127

ORNL-2614
Physics and Mathematics
TID-4500 (14th ed.)

SOLID STATE DIVISION

ANNUAL PROGRESS REPORT

FOR PERIOD ENDING AUGUST 31, 1958

OAK RIDGE NATIONAL LABORATORY
operated by
UNION CARBIDE CORPORATION
for the
U.S. ATOMIC ENERGY COMMISSION

Printed in USA. Price $3.00 cents. Available from the
Office of Technical Services
U. S. Department of Commerce
Washington 25, D. C.

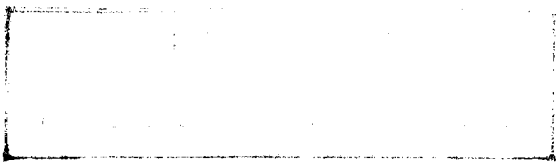

ORNL-2614
Physics and Mathematics
TID-4500 (14th ed.)

Contract No. W-7405-eng-26

SOLID STATE DIVISION

ANNUAL PROGRESS REPORT

For Period Ending August 31, 1958

D. S. Billington, Director
J. H. Crawford, Jr., Assistant Director

DATE ISSUED

NOV 7 1958

OAK RIDGE NATIONAL LABORATORY
Oak Ridge, Tennessee
operated by
UNION CARBIDE CORPORATION
for the
U.S. ATOMIC ENERGY COMMISSION

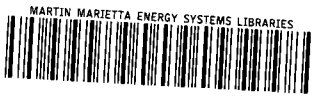

CONTENTS

SUMMARY

Effect of 14-Mev Neutron Irradiation upon Carrier Lifetime in Germanium

The effect of 14-Mev neutron irradiation upon the lifetime of current carriers in germanium has been investigated. The recombination process is apparently different from that in reactor-irradiated material. The position of the energy level responsible for recombination has been determined and the capture cross section for holes and electrons has been estimated.

Irradiation of Germanium with 14-Mev Neutrons

The conduction-electron removal rate of several high-purity single-crystal samples of n-type germanium has been determined following irradiation with 14-Mev neutrons that were produced by a Cockcroft-Walton accelerator by the $T(d,n)He^4$ reaction. The average value for several experiments is ~ 8 current carriers per incident 14-Mev neutron, where the carrier concentration was determined at 77°K. No low-temperature thermal instability or minority-carrier trapping effects were observed between 77°K and room temperature following irradiation at 77°K.

Gamma-Radiation Effects on Germanium

Single-crystal n- and p-type germanium plates were exposed to the 1.17- and 1.33-Mev gamma rays of Co^{60}. Two acceptor levels were observed for n-type germanium. One level is only effective as an electron trap below ~ 250°K and is removed by annealing at ~ 373°K. The other level is effective at all temperatures below intrinsic conditions and is not removed by annealing at ~ 373°K. Irradiation to nearly intrinsic conditions without annealing indicates that the first level is ~ 0.2 ev below the conduction band. This level is similar to one introduced by fast neutrons and is attributed to the first ionization of a radiation-produced interstitial. Annealing therefore suggests that preferential interstitial migration takes place. Some recovery toward initial conditions also occurs, particularly with extended anneals. Conversion of n-type to p-type by irradiation indicates an acceptor level at ~ 0.24 ev above the valence band. Extended irradiation does not further increase the apparent hole concentration significantly or reveal any low-lying acceptor states of the type observed with fast neutrons. Anneals at moderate temperature (~ 373°K) do not alter the ~ 0.24-ev level, and recovery toward initial conditions is not observed, even with extended anneals.

Annealing Studies of Irradiated Germanium

The anticipated annealing structure at low temperoture was not found in the experiments performed. These experiments differ from those in which the structure was found in that here the sample was removed from the reactor and stored at liquid nitrogen temperature to allow radioactive decay.

Electron Microscope Studies

A study is being made on the effect of irradiation on the etching behavior of germanium. Evidence is shown which indicates that irradiation modifies chemical behavior in such a way that a coherent surface film is formed in bromine-free CP-4 etchant. The changes in etching behavior are ascribed to this surface film. Other work in progress is directed toward studies of thin films and of plastic deformation of copper. Techniques have been developed and equipment is being built for the remote replication of surfaces of radioactive specimens.

Magnetic Susceptibility of Unirradiated and Neutron-Irradiated n-Type Silicon

Neutron irradiation of n-type silicon introduces deep traps, which at first seem to cause a disappearance of the donor paramagnetism. Upon longer irradiation, however, the trap paramagnetism increases again.

Magnetic Susceptibility of Manganese Sesquioxide

Susceptibility measurements between 50°K and room temperature have confirmed the existence of a magnetic phase change at 79°K and have shown that below that temperature Mn_2O_3 is antiferromagnetic.

Gamma Irradiation of n-Type Silicon

This work is in its beginning phase. The introduction rate of deep traps in an originally 12-ohm-cm phosphorus-doped silicon sample is 1.1×10^{-3} levels per Co^{60} photon per centimeter.

Radiation Effects in Indium Arsenide

The donor concentration of n-type samples of the semiconducting intermetallic compound InAs increases under fast-neutron irradiation. The hole concentration of p-type material decreases until the sample is converted to n-type. Further irradiation then increases the donor concentration. A major portion of the electron increase in p-type material can be thermally annealed; however, only about 25% of the electron increase in n-type material can be thermally annealed.

Optical Absorption Studies of Irradiated Solids

Neutron bombardments (10^{17} to 3×10^{20} fast neutrons/cm^2) of eight different crystalline and vitreous quartz samples are being completed for optical studies from 1400 to 26,000 Å. Three crystalline quartz samples were bombarded with 10^{17}, 10^{18}, and 10^{19} fast neutrons/cm^2 and then gamma-irradiated with a total of 5×10^7 r. No significant change was observed; this indicated that all neutron-created defects were filled. A low-temperature (−110°C) bombardment of 1.2×10^{17} fast neutrons/cm^2 indicated little difference from 60°C conditions for crystalline quartz; however, more of the far-ultraviolet absorption was observed in the vitreous quartz samples. Long-term gamma irradiation of crystalline quartz indicates that the coloration reaches a saturation value at about 5×10^7 r and does not bleach up to 3×10^9 r. The C band is not prominent in these samples, only the far-ultraviolet absorption. Under the same conditions, Corning No. 7940 and Vitreosil O.H. show radiation bleaching of the C band after 5×10^8 r, but Ultrasil continues to color at 3×10^9 r. No apparent difference in colorability with gamma irradiation was noticed with Corning silica samples heated at temperatures up to 1400°C and quenched.

Vacuum Ultraviolet Spectrophotometer

A spectrophotometer has been constructed and tested to cover the range from 900 to 3000 Å. The ratio of signal to scattered light is about 500 to 1 on the average. Most of the operational difficulties have been solved except for short- and long-term stability.

Optical Absorption Bands and Paramagnetic Resonance Centers in Silica and Quartz

By comparing the optical absorption bands and electron spin resonance (ESR) spectra of silica and quartz from several sources, after gamma-ray irradiation, after neutron irradiation in doses from 10^{17} to 3×10^{20} fast neutrons/cm^2, and after various heat treatments (after neutron bombardment), it is evident that the optical band at 2150 Å and the ESR line system centered at $g = 2.0010$ have correlation that is close to 1. A similar correlation is found for the 1650 Å band and the ESR line system centered at $g = 2.0090$. It is suggested that two forms of interstitial oxygen, O^{--} and O_2^-, and broken Si − O bonds may account for the observed ESR spectra.

Concentration of Paramagnetic Defects Produced in Silica and Quartz by Neutron Irradiation

The ESR technique has been used to establish the concentration of magnetic centers in each of the components of the ESR spectra by comparison with the concentration in the free radical diphenylpicrylhydrazyl. The total concentration of magnetic centers found by this method is in agreement with the concentration found by the magnetic susceptibility measurement. The concentration of paramagnetic centers in a specimen of natural quartz irradiated in BEPO, Harwell, England, has been determined. The concentration was found to follow the curve of concentration vs fast neutron dose found by Stevens *et al.* By comparing the ESR spectra in various materials and for various treatments, it can be shown that it is reasonable to assume that the intensities of the ESR spectra and of the optical absorption bands, after neutron irradiation, represent all the available defects of the kind which are observed by these techniques. More complex defect structures may be present but they are neither paramagnetic nor active optically.

Short-Range Order and Defects in Silicas

Some degree of short-range order, possibly extending over several unit cells, has been shown to exist in some silicas. One silica has been found which does not exhibit such short-range order and which shows much more rapid initial

growth of the 2150-Å band and the ESR line, $g = 2.0010$, than do the other silicas. The order in this silica is shown to be that characteristic of heavily irradiated ($\sim 10^{20}$ fast neutrons/cm^2) quartz and silica. The density of the two silicas seems indicative of the difference in short-range order between the two forms.

Low-Temperature Thermal Conductivity of Lithium Fluoride Crystal upon Irradiation by Thermal Neutrons and Co^{60} Gamma Rays

The nature of the radiation damage in thermal-neutron-irradiated lithium fluoride crystal has been examined through measurements of low-temperature thermal conductivity up to doses of $\sim 5.3 \times 10^{17}$ neutrons/cm^2. The thermal conductivity results indicate that the low-temperature thermal resistance is in large part due to clusters of point defects rather than to isolated defects, even at neutron doses as low as 4.5×10^{15} neutrons/cm^2. The observed thermal resistance maximum is followed by a decrease at higher neutron dose which is probably related to the decrease in lattice expansion observed previously. The thermal resistance introduced by Co^{60} gamma rays is qualitatively similar to that observed following thermal-neutron irradiation.

Effect of Fast-Neutron Bombardment on the Thermal Conductivity of Silica Glass at Low Temperature

Fast-neutron bombardment markedly alters the structure of both quartz and fused silica. Both approach a limiting density intermediate between those of the two forms, which suggests an intermediate state of order. However, x-ray studies show that irradiated silica is amorphous. The low-temperature thermal conductivity K, which is sensitive to crystalline order through the phonon mean free path, was measured on silica glass before and after successive exposures up to a maximum dosage of 7×10^{19} fast neutrons/cm^2. At 5°K, K was observed to double after the heaviest exposure. Moreover, the increase in both K and density appeared to have saturated. This behavior indicates that the short-range order in the glass improves with exposure. Annealing at ~ 900°C causes K to recover toward its preirradiated value.

Thermal Conductivity of Monoisotopic Ionic Crystals (Sodium Fluoride and Cesium Iodide) at Low Temperatures

The thermal conductivity, K, of NaF single crystals has been measured at low temperatures. It appears that grown-in defects are important factors limiting K. In CsI, K at the lowest temperatures appears to be limited by the presence of a high density of dislocations. Thermal annealing of a crystal of CsI containing 0.1% thallium resulted in an increase in the low-temperature thermal conductivity.

Stored Energy in Irradiated Graphite

The release of stored energy of graphite taken from the lattice of the ORNL Graphite Reactor was measured. A new method was used that depends upon the transfer of heat by radiation between the walls of the evacuated calorimeter and the sample. Approximately 26 cal/g was released upon heating the samples to 217°C.

Studies on Graphite from the ORNL Graphite Reactor

Measurements on graphite from the ORNL Graphite Reactor have included operating temperatures, c_0 parameters before and after annealing, and stored energy.

The results of the investigation show that the growth of the 200°C stored energy peak is very critically dependent upon irradiation temperature, even as low as 30°C. It was also found that correlation between c_0 axis expansion and stored energy can be employed if the irradiation temperatures are known.

The maximum amount of stored energy, to 250°C, in the Graphite Reactor is about 32 cal/g, and the damaged region of the graphite stack that contains this energy comprises only about 5% of the total graphite volume. From these results it is clear that the reactor is in a safe condition and that the buildup of the 200°C stored energy peak is only about 2 cal·g^{-1}·year^{-1} at the present rate of growth.

Young's Modulus and Internal Friction Studies

A study of the amplitude-independent internal friction and Young's modulus in copper from 14°K to room temperature, both before and after neutron

irradiation, indicates that there are two dislocation components in these quantities. These have been tentatively identified as a relaxation component, studied in detail theoretically by Seeger, and a background component, which appears to be characteristic of Koehler's bowing mechanism. It is felt that these two components are probably quite intimately related, for the background internal friction rises at just slightly higher temperatures than the maximum of the individual relaxation processes, and the activation energy of the background process is about twice the kink energy obtained from Seeger's theory. Moreover, the Bordoni, or relaxation spectrum, is shown to be considerably more complex than has been previously indicated in that there appear to be at least four principal relaxations. As a result of the analysis attempted in the present work, it appears that the more obvious difficulties of Seeger's theoretical treatment are alleviated.

Neutron Damage Effects in Metals at Low Temperatures

The temperature dependence of the critical shear stress of an irradiated copper single crystal has been measured and found to be in close agreement with theory over a large temperature range. Isochronal annealing studies have been made on high-purity beryllium and magnesium irradiated at 19.5°K. The annealing of these materials is quite different from that found in copper. Studies on the damage rate and annealing differences between annealed and cold-worked copper bombarded at low temperatures have been made. It is believed that the neutron damage rate (measured by changes in residual resistivity) in cold-worked copper is higher than in annealed copper. It has been found that the residual resistivity of high-purity copper can be greatly reduced by annealing in the presence of oxygen.

Reactor Bombardments Near 4°K

A helium liquefier system has been operated successfully in the ORNL Graphite Reactor. The system uses a closed helium circuit and operates continuously. Two neutron bombardments have been made, one for 80 hr and one for 160 hr at 4.17°K with the reactor at full power.

Hole 50 Liquid-Nitrogen Cryostat

A liquid-nitrogen cryostat has been built for hole 50 of the ORNL Graphite Reactor. A new heat exchanger and compressor system is being designed for this cryostat. Experience derived from the hole 52 cryostat and the hole 12 cryostat is being utilized on all components in an attempt to produce the best machine possible for this temperature range.

Chemical Properties of Metal Surfaces

An investigation was made of the polygonization of copper by using etch pits and x-ray diffraction to observe polygonization. These techniques for observing dislocations were used to determine the relation between oxide nuclei and dislocations. It was found that nuclei form at dislocations if certain impurities are present in the copper. Studies of the dissolution of copper crystals in aqueous solutions have shown that many dissolution reactions for copper occur by a mechanism which involves the oxygen dissolved in the solution.

Migration of Deuterium in Copper

The possibility of measuring the rate of diffusion of deuterium in copper has been investigated by using deuterons from a conventional radio-frequency ion source accelerated to 176 kev and focused on a thin copper target. The neutrons resulting from the $D(d,n)He^3$ reaction were counted with $B^{10}F_3$ proportional counters whose output was recorded automatically. The target temperature, held down by a spray of tap water, was monitored with thermocouples attached to its back side. For irradiation times up to 3 hr no evidence of saturation of the deuteron buildup curves occurs, although the deuterium content of the target decreases when the target is left standing in a vacuum. An equation has been developed which gives the counting rate as a function of the diffusion coefficient, D, and the range, R. The values obtained for a selected target are $D/R^2 = 1.21 \times 10^{-3}$ sec^{-1} and $D = 3 \times 10^{-11}$ cm^2/sec. An Oracle program for evaluation of the diffusion coefficient by the method of least squares is under development. Since the above-mentioned equation requires a knowledge of cross sections as a function of penetration, a range-energy graph was constructed by graphical integration of data from the literature.

Irradiation and Quenching Experiments on Copper-Aluminum Alloys

Upon neutron irradiation near room temperature a decrease in the electrical resistivity of Cu-Al

alloys takes place. The process that causes this decrease in resistivity is apparently diffusion-controlled, since no decrease takes place when the irradiation temperature is −120°C. The possibility is considered that the alloy is initially in a metastable state and that the irradiation near room temperature accelerates the return to an equilibrium configuration, with an attendant decrease in resistivity. In order to investigate the nature of this metastability, resistivity measurements on unirradiated material have been made at temperatures up to 650°C and as a function of air-cooling and water-quenching. It has been found that an additional contribution to the resistivity appears at temperatures above 200°C. The energy of formation of the configuration responsible for this excess resistivity is about 0.2 ev. Also, the activation energy for the annealing of the excess resistivity retained upon quenching from 450°C was determined. These effects are discussed in terms of short-range ordering and the annealing of lattice defects.

Miscellaneous Small-Angle X-Ray Scattering Studies of Al-Ag

A pair of particularly homogeneous foil samples of an Al–20 wt % Ag alloy, one irradiated and one unirradiated, were given thorough examination for the rate of zone growth, the activation energy for zone growth, and the zone size distributions throughout aging until onset of true precipitation. Other studies of samples formed by various techniques and given various irradiations were conducted, and some of the results are described.

Some Mechanical Yield Phenomena in Unirradiated and Fast-Neutron-Irradiated Pure Copper Single Crystals

Mechanical yielding at 78 and 300°K in unirradiated and fast-neutron-irradiated copper single crystals has been studied from the load-elongation curves after various interrupted and alternated extensions at these two temperatures. Values of $\Delta\sigma$ are plotted vs plastic strain and are seen to be strongly affected by previous irradiation and in some cases strongly dependent on crystal orientations. Also, three distinct types of yield points are seen to exist in a sample with 5×10^{17} *nvt* which is of unique orientation.

HRP Radiation Metallurgy

The following conclusions regarding the behavior of irradiated iron alloys are discussed:

The notch-impact transition-temperature shift is strongly dependent on both temperature of irradiation (between 500 and 600°F) and fast-neutron dose (between 10^{18} and 2×10^{19} fast neutrons/cm^2).

High-purity iron normalized to produce a grain size between 0.1 and 1 mm shows the lowest increase in transition temperature of any iron alloy yet tested at doses of 10^{20} fast neutrons/cm^2. A higher initial transition temperature and a greater irradiation-induced increase were observed in the same iron with a much finer grain size produced by a subcritical anneal.

High-purity iron alloyed with 0.14% carbon shows a much lower transition-temperature increase than steels of equivalent carbon content. Therefore, the great sensitivity to irradiation-induced transition-temperature increase in steels is not a basic property of the carbon-containing body-centered-cubic structure.

Tensile fractures without localized necking have been observed in three alloys after high-dose, elevated-temperature irradiations. In all three cases the rate of work-hardening was greater than in the unirradiated metal. In all other cases the work-hardening rate was lower in the irradiated metal.

The generally lower uniform elongation of irradiated iron and steels of low carbon content does not correlate with the magnitude of the notch-impact transition-temperature shifts. This conclusion may not be valid in large or complex structures or where ductile fracture is involved.

Radiation Metallurgy

The stress-rupture life of tube-burst specimens of Inconel in air was determined in the MTR at several stresses at 1500°F. The rupture life is shortened at high stresses under irradiation. Earlier tests in a helium atmosphere showed a greatly shortened rupture life that was partially caused by contamination of the helium atmospheres by furnace insulation. The contamination caused thermocouple errors.

Oxidation in air of a ruptured tube-burst specimen apparently can fill the rupture fissures with metal oxides that have enough strength to hold the test

stress formerly applied for periods of hours before rupture occurs again.

Engineering of equipment for the four or five facilities to be used in the ORR is in progress. Locating equipment has been installed on the pool side of the reactor tank. Measurements of the fast flux in ORR facilities to be used have been completed. A number of measurements of fast and thermal flux in the LITR and ORR are reported.

The Np^{237} Fission Reaction as a Relative Monitor for Displacement Reactions

The Np^{237} and U^{238} fission reactions and the $S^{32}(n,p)P^{32}$ reaction are compared as relative monitors for radiation damage effects caused by displacements. From data on the conductivity changes of graphite and *n*-type germanium, the Np^{237} fission reaction gives the best agreement. Neutron flux values from this threshold reaction are given for holes A, 19, 51N, 52, and 1768 of the ORNL Graphite Reactor. The flux ratio between 1768 and A is in agreement with data on a copper-aluminum alloy.

Comparison of Reactor and Gamma Irradiation of Polymers

The reaction rates for three cleavage and three gassing reactions were compared for reactor and gamma irradiations. The ratios of the reaction rates were found to be roughly consistent with hydrogen content for gassing reactions in polyethylene, nylon, and allyl diglycol carbonate and for the cleavage reaction in poly-α-methylstyrene. The ratios for the cleavage reactions in Teflon and polymethyl methacrylate indicated that the reactor radiation was less efficient, by a factor of 2, than for the other reactions.

Effects of Radiation on Plastics and Elastomers

To permit quantitative interpretation of earlier infrared spectral studies of irradiated polymer films, absorption coefficients are being obtained by curve-fitting techniques applied to absorption measurements on standard hydrocarbon solutions. Further determinations of absorptivities are being made on films of polybutadienes having known concentrations of several olefinic groups.

The effect of molecular orientation on cross-linking or scission by radiation in amorphous polymers has been investigated. Orientation was observed to reduce the radiant energy required for cross-linking in polystyrene. On the other hand, orientation did not produce a measurable change in the energy required per scission in polymethyl methacrylate.

Irradiation of polystyrene to doses five- or tenfold larger than that required for complete cross-linking imparted significant resistance to crazing under flexural loads. There was evidence, however, that the time-to-rupture property was adversely affected.

Radiation Stability of Ceramic Materials

A technique has been developed for measuring the temperature coefficient of the Young's modulus of $\frac{3}{4}$-in.-long ceramic specimens. The sensitivity is improved for longer specimens. The resonant frequency was followed when the specimen was vibrated as a clamped free bar; the resonant frequency was in the range from 1000 to 5000 cps. In the temperature range from -50 to $0°C$, the temperature coefficient of the modulus of plate glass is much less sensitive than the Knoop hardness or the density to an exposure of 6×10^{20} nvt epithermal neutrons.

Energy Absorption in the Reactor by Calorimetry

Energy absorption in hole 19 in the Graphite Reactor was measured with a small calorimeter for graphite and for a hydrogen-containing material. From the measurements for the two materials and from the cross sections for interaction with neutrons and gamma radiation, the components of the total energy absorption which result from gamma radiation and fast neutrons may be calculated. The result is not very sensitive to the exact values taken for the cross sections or to the neutron spectrum, since for the mixed radiation field in the reactor the energy absorption in hydrogen is largely from fast neutrons and the energy absorption in graphite is largely from gamma radiation.

Gas-Cooled Reactor Fuels

An irradiation program was started to evaluate the stainless-steel-canned UO_2 fuel element for the Gas-Cooled Reactor prototype. Fuel element integrity and fission gas release will be primary objectives. Fission gas evolution was measured from UO_2 of 96% theoretical density irradiated at a temperature of 1770°F, and the rate was found

to be of the order of 1% of the production rate. Long-range studies were continued on more advanced fuel materials. A UO_2 fuel plate clad with Cr-Al_2O_3 was examined after irradiation at 1800°C to 14.5% U^{235} burnup. High-temperature cladding for graphite is being investigated for use as a fuel canning material and as a moderator material. Construction began on a closed gap loop facility to test advanced high-temperature fuels. A thermocouple irradiation damage program was initiated for high-temperature application, and also an alternative device is being developed for this purpose.

High-Radiation-Level Examination Laboratory

The design criteria have been established and conceptual design is completed for part I of the new hot cell laboratory. This laboratory is designed for complete containment and wholly remote maintenance and will be used for work with materials containing mixtures of high-level alpha, beta, and gamma radiations.

Recycling Viscometer

Preliminary testing of the recycling viscometer has been completed. These tests were carried out with standard mixtures of water and glycerol of known viscosity. In order to make the solutions conducting, a small amount of KCl was added to each, but the effect on the viscosity of the solutions was negligible. Results obtained indicate that viscosities can be determined with an error no greater than ±1% in the range of 5 to 10 centipoises. No attempt was made to determine any values outside this range.

Electrodeposition in Molten Fluorides

The equipment for investigating electrodeposition in molten salts has been completed and should prove adequate for studies of the electrical properties of high-temperature liquid systems.

Fused Salt Polarography

The fused salt polarograph has been under development and will be satisfactory for fused nitrates. Application to high-temperature fluoride systems will require further development.

Volatility Process Studies

A study of the volatility behavior of molybdenum indicates that MoF_5 is converted to MoF_6 by fluorine. Molybdenum hexafluoride and technetium are adsorbed on sodium fluoride at 100°C, technetium fluoride being more strongly adsorbed than MoF_6. The vapor pressure of MoF_6 is too high to permit satisfactory trapping at the temperature of dry ice. The behavior of volatile fission product fluorides is such that (1) ruthenium and niobium fluorides are volatile from fused salts during fluorination, and (2) molybdenum and technetium are not volatile during hydrofluorination but are volatilized by excess fluorine.

Effect of Radiation on Corrosion of Structural Materials by Molten Fluorides

In the many capsule tests and in the three in-pile loop tests, no major changes have occurred in the fuel mixtures that can be attributed to irradiation effects, other than normal burnup of uranium. Metallurgical examinations of the Inconel capsules and tubing have likewise shown no changes in corrosion that can be the result of radiation damage.

Effect of Radiation on Static Corrosion of Structural Materials by Fused Salt Fuels

The study of the effect of radiation on the corrosion of structural materials by fused salt fuels has been continued. The following systems were under investigation: Hastelloy B containing NaF-KF-LiF-UF_4 at 1500°F, graphite and Inconel containing LiF-BeF_2-UF_4 at 1250°F, and INOR-8 containing LiF-BeF_2-UF_4 at 1250°F.

Molten-Salt Reactor Program In-Pile Convection Loop

An in-pile thermal-convection loop with LiF-BeF_2-UF_4 fuel in an INOR-8 container is being prepared for operation in the LITR. An electrically heated mockup of this loop is in operation. Improved thermocouples have been developed to withstand the effects of differential thermal expansion of the loop.

Fused Salt Forced-Circulation LITR Loop

The Inconel in-pile forced-circulation fused salt loop previously operated for 235 hr in the LITR at 1600°F was examined for corrosion. The corrosion was the same as that which would have been expected under the same conditions in the absence of radiation.

Gaseous Fission Product Disposal

Investigation of the holdup or retention of gaseous fission products was continued. Some of the studies related directly to the HRT charcoal adsorber system, while others were of more general applicability. In a number of experiments a gas-solid chromatographic technique was employed, with Kr^{85} used as a tracer. Experiments of this type include (1) comparison of the holdup performances of a wide variety of adsorbents such as activated carbons, Linde molecular sieves, and porous glass; (2) the effect of moisture on the adsorption efficiency of charcoal; (3) comparison of holdups when different carrier or sweep gases are used; (4) effect of fission gas partial pressure on holdup; and (5) comparison of krypton and xenon holdup, which involved the use of an additional tracer, Xe^{133}. Similar experiments now in progress are concerned with the effects of trap geometry and linear velocity of the sweep gas on holdup and on the shape of the elution curves. Holdup measurements were made on the actual HRT adsorbers prior to operation of the reactor, and currently the behavior of the charcoal beds is being studied by means of gamma spectrometry. Also, since the HRT employs oxygen as the carrier for the fission gases, the ignition and combustion of charcoal in oxygen was investigated both experimentally and theoretically. A rather brief study was made of the removal of iodine from gas streams by adsorbents.

Hot Cell Operations

The Hot Lab Section has operated as a service group since July 1, 1957. It has processed over 450 radioactive specimens and 54 experiments within the last year.

Several new pieces of equipment have been added; also, a dry storage facility and a cell vacuum cleaning system are under construction. Design for cell modification to make possible the handling of alpha-, beta-, and gamma-active specimens is in progress.

EFFECT OF 14-Mev NEUTRON IRRADIATION UPON CARRIER LIFETIME IN GERMANIUM

O. L. Curtis, Jr.

The effect of 14-Mev neutron irradiation upon the lifetime of excess current carriers in germanium is being investigated. Table 1 shows the results of the first irradiation of 1.05×10^{11} neutrons/cm^2 on n- and p-type samples having a range of resistivities. Listed are the carrier concentration (which did not change measurably during the irradiation), the initial lifetime τ_0, and the lifetime after irradiation, τ. From the initial and final lifetimes is obtained the quantity $(1/\tau - 1/\tau_0)$, a measure of the effect of the irradiation upon recombination. The estimated amount of reactor irradiation (approximately a fission spectrum) required to produce an equivalent effect[1] in each sample has been tabulated as obtained from Fig. 1 for n-type material and from similar data[2] for p-type material. Due to the complexity of the situation in p-type material,[2] we shall attempt an analysis only of the recombination centers in n-type material.

A comparison of the equivalent reactor irradiations for high- and low-resistivity material indicates the possibility of a difference in the nature of the recombination centers introduced by the two types of irradiation. This difference is indicated more strikingly by comparing Figs. 2 and 3, which are plots of ln τ vs $1/T$ for similar material following the two types of irradiation. On the basis of simple theory, the data of Fig. 2 suggest a recombination level at 0.35 ev from a band edge, as compared with a value of 0.20 ev obtained for centers induced by reactor neutrons.[1,2] (These numbers include a $T^{3/2}$ correction from the observed slope.)

An analysis of this behavior can be made on the basis of the Hall-Shockley-Read theory.[3,4] The

[1] O. L. Curtis, Jr., *et al.*, *J. Appl. Phy.* 28, 1161 (1957).

[2] O. L. Curtis, Jr., J. W. Cleland, and J. H. Crawford, Jr., *J. Appl. Phy.* (to be published).

[3] R. N. Hall, *Phys. Rev.* 87, 387 (1952).

[4] W. Shockley and W. T. Read, Jr., *Phys. Rev.* 87, 835 (1952).

Table 1. Effect of Irradiation with 14-Mev Neutrons on Carrier Lifetime in Germanium

Sample	Initial Properties			τ* (μsec)	$1/\tau - 1/\tau_0$ (sec^{-1})	Estimated Equivalent Reactor Irradiation** (neutrons/cm^2)
	n (cm^{-3})	p (cm^{-3})	τ_0 (μsec)			
					$\times 10^3$	
A5 - 1	5.1×10^{13}	4.9×10^{12}	1070	410	1.51	4×10^{11}
A6 - 1	1.5×10^{14}		960	155	5.41	8×10^{11}
AB7 - 1	3.1×10^{14}		410	66	12.7	1×10^{12}
A4 - 1	7.6×10^{14}		170	18.4	48.5	1.5×10^{12}
CH - 6	2.6×10^{15}		44	11.8	62	1.1×10^{12}
D1 - 1	3.1×10^{12}	8.0×10^{13}	760	400	1.2	4×10^{11}
F2A - 1		3.4×10^{14}	460	155	4.3	6×10^{11}
D3 - 1		1.6×10^{15}	220	65	10.8	

*Carrier lifetime after irradiation with 1.05×10^{11} neutrons/cm^2 (energy 14 Mev).

**Average neutron energy $\sim$1.5 Mev.

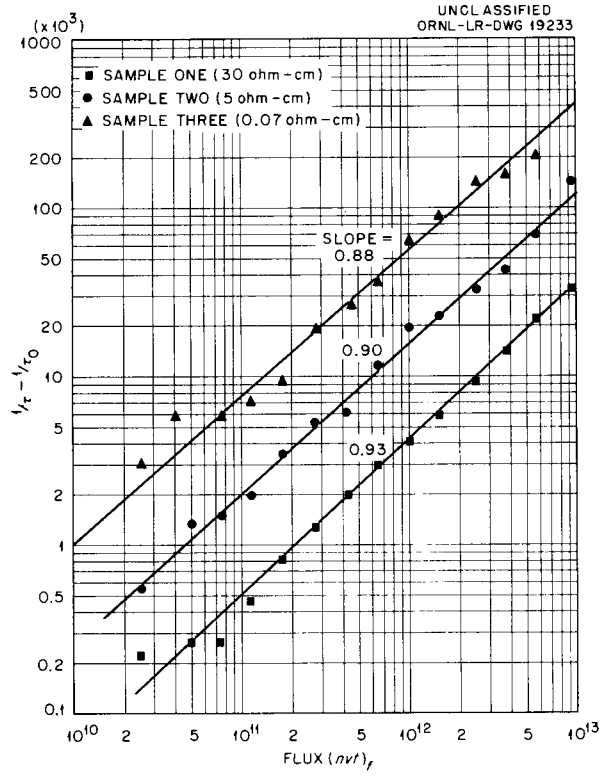

Fig. 1. Plot of $1/\tau_0 - 1/\tau$ vs Integrated Fast Neutron Flux, $(nvt)_f$, for n-Type Germanium, Reactor-Irradiated.

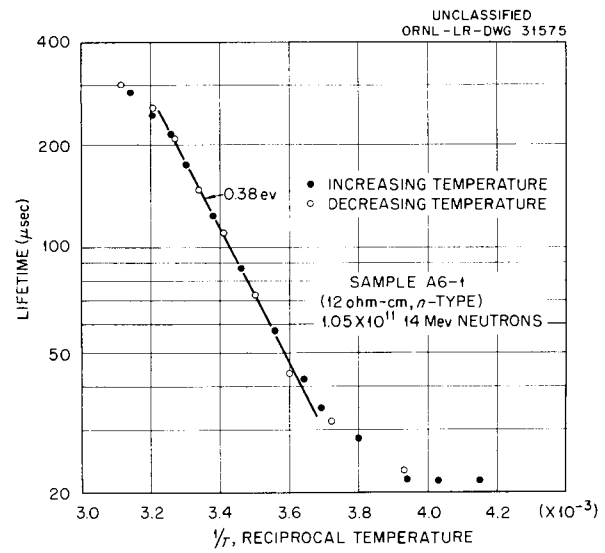

Fig. 2. Plot of τ vs $1/T$ for an n-Type Specimen of Germanium Irradiated with 14-Mev Neutrons.

recombination equation can be written:

$$\tau = \frac{(p + p_1)/c_n + (n + n_1)/c_p}{N_t(n + p)} ,$$

where τ is lifetime, n and p are the initial electron and hole concentrations, respectively, c_n and c_p are electron and hole capture probabilities, n_1 and p_1 are the concentrations if the Fermi level is at the position of the recombination center, and N_t is the number of recombination centers. For n-type material $n >> p$. For a level near the center of the band, $p_1 >> p$, $n >> n_1$. The recombination equation reduces to:

$$\tau = \frac{p_1}{c_n N_t n} + \frac{1}{c_p N_t} .$$

Aside from the possibility of a small variation of c_p with temperature, the second term is temperature-independent and represents the leveling-off of the τ-vs-$1/T$ curve at low temperature. We do not know N_t. However, we can make the same assumption as previously[1,2] and say that one recombination center is added for each two carriers removed. This may not be a valid assumption, since the nature of these low-lying levels is not well understood. Cleland (see "Radiation of Germanium with 14-Mev Electrons," this report) has measured the rate of carrier removal and found it to be approximately 8 per incident 14-Mev neutron. On this basis $N_t = 4.2 \times 10^{11}$ cm^{-3}. For these samples at low temperature we have:

$$\tau^* = \frac{1}{c_p N_t} ,$$

or

$$c_p = \frac{1}{\tau^* N_t} ,$$

where the limiting value τ^* is about 20 μsec, giving $c_p = 1.2 \times 10^{-7}$ cm^3/sec. The temperature-dependent portion of the curve should be given by:

$$\tau = \frac{p_1}{c_n N_t n} .$$

We need only to calculate p_1 to determine c_n. We have:

$$p_1 = N_v e^{(E_v - E_t)/kT} ,$$

where N_v, the number of states in the valence band, is equal to 4.55×10^{18} cm^{-3} at room temperature and is proportional to $T^{3/2}$. The quantity $E_t - E_v$ is the position of the recombination center measured from the valence band. This is obtained from the slope of the curve: $E_t - E_v = 0.35$ ev. The electron concentration, n, is equal to

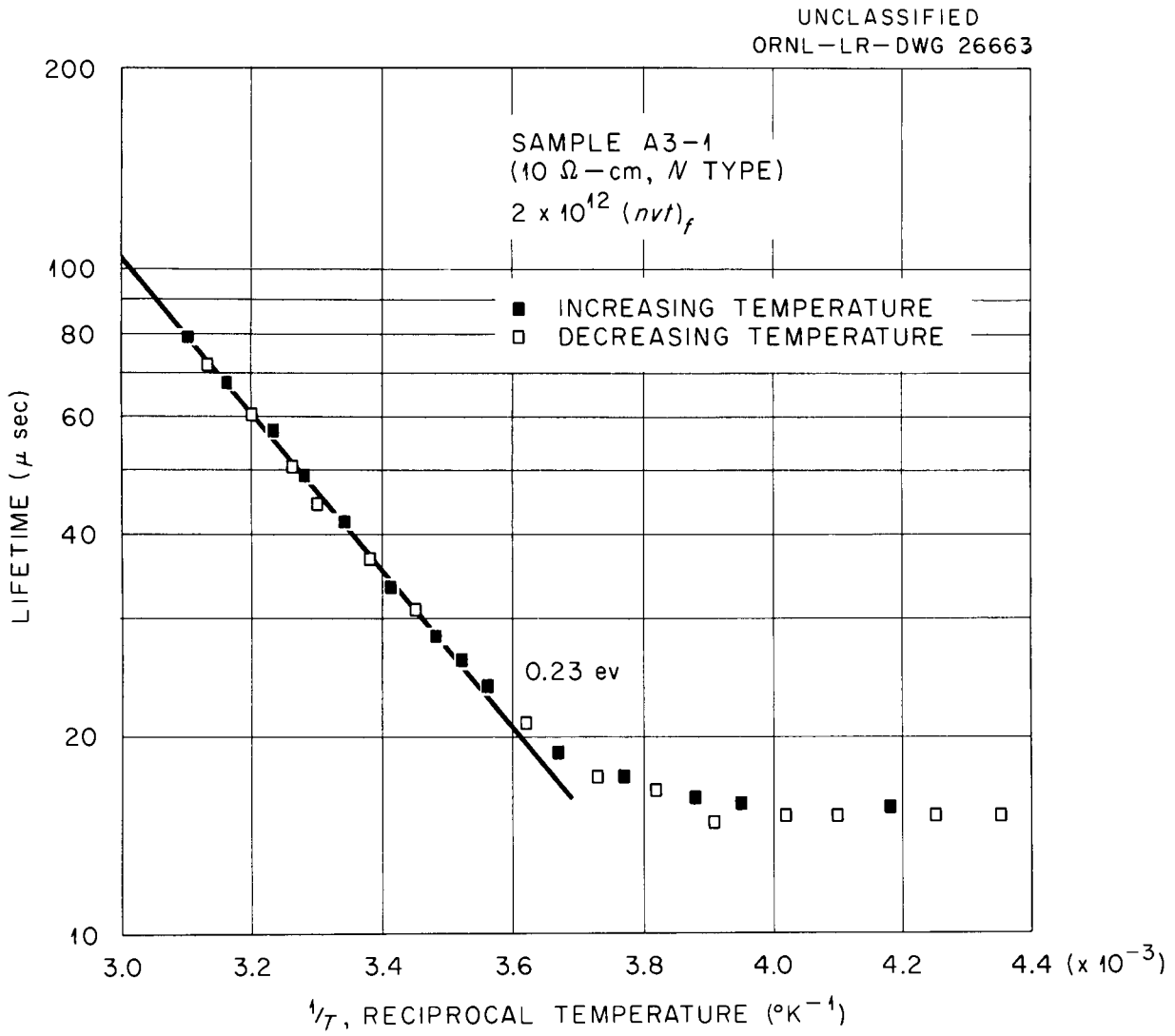

Fig. 3. Plot of τ vs $1/T$ for an n-Type Specimen of Germanium Irradiated with Reactor Neutrons.

1.5×10^{14} cm^{-3}. Since we know the initial room-temperature lifetime, τ_0, we can correct the post-irradiation lifetime, τ, for the original recombination. The corrected lifetime is given by $(1/\tau - 1/\tau_0)^{-1}$ and is equal to 185 μsec. Inserting these values, we have $c_n = 5 \times 10^{-10}$ cm^3/sec. From the relationship $c = \sigma\langle v\rangle$, where $\langle v\rangle$ is the mean carrier velocity (1.8×10^7 cm/sec for holes and 1.1×10^8 cm/sec for electrons), we obtain the capture cross sections, $\sigma_n = 4.5 \times 10^{-18}$ cm^2 and $\sigma_p = 6.7 \times 10^{-15}$ cm^2.

In Fig. 4 the temperature variation for a p-type specimen is plotted. The results are similar to those for reactor-irradiated specimens,[2] except that again a stronger temperature dependence is noted.

Further studies using 14-Mev neutrons are planned, and a more complete analysis of the recombination process will be attempted.

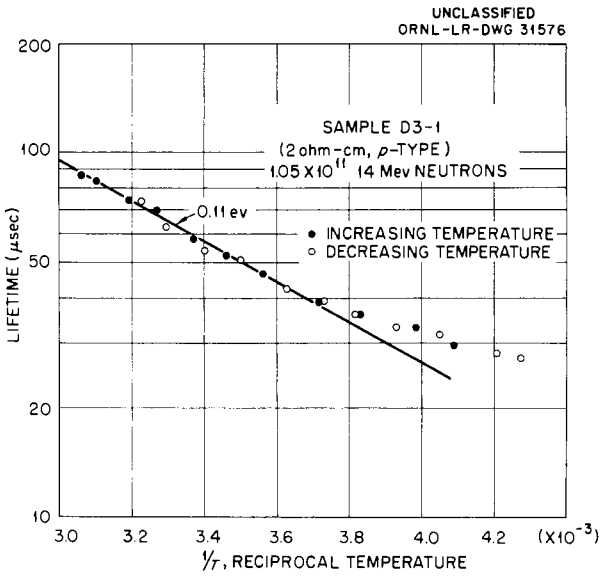

Fig. 4. Plot of τ vs $1/T$ for a p-Type Specimen of Germanium Irradiated with 14-Mev Neutrons.

IRRADIATION OF GERMANIUM WITH 14-Mev NEUTRONS

J. W. Cleland O. L. Curtis, Jr. J. H. Crawford, Jr.

The availability of a Cockcroft-Walton accelerator in the Biology Division of the Oak Ridge National Laboratory[1] has recently permitted irradiation-effect studies on germanium, utilizing the 14-Mev neutrons produced in a platinum–zirconium tritide target by deuterons. The extreme sensitivity of the electrical properties of germanium is such that the average flux of $\sim 1.5 \times 10^8$ neutrons·cm^{-2}·sec^{-1} at the wall of the target tube is sufficient for certain experiments. Actual total dosage at about 3 in. from the wall of the target tube is approximately 3×10^{11} neutrons/cm^2 for an irradiation time of 6 hr, which is the expected lifetime of a target.

High-purity single-crystal specimens of n- and p-type germanium have been cut into bars for lifetime measurements and into plates for Hall coefficient and conductivity studies. Several preliminary measurements of the change in carrier concentration of n- and p-type samples have been made, and one conductivity experiment has been conducted at liquid nitrogen temperature.

Figure 5 shows the conductivities of two n-type samples and of one p-type sample of germanium at 77°K as a function of the integrated incident flux of 14-Mev neutrons. The slopes are essentially linear. The incident flux actually decreases during irradiation as the target is exhausted, and the incident flux also varies as different portions of the rotating target are employed. The conductivity data reported were actually obtained as a function of total counts of slow neutrons from a long counter but are plotted as a function of time. An alpha counter was also employed in some of the irradiations and indicated that the total flux was within 12% of that indicated by the slow-neutron counter.

The samples of Fig. 5 were slowly warmed to room temperature after irradiation and were then recooled to 77°K. No evidence of any form of thermal instability of defects, annealing, or minority-carrier trapping was observed. This is in contrast to low-temperature reactor irradiation results, where extensive minority-carrier trapping

[1] The authors are indebted to M. L. Randolph of the Biology Division for the use of the machine and for operating it during the experiment.

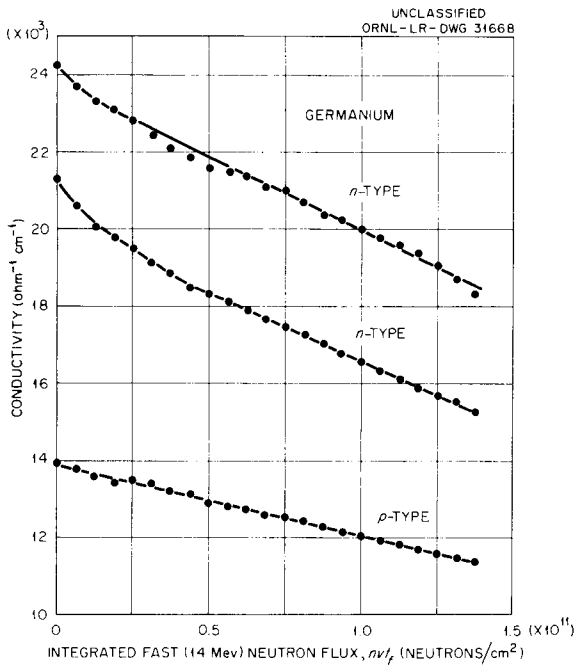

Fig. 5. Conductivity of Germanium at 77°K vs Integrated Fast (14 Mev) Neutron Flux.

effects were observed.[2] The conductivity of the two *n*-type specimens returned to the postirradiation value at 77°K following thermal cycling to room temperature. The *p*-type sample could not be measured, apparently because of a loose resistivity-probe contact. The two *n*-type samples were not appreciably photosensitive at 77°K prior to exposure; however, they became extremely photosensitive as a result of the irradiation. Another *n*-type sample, changed to essentially intrinsic conditions by a room-temperature irradiation of greater magnitude, varied in resistance at 77°K from many megohms in the dark to only hundreds of ohms with a small amount of ambient light.

The electron removal rate of the two *n*-type samples, determined by Hall coefficient measurements at 77°K before exposure and subsequent to exposure and thermal cycling, was 7 ± 1.5 per incident 14-Mev neutron. The removal rate of another *n*-type specimen, irradiated at room temperature, was 9 ± 1 per incident 14-Mev neutron as determined at 77°K.

[2] J. W. Cleland and J. H. Crawford, Jr., *Solid State Ann. Prog. Rep. Aug. 31, 1957*, ORNL-2413, p 28.

The removal rate of conduction electrons in high-purity Ge has been determined for monoenergetic neutrons of other energies by Ruby, Schupp, and Wolley of the Westinghouse Electric Corporation.[3] A Van de Graaff accelerator provided 2-Mev deuterons, and the $D(d,n)He^3$ reaction produced approximately 10^7 neutrons·cm^{-2}·sec^{-1} of 4.8, 3.2, and 1.7 Mev energy at angles of 0, 90, and 145° from the incident deuteron direction. They measured carrier concentration changes at 77°K subsequent to irradiation at 77°K without thermal cycling, and obtained experimental removal rates of conduction electrons per unit of neutron flux of 12, 12, and 21 at neutron energies of 4.8, 3.2, and 1.7 Mev, respectively.

Reactor irradiation results on the removal rate of conduction electrons in *n*-type germanium were originally listed as ~3.2 per incident fast neutron as obtained in a cylindrical uranium donut or fission chamber located in hole 51N of the ORNL Graphite Reactor. This value has been employed as a standard to permit comparison with other reactor positions. More recent measurements[4] utilizing fission reactions as threshold detectors have indicated that the fast neutron flux capable of displacing germanium atoms in hole 51 is more probably $\sim 4 \times 10^{11}$ than the value $\sim 8 \times 10^{11}$ originally employed. Such a correction would essentially double the probable removal rate of conduction electrons in a reactor fission spectrum. Under these assumptions, the present experimental data can be tabulated as follows:

	Neutron Energy (Mev)	Charge-Carrier Removal Rate, $-dn/d\phi$
Reactor, Oak Ridge	Fission spectrum	6.4
$D(d,n)He^3$, Westinghouse	1.7	21
	3.2	12
	4.8	12
$T(d,n)He^4$, Oak Ridge	14	8

[3] S. L. Ruby, F. D. Schupp, and E. D. Wolley, "Effect of Monoenergetic Fast Neutrons on *N*-type Ge," *Phys. Rev.* (submitted for publication).

[4] D. Binder, *Solid State Ann. Prog. Rep. Aug. 31, 1957*, ORNL-2413, p 122.

GAMMA-RADIATION EFFECTS ON GERMANIUM

J. W. Cleland J. H. Crawford, Jr.

Introduction

It has previously been observed[1] that high-energy photons (Co^{60} gamma rays) alter the electrical properties of germanium. Electron trapping levels (acceptors) were observed which are quite similar to those produced by fast-neutron irradiation.[2] In the present work, the position and ionization behavior of photon-introduced donor and acceptor states are determined more exactly, and certain consequences of annealing studies are presented.

Experiment

High-purity single-crystal n- and p-type plates of germanium were exposed to 1.17- and 1.33-Mev gamma rays from an 1800-curie Co^{60} source. The temperature during exposure was below 40°C. The photon flux was determined by cerium sulfate dosimetry as $\sim 2.3 \times 10^6$ r/hr. One roentgen is taken as 1.5×10^9 gammas/cm^2. Thus the incident photon flux was $\sim 10^{12}$ per square centimeter per second. The total-flux figures listed previously[1] were in error, being too low by a factor of 2. The addition rate of defects in n-type germanium as determined from carrier concentration changes in these experiments and the rate previously determined[1] are both consistent with a value of $\sim 6 \times 10^{-4}\phi$, where ϕ is the incident photon flux.

Measurements of the Hall constant, R, and of resistivity, ρ, were made as a function of temperature. Soft-soldered electrical leads were employed, and all anneals were conducted in air.

Results

The effect of a series of exposures on n-type germanium is shown in Fig. 6, where log R and log ρ are separately plotted vs reciprocal temperature. The introduction of two acceptor levels is indicated by curves II and III. One is evidently only effective below ~250°K, whereas the other is effective at all temperatures below essentially intrinsic conditions. Continued irradiation to nearly intrinsic n-type conditions suggests that one level is located ~0.2 ev below the conduction band.[1] A similar level has been observed for fast-neutron irradiation[3] and has been attributed to the first ionization of a radiation-produced interstitial atom.

Some of the radiation-induced carrier concentration decrease of the sample of Fig. 6 was removed by a thermal anneal of 1 hr at ~373°K (curve V). However, some evidence of two acceptor levels remained. An extended anneal, 18 hr at ~373°K, removed a major portion of the radiation-induced carrier concentration decrease; and curve VI shows no evidence for two different levels. The sample of Fig. 6 was reirradiated with 4×10^{17} photons and attained essentially

[1] J. W. Cleland, J. H. Crawford, Jr., and D. K. Holmes, *Phys. Rev.* 102, 722 (1956).

[2] J. W. Cleland, J. H. Crawford, Jr., and J. C. Pigg, *Phys. Rev.* 98, 1742 (1955).

[3] J. W. Cleland, J. H. Crawford, Jr., and J. C. Pigg, *Phys. Rev.* 99, 1170 (1955).

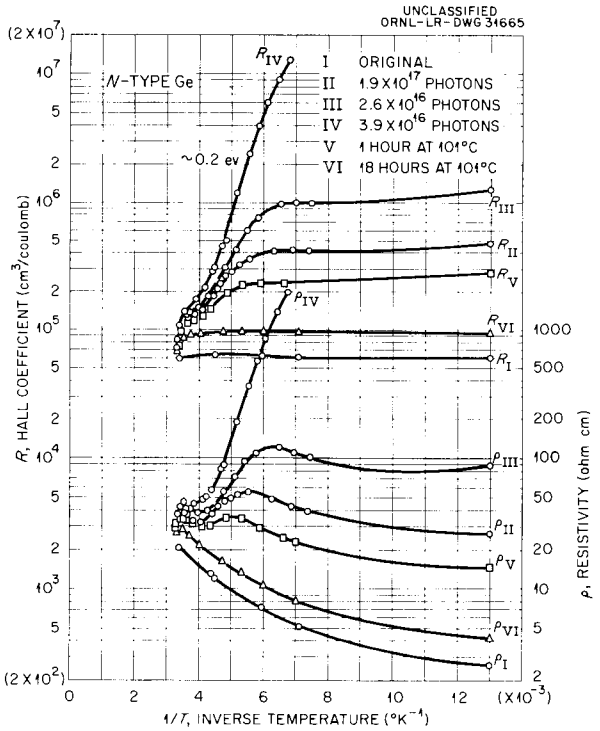

Fig. 6. Plot of Hall Coefficient, R, and Resistivity, ρ, vs Reciprocal Temperature for n-Type Germanium.

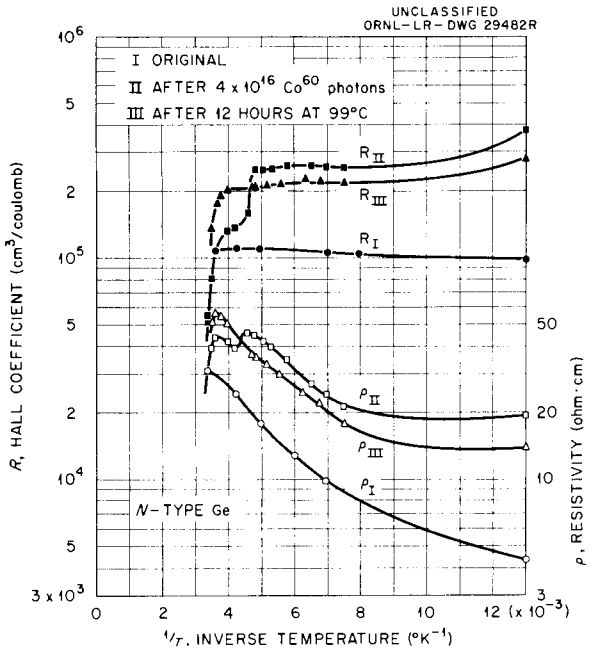

Fig. 7. Plot of Hall Coefficient, R, and Resistivity, ρ, vs Reciprocal Temperature for n-Type Germanium.

intrinsic n-type properties at temperatures down to the lowest at which electrical measurements could be made. A thermal anneal at ~373°K again removed a large number of the radiation-induced defects and returned the carrier concentration to about one-third of the original value.

The apparent role of the energy level tentatively located at ~0.2 ev below the conduction band is shown in greater detail in Fig. 7, where log R and log ρ have been separately plotted vs reciprocal temperature for another sample. Analysis of the carrier concentration changes of the two levels indicated (curve II) reveals that they are present in approximately equal concentration. Annealing at ~373°K (curve III) indicates almost total removal of the shallow state. Such behavior is very suggestive of preferential interstitial migration, since the energy level previously attributed[1,2] to the first ionization of the radiation-produced interstitial has been almost totally removed. Some total annealing also occurs; however, most of the conduction electrons previously released by ionization of the ~0.2-ev state above ~200°K before the anneal (curve II) are now trapped below approximately intrinsic temperatures by a deeper state (see below) after the anneal (curve III). Comparison of the data of Figs. 6 and 7 also reveals a marked variation between specimens in the amount of differential annealing, which is therefore assumed to be structure-sensitive.

Conversion of n-type germanium to p-type by photon irradiation is shown in Fig. 8, where log R is plotted vs reciprocal temperature. Only $\sim 2 \times 10^{16}$ photons were required to produce p-type material (curve III). Extensive irradiation (as much as 6×10^{18} photons) did not increase the effective hole concentration of any of several samples beyond the approximate amount indicated by curve IV of Fig. 8. In addition, the apparent acceptor-level position of this and other converted samples, after extended irradiation, did not indicate the introduction of any low-lying acceptor states of the type observed following conversion of n-type germanium to p-type by fast neutrons.[3]

Annealing effects at ~373°K following conversion to p-type and extended irradiation are also shown in Fig. 8. No evidence of defect removal is

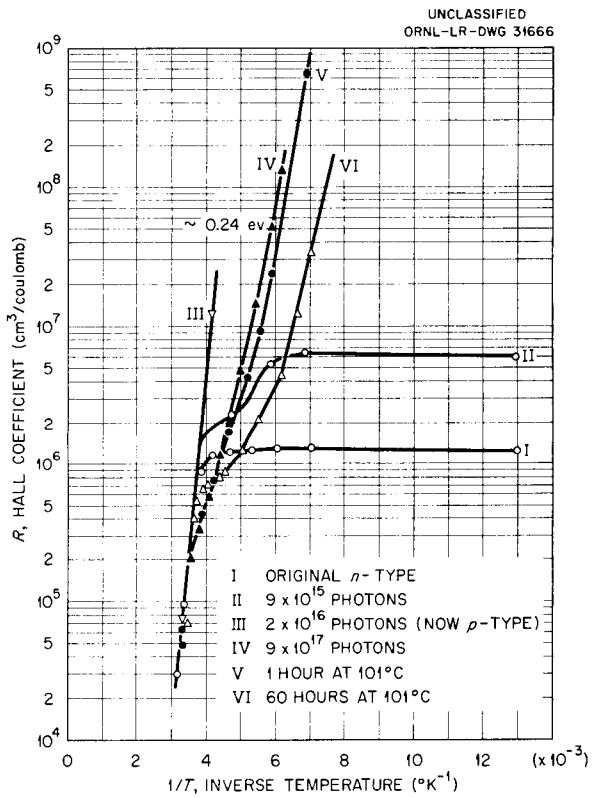

Fig. 8. Plot of Hall Coefficient, R, and Resistivity, ρ, vs Reciprocal Temperature for n-Type Germanium Converted to p-Type.

observed at this annealing temperature, and the position of the acceptor level is not appreciably altered. Extensive recombination of interstitials and vacancies would be expected to decrease the effective hole concentration, as would also any preferential migration of vacancies. Preferential migration of interstitials, however, would presumably enhance the acceptor efficiency of the lower-lying acceptor state that was predicted from the *n*-type results. Such migration would then account for the observed increase in hole concentration (curves V and VI), since compensation in this level would be decreased as the electrons originally associated with interstitials are removed.

Continued irradiation of the sample of Fig. 8, after conversion and extended anneal, actually decreased the apparent hole concentration back to about the region of curves IV and V. A second extended anneal then increased the apparent hole concentration to approximately that of curve VI. This cycle was repeated several times. The apparent acceptor level remained at ~0.24 ev during all such experiments. A previous statement[1] regarding a decrease in apparent acceptor-level position by annealing at approximately these temperatures following conversion was not verified and is now believed to be in error.

Several samples of initially *p*-type germanium of extremely high resistivity were also irradiated. Figure 9 shows the results for one sample, when log R and log ρ are plotted vs reciprocal temperature. The hole concentration increased upon exposure (curve II); however, the indicated increase is apparently a saturation value, since additional exposure produced no further increase (curve III). Annealing at ~373°K removed approximately half the hole concentration increase (curve IV) for this and other samples, after which successive irradiations and anneals merely oscillated the apparent hole concentration between the limiting (curve III) and annealed (curve IV) positions in a manner analogous to that for the converted specimen (Fig. 8).

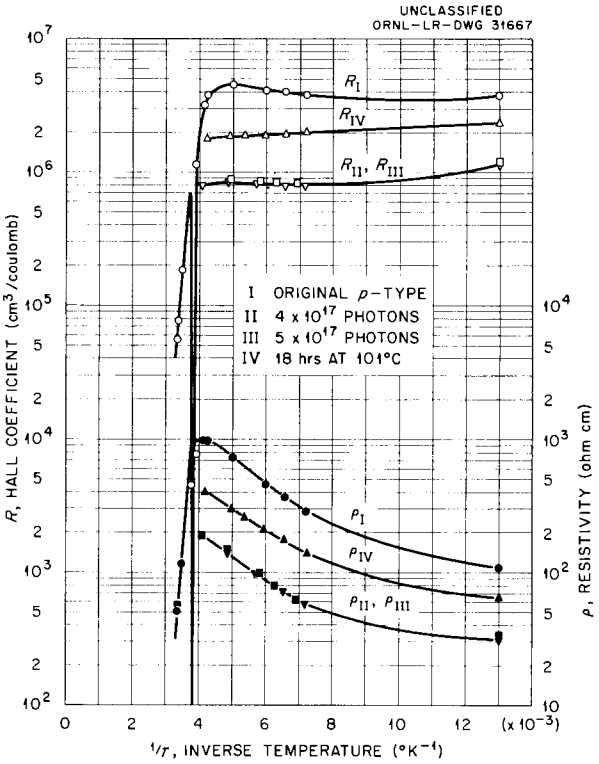

Fig. 9. Plot of Hall Coefficient, R, and Resistivity, ρ, vs Reciprocal Temperature for *p*-Type Germanium.

Discussion

The cross section per atom for displacement by a gamma ray may be calculated using the information summarized by Bethe and Ashkin.[4] If the displacement threshold energy for a lattice atom in germanium is taken as 25 ev, the displacement cross section is $\sim 1.23 \times 10^{-25}$ cm^2. This cross section is primarily (~95%) due to the energetic Compton electrons produced by the gamma rays.[5] A previous statement,[1] which assigned an equal contribution to photoelectrons, is in error. Photoelectric recoils of sufficient energy are negligible for gammas of this energy.

Experimentally, under the assumption that two electrons are removed per displaced atom, the cross section for the displacement of atoms by Co^{60} photons in germanium for these and previous[1] experiments is only $\sim 7.5 \times 10^{-27}$ cm^2. The large difference between this value and that calculated is presumably due to uncertainty regarding the displacement threshold energy, the amount of annealing during the irradiation, and the actual effectiveness of interstitials and vacancies as electron traps. Low-temperature irradiation experiments might aid in explaining the difference

[4] H. A. Bethe and J. Ashkin in *Experimental Nuclear Physics* (ed. by E. Segre), vol 1, p 166, Wiley, New York, 1953.

[5] D. O. Thompson and D. K. Holmes, *J. Phys. Chem. Solids* 1, 275–78 (1957).

between theory and experiment if the additional complication of minority-carrier trapping could be dealt with successfully.

Application of the model of James and Lark-Horovitz,[6] which suggested multiple ionization of irradiation-produced interstitials and vacancies, has been of benefit in previous studies. Because of the low energy of the Compton electrons (<1 Mev), only isolated interstitial-vacancy pairs are expected. Each such pair will, on the average, be many thousands of lattice spacings from the nearest neighboring pair.

The creation of an interstitial-vacancy pair by a Compton electron results in the removal of at least one electron, and more probably two, from the conduction band. Presumably, one state is sufficiently shallow (~0.2 ev below the conduction band) that it empties above ~250°K. The lower state (~0.26 ev above the filled band) is effective at all temperatures. Annealing that recombined such pairs would then release electrons to the conduction band. Preferential migration of the interstitial atom to dislocations or clusters, however, would make the more effective lower state available for interstitial-electron removal in *n*-type specimens. Therefore, interstitial removal during anneals at moderate temperature (100°C) effectively replaces the 0.2-ev state by a much deeper level.

Conversion to *p*-type material essentially eliminates the role of the upper level, since the Fermi ζ level is below the middle of the gap. The limiting position of the ζ level is evidently ~0.26 ev above the valence band. For high-resistivity *p*-type material, interstitial migration increases the acceptor efficiency of the ~0.26-ev level somewhat by decreasing compensation in this level; and reirradiation serves to raise the ζ level slightly. For low- and medium-resistivity *p*-type material, the acceptor states introduced are well above the ζ position. Hence the effect of irradiation is almost negligible. The saturation of hole concentration change in both converted samples and samples initially *p*-type is not yet understood.

[6] H. M. James and K. Lark-Horovitz, *Z. physik. Chem. (Leipzig)* 198, 107 (1951).

ANNEALING STUDIES OF IRRADIATED GERMANIUM

J. C. Pigg

The instrument reported previously[1] has been utilized to follow the annealing behavior in several neutron-irradiated germanium samples. The results of one such experiment are shown in Fig. 10.

The concentration and mobility obtained from the Hall coefficient and the resistivity are shown as a function of annealing time. The annealing temperatures are indicated. The measurements were made at the indicated times after the sample had returned to liquid nitrogen temperature.

The expected annealing peaks[2] at 135 and 165°K do not appear. In order to account for the possibility of loss of this detail during anneal, the experiment was repeated taking Hall and resistivity measurements at liquid nitrogen temperature after hourly pulses (Fig. 11). Although some structure is clearly evident, it is not of the type expected. A scatter in the data is also noted that is greater than the range of error expected from the sensitivity of the instrument.

The data scatter in both experiments can be understood on the basis of photoconductive modulation resulting from variations in light intensity in the room; for example, readings taken during the day showed higher conductivity than those taken at night even though no annealing pulse intervened. Subsequent experiments will be shielded from light variations as much as is practicable.

[1] J. C. Pigg, *Solid State Ann. Prog. Rep. Aug. 31, 1957*, ORNL-2413, p 34–35.

[2] J. W. Cleland, J. H. Crawford, Jr., and J. C. Pigg, *Solid State Semiann. Prog. Rep. Feb. 28, 1955*, ORNL-1852, p 15–17.

Sample 5-1-4-13 was subjected to anneals of length indicated by the points in Fig. 10. Sample EP3-B received 1-hr pulses, although the points are not plotted every hour. It does not appear that failure to observe the expected structure was due to length of pulse. The experiments in which the low-temperature structure was found were performed in an intense gamma field in the reactor, and the annealing was conducted immediately without time for radioactive decay in the germanium. The experiments reported here were performed outside the reactor; the samples had been stored at liquid nitrogen temperature to permit decay in the germanium.

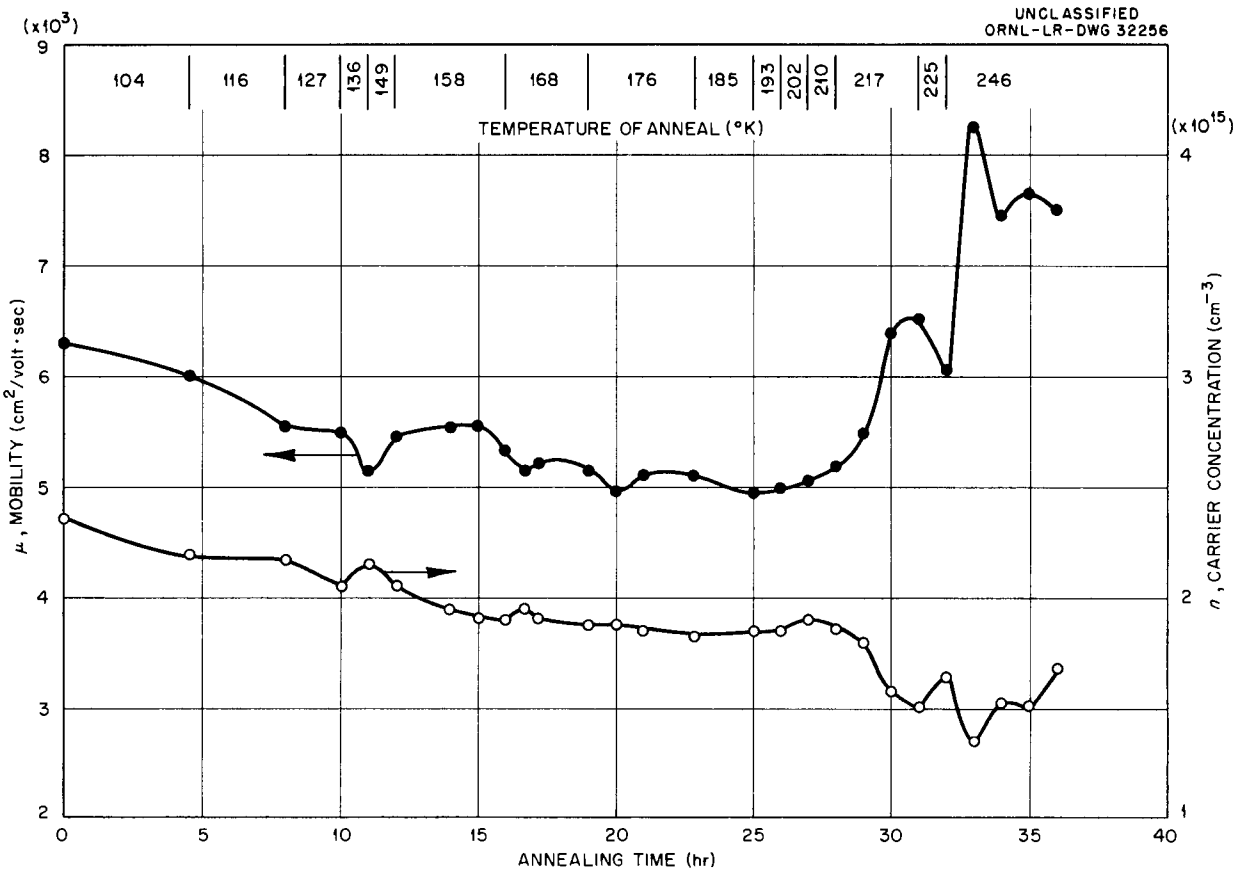

Fig. 10. Annealing of Germanium After Reactor Irradiation at 77°K (Long Annealing Pulse).

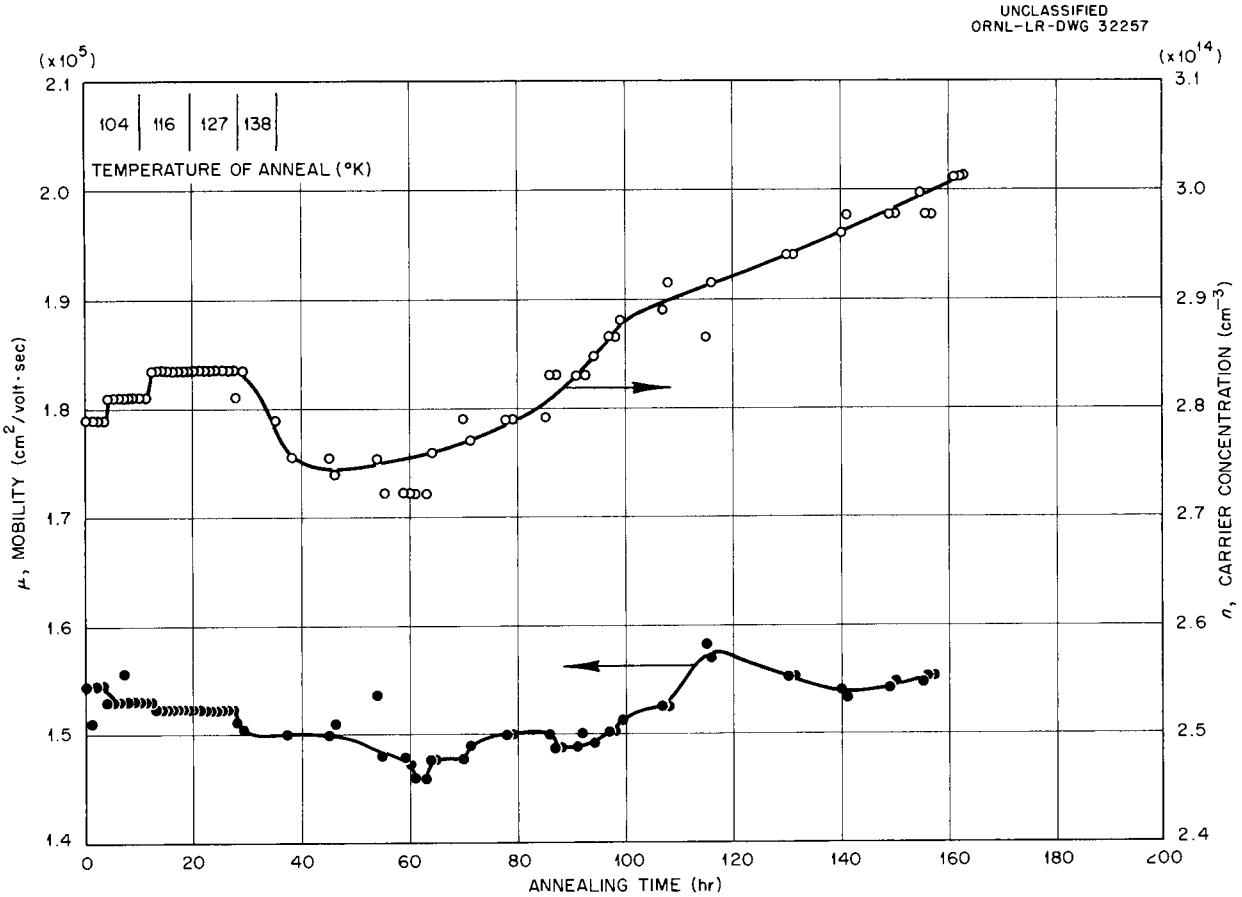

Fig. 11. Annealing of Germanium After Reactor Irradiation at 77°K (1-hr Pulses).

ELECTRON MICROSCOPE STUDIES

T. S. Noggle J. O. Stiegler

An investigation of the etching characteristics of irradiated germanium has recently been initiated. This work is an extension of work carried out by R. Chang which has been reported in the literature.[1] This earlier work established that a fine, dotlike structure was present on the (111) face after etching in the standard CP-4 etchant[2] and that subsequent annealing eliminated this behavior. In that this surface structure apparently arises from radiation effects in the germanium, it is of interest to use electron microscope and electron diffraction techniques to more clearly define and identify this structure and its relation to radiation effects in the material.

Chang[1] noted that the etching characteristics of germanium single crystals gave rise to network structures of three different orders of magnitude as shown in Fig. 12. The so-called first-order structure appears as heavy horizontal and vertical lines in the micrograph; it has an average diameter of 100 μ. A smaller second-order network having an average diameter of the order of 10 μ is clearly

[1] R. Chang, *J. Appl. Phy.* 28, 385–87 (1957).

[2] 50 ml HNO_3, 30 ml CH_3COOH, 30 ml HF, 0.6 ml liquid bromine.

visible within the first-order structure. The third-order structure of approximately 0.5 μ diameter is shown as faint dots within the second-order net. These structures are only observed when the surface under examination lies within a few degrees of a (111) orientation. The standard CP-4 etchant with or without liquid bromine brings out the conical etch pits and the first-order network. This same etchant will also reveal a third-order structure on irradiated crystals, while CP-4 heavily enriched in liquid bromine is necessary to delineate the second- and third-order networks on unirradiated crystals.

Preliminary observations on the etching behavior of germanium have shown that the first-order structure mentioned by Chang can be readily reproduced, but is associated with specimen preparation techniques. Slight changes in preliminary surface grinding or etching times lead to large variations in this structure. The coarse "cobblestone" appearance of the first-order structure is aligned in the direction of grinding as shown in Fig. 13, in which two adjoining regions were ground in perpendicular directions, then etched in CP-4. Figures 14 and 15 illustrate changes observed in the "cobblestone" pattern with increased etching time. The initially fine network coarsens and is eliminated entirely after a sufficiently long etching period. Electron microscope examination of these structures leads to the conclusion that the first-order network marks the boundary between plateaus of slightly different elevations. This boundary is not abrupt but a rather gradual transition from one level to the other and devoid of any fine structure peculiar to this boundary region.

The nature and origin of the second-order structure are less certain. This structure is readily produced only in the bromine-enriched etchant, and is not sufficiently reproducible that definite conclusions about it can be made. Apparently it is of the same general nature as the first-order structure, that is, small elevation differences within the first-order plateaus; but the etchant that displays this structure leaves the surface so roughened that electron microscope observations fail to identify topographical features which could unambiguously be attributed to this structure.

The studies on irradiated germanium have been made on 5-ohm-cm p-type germanium crystals irradiated to 10^{17} and 10^{18} nvt. These specimens were cut within half a degree of a (111) face. Prior to irradiation the specimens were etched in

Fig. 12. Unirradiated p-Type Germanium, (111) Face. Bromine-enriched CP-4 etch. 500X.

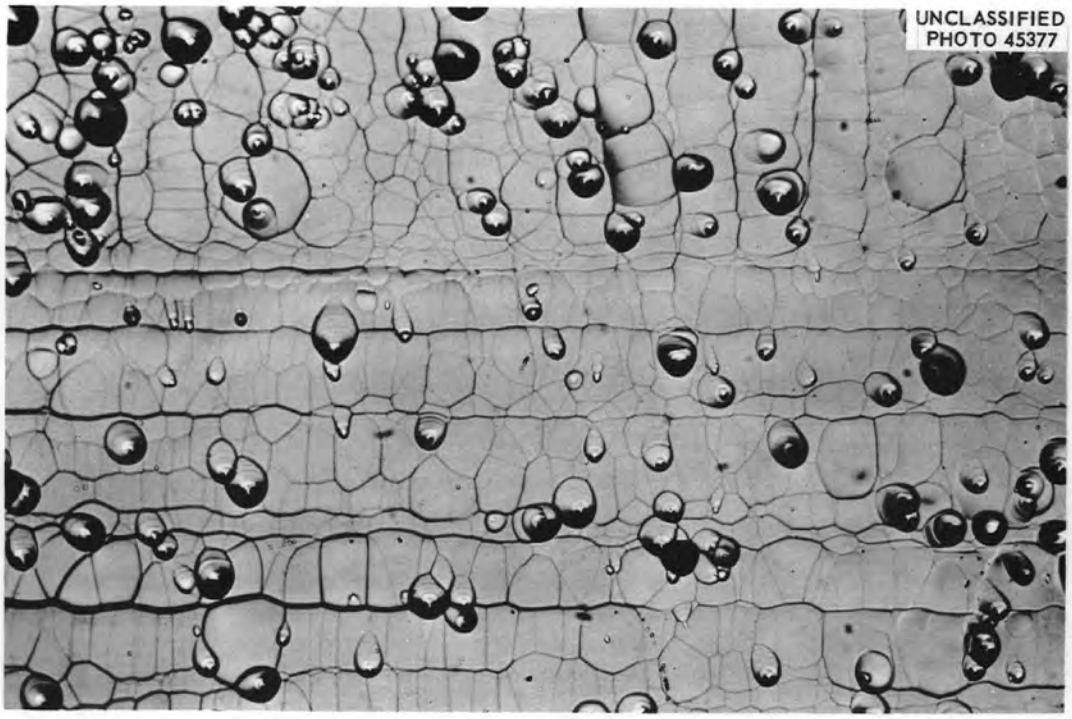

Fig. 13. Unirradiated *p*-Type Germanium, (111) Face. CP-4 etch. 100X.

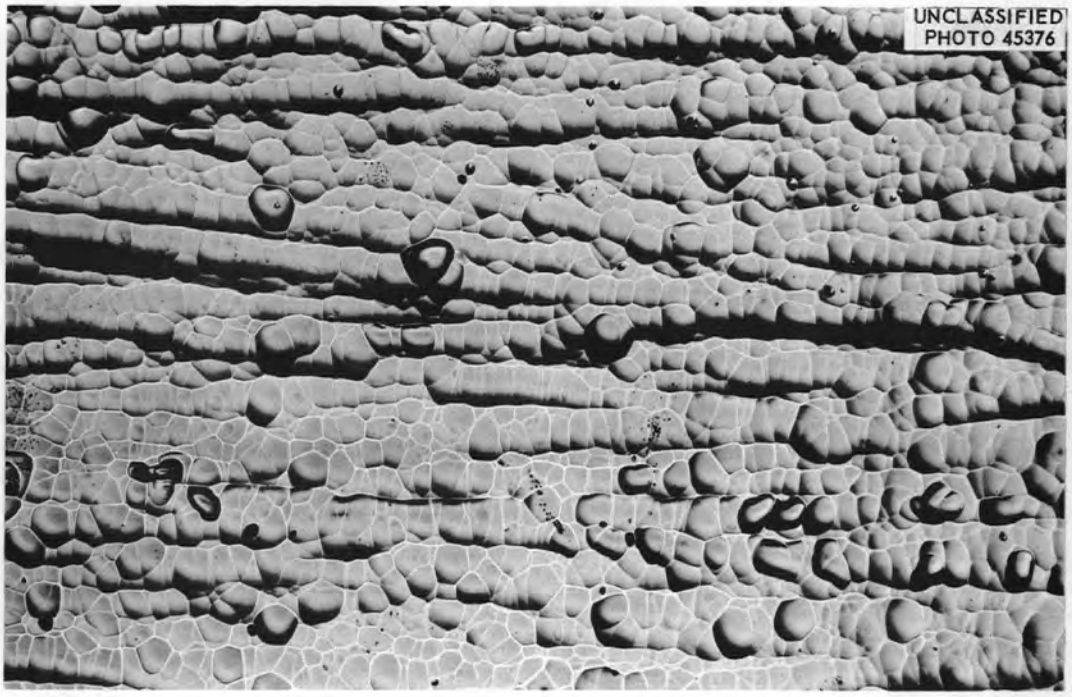

Fig. 14. Unirradiated *p*-Type Germanium, (111) Face. CP-4 etch, 2 min. 100X.

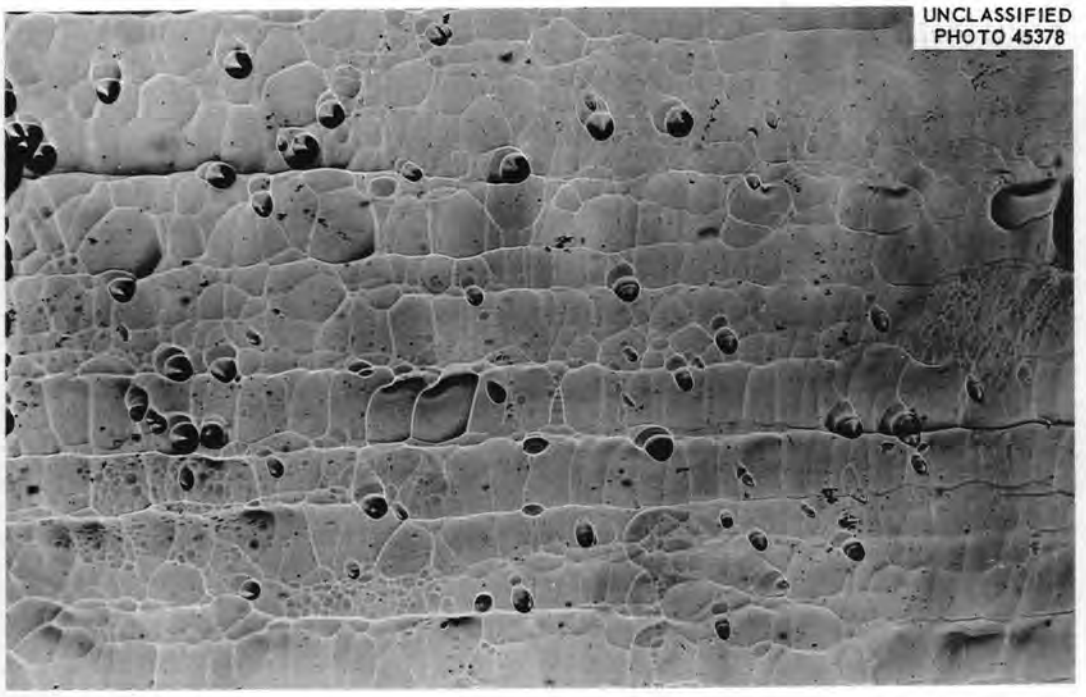

Fig. 15. Unirradiated *p*-Type Germanium, (111) Face. CP-4 etch, 4 min. 100X.

CP-4 until only conical etch pits were visible on the surface.

After irradiation and subsequent to etching in bromine-free CP-4, the specimens show the third-order dotlike structure. The irradiated specimens show an extended period in which the etching rate is quite slow with very slight gas evolution, followed by the normal etching behavior in which copious amounts of gas are evolved. This abnormal behavior has been observed to last as long as 30 min. During this period material is removed from the surface at relatively slow rates, and observations of the surface show only a washed-out appearance in which neither pits nor fine structure is clearly defined.

Reflection electron diffraction patterns from the as-irradiated specimens show only the single-crystal spots and intense Kikuchi lines, unchanged from the unirradiated material. Subsequent to etching in bromine-free CP-4, the patterns from the irradiated material show a polycrystalline component as indicated by the rings in Fig. 16. The diffraction rings observed do not relate definitely to any known germanium compound and most nearly fit the indexing for germanium. However, small differences in the apparent d spacings are present which make this identification uncertain at the present time. Diffraction patterns from specimens removed from the etchant during the abnormal-etching period show several diffuse rings which do not lie near the sharp rings observed after normal etching sets in. Figure 17 shows a typical pattern obtained under these conditions. Electron microscope examination of the surfaces of the irradiated specimens showing normal etching behavior has shown a distinct structure which has not been observed on the other materials similarly etched. Figure 18 illustrates the type of structure observed in which discrete patches several microns in length lying a few hundred angstroms below the general surface level are visible. The texture of the surface within the patches appears smoother than that outside and appears to be the same as that observed on unirradiated specimens. This structure is associated with the breaking up or dissolution of a surface film. Figure 19 shows an isolated case in which a portion of this film is folded upon itself.[3] The

[3] This figure unambiguously demonstrates that a coherent surface film was present on this specimen. The replica technique employed involves preshadowing with a gold-chromium alloy, then carbon replication. The carbon replica thus serves only as a carrier for the contrast-forming shadowing material, and the observed structure could not occur from any artifact in the replica, such as, for example, folding of the replica during processing.

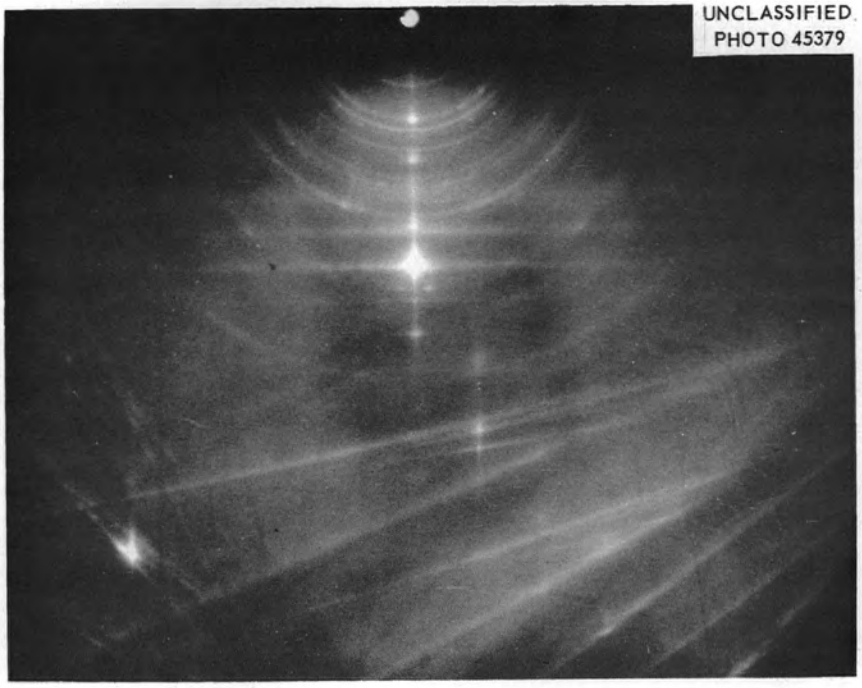

Fig. 16. Reflection Electron Diffraction Pattern from (111) Face of Irradiated Germanium After Normal Etch.

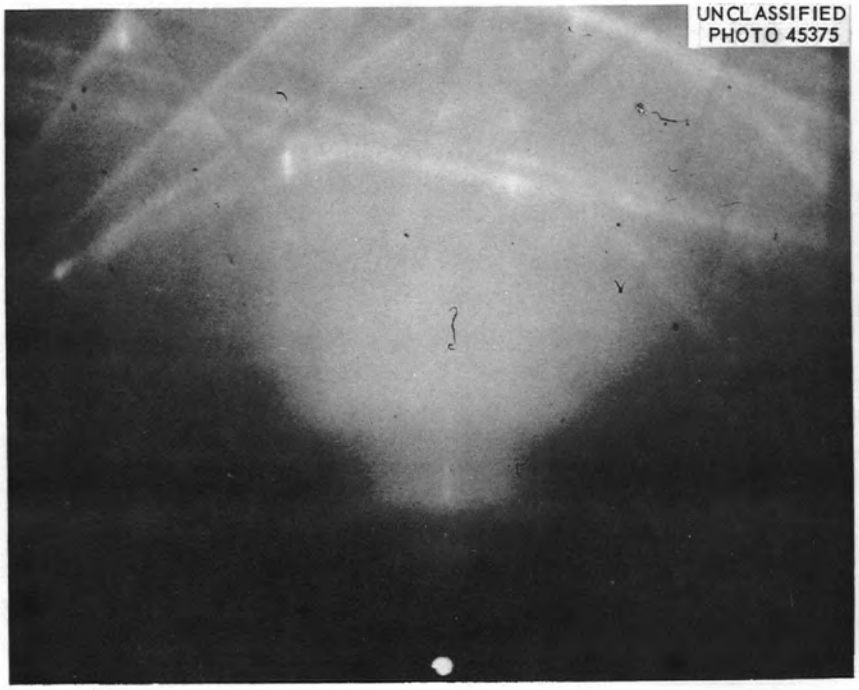

Fig. 17. Reflection Electron Diffraction Pattern from (111) Face of Irradiated Germanium After Abnormal Etch.

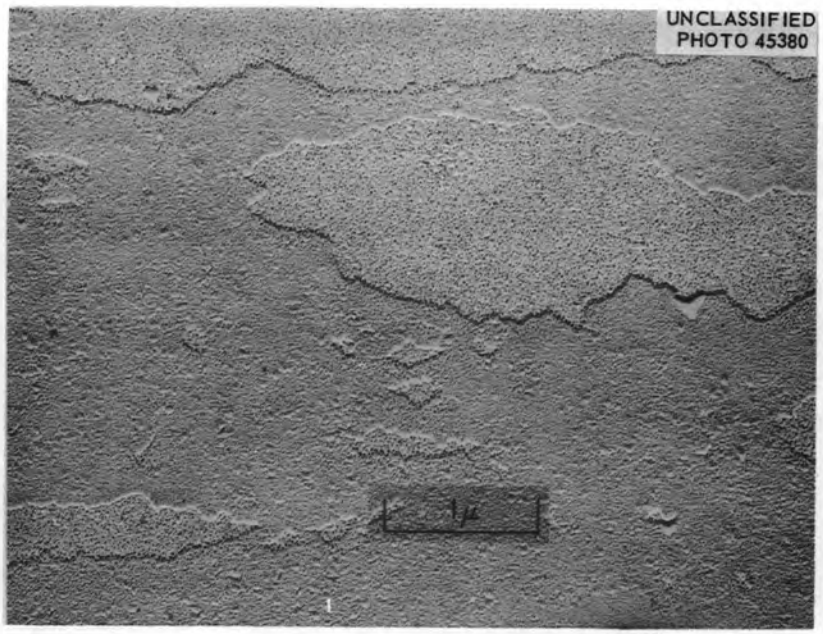

Fig. 18. p-Type Germanium, Irradiated to $\sim 10^{17}$ nvt, (111) Face. Bromine-free CP-4 etch, shadowed with AuCr at $\theta = \tan^{-1} \frac{1}{5}$. 20,000X.

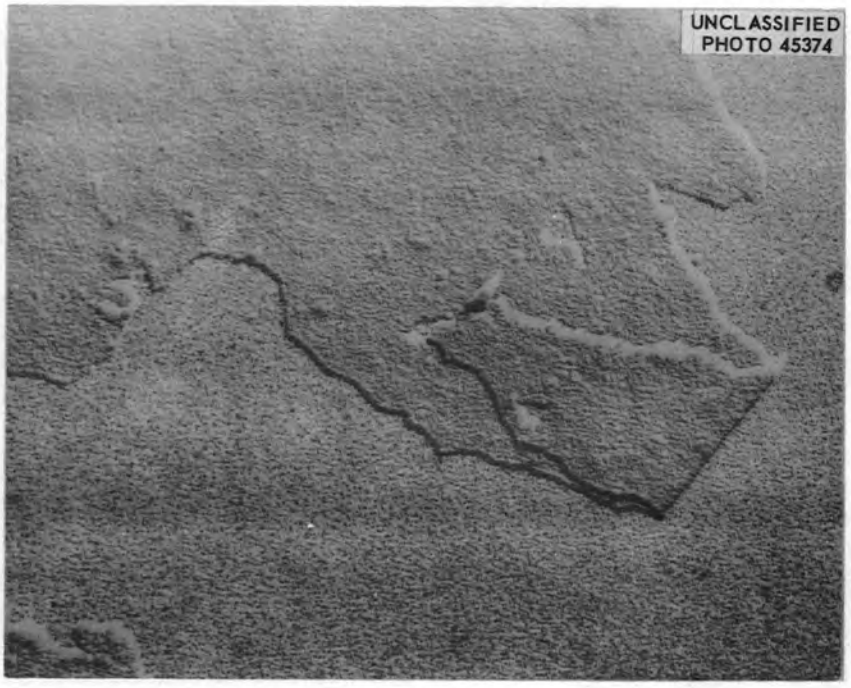

Fig. 19. Same Surface as in Fig. 18. 40,000X.

general size of the patches is approximately that of the third-order structure observed with the optical microscope on this material, but further work to establish a one-to-one correspondence between the two is necessary. Efforts are being made to strip this film for study in the electron microscope.

The results of this investigation to date suggest that irradiation of germanium with pile neutrons changes the chemical reactivity of the surface, leading to the formation of a film on the surface upon initial exposure to the etching reagent, and that this film is subsequently dissolved by the etchant. The third-order structure then may reflect the pattern of breaking-up of this surface film. Future work is planned to study the abnormal etching behavior in greater detail and extend all types of observations to more highly irradiated specimens, different crystallographic faces, and germanium of various purities.

Other electron microscope work in progress will not be reported in detail, but the nature of some of the work will be outlined.

Preparation of evaporated films of gold oriented to (111) and (100) orientations has been carried out. These films are basically of the orientations noted, but show profuse twinning. Attempts are now being made to eliminate or substantially reduce the amount of twinning present in these films so that the intended studies on radiation effects may be carried out.

Tensile specimens of copper have been prepared for the study of the effect of neutron irradiation on the surface structures developed by plastic deformation.

A vacuum evaporation unit suitable for remote operation in the hot cells is nearly completed. Remote techniques for the removal of carbon replicas from metallographic specimens have been developed and will be applied to radioactive specimens when the construction of the vacuum evaporation unit is finished.

MAGNETIC SUSCEPTIBILITY OF UNIRRADIATED AND NEUTRON-IRRADIATED *n*-TYPE SILICON

E. Sonder

The analysis of the magnetic properties of unirradiated *n*-type silicon has been completed and published. An abstract of the paper appears below:

Magnetic Properties of *n*-Type Silicon.[1] E. Sonder and D. K. Stevens. – The magnetic susceptibility of *n*-type silicon samples with a wide range of donor concentrations (3×10^{16} to 3×10^{19} atoms/cm^3) has been measured as a function of temperature from 3°K to 300°K. By utilizing conduction-electron concentrations obtained from Hall coefficient measurements on comparison specimens over the range from 50°K to 400°K, the contributions to the susceptibility arising from the conduction electrons and electrons trapped on donor atoms have been analyzed. In the upper range of temperature the diamagnetic contribution of conduction electrons is dominant and is consistent with the model of six energy minima in the conduction band. However, comparison of the squared reciprocal mass ratio with that obtained from cyclotron-resonance experiments reveals that the former is appreciably smaller than the latter (~8 as compared to ~13). As the temperature is lowered, the conduction-electron contribution at low temperatures leads to a Curie-law paramagnetism in the specimens of higher purity, whereas in the more impure samples, deviations from Curie's law occur which are attributed to interactions between closely spaced donor centers.

It has been shown[2,3] that neutron irradiation of silicon introduces deep-lying traps, which remove conduction electrons at temperatures as high as room temperature. In order to try to understand the nature of the radiation-induced centers it is useful to probe their magnetic as well as their electrical properties. Irradiations are being made

[1] E. Sonder and D. K. Stevens, *Phys. Rev.* 110, 1027 (1958).

[2] J. H. Crawford, Jr., and J. W. Cleland, *Progress in Semiconductors* (ed. by A. F. Gibson, R. E. Burgess, and P. Aigrain), vol 2, p 67, Heywood, London, 1957.

[3] G. K. Wertheim, *Phys. Rev.* (to be published).

of n-type silicon susceptibility cubes and companion Hall plates. In an exploratory investigation a few years ago[4] three samples (one n-type, one p-type, and one intrinsic) were irradiated and their susceptibility between liquid nitrogen and room temperatures was determined. In the case of the n-type sample a disappearance of the conduction-electron diamagnetism and an appearance of a paramagnetic component in the liquid nitrogen temperature range were observed.

The present measurements have been extended to liquid helium temperatures, and an attempt is being made to see how the radiation effects vary with neutron dosage. Some early results are reproduced in Fig. 20, where the diamagnetic susceptibility of a 0.03-ohm-cm (carrier concentration of 6×10^{17} arsenic atoms per cubic centimeter) sample of silicon is plotted as a function of temperature. Data are shown for the unirradiated sample as well as for the specimen after two exposures to fast neutrons. The surprising and most interesting thing about the results is that the paramagnetic contribution in the liquid helium range seems, at first, to decrease and then to increase with neutron dosage. This is shown more clearly in Fig. 21, where the susceptibility component that can be attributed to all traps, including donors, is plotted vs inverse temperature. The slopes of the curves give 6.6×10^{17} magnetic centers for the unirradiated sample, 1.4×10^{17} centers for an irradiation of 1.1×10^{17} nvt, and 2.1×10^{17} magnetic centers for a dose of 2.1×10^{17} nvt.

A decrease of the number of centers is consistent with the idea that electrons leave donor centers and go into deeper, irradiation-induced traps, if in these traps the electrons lose their spin paramagnetism. However, since upon longer irradiation the number of magnetic centers increases again, it would seem that a more complicated situation exists. At least two types of levels must be invoked to explain the results. For further, more quantitative analyses, more data are necessary. It might be noted that the increase of paramagnetism at high irradiation doses is in agreement with the results found in the past.[4]

[4] D. K. Stevens *et al.*, *Solid State Semiann. Prog. Rep. Aug. 30, 1956*, ORNL-2188, p 11.

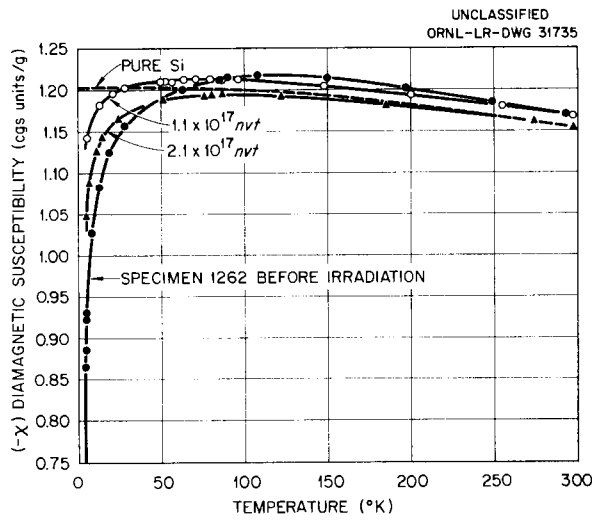

Fig. 20. Magnetic Susceptibility of Neutron-Irradiated n-Type Silicon.

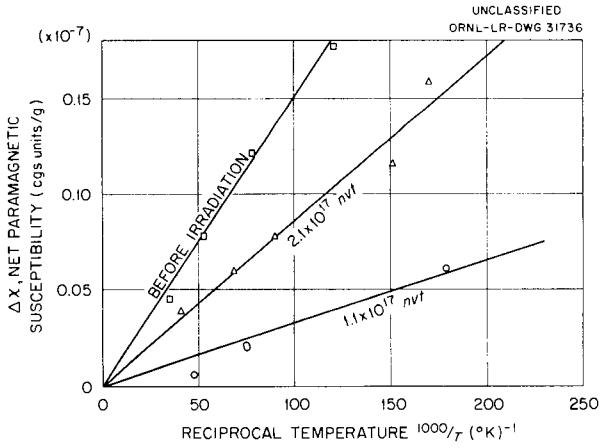

Fig. 21. Magnetism of Donor and Trapping Centers as a Function of Reciprocal Temperature for n-Type Silicon.

MAGNETIC SUSCEPTIBILITY OF MANGANESE SESQUIOXIDE

E. Sonder

In order to facilitate interpretation of neutron spectroscopy data obtained by other members of the Laboratory,[1] a determination of the magnetic susceptibility of Mn_2O_3 was desirable. The neutron scattering which had been observed could be explained by assuming that an ordered magnetic structure existed below about 88°K. Furthermore, it was known from heat capacity data[2] that a second-order phase change occurred at 79°K. The nature of the ordered phase was not known conclusively but could be obtained simply from the magnetic susceptibility. Therefore a sample of Mn_2O_3 powder was measured between 50°K and room temperature. Figure 22 shows the results. The break of the curve occurs at 79°K, in good agreement with the specific heat measurements.[2]

The decrease of paramagnetism below that temperature shows clearly that the material is antiferromagnetic in that range.

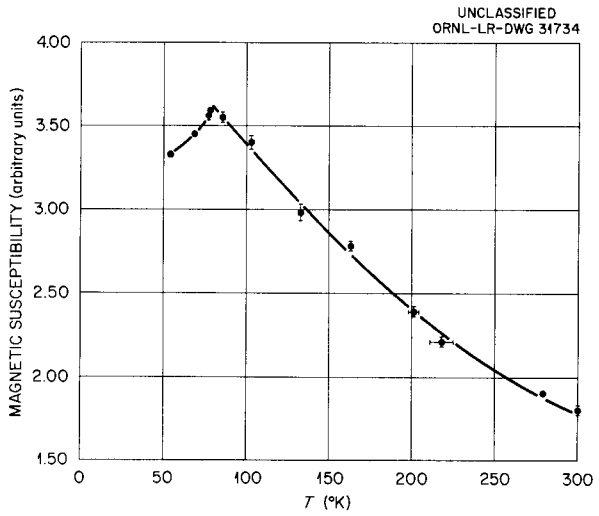

Fig. 22. Magnetic Susceptibility of Manganese Sesquioxide.

[1] J. W. Cable *et al.*, *Phys. Semiann. Prog. Rep. March 10, 1957*, ORNL-2302, p 43.

[2] E. G. King, *J. Am. Chem. Soc.* **76**, 3289 (1954).

GAMMA IRRADIATION OF *n*-TYPE SILICON

E. Sonder L. C. Templeton

Analysis of particle-irradiation effects in solids is often complicated by the fact that the damage may be nonuniform and of a very complicated nature. A first step in understanding such processes involves obtaining a simple type of damage. This may be partially accomplished by using electrons or gamma rays of not too high an energy (about 1 Mev) which will produce a preponderance of uniformly distributed vacancy-interstitial pairs. This approach is being used for silicon. Samples are being irradiated at room temperature with Co^{60} gamma rays from a source[1] capable of producing about 10^{12} gammas·cm^{-2}·sec^{-1}.

Some preliminary results are shown in Fig. 23, where the Hall coefficient of an originally 12-ohm-cm phosphorus-doped silicon sample is plotted vs reciprocal temperature. In the range above 150°K, where most of the donor sites are empty, the change in the number of conduction electrons with irradiation reflects the introduction of deep traps. From the data, an introduction rate of the traps can be calculated. It turns out to be 1.1×10^{-3} trapping level per gamma ray per centimeter.

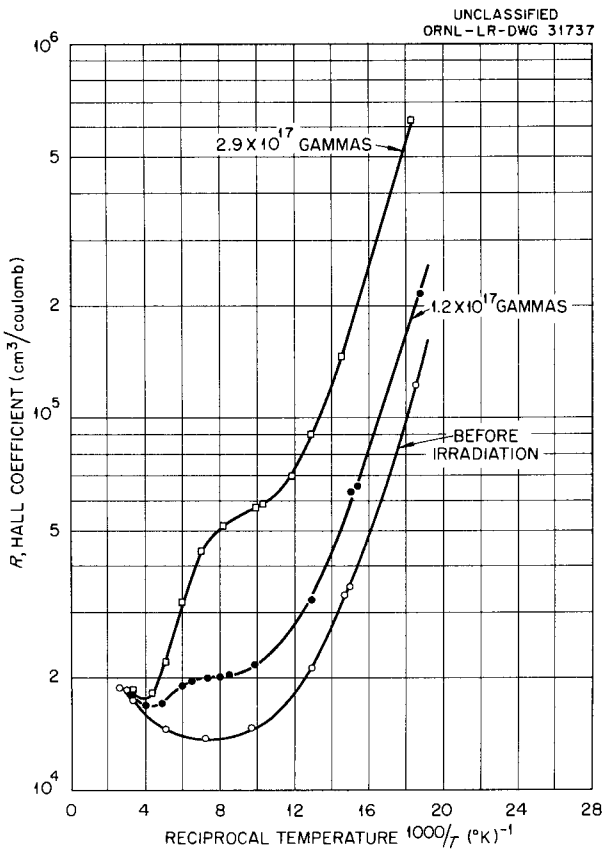

Fig. 23. Plot of Hall Coefficient vs Reciprocal Temperature for *n*-Type Silicon.

[1] J. W. Cleland, *Solid State Ann. Prog. Rep. Aug. 31, 1957*, ORNL-2413, p 73.

RADIATION EFFECTS IN INDIUM ARSENIDE

J. W. Cleland J. H. Crawford, Jr.

The semiconducting intermetallic compound indium arsenide, InAs, is of considerable interest because of its large electron mobility, 25,000 cm^2·v^{-1}·sec^{-1} at room temperature. *n*-Type large-grain-size polycrystalline specimens with extrinsic electron concentrations of $\sim 5 \times 10^{16}$ and $\sim 2 \times 10^{17}$ cm^{-3} and *p*-type large-grain-size polycrystalline specimens with an extrinsic hole concentration of $\sim 3 \times 10^{17}$ cm^{-3} were supplied by personnel of the Naval Ordnance Laboratory. Hall-coefficient plates were fashioned by diamond-saw cutting, and copper leads were soft-soldered using tin. Fast-neutron irradiations were conducted in a water-cooled fission-chamber facility of the ORNL Graphite Reactor at about 30°C. The samples were shielded with indium and cadmium foil to reduce the incident flux of thermal and resonance neutrons that would produce transmutation to donor-type elements.

Figure 24 shows the conductivity of *n*- and *p*-type samples as a function of fast-neutron irradiation. The increase in *n*-type conductivity was not expected but has also been observed at Battelle Memorial Institute using fast neutrons and at

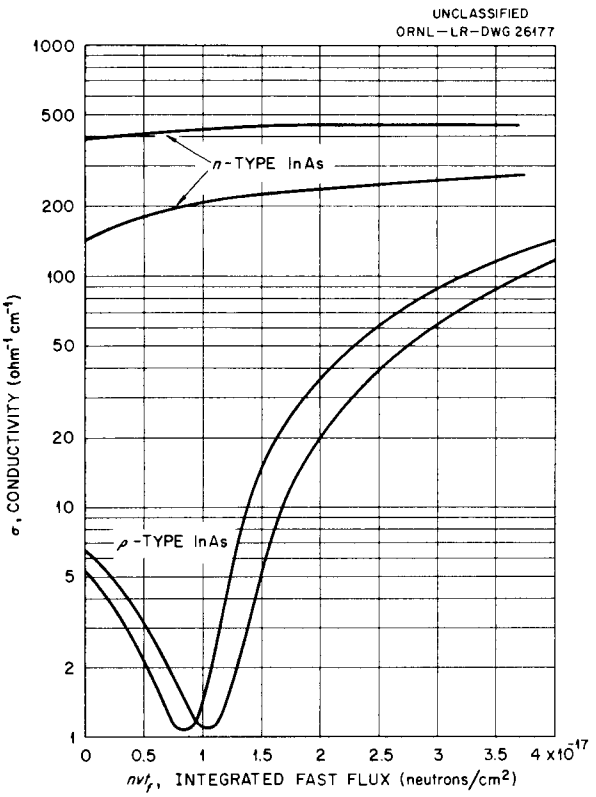

Fig. 24. Conductivity of Indium Arsenide vs Integrated Fast Neutron Flux.

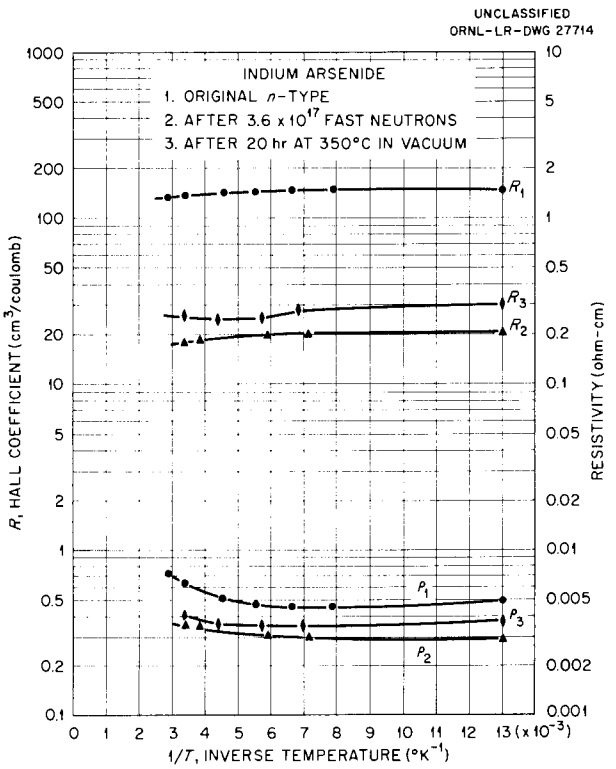

Fig. 25. Plot of Hall Coefficient, R, and Resistivity, ρ, vs Reciprocal Temperature for n-Type Indium Arsenide.

Purdue University using 4.5-Mev electrons at 77°K. The conductivity of p-type reaches a minimum value which is somewhat greater than the intrinsic value expected for the temperature of irradiation. Continued irradiation increased the conductivity to approximately the same value as that attained by the n-type samples.

Figure 25 shows the Hall coefficient and resistivity of n-type material as a function of inverse temperature. The addition rate of conduction electrons was approximately one per incident fast neutron for several samples for a total integrated fast flux of from 2 to 4×10^{17} neutrons/cm^2. A considerable decrease in mobility is also evident. A 20-hr anneal at 101°C after irradiation resulted in the removal of less than 2% of the carriers added by irradiation. A further anneal in vacuum for 20 hr at 350°C resulted in the removal of only about 25% of the carriers added by irradiation. This result also was not expected.

Figure 26 shows the Hall coefficient and resistivity of p-type material as a function of inverse temperature. The total addition rate of electrons was again approximately one per incident fast neutron for several samples for a total integrated fast flux of about 4×10^{17}. The sample was converted to n-type after the conductivity minimum indicated in Fig. 24. Annealing for 20 hr at 101°C again produced little change; however, 20 hr at 350°C returned the sample to p-type and to approximately the original condition. Transmutation effects would be expected to decrease the final hole concentration somewhat. However, the total thermal-neutron leakage through the cadmium-indium shield was measured in indium antimonide, InSb, as only ~6% under similar experimental conditions.[1] The net result, therefore, is that a major portion of the electron increase in p-type material can be thermally annealed; however, only about 25% of the electron increase in n-type material can be thermally annealed at 350°C.

[1] J. W. Cleland and J. H. Crawford, Jr., *Phys. Rev.* 95, 1177 (1954).

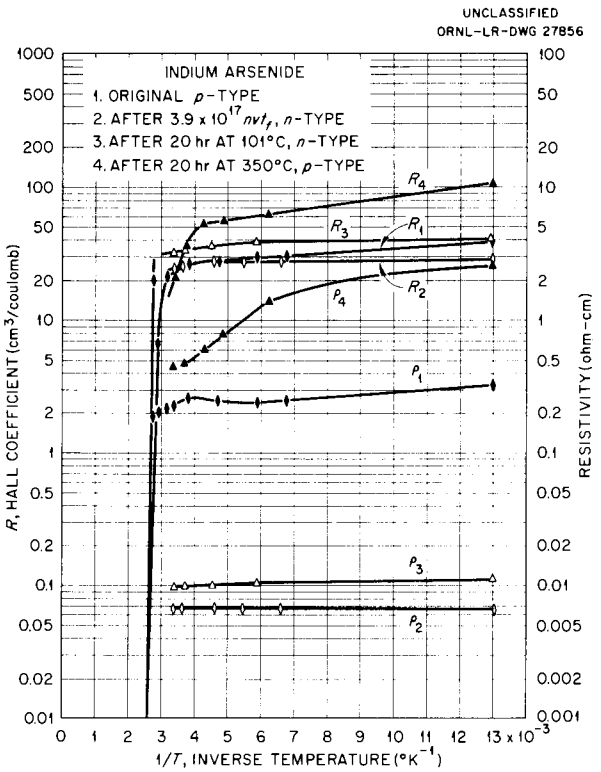

Fig. 26. Plot of Hall Coefficient, R, and Resistivity, ρ, vs Reciprocal Temperature for p-Type Indium Arsenide.

Folberth and Weiss[2] have reported measurements on an originally n-type specimen containing 3×10^{16} electrons/cm^3 to which they added varying quantities of zinc. Polycrystalline Hall plates with $\sim 2 \times 10^{17}$ zinc atoms added exhibited a normal p-type behavior quite similar to curve 1 of Fig. 26. Decreasing the added zinc concentration, however, produced a double reversal of Hall coefficient sign. The lower-temperature reversal occurred at about $-100°$C for a sample with about 1×10^{17} zinc atoms. The Hall curve was negative and independent of temperature below this reversal. The higher-temperature reversal occurred around room temperature. A further decrease in added zinc concentration finally converted the sample to n-type; however, there was still a large dip in the Hall coefficient value in the vicinity of room temperature.

Fast-neutron irradiation of p-type InAs essentially duplicates the results obtained by Folberth and Weiss using varying quantities of zinc. Figure 27 shows the Hall coefficient of a p-type specimen as a function of inverse temperature. About 5×10^{16} fast neutrons produced a double minimum, and the higher-temperature n-type dip after about 6×10^{16} fast neutrons is quite similar to that in the data of Folberth and Weiss for a sample with 3×10^{16} donors and 5×10^{16} added zinc atoms.

Dixon and Enright[3] have duplicated the low-temperature double reversal in p-type InAs by zinc addition, and have then eliminated it by certain annealing experiments. An originally p-type specimen, held at 850°C for 280 hr and then quenched, was converted to n-type material.

[2] O. G. Folberth and H. Weiss, *Z. Naturforsch.* 11a, 510 (1956).

[3] J. R. Dixon and D. P. Enright, *Effect of Heat Treatment on the Electrical Properties of Indium Arsenide*, U.S. Naval Ordnance Laboratory, White Oak, Md. (to be published).

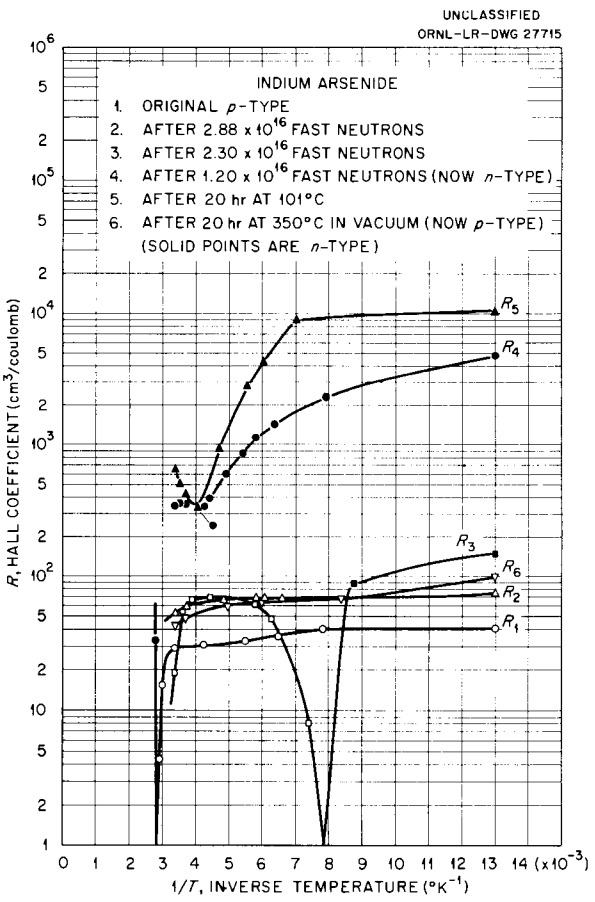

Fig. 27. Plot of Hall Coefficient vs Reciprocal Temperature for p-Type Indium Arsenide.

Additional annealing for 400 hr at 100°C restored the specimen to *p*-type. They propose a mechanism of segregation and dispersion of donor impurities to and from dislocations or grain boundaries to account for the presence or absence of the low-temperature reversal.

The equivalence of irradiation effects and heat-treatment effects in InAs is of interest. However, the irradiation data are not yet sufficient to permit the formulation of a model for this material. Additional experiments, including low-temperature irradiation of single-crystal samples, should permit an analysis of the type of irradiation defect responsible for the addition of extremely shallow *n*-type donors to *n*-type material, an effect which incidentally has not been observed in any other semiconductors. The difference in annealing behavior between irradiated *n*- and *p*-type material and the double reversal at low temperature might also be understood if the annealing results of Dixon and Enright were correlated with irradiation results on similarly annealed samples.

OPTICAL ABSORPTION STUDIES OF IRRADIATED SOLIDS

C. M. Nelson R. E. Lide[1] W. J. Pegram[2]

The general effects of fast-neutron and Co^{60} gamma irradiation on both crystalline and vitreous silica have been observed and reported.[3] During the past year some of these experiments have been continued and other experiments have been performed to elucidate the nature of the defects which give rise to optical absorption. A separate report has been written discussing the evidence for correlation between the prominent ultraviolet absorption band (the 2150-Å or *C* band) and the group of narrow spin resonance lines ($g = 2.0010$).

Another comprehensive series of neutron bombardments is being completed and will cover a range from 10^{17} to 3×10^{20} fast neutrons/cm^2. The materials bombarded include: crystalline quartz (both with *c* axis perpendicular to face and with *c* axis parallel to face) – General Electric Ltd. synthetic, Bell synthetic, and Thermionic natural; vitreous quartz – Corning No. 7940, Corning No. 7943 (waterless), General Electric type III, Amersil O.G. 1, and Ultrasil. The measurements and discussion of the results will probably be published as soon as they are completed.

In order to see if all the defects were filled following fast-neutron bombardments, three crystalline quartz samples which had been bombarded with 10^{17}, 10^{18}, and 10^{19} fast neutrons/cm^2 were gamma-irradiated. These samples were exposed seven times, to a total of 5×10^7 r, with no additional coloration for any of the samples except perhaps a 3% increase for the 10^{19} sample. This increase may not be significant.

A low-temperature (–110°C) fast-neutron bombardment (1.2×10^{17} fast neutrons/cm^2) was made in order to see if the temperature of bombardment would have an effect on the coloration. There are indications of the *C* band being present in the crystalline quartz samples, but the far-ultraviolet is the most prominent absorption. In the case of the vitreous quartz samples, the shape of the absorption curve is different from that produced by the usual 60°C bombardments. The far-ultraviolet absorption now is more prominent and another band near 2400 Å becomes noticeable (see Fig. 32).

Samples of crystalline quartz from different sources (natural, Bell synthetic, and G.E. Ltd. synthetic) have been irradiated with over 10^9 r of Co^{60} gamma rays in an effort to discover a long-term effect. However, there does not seem to be any decided effect even after 3×10^9 r; the coloration reaches saturation at about 5×10^7 r and thereafter does not bleach. The *C* band is not prominent in any of these samples. Also, it

[1] Summer employee.

[2] Co-op employee.

[3] C. M. Nelson, *Solid State Ann. Prog. Rep. Aug. 31, 1957*, ORNL-2413, p 58.

appears that the amount of far-ultraviolet absorption is dependent on the amount of visible impurity bands. Consequently, it is important to be careful of sample placement in case the impurities are not homogeneously distributed.

On the other hand, samples of high-purity vitreous quartz from different sources (Corning No. 7940, Ultrasil, and Vitreosil O.H.) showed some interesting effects from long-term (4×10^9 r) Co^{60} gamma irradiation (Fig. 28). The Ultrasil sample continued to develop very slowly the *C* band and the far-ultraviolet absorption. However, the Vitreosil O.H. and Corning No. 7940 samples show a maximum (near 5×10^8 r) in the development of the *C* band before an "optical bleach." These experiments are very interesting and will be continued. Radiation bleaching of the visible coloration has been observed before by many people. This visible coloration is due to impurities, whereas the *C* band has been assumed to be due to a lattice defect. No adequate explanation has been found for this effect.

Another set of experiments has been carried out in an effort to introduce more defects into the vitreous quartz structure. Specimens were heated for 1 hr at various temperatures from 600 to 1400°C and air-quenched. It was thought that at some high temperature additional vacancies might be produced which would be detected by gamma irradiation. However, essentially no difference was noted between these quenched samples, an unheated sample, and one which was heated to 1400°C for 1 hr and slowly cooled (about 60°C per hour). After 10^9 r there seems to be some difference between the high-temperature-treated samples. The 1300 and 1400°C quenched samples do not bleach as readily as do the other samples with longer gamma irradiation. The difference appears significant but is not the effect originally sought.

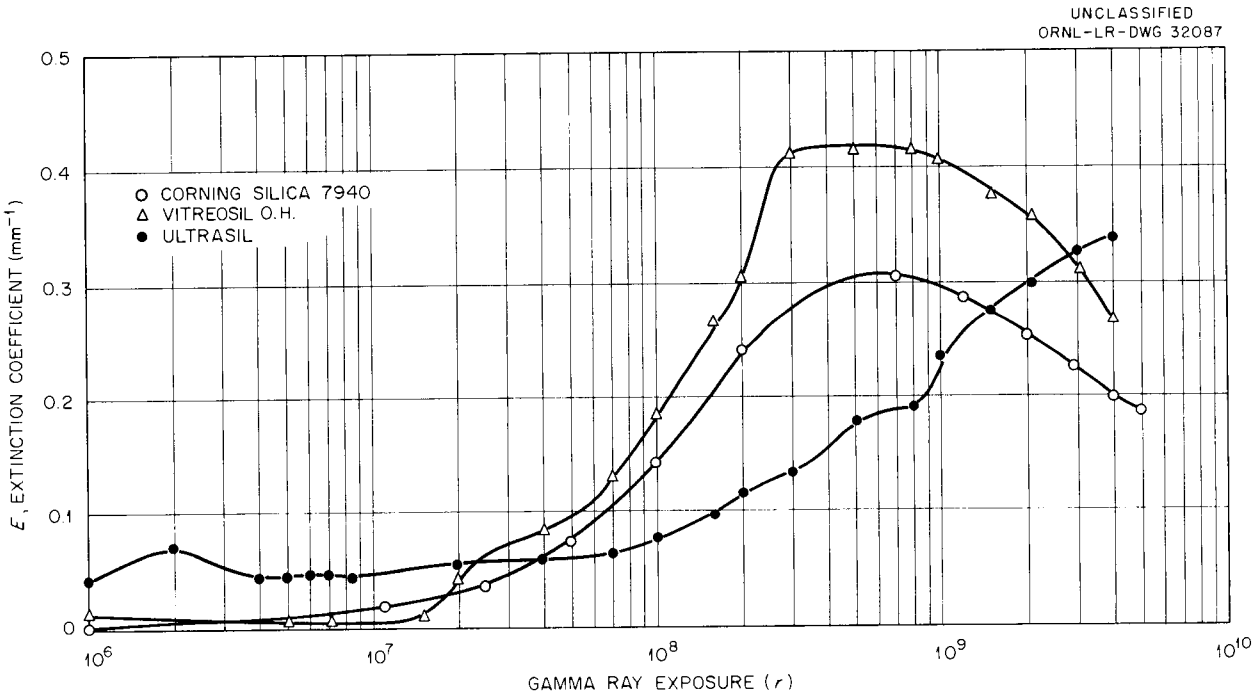

Fig. 28. Buildup of Coloration in Vitreous Silica with Gamma-Ray Exposure.

VACUUM ULTRAVIOLET SPECTROPHOTOMETER

C. M. Nelson R. E. Lide[1] W. J. Pegram[2]

A vacuum ultraviolet spectrophotometer has been under construction and test at ORNL. It is similar to one constructed at the University of Missouri by G. Reiling for his Ph.D. thesis. This instrument will cover the range from 900 to 3000 Å so that optical absorption measurements can be made down to the fundamental absorption edge of solids. Together with the Cary model 14 spectrophotometer (1850 to 26,000 Å) in current use, all absorption bands will now be able to be studied.

This instrument has a concave grating blazed at 1500 Å and ruled with 600 lines per millimeter. There are no windows or lenses in the design, so the limit of usefulness will be that of hydrogen absorption near 900 Å. The entire instrument is filled with hydrogen at a pressure of about 2 mm Hg. A very small flow of hydrogen is maintained through the assembly. The exit slit system is placed close to the entrance slit with the slits open to 0.010 in. It is a single-beam instrument, but a rotating sample holder has been provided so that three samples and a blank can be measured without opening up the system.

The instrument is almost ready to be used for accurate absorption measurements. It has been calibrated with the Hg arc lines, and a plot of wavelength vs micrometer reading was linear, as expected. The detection system uses a 1P28 photomultiplier tube coated with sodium salicylate as a fluorescent material. A hydrogen arc tube has been constructed with operating characteristics of about 50 v and 2.5 amp. In the wavelength region of particular interest for studies of crystalline and vitreous quartz, the ratio of signal to scattered light is about 500 to 1 on the average. Considerable difficulty has been experienced in learning how to start and operate the arc. At the present time trouble has been noticed in short- and long-time arc current stability. An arc current regulator has been built by the Instrument Department to act as a power supply and regulator, and by suitable alteration of some of the components the desired stability should be achieved.

[1] Summer employee.

[2] Co-op employee.

OPTICAL ABSORPTION BANDS AND PARAMAGNETIC RESONANCE CENTERS IN SILICA AND QUARTZ

C. M. Nelson R. A. Weeks R. E. Lide[1] W. J. Pegram[2]

The study of the defect structure of crystalline solids requires that the various experimental phenomena associated with such defects be related in a consistent manner. In the alkali halides the experimental results of the studies of optical absorption bands, luminescence, and ionic conductivity have been related in a fairly consistent fashion.[3] Electron spin resonance (ESR) spectra have provided in some cases, such as that of the V center,[4] unequivocal evidence as to the structure of the defect. Similar results were obtained in the identification of an F center produced in MgO by fast-neutron bombardment.[5] In the study of more complex crystalline structures such as quartz, the ESR evidence has not been entirely sufficient in identifying the structure of some of the defects produced by fast-neutron bombardment. By the ESR technique it has been possible, however, to identify defects of the quartz lattice.[6]

Ionization states of certain impurity atoms in quartz have been identified and an optical absorption band has been associated with the aluminum

[1] Summer employee.

[2] Co-op employee.

[3] F. Seitz, *Revs. Modern Phys.* 26, 7 (1954).

[4] W. Kanzig, *Phys. Rev.* 99, 1890 (1955).

[5] J. E. Wertz *et al.*, *Phys. Rev.* 107, 1535–37 (1957).

[6] R. A. Weeks, *J. Appl. Phy.* 27, 1376 (1956).

ionization state.[7,8] If it is assumed that the crystalline field interactions with a paramagnetic defect, such as a trapped electron, are similar in magnitude and direction, as are those in the alkali halides,[9] then it is possible to state that the ESR data[6] do show that one of the irradiation-produced defects is a trapped electron and the other is a trapped hole. Van Wieringen,[10] in a study of the optical absorption bands and ESR spectra produced by x rays in glass doped with alkali impurities, assumed that this hypothesis was valid. Mitchell and Paige,[11] on the basis of the far infrared absorption and the large magnetooptic anomaly, have assumed that the binding in quartz is ionic.

Numerous experiments now indicate a correlation between the 2150-Å (C) band and a group of ESR lines observed in irradiated quartz and a single line in the silica ($g = 2.0010$).[6] Initial development of the C band is markedly dependent upon the previous history and type of irradiation. Samples of crystalline quartz from three different sources (Brazilian natural, Bell synthetic, and General Electric Ltd. synthetic) were gamma-irradiated with 10^9 r. The induced optical absorption (Fig. 29) indicates little, if any, formation of the C band in the crystalline materials. The G.E. Ltd. sample showed very little coloration even in the far ultraviolet. On the other hand, the Bell sample showed considerable visible coloration as well as far ultraviolet absorption. The natural quartz sample had intermediate absorption in the visible and far ultraviolet. In general, the far ultraviolet absorption appears to be proportional to the visible coloration. Mitchell and Paige have also observed a correlation between the intensities of the C and A bands after x-ray irradiations.[11]

Although the crystalline material showed almost insignificant development of the C band with gamma irradiation, samples of vitreous silica from four different sources (Corning No. 7940, Vitreosil O.H., Ultrasil, and Amersil O.G. 1) develop an intense C band with such an irradiation (Fig. 28). The intensity of the C band produced varies with the source material, as do the weak intensities of bands at longer wavelengths. The absorption at 1850 Å is also a function of material source. Where there is visible coloration in the silicas, the shape of the absorption curve is so altered as to indicate a possible development of more far ultraviolet absorption than that in the uncolored samples. No relation can be established between the C band and the visible coloration (note the crossing of the Ultrasil curve).

After fast-neutron bombardment (10^{17} fast nvt), the absorption curves (Fig. 30) are similar to those obtained after gamma irradiation. The C band is quite intense in Amersil and the other silicas but

[7] J. H. E. Griffiths *et al.*, in *Conference on Defects in Crystalline Solids*, p 81, Physical Society, London, 1955.

[8] R. W. Ditchburn *et al.*, in *Conference on Defects in Crystalline Solids*, p 92, Physical Society, London, 1955.

[9] A. H. Kahn and C. Kittel, *Phys. Rev.* 89, 315 (1953).

[10] J. S. van Wieringen and A. Kats, *Philips Research Repts.* 12, 432 (1957).

[11] E. W. J. Mitchell and E. G. S. Paige, *Phil. Mag.* [8]1, 1085 (1956).

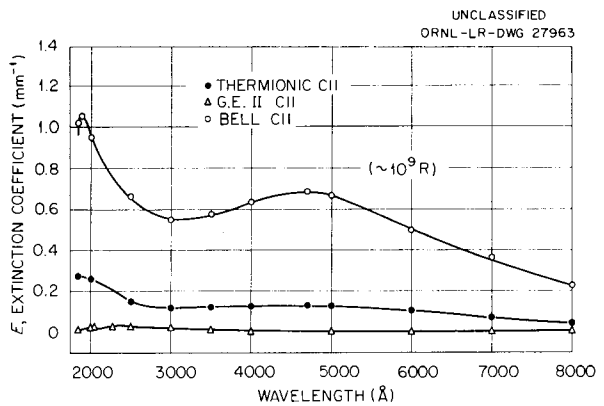

Fig. 29. Absorption Spectra of Samples of Crystalline Quartz After Gamma Irradiation (~10^9 r).

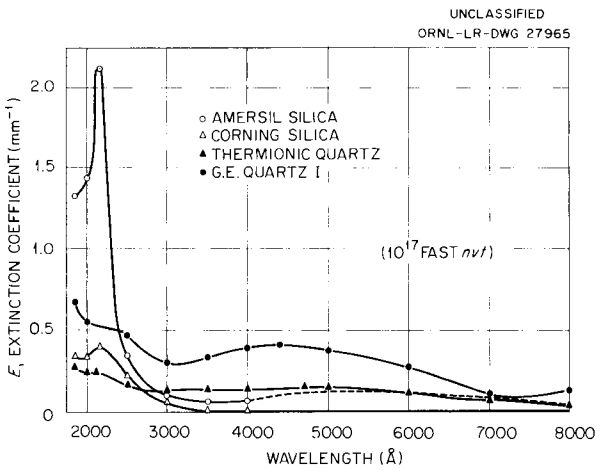

Fig. 30. Absorption Spectra of Samples of Quartz and Silica After Bombardment with Fast Neutrons. $(nvt)_f = 10^{17}$.

very weak in the crystalline quartz specimens. As noted for the gamma irradiations, the far ultraviolet absorption seems to follow the visible coloration. (Table 2 gives the extinction coefficient of the *C* band for various materials bombarded with 10^{18} fast neutrons/cm^2.) After $\sim 3 \times 10^{20}$ fast neutrons/cm^2 the absorption spectrum of crystalline

Table 2. Relative Intensities of the 2150 Å Absorption Band and the ESR Line, $g = 2.0010$, in Various Silicas and a Single Crystal for a Dose of 10^{18} Fast Neutrons/cm^2

Specimen	ESR Line, $g = 2.0010$ (centers/cm^3)	Extinction Coefficient (cm^{-1})	
		2150 Å	1850 Å
Amersil silica (O.G. 1)	5×10^{18}	4.4	4.4
Corning silica (No. 7940)	2.7×10^{18}	3.7	3.2
G.E. type III silica	2×10^{18}	3.7	3.2
G.E. synthetic quartz	4.5×10^{17}	1.9	2.0

quartz is similar to that of silica (Fig. 31). However, the absorption at 1850 Å does seem to vary from the crystalline material to the silicas.

Several neutron bombardments were made at low temperatures (−110°C). Observations were then made from 1850 Å to longer wavelengths on the various materials which had been irradiated. As shown in Fig. 32, there is less development of the *C* band and more development of the far ultraviolet absorption, particularly in the case of Amersil. Another color center is apparent in the Corning sample near 2500 Å.

A sample of Corning silica bombarded with 1.1×10^{18} fast neutrons/cm^2 developed an intense *C* band. It was then thermally annealed in 50°C steps up to 550°C. After 30 min at 550°C (Fig. 33) the *C* band was apparently gone, leaving some far ultraviolet absorption and another quite weak band at 2350 Å. A similar experiment on a synthetic crystal has been reported.[12]

[12] C. M. Nelson, *Solid State Ann. Prog. Rep. Aug. 31, 1957*, ORNL-2413, p 62.

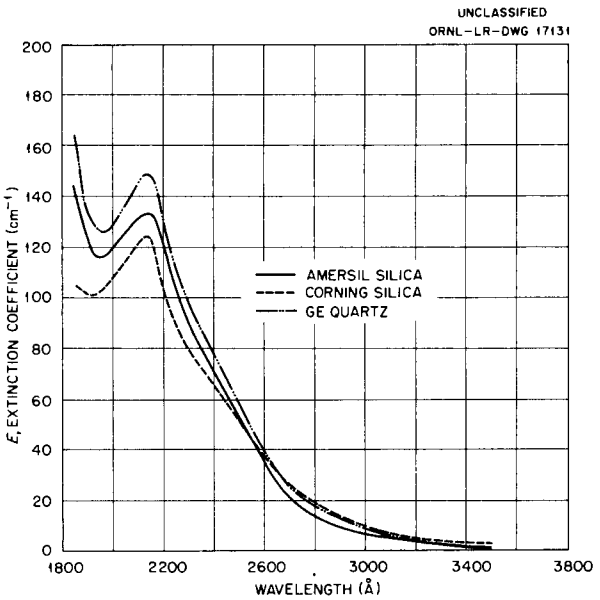

Fig. 31. Absorption Spectra of Samples of Quartz and Silica After Bombardment with Fast Neutrons. $(nvt)_f = 2.9 \times 10^{20}$.

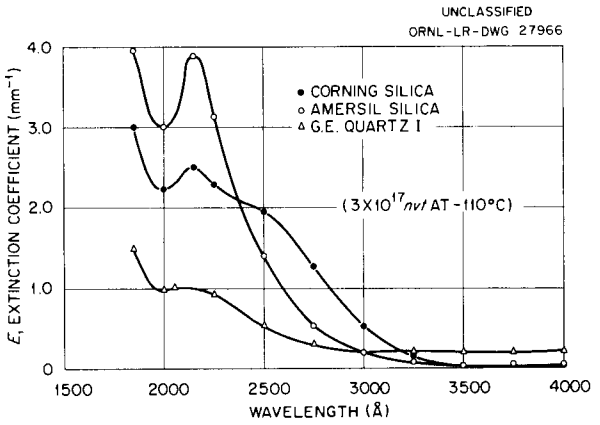

Fig. 32. Absorption Spectra of Samples of Quartz and Silica After Bombardment with Fast Neutrons at −110°C. $(nvt)_f = 3 \times 10^{17}$.

The four silicas and single crystals of the three quartzes were also examined by the ESR technique. The ESR spectra produced by Co^{60} gamma-ray irradiation of the various silicas and single crystals show a great variety of lines. Using the previously obtained[6] identifications of the lines which arise from defects of the quartz structure in neutron-irradiated specimens and of those which are probably associated with impurities, it was possible to correlate the observed spectra with some

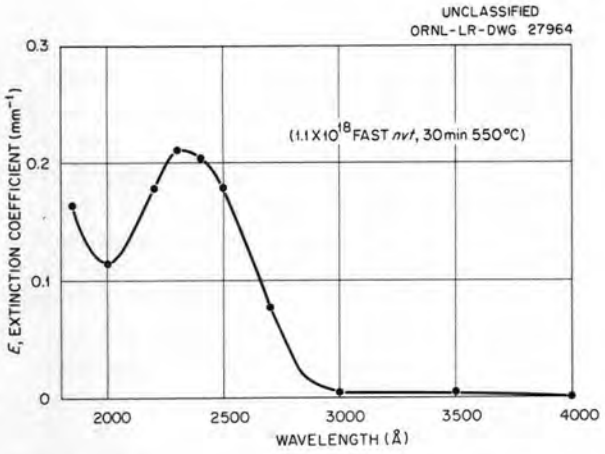

Fig. 33. Absorption Spectrum of a Sample of Corning Silica After Bombardment with Fast Neutrons $[(nvt)_f = 1.1 \times 10^{18}]$ and Annealing for 30 min at 550°C.

of the optical results. In the natural quartz crystal two principal groups of lines were found to be the same as the ESR lines,[13] $g = 2.0010$ and $g = 2.0090$, observed in the silicas. In Fig. 34 the ESR spectra produced in these materials are shown. In the G.E. Ltd. synthetic crystal with its c axis parallel to H, the magnetic field, a pair of lines of equal intensity were observed. These could not be definitely associated with the narrow resonance system although their g values were 2.0010 and 2.0009. In addition to this group there was another system of four lines equally spaced and centered on the line at $g = 2.0009$. These lines were approximately one-fifth as intense as the two more intense lines. An impurity with a nuclear spin of 3/2 (Li^7, Na^{23}, and K^{39} are possibilities) could produce such a group. If the synthetic crystal was grown by the usual technique, that is, from an Na_2CO_3 solution, then Na^{23} is probably the impurity.

In all of these gamma-ray irradiated crystals the development of the ESR line, $g = 2.0010$, was always small when compared with that of the components of the broad resonance system, except

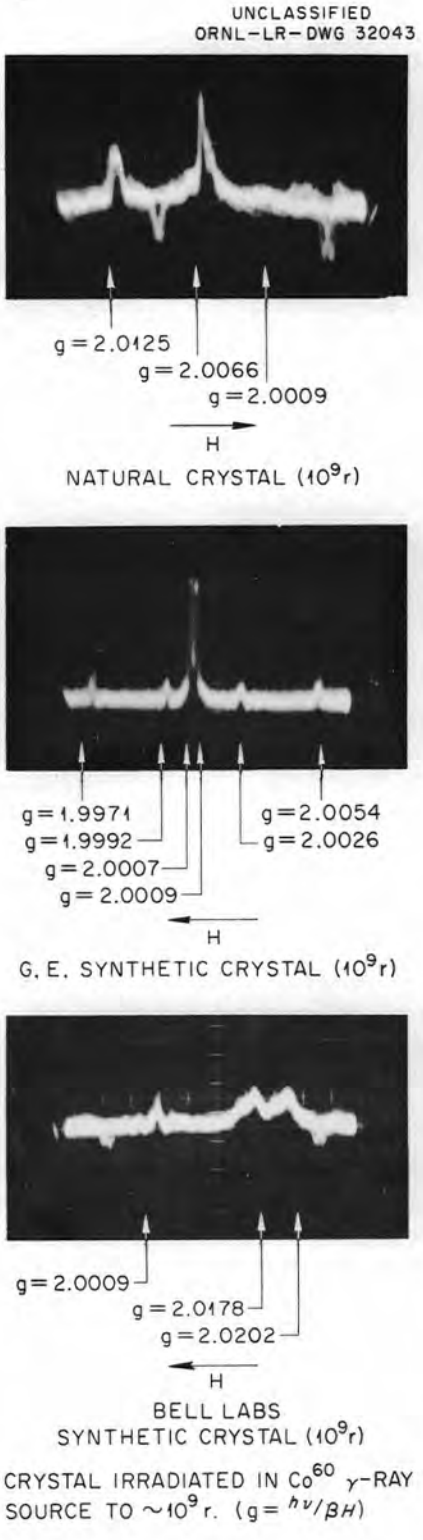

Fig. 34. Electron Spin Resonance Spectra of Samples of Crystalline Quartz After Gamma Irradiation (~10^9 r).

[13] This ESR line centered at $g = 2.0090$ in the silicas is composed of many lines in the single crystals whose g's, as a function of orientation, range from 2.0020 to 2.0410. The analysis of the orientation data on these lines is not complete. The whole system of lines will be labeled "ESR line, $g = 2.0090$," for both the silicas and single crystals. The ESR line centered at $g = 2.0010$ in the silica has from one to six components depending on orientation in the crystal; it will be labeled "2.0010."

that in the case of the G.E. Ltd. crystal the other lines in the spectra complicate the identification. Gamma-ray irradiation of the silicas produced a strong ESR line, $g = 2.0010$, and the 2150 Å absorption band was also intense. The ranking of the silicas according to the intensity of the narrow resonance system is the same as the ranking according to the intensity of the 2150 Å band; for neutron bombardments of short duration (10^{17} fast neutrons/cm^2) the silicas and single crystals can be ranked in the same order. Again the agreement of the ESR data with the optical data on the 2150 Å band is excellent.

Two varieties of high-purity Corning silica (Nos. 7940 and 7943), one of which was presumably manufactured in a manner similar to that of previous shipments and one, the "waterless" variety, in which special precautions were taken to exclude water, were obtained. A specimen of each was irradiated with 5×10^{17} fast neutrons/cm^2, and the relative intensities of the ESR line, $g = 2.0010$, and the 2150-Å band were measured. The ratio of the intensity of the ESR line in the waterless to that in the usual silica was found to be 4.5, while the ratio of intensities of the 2150-Å bands was 7. There is a difference in the optical measurement, probably accounted for by the difference in the background absorption. In the "waterless" silica the background absorption at 1850 Å is much higher than in the other silica. If this background is subtracted the agreement is much better. It was unfortunate that the optical absorption in this particular sample was so large. Since the slits on the spectrophotometer were wide open, the shape and intensity of the absorption band became rather indefinite. In any case, qualitatively there was tremendous absorption in the C-band region. As soon as more waterless material is available, a quantitative measurement of the C-band absorption will be made. There have been many indications of a considerable complexity of the optical absorption from 2000 to 2500 Å.[14–17]

If the relative intensities of the narrow resonance system and the 2150-Å band are compared for a neutron dose at which the neutron-introduced defects become a significant fraction of the total defect concentration, again an excellent correspondence is observed. In Table 2 the relative intensities are compared for a dose of 10^{18} fast neutrons/cm^2. If the background, as indicated by the optical absorption at 1850 Å (last column in the table), is taken into account the agreement is improved.

If a comparison is made after a dose $>3 \times 10^{19}$ fast neutrons/cm^2 at which the intensity of the 2150-Å band and that of the ESR line, $g = 2.0010$, have saturated (Fig. 38 in this report and Fig. 23, p 59, ORNL-2413), a one-to-one relationship is again found. After such neutron doses all optical bands have disappeared except for the 2150-Å band and those below 1850 Å.[11]

Mitchell and Paige[11] have shown that there are at least two optical bands between the 2150-Å band and the optical absorption edge at 1450 Å. The E band (1650 Å) is the most intense band in this region for doses $>10^{17}$ fast neutrons/cm^2.

The question then arises as to the correct assignment of the ESR lines to the available optical absorption bands. The data on the gamma-ray irradiation and low neutron dose ($\sim 10^{17}$) strongly suggest that the 2150 Å band is the same as the ESR line, $g = 2.0006$. A further verification of this assignment and the relation between the E band and the ESR line, $g = 2.0090$, is found in the annealing data shown in Figs. 35 and 36. In the top part of Fig. 35 the ESR spectrum observed in a Corning silica specimen is shown after a dose of 10^{19} fast neutrons/cm^2. The derivative of the absorption is plotted as a function of field intensity. The ESR line, $g = 2.0010$, is off scale, the ESR line, $g = 2.0090$, is easily identified, and two more lines are apparent on either side of the narrow resonance system. The intensity of these two lines is of the order of 1% of the intensity of the ESR line, $g = 2.0010$. In the bottom part of this figure the spectrum after annealing is shown. The line, $g = 2.0010$, is completely annealed and a portion of the line, $g = 2.0090$, in the region of $g = 2.0090$ has disappeared. As indicated above, the optical spectrum showed the complete disappearance of the 2150-Å band but the absorption below 1850 Å, as shown by the small change in absorption at 1850 Å, was still present.

In Fig. 36 the results of a similar annealing experiment on a natural crystal are shown. Figure 36a shows the spectrum with the crystal oriented in the strong magnetic field H_0 with the c axis parallel to H_0. The intense line on the high-field

[14] R. Yokota, *J. Phys. Soc. Japan* 7, 316 (1952).

[15] E. W. J. Mitchell and E. G. S. Paige, *Phil. Mag.* [8]1, 1085 (1956).

[16] A. J. Cohen, *Phys. Rev.* 105, 1151 (1957).

[17] P. Levy, private communication.

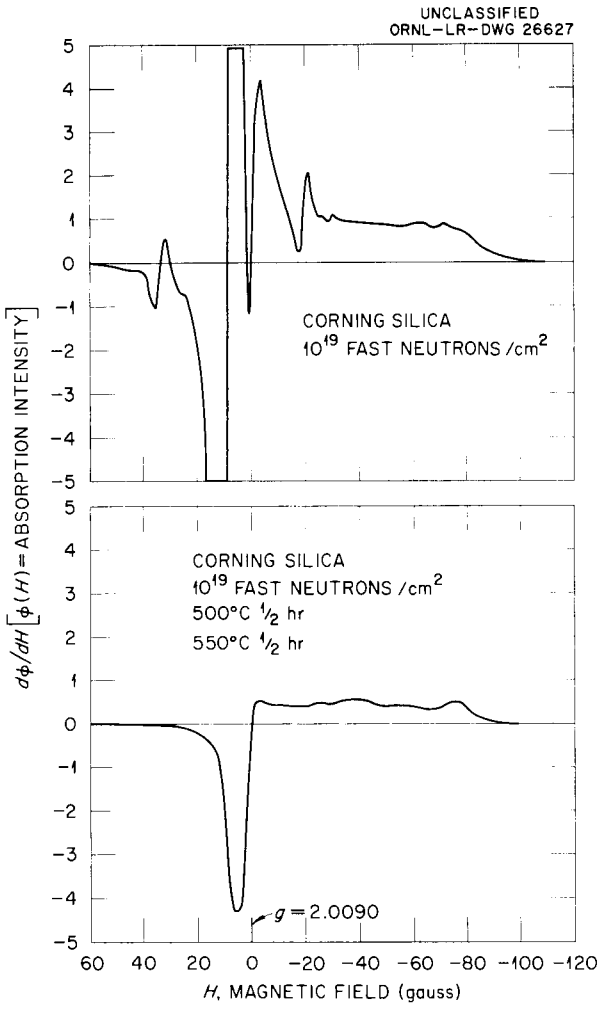

Fig. 35. Annealing of Electron Spin Resonance Centers in Corning Silica.

end of the spectrum is the same as the line, $g = 2.0010$, in the silica. The line just resolved on the low-field side is a component of the line, $g = 2.0090$, as is the other line on the low-field side. These two lines for this orientation of the crystal then comprise the ESR line, $g = 2.0090$, observed in the silica.

Figure 36*b* shows the spectrum after an anneal approximately one half as long as that given the Corning specimen. The line, $g = 2.0010$, and one component of the line, $g = 2.0090$, are approximately an order of magnitude less intense; the other component of the line, $g = 2.0090$, has decreased approximately 30%. On the basis of the annealing data on the Corning silica and the natural crystal, the ESR line, $g = 2.0090$, is probably composed of two components with different annealing rates. This interpretation would indicate two different spin systems and hence different kinds of defects.

If these data are compared with the optical data of Mitchell and Paige[11] for similar conditions of temperature and time, an identity can be established between the E band they observed and the component of the ESR line, $g = 2.0090$, least affected by the thermal treatment. Mitchell and Paige[11] observed that for a similar thermal treatment on a natural crystal the C band decreased by an order of magnitude and the E band decreased approximately 30%. A comparison of the ESR heat-treatment data with the optical data for similar conditions shows that the E band and one component of the ESR line, $g = 2.0090$, arise from the same center. These authors suggest that the C band is due to an electron trapped at an oxygen vacancy and that the E band is due to a hole trapped at an interstitial oxygen ion. Such a suggestion does agree with the observed sign of Δg (ref 9) for each center where

$$\Delta g = g_{\text{center}} - g_{\text{free electron}}$$

and g is defined as the spectroscopic splitting factor in the relation

$$h\nu = g\beta H_0$$

in which h is Planck's constant, ν is the frequency of the oscillating magnetic field, β is the Bohr magneton, and H_0 is the fixed field perpendicular to the oscillating magnetic field.

In some of the silicas (Amersil, G.E. type III, Corning, and Vitreosil) a gamma-ray (Co^{60}) dose of 10^8 r can produce a very intense C band (Fig. 29), as compared with the crystalline material. The ESR line, $g = 2.0006$, is much more intense in the silicas than in the crystalline material. An irradiation of 10^{17} fast neutrons/cm^2 also produces the ESR line, $g = 2.0010$, in the same relative intensity. As described above the usual form of the Corning high-purity silica and the special form in which water was excluded were given the same neutron dose. The C band and the ESR line, $g = 2.0010$, were approximately five times as intense in the waterless as in the usual form. In the section "Short-Range Order and Defects in Silicas" evidence is shown that indicates that the waterless silica is more highly disordered than the usual forms of silica. In Fig. 39 the ratio of

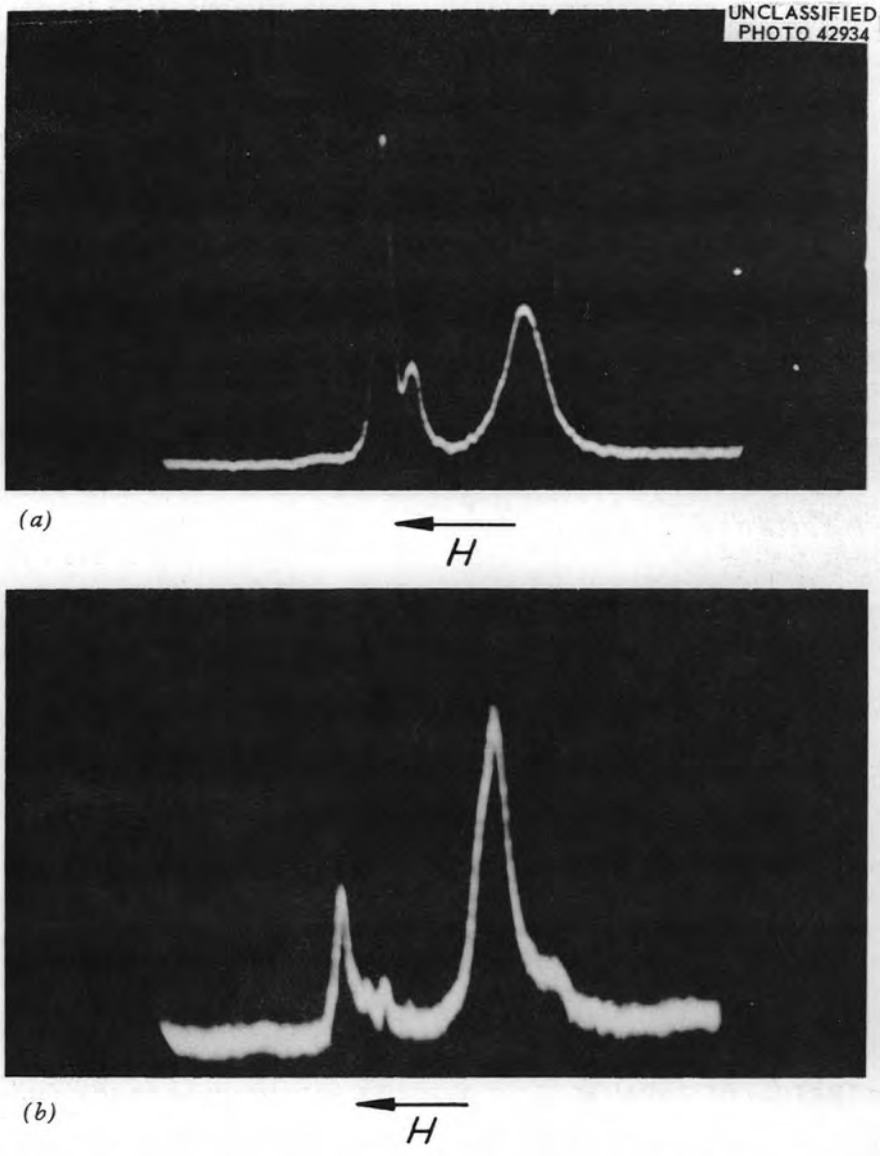

Fig. 36. Annealing of Electron Spin Resonance Centers in Natural Quartz. (*a*) Spectrum after irradiation with 5×10^{18} fast neutrons/cm^2. (*b*) Spectrum after annealing at 450°C for 2 hr; oscilloscope gain, 3.7.

the "electron" line, $g = 2.0010$, to the two "hole" lines, $g = 2.0090$, in some of the silicas and single crystals is plotted as a function of neutron dose. The silicas that show the initial high production of the "electron" line have a ratio of "electron" to "hole" concentration greater than 1, after irradiation with 10^{17} fast neutrons/cm^2. For doses greater than 10^{18} fast neutrons/cm^2 the ratio drops to ~ 0.7 and remains at this value to saturation of concentration at 4×10^{19} and beyond. The ratio for G.E. synthetic crystal begins at 0.3 at 3×10^{17}, shows a gradual increase to 0.6 at 10^{18} nvt_f and remains constant to $\sim 3 \times 10^{19}$. The ratio then begins a rapid increase up to a value of 1.3 at 8×10^{19}. It then decreases to 0.7 at 3×10^{20}. These variations in the relative concentration of the two or three principal kinds of defects seem to be closely correlated with the rapid decrease in the density between 3×10^{19} and 10^{20} nvt, reported by Wittels[18] and others,[19] and with the peak in the total concentration of paramagnetic

[18] M. C. Wittels, *Phil. Mag.* [8]2, 1445 (1957).

[19] W. Primak, *Phys. Rev.* 110, 1240 (1958).

centers at 4×10^{19} *nvt*, described by Stevens *et al.*[20]

The initial high rate of production of the "electron" center in some of the silicas with gamma-ray and neutron bombardment, the rapid growth of the "electron" center between 3×10^{19} and 8×10^{19} in the crystalline material, and the very high rate of production at low neutron dose ($\sim 5 \times 10^{17}$) in the Corning waterless silica, which has a line shape for the ESR spectra and a density suggestive of the highly disordered material resulting from a fast neutron bombardment of 5×10^{19}, indicate that this defect is closely linked with the Si – O bonds. It is suggested that the defect is due to a broken Si – O bond[20] rather than to an actual displacement of the O. The observed complexity of the absorption in the region from 2000 to 2300 Å could arise from a variety of defects. The ESR spectrum which has been associated with the peak at 2150 Å does not reveal any great variation from crystal to crystal, except in intensity. However, in the silicas, as has been noted there can be considerable variation in the shape of the ESR line (see the section "Short-Range Order and Defects in Silicas"). Also, the two varieties of Corning silica, Nos. 7940 and 7943, do not show any difference in their optical spectra except at 1850 Å, and the only other difference is in the shape of the ESR line. These data suggest that the local environment of the center can cause a shift in the peak of the optical absorption.

The two components of the "hole" defect may be two different forms of interstitial oxygen. If such were the case, then the optical absorption bands from the two forms could fall in the same wavelength range. In the alkali halides an optical absorption band has been observed for O^{--} and for OH^- (ref 21). The peak of the OH^- band falls at a slightly higher energy than that of the O^{--} band, whose peak falls at 6 ev. In quartz, which has a more open structure and a lower dielectric constant, the peak of an O^{--} band might be expected to fall at a considerably higher energy. This suggestion is in agreement with observation of the peak of the *E* band at 7.6 ev. The first ionization state of the O_2 molecule is about 9 ev.[22] Taking into account the dielectric constant of the quartz, this might well be depressed to the 7.6 ev observed for the *E* band. It is therefore suggested that it may not be possible to distinguish between the O^{--} ion and the O_2^- ion optically but that the ESR spectra of two such entities might be resolved. The two components of the trapped "hole" may arise from two such entities.

[20] D. K. Stevens, W. J. Sturm, and R. H. Silsbee, *J. Appl. Phy.* 29, 66 (1958).

[21] J. Rolfe, *Phys. Rev. Letters* 1, 56 (1958).

[22] G. Herzberg and L. Herzberg, in *American Institute of Physics Handbook* (ed. by D. E. Gray), p 7–145, McGraw-Hill, New York, 1957.

CONCENTRATION OF PARAMAGNETIC DEFECTS PRODUCED IN SILICA AND QUARTZ BY NEUTRON IRRADIATION

R. A. Weeks E. Sonder R. E. Lide[1] W. J. Pegram[2]

Magnetic susceptibility[3] and electron spin resonance (ESR) measurements[4–6] have shown that some of the defects produced in quartz and silica by irradiation with fast neutrons are paramagnetic. In the susceptibility measurements the total concentration of paramagnetic defects is found, and in this technique there is no way of distinguishing between contributions from ionization states of impurities and defects of the basic structure. The ESR technique does allow the contributions from the various kinds of paramagnetic defects to be separated, and defects of the lattice can usually be separated from paramagnetic ionization states of impurities.

[1] Summer employee.

[2] Co-op employee.

[3] D. K. Stevens, W. J. Sturm, and R. H. Silsbee, *J. Appl. Phy.* 29, 66 (1958).

[4] R. A. Weeks, *J. Appl. Phy.* 27, 1376 (1956).

[5] J. S. van Wieringen and A. Kats, *Philips Research Repts.* 12, 432 (1957).

[6] E. W. J. Mitchell and E. G. S. Paige, *Phil. Mag.* [8]1, 1085 (1956).

The susceptibility measurements of Stevens *et al.*[3] on neutron-irradiated quartz give a value of 3.7 centers (moment equal to one Bohr magneton) per incident fast neutron. These authors assume that these centers are divided equally between two species of paramagnetic centers.[4] Then, using the optical absorption data and the conclusions of Mitchell and Paige[6] with respect to the defects giving rise to the *C* and *E* bands (Mitchell and Paige notation), they calculate for the two bands an oscillator strength which is reasonable on the basis of the Mitchell and Paige assignment of the bands. Their conclusion as to the origin of the bands is that the *C* band is due to an electron trapped at an oxygen vacancy, and the *E* band due to a hole trapped at an oxygen interstitial. These two defects should be produced in equal numbers by neutron bombardment. It is possible to determine the relative concentration of each paramagnetic species by means of the ESR technique since the contributions of the various species to the paramagnetism are resolved into spectral lines whose areas can be measured.

If measurements are made at the same time on an ESR line of unknown concentration and on a measured quantity of a material with a known concentration of paramagnetic centers, then a value can be obtained for the concentration of the unknown.[7] Such measurements have been made on the ESR lines,[8] $g = 2.0010$ and $g = 2.0090$, in a neutron-irradiated specimen of Amersil, using as the standard a crystal of diphenylpicrylhydrazyl (DPPH). In order that the comparison be as accurate as possible, the number of centers in the standard should be of the same order as in the unknown. For this measurement a specimen of Amersil O.G. 2, $0.97 \times 2.28 \times 0.051$ cm in dimensions, was irradiated in the Graphite Reactor at −105°C to a dose of 8.3×10^{16} fast neutrons/cm^2. After the irradiation a small crystal of DPPH whose volume had been determined by measuring its dimensions was inserted into a small hole (0.1 cm diameter) that had been drilled in the center of the Amersil specimen. Measurements were then made on the resonance in the Amersil and the DPPH at the same time and under identical conditions. The DPPH and Amersil ESR lines are shown in Fig. 37.

The DPPH was assumed to have a density[9] of 1.35 and its measured volume was 1.13×10^{-4} cm^3. The density is for crystals grown from a benzene solution and the molecular weight is 472 including the benzene of crystallization. The DPPH used was made at this laboratory and the crystals were grown from a chloroform solution.[10] In these measurements, however, the data on the DPPH grown from a benzene solution were used.

The derivatives of the lines were recorded, and since the center of the Amersil resonance was at $g = 2.0010$ and that of the DPPH at $g = 2.0039$, the lines were adequately resolved and appropriate numerical integration could be performed without difficulty. Taking into account the filling factor of the Amersil specimen, the concentration of centers in the narrow resonance was found to be $(7.2 \pm 1.5) \times 10^{17}$ cm^{-3}. The error takes into account the uncertainty in the molecular weight to be used for this DPPH, the error in the volume measurement, and the error in the numerical integration. Using the values obtained for this

[7] R. H. Silsbee, *Phys. Rev.* **103**, 1675 (1956).

[8] These *g* values are the centers of the lines observed in the silicas. In single crystals there are three groups of lines which have been identified with the two lines observed in the silicas (see footnote 13 to "Comparison of Optical Absorption Bands and Paramagnetic Resonance Centers in Silica and Quartz," this report).

[9] J. Berthet, thesis, University of Paris.

[10] S. Goldschmidt and K. Euler, *Ber. deut. chem. Ges.* **55**, 616 (1922).

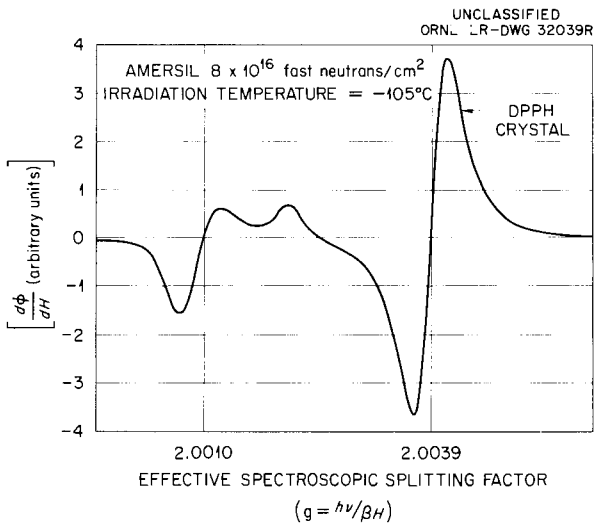

Fig. 37. Electron Spin Resonance Spectrum of Amersil Silica After Irradiation at −105°C with Fast Neutrons $[(nvt)_f = 8 \times 10^{16}]$. Direct comparison with DPPH crystal. Amersil line $g = 2.0006$.

specimen of Amersil as a reference point, comparisons were then made with specimens of Corning, Amersil, Vitreosil, and G.E. type III silicas and with natural Brazilian quartz and G.E. Ltd. synthetic crystals. These materials were all irradiated in the C-28 facility of the LITR with doses ranging from 10^{17} to 3×10^{20} fast neutrons/cm^2. The results of this comparison are shown in Fig. 38. The estimated error in these comparisons is ±70% between different doses. In the case of the specimens with the 10^{18} dose the relative accuracy is estimated at ±20%. The Amersil shows the greatest increase in concentration initially (at $\sim 10^{17}$) but then seems to saturate at a concentration identical with that in the other silicas. The crystalline material shows very low relative concentration at 10^{18}, but rises at $\sim 4 \times 10^{19}$ fast neutrons/cm^2 to a concentration that is the same as that in the silicas. These concentration data do not indicate a peak in this particular defect as do the data for total concentration of magnetic defects.[3] The accuracy of the data, however, does not justify any conclusions about the existence of such a peak for this particular center.

Since two ESR lines are observed in the silicas and these data represent the contribution to the magnetic defect concentration of only one of them, each of the points in Fig. 38 should be increased by a certain amount to represent the total magnetic defect concentration. This additional component has been found for some specimens by measuring the ratio of the concentration of centers in each line (g = 2.0010 and g = 2.0090). The accuracy of such a ratio for the silica specimens is ±10%. For the crystalline specimens the crystal must be oriented with its c axis parallel to the strong magnetic field. In this orientation the ESR line, g = 2.0010, is a single line at g = 2.0010 and the other ESR line, g = 2.0090, is composed of two lines at g = 2.0023 and 2.0065 (see Fig. 36). For this orientation the accuracy of the ratio is probably ±15%. For neutron doses $>4 \times 10^{19}$ fast neutrons/cm^2 orientation is no longer necessary (see Fig. 42). The plot of these data is shown in Fig. 39. In the silicas there is a rather wide

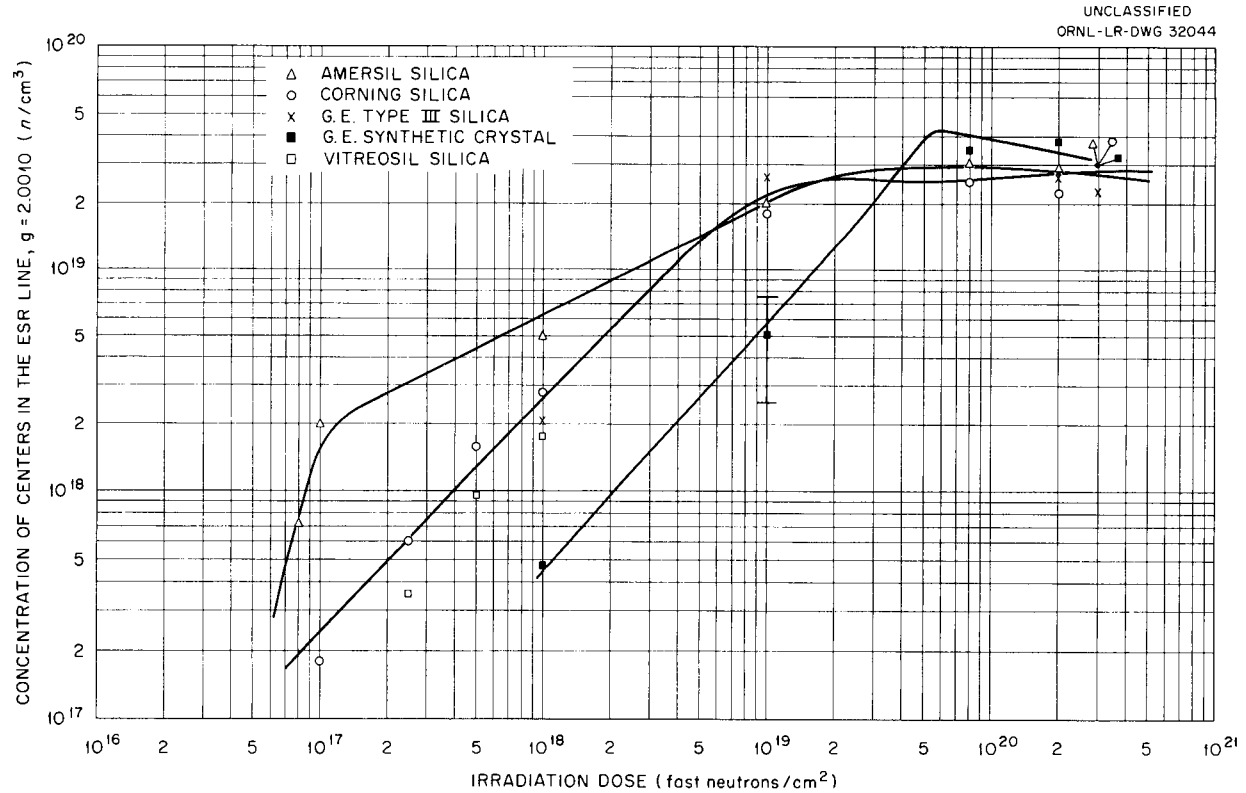

Fig. 38. Concentration of Magnetic Centers in the ESR Line, g = 2.0010, vs Fast-Neutron Dose.

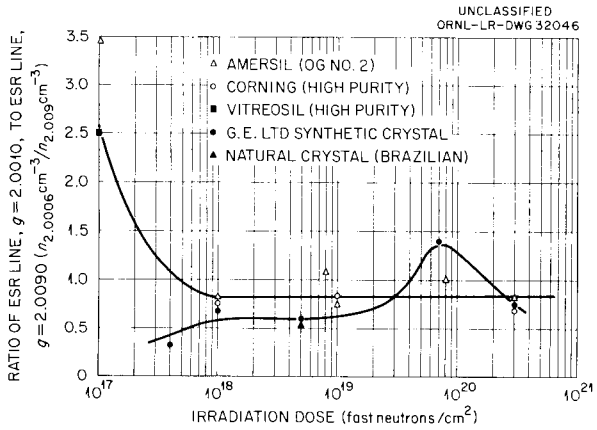

Fig. 39. Ratio of Concentrations of Magnetic Centers in the ESR Lines, $g = 2.0010$ and $g = 2.0090$.

range of this ratio at low neutron dose (10^{17} fast neutrons/cm^2). Amersil has the highest ratio. The G.E. Ltd. synthetic crystal has quite a low ratio, 0.3, at 3×10^{17}. In the silicas this ratio settles down to a value of ~0.7 at 10^{18} fast neutrons/cm^2 and remains there to 3×10^{20}. There is some scatter at 8×10^{18} and at 8×10^{19} that is outside the error given above. Further measurements need to be made to elucidate this discrepancy.

The ratio in the crystalline material shows a rise to ~0.6 at 10^{18} and is constant up to ~3×10^{19}, at which point a rather sharp increase is observed. The highest value is 1.4 at 8×10^{19}. Considerably more data are necessary in this region. The ratio then falls to that of the silicas at 3×10^{20}. (See the section "Optical Absorption Bands and Paramagnetic Resonance Centers in Silica and Quartz" for further discussion of this figure.) If the contribution to the magnetic defect concentration is added to that shown in Fig. 38, then the agreement with the data of Stevens *et al.*[3] is within the error of the ESR measurements.

In addition to these measurements on concentration of paramagnetic defects a cooperative effort with E. W. J. Mitchell of the University of Reading, Reading, England, was undertaken. Some single crystals of Brazilian natural quartz, which were irradiated in the BEPO reactor at Harwell, England, and on which Mitchell had made optical measurements were sent by him to ORNL. One of these crystals was suitable for magnetic susceptibility measurements. This crystal had received a dose of 5.1×10^{18} thermal neutrons/cm^2. Using the equation of Mitchell and Paige[6] the fast dose (100 ev to 2 Mev) was found to be 1.1×10^{18} fast neutrons/cm^2. The susceptibility measurements are shown in Fig. 40, in which the diamagnetic susceptibility is plotted as a function of reciprocal temperature. Assuming a Curie-law paramagnetism[3] the density of centers is related to the measured gram susceptibility by

$$\chi = \chi_{\text{diamagnetic}} + \sum_i \frac{N_i B_i^2}{\rho k T} \quad ,$$

where N_i is the number of centers with magnetic moment B_i and ρ is the density of the material. The spin resonance data[4] indicate that all the centers have spin 1/2 and no orbital contribution to the magnetic moment ($g = 2$); thus $B_i = B$, the Bohr magneton. The slope of the curve in Fig. 40 then gives the density of centers. The concentration of paramagnetic defects is 7.2×10^{18} cm^{-3}. If this value is compared with the curve given in reference 3, where concentration is plotted vs fast-neutron dose, it falls on the curve. Of course this value includes contributions from paramagnetic impurities (e.g., aluminum)[11] which have also been produced by the irradiation. However, if the intensity of the optical absorption can be taken

[11] J. H. E. Griffiths *et al.*, in *Conference on Defects in Crystalline Solids*, p 81, Physical Society, London, 1955.

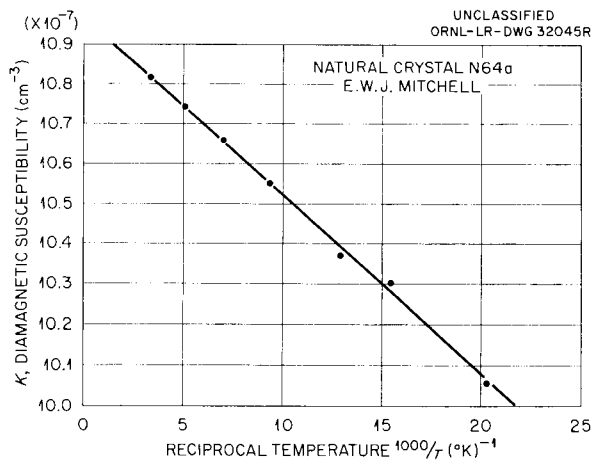

Fig. 40. Diamagnetic Susceptibility of Irradiated Natural Quartz (1.1×10^{18} fast neutrons/cm^2).

as an indication of the concentration of the aluminum impurity, then the contribution to the paramagnetism from this source is much smaller than the total concentration observed.

In view of this agreement it can be concluded that the ESR spectra observed at 25°C represents nearly all the paramagnetic centers, with the exception of the paramagnetic ionization state of the substitutional aluminum.[12] In the best crystalline material available the aluminum concentration is $\leq$0.01%. It is evident that this center can make only a small contribution to the susceptibility at fast-neutron doses $>10^{18}$ cm^{-2}. On the basis of the ESR optical data (see the preceding section, "Optical Absorption Bands and Paramagnetic Resonance Centers in Silica and Quartz") there are two, probably three, basic defects produced by neutron bombardment in the quartz structure. Two of these, the *C* and *E* optical absorption bands, have been related to the trapped electron ($g = 2.0010$) and trapped hole ($g = 2.0090$), respectively.[8] The resonance that has been identified with the trapped hole may be two distinct defects as indicated by annealing data (see preceding section).

One other aspect of the measurements of defect concentration by these techniques is the possibility that the defects may not have trapped an electron and a hole. Optical and ESR measurements were made to check this possibility in the following manner (see the section "Optical Absorption Studies of Irradiated Solids," this report). Specimens of silica and of synthetic and natural quartz were irradiated in the LITR at a temperature of ~50°C. Optical and ESR measurements were then made. Gamma-ray irradiation in a Co^{60} source was then applied, of sufficient duration to ensure saturation of available defects. The optical and ESR measurements were then repeated. No difference was observed between the two measurements.

On the basis of the evidence presented above it seems reasonable to conclude that all the *C*-band defects have trapped an electron and hence are observable by the various techniques described above. Although similar experimental verification has not been obtained for the *E* band it seems reasonable that similar conditions prevail. Neutron irradiation may, however, produce defects that are more complex than those described and that are neither paramagnetic nor active optically.

In the early experiments[2] the reactor irradiations were carried out at a temperature of ~250°C and at doses of 10^{18} fast neutrons/cm^2 or higher. The evidence from these experiments indicated that all the observable defects were point defects. The width (separation of inflection points) of the ESR line for these crystals oriented with their *c* axis parallel to the strong magnetic field was $\leq$0.1 gauss. Single crystals of natural and synthetic quartz irradiated at temperatures of 50 and −105°C (dose ~10^{17} fast neutrons/cm^2) had line widths of 0.7 gauss. In addition to the difference in width the shape of this line was different for each temperature of irradiation. As can be seen in Fig. 41 there is evidence of an underlying structure indicated by the arrows in the figure. There are two possibilities that should be considered: (1) There is another paramagnetic center whose *g*, for this orientation of the crystal, has the same value as that of the center which has been labeled "$g = 2.0010$" above. (2) The underlying structure is due to vitreous regions created by the fast-neutron bombardment; the centers in these vitreous

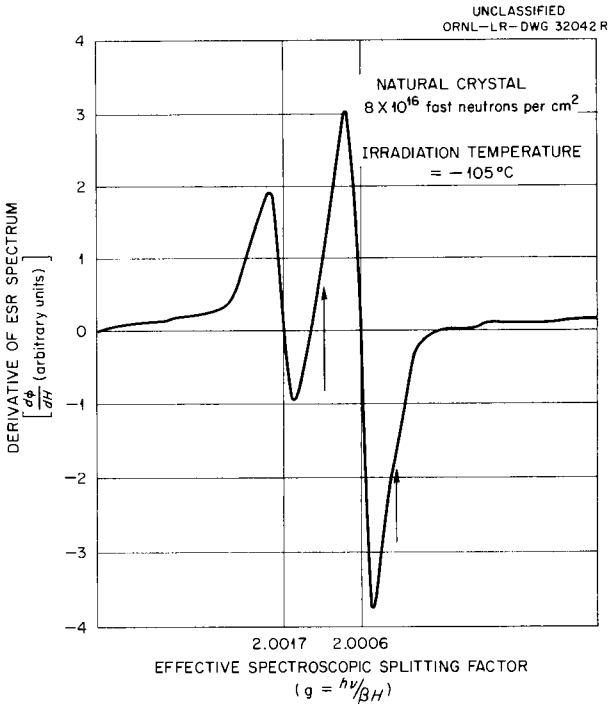

Fig. 41. Electron Spin Resonance Spectrum of Natural Quartz After Irradiation at −105°C.

[12]The resonance of the ionization state of the aluminum substituted for silicon in the quartz can only be observed at liquid nitrogen temperature or lower.

regions would then display a line similar to that displayed by the silicas.

Wittels[13] has shown that there are no vitreous regions present that can be detected by the x-ray diffraction pattern technique up to neutron doses of 3×10^{19} fast neutrons/cm^2. However, the ESR technique is particularly sensitive to the degree of crystalline order in the region, around the center, extending over a few atomic distances. Although such regions in the crystal would not be large enough to be detected by the x-ray diffraction technique, nevertheless the center would be in a vitreous region. Low-temperature thermal-conductivity measurements[14,15] may also indicate the presence of disordered regions. Mitchell and Paige have suggested that such regions are formed from the onset of irradiation. If the line-width increase is due to such disordered regions, then for irradiation temperatures between 100 and 250°C these regions fail to form even though, as indicated by the data of Stevens *et al.*,[3] the higher temperature does not greatly change the rate of formation of paramagnetic centers.

Orientation data do not clearly indicate either the presence or the absence of an additional line that moves away from the ESR line, $g = 2.0010$, as the crystal is rotated. There is very little evidence to indicate that (1), above, is the correct explanation of the observed line broadening.

The point of this digression was to indicate that complex disordered regions may be present in neutron-irradiated crystals. The data of Stevens *et al.*,[3] in conjunction with the optical and ESR data, indicate that most of the available hole and electron traps are filled after irradiation in a reactor. However, the concentrations of hole and electron traps derived from the ESR and magnetic susceptibility data may not represent the total defect concentration present as a result of reactor bombardment.

[13] M. C. Wittels, *Phil mag.* [8]2, 1445 (1957).

[14] R. Berman, *Proc. Roy. Soc.* (*London*) **A208**, 90 (1951).

[15] P. G. Klemens, *Prog. Roy. Soc.* (*London*) **A208**, 108 (1951).

SHORT-RANGE ORDER AND DEFECTS IN SILICAS

R. A. Weeks R. E. Lide[1] W. J. Pegram[2]

The structure of silica has been the subject of very extensive investigations. As reported by Morey,[3] the x-ray evidence would seem to indicate a short-range order extending from one SiO_4 tetrahedron to the next, and a complete absence of long-range order. It might then be assumed that reactor irradiation would produce only very small changes in the density of the material and that defects produced by such irradiations would exist in a completely disordered environment. Wittels[4] has reported that upon prolonged neutron irradiation (10^{20} fast neutrons/cm^2) the density of silica does change, increasing as much as 3.0%. Cohen[5] has shown that the low-temperature thermal conductivity of silica increases by a factor of 2 with bombardment of 5.8×10^{19} fast neutrons/cm^2.

It has also been shown that the defects produced in silicas and single crystals by bombardment up to 10^{19} fast neutrons/cm^2 have similar environments.[6] This was shown by comparing the shape of one ($g = 2.0010$) of the electron spin resonance (ESR) lines found in the silicas with a line with the same g value observed in a crushed crystal. The identity of the lines was also established by other measurements.[6] Since the line shape in the silica was the same as in the crushed crystal, it is reasonable to assume that the environment of the spin center is the same in both materials.

The shape of the ESR line, $g = 2.0010$, in the silicas changes with increasing reactor irradiation. In Fig. 42 the shape of the line, $g = 2.0006$, in

[1] Summer employee.

[2] Co-op employee.

[3] G. W. Morey, *The Properties of Glass*, p 548–71, Reinhold, New York, 1954.

[4] M. C. Wittels, *Phys. Rev.* 89, 656 (1953).

[5] A. F. Cohen, *Solid State Ann. Prog. Rep. Aug. 31, 1957*, ORNL-2413, p 70.

[6] R. A. Weeks, *J. Appl. Phy.* 27, 1376 (1956).

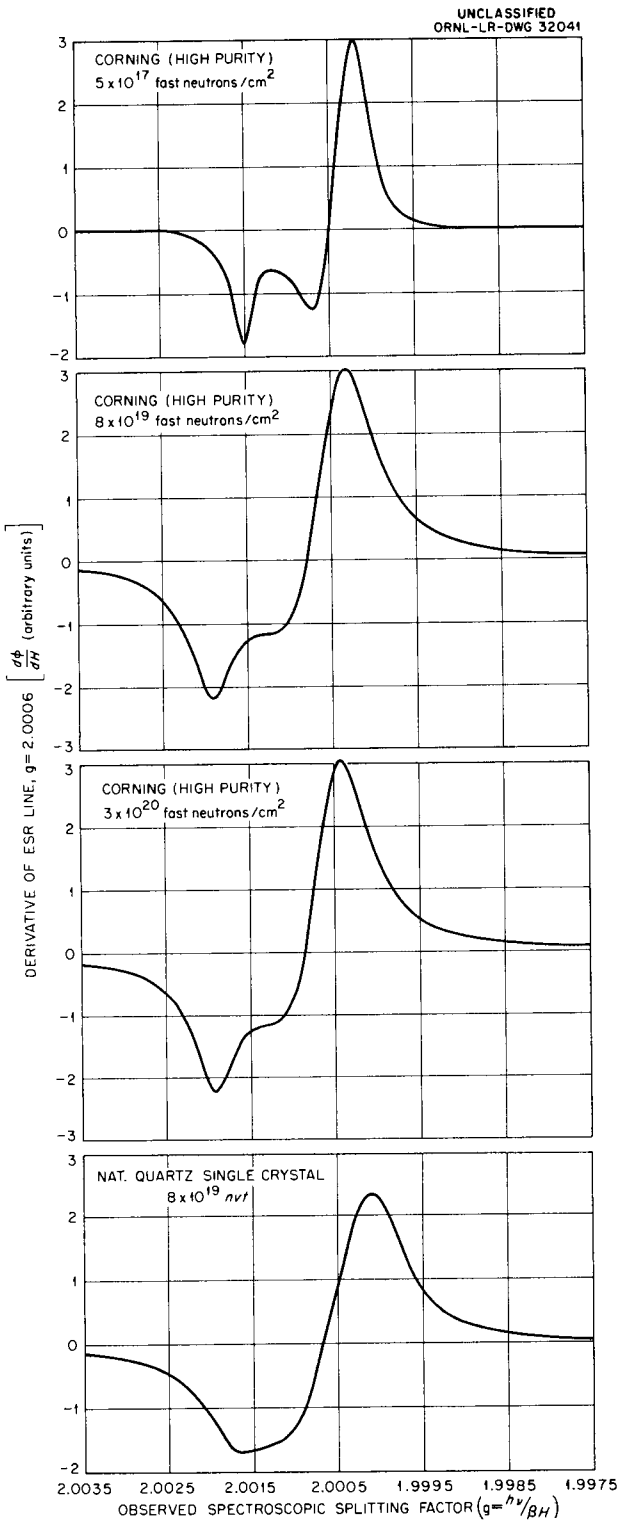

Fig. 42. Electron Spin Resonance Spectra of Corning Silica and Natural Quartz After Fast-Neutron Irradiation.

Corning silica (high-purity) as a function of neutron dose is shown. Also shown is the ESR line observed in a natural quartz single crystal after the indicated neutron dose. The orientation of the single crystal is immaterial at this point, the line being the same for any orientation. Of course, at a neutron dose $<10^{19}$ fast neutrons/cm^2, one to six lines may be resolved depending upon the orientation of the crystal.[6]

As can be seen in Fig. 42, the line shape of the heavily irradiated crystal is quite similar to that of the heavily irradiated silicas. There is a small difference still present. Because of the similarities of line shape it is reasonable to assume that the crystalline order around the center is approximately the same in the silicas and the single crystal after a neutron dose $\geq 5 \times 10^{19}$ fast neutrons/cm^2. This conclusion is further supported by the fact that the density of the silicas is the same as that of the quartz after such a neutron dose.[7]

A specimen of the Corning high-purity silica has been obtained on which special precautions were taken to exclude water. This waterless silica was given a neutron dose of 5×10^{17} fast neutrons/cm^2. The narrow resonance, $g = 2.0010$, is shown in Fig. 43. The shape of the line is quite similar to that found in heavily irradiated silicas,

[7] M. C. Wittels and F. A. Sherrill, *Phys. Rev.* 93, 1117 (1954).

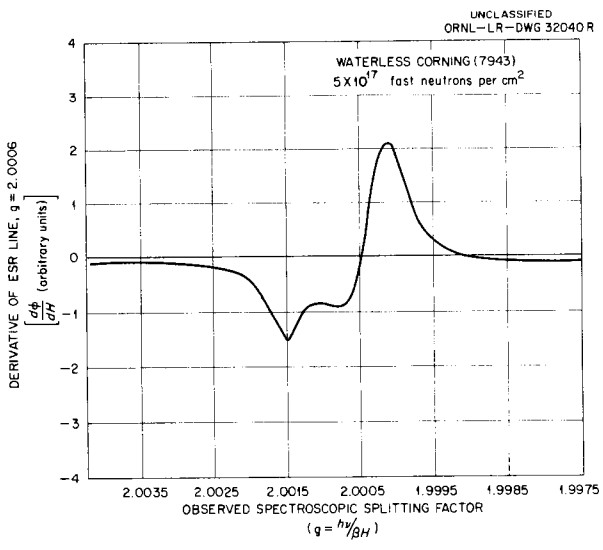

Fig. 43. Electron Spin Resonance Spectrum of Waterless Corning Silica After Fast-Neutron Irradiation.

as can be seen by comparing with Fig. 42. This similarity of line shape suggests that the order in the waterless silica is the same as that in the heavily irradiated silica of the usual kind.

The densities of the following specimens are tabulated below: Amersil O.G. 1; Corning No. 7940 (high-purity); three samples of the first shipment received of very high-purity Corning silica (one unirradiated, one lightly, and one heavily irradiated); and Corning No. 7943 (waterless).

Material	Irradiation	Density
Amersil O.G. 1	None	2.2004 ± 0.0001
Corning No. 7940	None	2.2005 ± 0.0001
Corning very high purity	None	2.2008 ± 0.0001
	10^{17} *nvt*	2.2027 ± 0.0001
	10^{20} *nvt*	2.2538 ± 0.0001
Corning No. 7943 "waterless"	None	2.2068 ± 0.0001

The waterless silica is 0.5% more dense than Amersil and the usual type of Corning. The heavily irradiated specimen of Corning is 2.5% more dense. Whereas in single crystals the rate of density change as a function of irradiation dose increases rapidly in the region of 4×10^{19} fast neutrons/cm^2 (ref 7), the density change in the silicas is much more gradual, saturating after $\sim 10^{20}$ fast neutrons/cm^2, as shown by the density of the heavily irradiated specimen.

The data on the shape of the narrow line suggest that in silicas whose density is 2.2008 there is short-range order extending over a small region around the defects introduced by neutron irradiation. The necessary extent of this region would be determined by the interaction of the wave function of the trapped defect with the surrounding lattice. Wertz *et al.*[8] give an estimate of the amount of overlap with the nearest neighbor atoms of the *F*-center wave function in MgO. If the spin center in the silica is a trapped electron, as assumed by Mitchell and Paige,[9] then the results on MgO may indicate, within an order of magnitude, the required extent of an ordered region in the silica. In these terms a region of crystalline order of the order of 50 Å in diameter around the defect might be expected to produce the observed line shape when averaged over random orientations.

The line-shape data given above suggest that upon long neutron bombardment this short-range order is destroyed. The resulting state of the silica and that of the single crystal subjected to a similar irradiation are approximately the same.[10] The data on the waterless specimen suggest that the "disordered" material may also be formed by appropriate manufacturing procedures.

[8] J. E. Wertz *et al.*, *Phys. Rev.* 107, 1535 (1957).

[9] E. W. J. Mitchell and E. G. S. Paige, *Phil. Mag.* [8]1, 1085 (1956).

[10] M. C. Wittels, *Phil. Mag.* [8]2, 1445 (1957).

LOW-TEMPERATURE THERMAL CONDUCTIVITY OF LITHIUM FLUORIDE CRYSTAL UPON IRRADIATION BY THERMAL NEUTRONS AND Co^{60} GAMMA RAYS

A. F. Cohen

Introduction

Lithium fluoride can easily be damaged by short neutron bombardments and has therefore been used for numerous radiation damage studies. Upon bombardment with thermal neutrons, the Li^6 isotope, which has a 7.5% natural abundance, undergoes fission via the reaction:

$$Li^6 + n^1 \longrightarrow H^3\ (2.7\ \text{Mev}) + He^4\ (2.1\ \text{Mev})$$

Numerous property changes and the nature of the various lattice defects introducted in LiF by thermal-neutron irradiation have been investigated. Among the defects to be considered are the tritium and helium atoms produced by the fission reaction as well as the many defects created by the 4.8 Mev of kinetic energy during its dissipation in the crystal. Considerable ionization is present, as is apparent from the large number of color centers produced at low irradiation doses. A flux of $\sim 9 \times 10^{17}$ *nvt* results in displacement of $\sim 1\%$ of all the atoms, and $\sim 9 \times 10^{13}$ *nvt* produces ~ 1

defect pair per million atoms.[1,2] The large numbers of displacements and defect pairs produced may be assumed to be in large part responsible for the observed property changes following irradiation.

Investigation of the lattice expansion that occurs in LiF during exposures up to 10^{19} *nvt* has been carried out by various methods.[3-10] The work of Mayer *et al.*[4] and Smallman and Willis[3] indicates that the lattice parameter a increases with flux to $\sim 3 \times 10^{17}$ *nvt* and then decreases at higher fluxes. Smallman and Willis have suggested that the decrease is associated with the disappearance of strains due to interstitials when the interstitials "coalesce" into clusters of defects. The radiation-induced changes in LiF are stable at room temperature, but most properties can be returned to the unirradiated state by annealing at temperatures of 300 to 500°C.

Gilman and Johnston[11] find from etch behavior following neutron irradiation that the etching is caused by aggregates of defects rather than by individual point defects. Bombardment of LiF crystals with 1.5-Mev electrons ($\sim 5 \times 10^{15}$ electrons/cm^2), with which there is no gas due to fission, results in etching effects similar to those from thermal-neutron irradiation. In addition, effects on etching behavior are produced by low thermal-neutron doses ($<10^{15}$ neutrons/cm^2) in LiF; consequently, aggregates or clusters of point defects are in evidence even at low neutron doses.

According to the thermal conductivity calculations of Klemens,[12] the temperature dependence of the introduced thermal resistance will be qualitatively different for isolated point defects and for clustered defects or dislocations. It was felt, therefore, that thermal conductivity measurements could be used to study the nature of damage induced in LiF by thermal neutrons or by Co^{60} gamma rays. In addition, density measurements were carried out with the purpose of correlating an additional property subjected to the same irradiation conditions.

Experimental

The thermal conductivity specimens used were long rods of approximately square cross section, cleaved from single-crystal lithium fluoride grown by the Harshaw Chemical Company. Measurements of the thermal conductivity were made by a static heat flow method. The temperature gradient was measured by means of thermal probes consisting of calibrated carbon resistors attached to nickel-silver clips which were in good thermal contact with the specimen.

The density measurements were carried out at room temperature by a conventional hydrostatic method. The liquid used was carbon tetrachloride, in which the solubility of lithium fluoride is negligible.

The LiF crystal used for irradiations with Co^{60} gamma rays was wrapped in aluminum foil, and the temperature of irradiation was approximately 40°C. This specimen was $\sim 0.165 \times 0.170$ in. in cross section. A 2000-curie source with a flux of $\sim 10^{12}$ photons·cm^{-2}·sec^{-1} was employed.

The LiF specimens for neutron irradiations were bombarded in the thermal-neutron facilities of the ORNL Graphite Reactor with a flux of about 0.7×10^{12} thermal neutrons·cm^{-2}·sec^{-1}. The specimens were wrapped in 2S aluminum foil, and the temperature of irradiation was approximately 60°C. These specimens were approximately square in cross section ($\sim 0.105 \times 0.105$ in.).

The thermal-neutron doses were measured by determining the gamma activity of pure cobalt foil monitors placed with the LiF samples. Since the samples were relatively thick, self-screening was appreciable, and appropriate corrections were made.[7] The thermal-neutron doses which will be

---

[1] F. Seitz and J. S. Koehler, in *Solid State Physics* (ed. by F. Seitz and D. Turnbull), vol 2, p 305, Academic Press, New York, 1956.

[2] D. Binder and W. J. Sturm, *Phys. Rev.* **107**, 106 (1957).

[3] R. E. Smallman and B. T. M. Willis, *Phil. Mag.* [8]2, 1018 (1957).

[4] G. Mayer *et al.*, *Proc. Intern. Conf. Peaceful Uses Atomic Energy, Geneva, 1955* 7, 647 (1956).

[5] W. J. Sturm, *Conference on Effects of Radiation on Dielectric Materials, Naval Research Laboratory, Washington, D.C., Dec. 14–15, 1954*, ACR-2, 97.

[6] D. T. Keating, *Phys. Rev.* 97, 832 (1955).

[7] D. Binder and W. J. Sturm, *Phys. Rev.* **96**, 1519 (1954).

[8] D. Binder and W. J. Sturm, *Phys. Rev.* **99**, 603 (1955).

[9] P. Senio and C. W. Tucker, *Radiation Effects in LiF*, KAPL-1727 (May 24, 1957).

[10] D. Binder and W. J. Sturm, *Phys. Rev.* 107, 106 (1957).

[11] J. J. Gilman and W. G. Johnston (to appear in *J. Appl. Phy.*); private communication.

[12] P. G. Klemens, *Proc. Phys. Soc. (London)* A68, 1113 (1955).

referred to below are corrected doses. There was, of course, some variation in dose through the sample.

Results

In Fig. 44, the logarithm of the thermal conductivity K is plotted against log T for an LiF crystal before and after successive irradiations with Co^{60} gamma rays. Figure 45 is a plot of the gamma-ray-induced thermal resistance (i.e., the reciprocal of K for the irradiated specimen minus the reciprocal of K for the unirradiated specimen) vs temperature. It has been shown for introduction of point defects by impurities in KCl crystals that the theoretically expected thermal resistance is approximately attained.[13] The present experiment indicates a greater thermal resistance at low temperatures than that expected for point defects. The observed temperature dependence of the induced thermol resistance is $\sim T^{-1.7}$ to $T^{-2.0}$.

Figure 46 is a plot of the thermal resistance induced in LiF crystal upon thermal neutron irradiation, the unirradiated thermal conductivity values having been very similar to those shown in Fig. 44. The thermal resistance has a maximum in the region of the dose indicated by curve D, since it decreases somewhat at higher dosage. This decrease is probably related to the decrease in lattice expansion, via strain release, postulated by Smallman

[13] G. A. Slack, *Phys. Rev.* 105, 832 (1957).

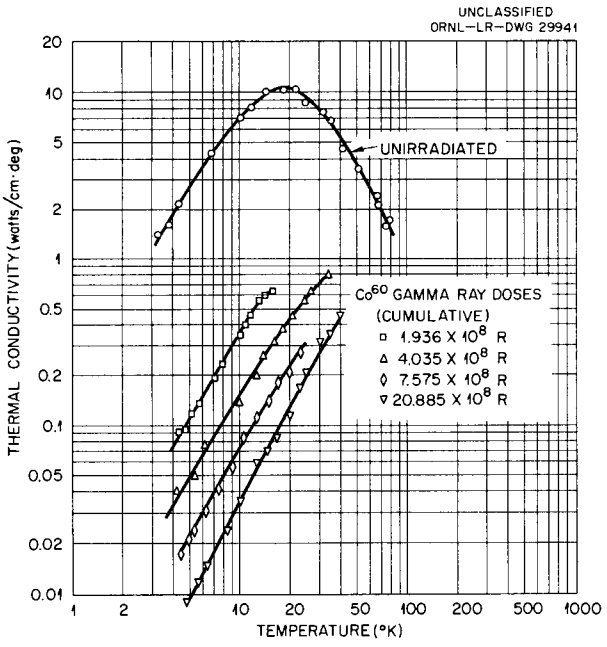

Fig. 44. Thermal Conductivity of LiF Crystal Before and After Successive Co^{60} Gamma Irradiation.

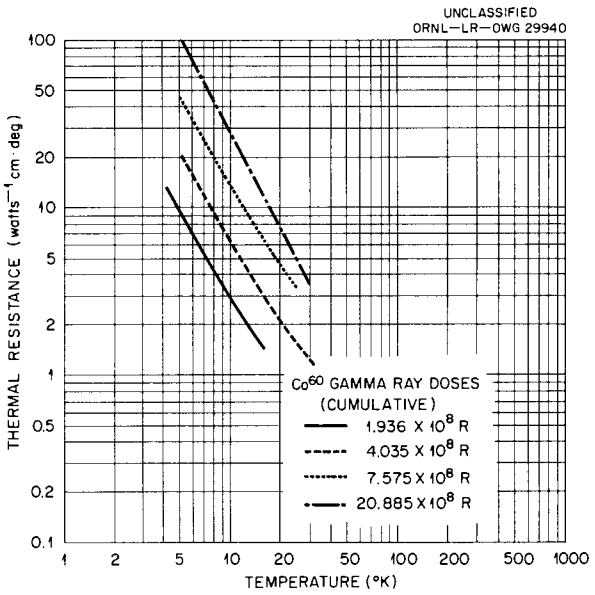

Fig. 45. Thermal Resistance Induced in LiF Crystal by Co^{60} Gamma Irradiation.

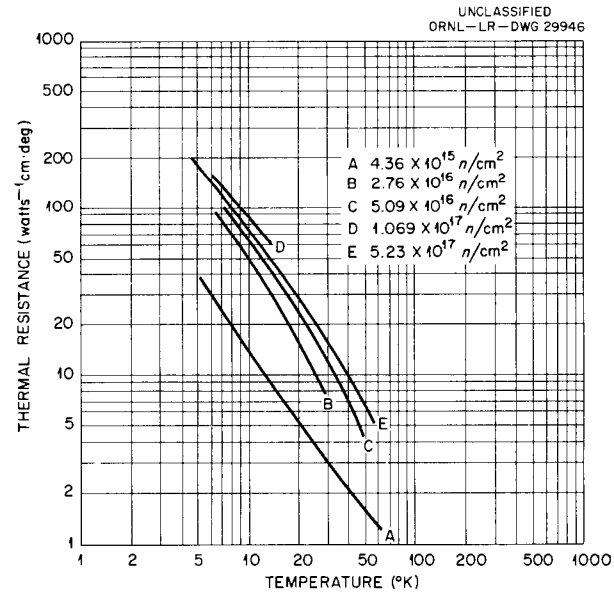

Fig. 46. Thermal Resistance Induced in LiF Crystal by Thermal-Neutron Irradiation.

and Willis.[3] It is seen even at doses as low as 4.5×10^{15} neutrons/cm^2 that the temperature dependence of the thermal resistance is different from that expected for isolated point defects and fairly similar to observations in the case of LiF irradiated with Co^{60} gamma rays. The temperature dependence of the neutron-induced thermal resistance is $\sim T^{-1.4}$.

Figure 47 shows the dose dependence of the measured density of LiF, where a monotonic decrease approximately equivalent to three times the average lattice-parameter increase found by Mayer *et al.*[4] and Smallman and Willis[3] at 3×10^{17} neutrons/cm^2 is observed. At higher doses, where the parameter decreases, the density continues to decrease, which is in general agreement with the behavior of density change vs neutron dose observed by Senio and Tucker.[9] In addition, they have found that the value of the quantitative density change in LiF is dependent on the sample temperature during irradiation.

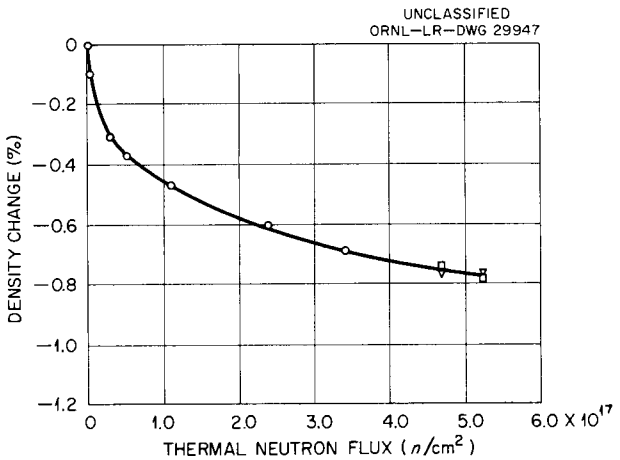

Fig. 47. Density Change Induced in LiF Crystal by Thermal-Neutron Irradiation.

Conclusions

The radiation damage in thermal-neutron-irradiated lithium fluoride crystals has been examined through measurements of low-temperature thermal conductivity up to doses of $\sim 5.3 \times 10^{17}$ neutrons/cm^2. The observed thermal resistance maximum is followed by a decrease at higher neutron dose which is probably related to the decrease in lattice expansion via strain release postulated by Smallman and Willis.[3] The introduced thermal resistance at low temperatures is different from that expected for isolated point defects and is more like a boundary resistance, suggesting therefore that clusters of point defects are responsible for a large part of the introduced resistance. Recent etch studies by Gilman and Johnston[11] also indicate that clusters of point defects exist in thermal-neutron-irradiated LiF even at low doses. The size of these clusters is estimated by them to be between 2 and 50 Å.

The thermal resistance introduced in LiF crystal by Co^{60} gamma rays is qualitatively similar to that observed following thermal-neutron irradiations. Since the etch behavior in LiF bombarded by 1.5-Mev electrons shows that clusters of point defects are present, it would not be unreasonable to expect qualitatively similar damage, that is, clusters of point defects, to be formed by Co^{60} gamma rays via the Compton electrons.

Therefore, the helium and tritium atoms produced in the neutron-irradiated LiF do not necessarily have an important role in producing the measured thermal resistance at low temperature, since a similar resistance is observed for gamma-irradiated LiF, where helium and tritium are not even present.

D. K. Holmes of this Laboratory has estimated the ratio of the initial rate of increase of thermal resistivity in the neutron case to that in the gamma-ray case, assuming that the observed effects are due to displaced atoms. He has found that the experimentally determined ratio seems to be a couple of orders of magnitude lower than the theoretical estimate.

Grown-in dislocations, present in unirradiated LiF, may in some way serve as centers to which point defects, formed by gamma rays or thermal-neutron irradiation, may attach. Consequently a clustering of defects may occur at the dislocations.

It would be of interest to extend the Co^{60} gamma irradiations to saturation with respect to the introduced thermal resistance and thereby to determine the difference between the effects of damage by Co^{60} gamma rays and thermal neutrons. It would also be of interest to anneal both the neutron- and gamma-ray-damaged crystals at various temperatures to study the recovery of the thermal resistance.

EFFECT OF FAST-NEUTRON BOMBARDMENT ON THE THERMAL CONDUCTIVITY OF SILICA GLASS AT LOW TEMPERATURE

J. H. Crawford, Jr. A. F. Cohen

Introduction

In this paper recent studies of the effect of prolonged fast-neutron bombardment and subsequent annealing on the low-temperature thermal conductivity of vitreous silica are described. This work represents an extension of previously reported results[1] in the following respects: Changes in conductivity K have been correlated with density measurements. Moreover, the exposure range has been extended to the point where saturation of changes in both K and density ρ has occurred. Finally, annealing experiments subsequent to bombardment have been made in order to ascertain the extent of recovery of both K and ρ.

The purpose of these studies is to obtain further information about the degree of order produced in a vitreous material by fast-neutron bombardment. Exposure of silica glass to reactor neutrons in the room-temperature range causes an increase in density.[2,3] This increase saturates for exposures $>5 \times 10^{19}$ fast neutrons/cm^2 (n_f/cm^2) at a value $\rho_s = 2.26$ g/cm^3, which corresponds to an increase in ρ of $\sim 3\%$. An even more significant fact is that this radiation-induced "phase" of silica is also produced by prolonged exposure of quartz, tridymite, and cristobalite. X-ray studies indicate that the "irradiation phase" is completely lacking in long-range order. Consequently, it appears that prolonged fast-neutron bombardment is capable of reducing crystalline forms of silica to a state of nearly complete long-range disorder which, at the same time, is more dense and, presumably, somewhat more highly ordered locally than vitreous silica prepared by more normal means.

A detailed analysis of x-ray diffraction patterns obtained from heavily irradiated fused silica and quartz has been carried out by Simon.[4] He finds that the Si – O distances are unchanged but that there is a decrease in distance between adjacent Si atoms after irradiation. He interprets this decrease in terms of a change in Si – O – Si bond angle from 142° before irradiation to 138° afterward. It also appears that irradiation increases the distribution of distances between atoms at greater separation, such as Si – 2nd O and O – O distances.

Consideration of this structural change ($\sim 3\%$ density increase) led Klemens to suggest that an increase in thermal conductivity would also be expected in irradiated vitreous silica.[1] Measurements have confirmed this prediction, and it was found that an exposure of 5.8×10^{19} n_f/cm^2 caused a twofold increase in K at 5°K.

In the following sections the more recent experiments are described and the results are discussed in terms of current theoretical concepts of heat conduction in glasses.

Experimental Details

The specimens used in this study were in the form of square rods of 19.8 mm^2 cross section. These were cut from a single piece of high-purity Corning fused silica. Measurements of K were performed by a conventional static method in which the temperature gradient was measured by thermal probes. The probes consisted of carbon resistance thermometers attached to silver clips, which made good thermal contact to the specimen.

Because of the high thermal resistivity of the silica glass, it was necessary to make careful corrections for heat loss along other paths. Good reproducibility of K for different arrangements in the cryostat and for different specimens was taken as evidence of the adequacy of these corrections.

Densities were measured by a conventional hydrostatic technique at room temperature.

The specimens were bombarded in a water-cooled fast-neutron facility in the LITR. The actual specimen temperature during exposure is not accurately known. However, since the specimen was always in good thermal contact with the reactor cooling water, its temperature should not have been in excess of ~ 80° C.

---

[1] A. F. Cohen, *J. Appl. Phy.* 29, 591 (1958).

[2] M. C. Wittels and F. A. Sherrill, *Phys. Rev.* 93, 1117 (1954).

[3] W. Primak, L. H. Fuchs, and P. Day, *J. Am. Ceram. Soc.* 38, 135 (1955).

[4] I. Simon, *Phys. Rev.* 103, 1587 (1956).

Anneals were carried out in air at 925°C for a period of 9 hr.

Results

In Fig. 48, log K is plotted against log T for the fused silica specimens after various treatments. The curve before exposure is somewhat higher than a similar one for the same temperature range obtained by Berman.[5] However, our specimens were Corning fused silica of very high purity and were nearly free from strains. Therefore this difference is probably due to a difference in materials used and is not caused by experimental inaccuracies.

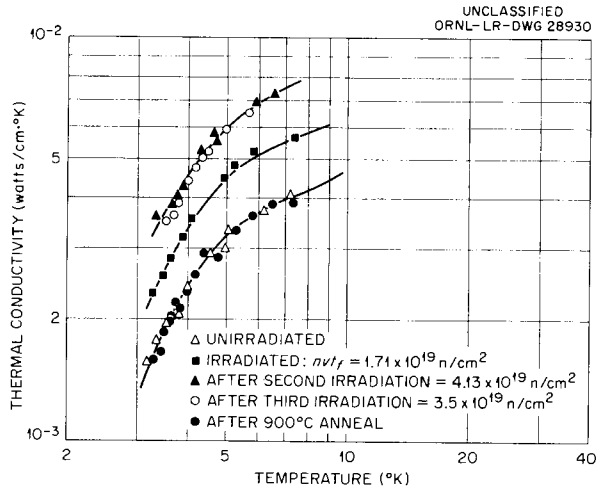

Fig. 48. Plot of Thermal Conductivity vs Temperature for Fused Silica Before and After Neutron Irradiation.

The curves denoted by the solid squares and the solid triangles were obtained after integrated exposures of 1.7×10^{19} and 5.8×10^{19} n_f/cm^2, respectively. The irradiation causes an increase in K by an almost constant factor over the temperature range investigated. An additional exposure of 3.5×10^{19} n_f/cm^2 (total exposure of 9×10^{19} n_f/cm^2) does not further increase K (curve denoted by open circles). Therefore it is concluded that 5.8×10^{19} n_f/cm^2 is an exposure sufficient to cause saturation. On annealing the specimens at 925°C for 9 hr it was found that, within experimental error, the log K vs log T curve returned to its initial, preirradiation position.

[5] R. Berman, *Proc. Roy. Soc.* (*London*) A208, 90 (1951).

The variation in density is shown in Fig. 49, in which ρ is plotted against exposure. Evidently, since little additional change with bombardment is observed above 5.8×10^{19} n_f/cm^2, K and ρ approach saturation together. The saturation value $\rho = 2.26$ g/cm^3 is in good agreement with the findings of Wittels and Sherrill[2] and of Primak and co-workers.[3] After the annealing treatment, ρ returned to very near its initial value. Before irradiation, $\rho = 2.2002$ g/cm^3; after irradiation and anneal, $\rho = 2.2045$ g/cm^3. This behavior is consistent with that in the annealing studies of Primak and Szymanski.[6]

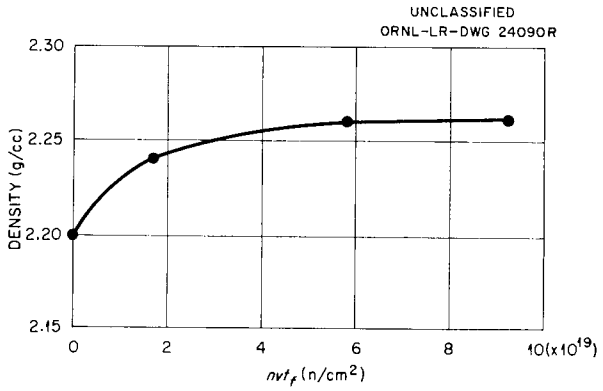

Fig. 49. Density Change of Fused Silica Upon Fast-Neutron Irradiation.

Discussion

The increase in K proceeds at a much more rapid rate during bombardment than does the density, which appears to approach saturation in the usual manner. A comparison of the changes in these two properties is made in Fig. 50, in which K is plotted against ρ for the several exposures. It is evident that K increases more rapidly than linearly with increasing ρ. Although K and ρ appear to be related because of similar saturation and annealing characteristics, the relationship may not be a direct one for reasons discussed below.

It is convenient to use the approximate Debye expression[7] for K in order to establish the origin

[6] W. Primak and H. Szymanski, *Phys. Rev.* 101, 1268 (1956).

[7] M. Planck *et al.*, *Vorträge über die kinetische Theorie der Materie und der Electrizität*, Teubner, Leipzig, 1914.

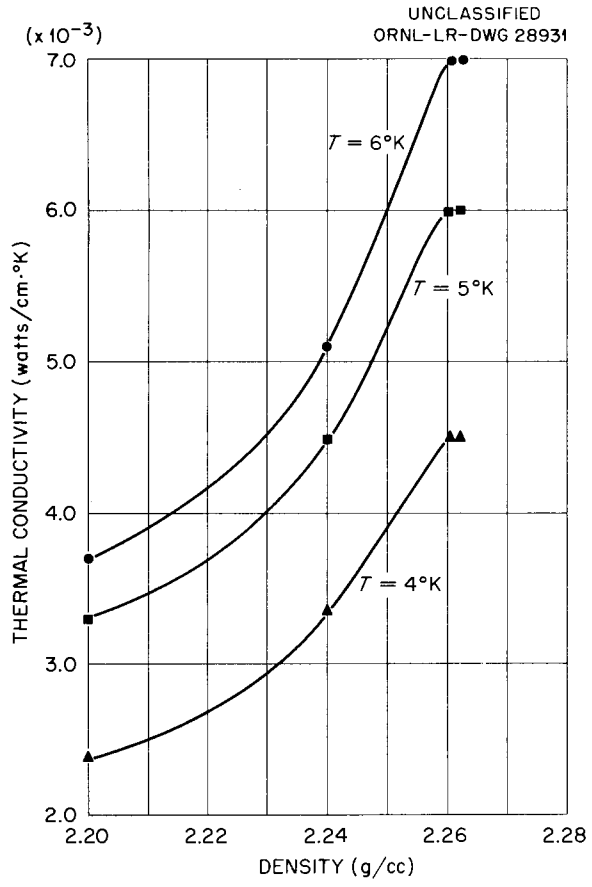

Fig. 50. Plot of Thermal Conductivity vs Density for Fused Silica Before and After Neutron Irradiation.

of the increase in K:

$$K = \tfrac{1}{3}cvl \quad , \tag{1}$$

where c is the heat capacity per unit volume, v is the phonon group velocity (velocity of sound), and l is the phonon mean free path or the effective relaxation length.

Neglecting second-order effects, one would expect the heat capacity per unit volume to be proportional to the concentration of molecules and hence the density, provided that the energy of interaction between adjacent atoms is not changed. This view is supported by the work of Simon and Lange,[8] who found that the specific heat was essentially the same for quartz and vitreous silica. Therefore we expect the 2.7% increase in ρ observed after the heaviest exposure to be reflected by a similar increase in c. The change in c is much too small to account for the observed increase in K.

The velocity of sound in a solid is given by

$$v = \sqrt{\frac{E}{\rho}} \quad , \tag{2}$$

where E is Young's modulus. Mayer and Gigon[9] have measured the effect of fast-neutron bombardment on the elastic constants of both quartz and silica glass. For the latter they find that an exposure of $7 \times 10^{18}\ n_f/\text{cm}^2$ causes an increase of 1.42% in E. This exposure corresponds to a 0.9% increase in ρ according to Fig. 49. If a linear relation between $\Delta\rho/\rho$ and $\Delta E/E$ is assumed (which is only approximately true for quartz), the 2.7% saturation increase in ρ would lead to a 4.2% increase in E. Therefore, since the effect of the increase in E is largely compensated by the increase in ρ, the increase in v can be no greater than 1%. Mayer and Gigon[9] find that v is virtually identical for quartz and fused silica. Therefore it is probable that the actual change in v is extremely small. We therefore conclude that the origin of the radiation-induced increase in K resides in the effective phonon relaxation length l.

Klemens[10] has proposed a theory which adequately accounts for the temperature dependence observed by Berman[5] in vitreous silica and other glasses. At higher temperatures (> 20°K) he finds that heat is carried predominantly by high-frequency phonons with a nearly constant mean free path l whose magnitude is approximately equal to the dimension (7 Å) of the fundamental structural unit, namely, the SiO_4 tetrahedron. In this temperature range, K is approximately proportional to c, as has also been pointed out by Kittel.[11] At lower temperatures (< 20°K), low-frequency phonons of wavelength λ much larger than the unit cell become an important part of the phonon distribution. The longitudinal branch of the low-frequency phonons may be treated on the basis of plane-wave propagation, and they are scattered by structural irregularities much

[8] F. Simon and F. Lange, *Z. Physik* 38, 227 (1926).

[9] G. Mayer and J. Gigon, *J. Phys. radium* 18, 109 (1956).

[10] P. G. Klemens, *Proc. Roy. Soc. (London)* **A208**, 108 (1951).

[11] C. Kittel, *Phys. Rev.* 75, 972 (1949).

greater in size than the unit cell. Although he does not specify the nature of such irregularities, it seems reasonable to identify them with strained regions or density fluctuations frozen into the glass during solidification.

The contribution to K of the low-frequency longitudinal phonons is characterized by their density and their value of l. Calculations of Klemens show that this contribution K_I rises linearly with temperature from $T = 0$ to a maximum value near 8°K for vitreous silica and then falls with increasing temperature according to $T^{-1/2}$. When superimposed on the contribution due to the transverse branch and the high-frequency phonons (K_{II}), it accounts for the hump on the K vs T curve observed by Berman[5] in the helium temperature range.

There does not appear to be a sensitive dependence of K_I on density in the theory.

In the previous paper[12] it was suggested that fast-neutron bombardment largely destroyed the quenched-in strain pattern or fluctuations in density initially present. This hypothesis seemed reasonable, since for large exposures each region of the specimen would have been subject to extensive atomic displacement and ionization effects which would tend to homogenize the material. However, in view of the complete recovery of K on annealing, this hypothesis is applicable only if the fluctuations in density, expected thermodynamically, that are introduced at 925°C have the same spatial pattern as the fluctuations present before bombardment. It is possible that such a situation could arise, provided the rate of cooling from the molten state is sufficiently slow. Additional experiments relating to the effect of quenching from high temperatures (>925°C) on K would either prove or disprove this explanation.

An alternative possibility is that appreciable order is established in the regions affected by each neutron collision. The size of such regions has been estimated variously[13] as containing 10^4 to 10^6 atoms for large energy transfers from a fission neutron. Moreover, Wittels and Sherrill[2] have found that on heavy neutron exposure ($\sim 2 \times 10^{20}$ n_f/cm^2) vitreous silica reverts to microcrystalline α-quartz on annealing above 900°C. This observation may be taken as evidence for an increase in order within the damaged regions, but it seems that higher exposures than those used here are necessary for the ordering to become more firmly established on annealing.

The manner in which an increase in order on this scale will affect K is not clear at the present time; however, an increase in relaxation length of the long-wavelength transverse phonons would give rise to a much greater temperature dependence ($\sim T^3$) of the increase in K. Therefore it would appear that only the longitudinal phonons are affected.

In summary it has been found that the increase of K at low temperatures in irradiated vitreous silica tends to saturate at the same exposure required for saturation of the density increase. Annealing at 925°C for 9 hr restores both K and ρ to their initial values. The increase in K appears to be connected with an increase in l governing the low-frequency longitudinal contribution K_I of Klemens' theory. A possible explanation of this behavior is that irradiation levels the density fluctuations initially present in the glass and that a similar strain pattern is introduced by the anneal. It is equally probable that an annealable increase in order, not presently understood, is imposed on the glassy matrix by irradiation and that this causes the increase in K at low temperatures.

[12] A. F. Cohen, *J. Appl. Phy.* 29, 591 (1958).

[13] H. Brooks, *Ann. Rev. Nuclear Sci.* 6, 215 (1956).

THERMAL CONDUCTIVITY OF MONOISOTOPIC IONIC CRYSTALS (SODIUM FLUORIDE AND CESIUM IODIDE) AT LOW TEMPERATURES

A. F. Cohen

The thermal conductivity, K, of single crystals of NaF was measured at low temperatures. In the best crystal, K_{max} was ~ 30 w·cm^{-1}·deg^{-1} at a temperature T_{max} of $\sim 17°$K. This crystal exhibited the exponential behavior expected at $T > T_{max}$ for crystals free of isotope scattering. In comparing K (from 3 to 30°K) of NaF crystals from different sources with nearly the same chemical purity, it appears that strains and grown-in defects[1] are important factors limiting K. In CsI the exponential behavior is observed at $T > 11°$K; however, at the lowest temperatures, K appears to be limited by the large density of dislocations present in this plastic crystal. In CsI containing 0.1% thallium, the impurity scattering as well as dislocations limit K. Upon thermal annealing of the thallium-doped crystal, K is increased somewhat, indicating partial annealing of dislocations.

[1] M. Moss, R. L. Sproull, and H. Weinstock, *Bull. Am. Phys. Soc.* 3, 126 (1958).

STORED ENERGY IN IRRADIATED GRAPHITE

M. S. Wechsler
R. R. Coltman
R. H. Kernohan
M. C. Wittels

The stored energy of graphite taken from the lattice of the ORNL Graphite Reactor was measured by a new technique. The method depends upon the transfer of heat by radiation between the walls of the calorimeter and the sample. The Stefan-Boltzmann radiation law is used to calculate the difference in the amount of heat received by the sample in two successive heating runs. This difference in heat gives a direct measure of the stored energy.

The experimental apparatus is shown in Fig. 51. The irradiated graphite sample was suspended in a copper can by duplex copper-constantan thermocouple wire, the junction of which was embedded in the sample. The thermocouple was removed from the assembly through a vacuum seal, and its output was fed to a temperature recorder. In addition, the temperature of the copper can was measured by recording the output of a thermocouple soldered to the outer wall of the can. A temperature-controlled oil bath, maintained at 199.1 ± 0.3°C, was mounted below the calorimeter on a platform attached to a motor-driven screw jack. For all runs, the bath was raised about the calorimeter can at the same rate. For each determination of the stored energy, two runs were made. The temperature vs time curve for the sample in the irradiated condition (first run) is given by T_1 in Fig. 52, and the corresponding curve for the second run is given by T_2.

The evacuated calorimeter can comprises a cavity whose interior walls are at a uniform temperature T_W. As such, the exchange of heat between the sample and the can is governed by the Stefan-Boltzmann radiation law. Since the initial and final temperatures are the same for the two runs, it can be shown[1] that the stored energy released during the first run is given by

$$(1) \qquad Q_{SE} = Ae\sigma \int_{t_i}^{t_f} (T_1^4 - T_2^4)\, dt \ ,$$

where A and e are the surface area and emissivity of the sample, σ is the Stefan-Boltzmann constant, T_1 and T_2 are the temperatures during the first and second runs, and the limits of integration t_i and t_f are times indicated in Fig. 52. The emissivity of the graphite was evaluated from the temperature-time curve of the second run by

[1] M. S. Wechsler *et al.*, *J. Appl. Phy.* (to be published).

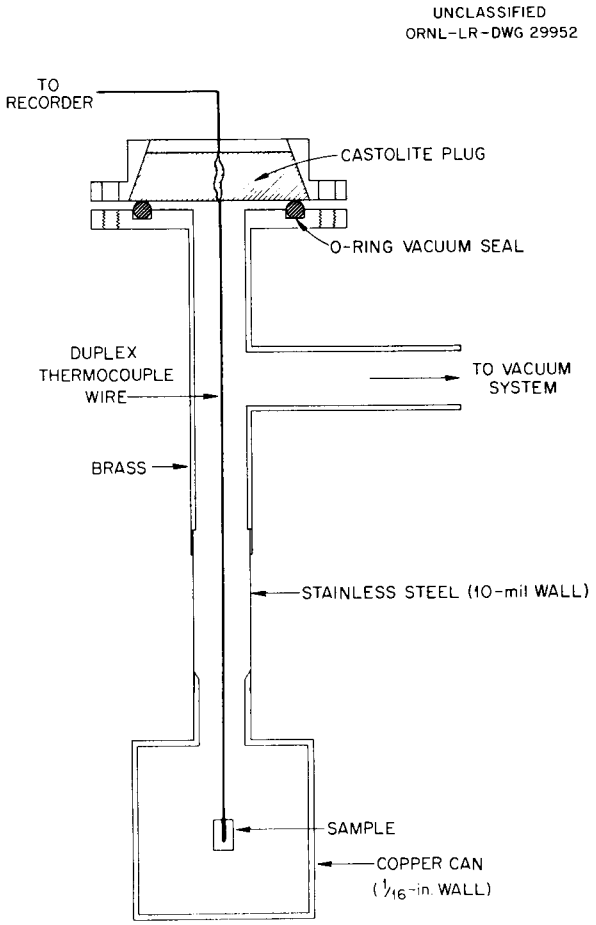

Fig. 51. Radiation Calorimeter for Measurement of Stored Energy.

using the expression

$$e = \frac{mc_p\, dT_2/dt}{A\sigma(T_W^4 - T_2^4)} ,$$

where m is the mass of the sample. The specific heat of the graphite, c_p, was calculated from the results of Kelley.[2] The value obtained for the

[2]K. K. Kelley, *U.S. Bur. Mines Bull.* No. 371 (1934).

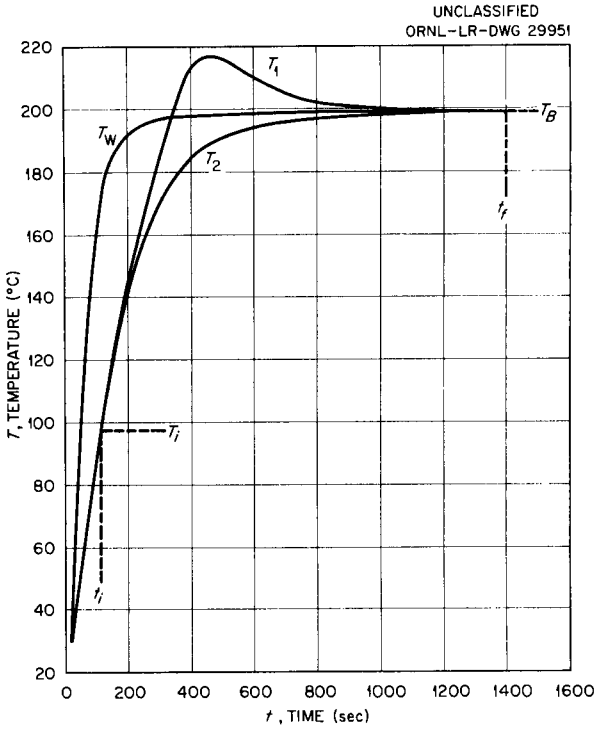

Fig. 52. Temperature vs Time Curves for Irradiated Graphite.

emissivity was $e = 0.85 \pm 0.06$. A correction to Eq. 1 arises from the difference in heat conduction losses along the thermocouple leads in the first and second runs. It can be shown that this correction is less than 2% of the stored energy released upon heating to 217°C.

Two samples were investigated for which the total integrated neutron flux was estimated to be 3×10^{20} neutrons/cm^2. The average temperature of irradiation was 45°C. The stored energy released upon heating to 217°C was 25.5 cal/g for the first sample and 26.1 cal/g for the second sample. These results compare favorably with those obtained on similar samples by other methods of measurement.

STUDIES ON GRAPHITE FROM THE ORNL GRAPHITE REACTOR

M. C. Wittels F. A. Sherrill

Introduction

Measurements on graphite from the ORNL Graphite Reactor have been conducted at the following laboratories: Solid State and Operations Divisions of the Oak Ridge National Laboratory, National Bureau of Standards, and Brookhaven National Laboratory. At each of these laboratories, different methods of measurement were employed so that independent analyses would be available. The samples were cored from the most severely damaged region of the graphite stack for the purpose of determining the most serious situation that exists. In addition, the measurements were designed to determine the validity of c_0 spacing correlations in stored energy estimates which have been employed in evaluating the state of the reactor.

Measurements at Oak Ridge National Laboratory

Radiation Calorimetry. – The stored energy to 218°C was measured in core samples taken from fuel channel 1766 at a distance of 6 ft 8 in. from the east face of the graphite stack. The measurements gave 26 cal/g, with an estimated accuracy of ±10%, in two separate runs. A radiation calorimeter[1] was employed in these experiments, and a brief description of the apparatus and method is given in another section of this report (see "Stored Energy in Irradiated Graphite").

The temperature-time curves for one of these experiments are shown in Fig. 52. It is noted that energy is released at temperatures as low as 120°C, and at approximately 165°C the slopes of the two curves begin to differ sharply. It should be noted that at temperatures near or above 120°C, stored energy is released under time periods as short as minutes. It is therefore reasonable to assume that substantial annealing would take place at these low temperatures for more extended but still reasonable times of, say, one day. Evidently, 165°C is the approximate temperature at which the specific heat of the damaged graphite becomes "negative" and a spontaneous energy release is propagated. The temperature rise from 165 to 218°C was completed in less than 3 min, and more than 95% of the entire release of stored energy was completed in approximately 10 min. These observations are interesting in considering the effects of spontaneous releases under actual reactor conditions where heat transfer by conduction and convection would contribute to even further restrictions in temperature excursions. A graphical plot of the numerical integration is shown in Fig. 53.

X-Ray Lattice Parameter Measurements. – Temperature traverses (see the next section of this paper) of the graphite stack by the Operations Division have revealed the north half of the reactor to be operated at the lowest temperatures. For this reason, fuel channel scrapings have been taken from channels 3268 and 3368, as well as from channels 2168 and 2768, which are contained in the middle horizontal plane of the stack, so that a series of c_0 spacings could be measured in the cool, high-flux portions of the reactor. These scrapings were taken from the upper portion of the fuel channel, above the fuel elements (Fig. 54). Shown in Fig. 55 is the east loading face with numbered channels. Channels are located by combining numbers, first horizontally and then vertically, to give a four-digit designation. Thus No. 1868 is the center channel of the reactor. The x-ray measurements have been completed, and estimates of the stored energy content to 250°C are shown in Fig. 56. It is noted that the c_0 spacings show the largest expansion (and therefore the most damage) at 6 to 7 ft from the cold east face of the graphite stack. The somewhat broadened curve for fuel channel 2768 is in large part due to a more extensive fuel loading in that channel, while the peculiar configuration for fuel channel 3268 in the 16-ft area is due to a control rod position. Fuel channel 3268 lies in the extreme northern row of channels; therefore it is apparent that the peak position for damage in this channel follows the flux distribution. According to the x-ray estimates, however, there is no stored energy at this extremity of the reactor which could be released spontaneously. Scrapings from channel 3368, which is 8 in. into the reflector region of

[1] M. S. Wechsler *et al.*, *J. Appl. Phy.* (to be published).

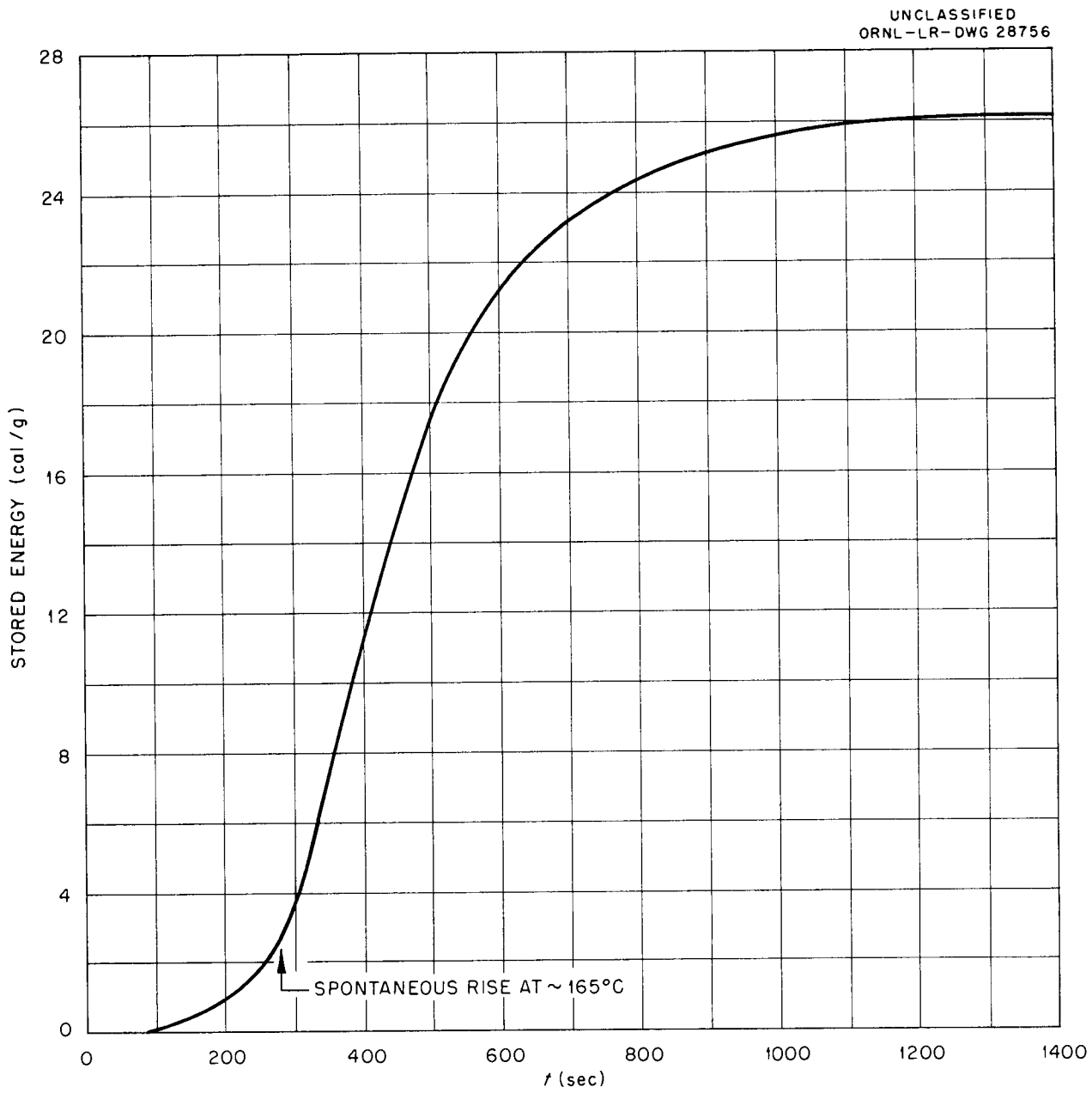

Fig. 53. Release of Stored Energy from Irradiated Graphite.

the stack, showed no significant damage within the limits of detection.

The region of the reactor containing the highest damage was therefore established by x-ray measurements, and solid cores were obtained from this area by the Operations Division through the use of a remote coring device which could cut upward into the fuel channel (Fig. 54). One such coring (fuel channel 1766, 6 ft 8 in. from the east face of the graphite stack) was examined for variations in damage as a function of distance from the fuel channel surface. Powder specimens for c_0 spacing measurements were obtained by means of jeweler-saw cuttings from spaced intervals along the core (Fig. 54). It is interesting to note that the damage near the fuel channel surface is considerably higher than the bulk damage through the core (Fig. 57). While it is apparent that the

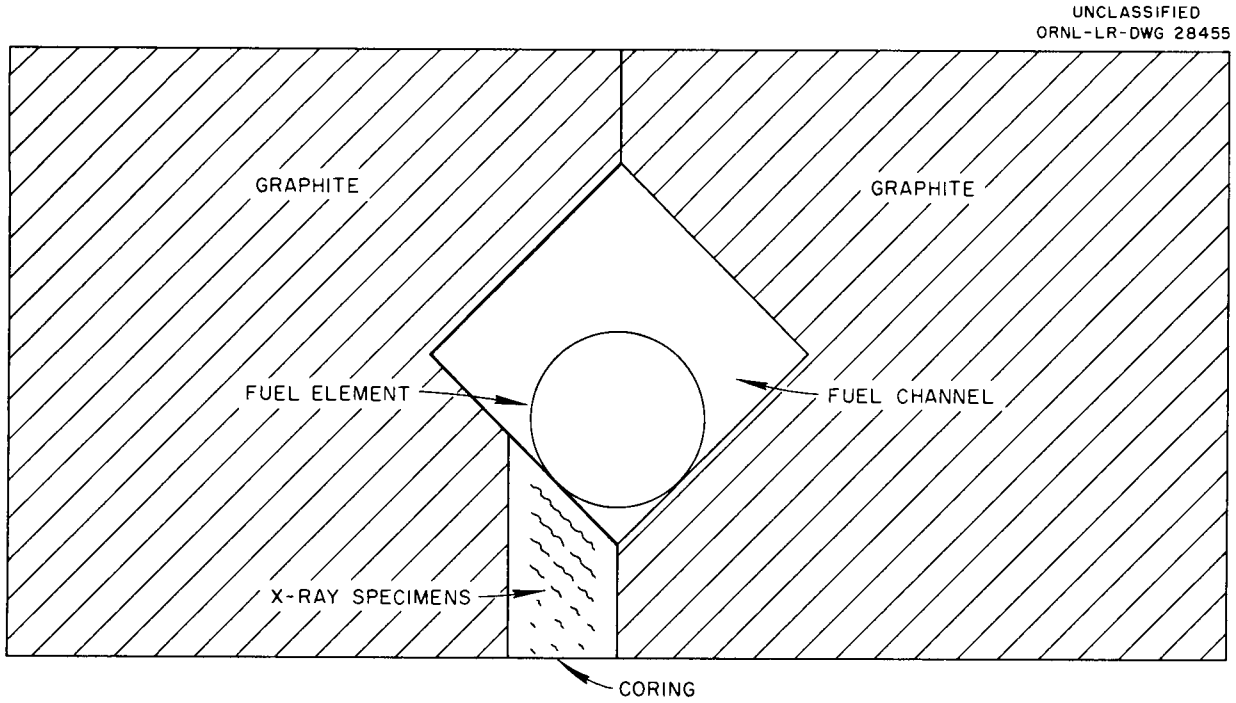

Fig. 54. Section Through a Fuel Channel of the Graphite Reactor.

temperature on the surface is lower as a result of the air stream contact, the temperature gradient into the graphite is not known, and a direct relation between the damage and the temperature is not quantitatively established. For this reason a precise conversion of c_0 spacings to stored energy is not feasible, as was the case for the scrapings, where a more uniform temperature condition exists. In addition to this probable temperature dependence, there exists the likelihood of an enhanced near-surface damage due to the higher concentration of displacements resulting from grazing angle collisions and the neutron mean free path consideration near the core surface. Samples later sent to the National Bureau of Standards were sectioned in an attempt to take these variations into closer account.

Graphite Reactor Temperatures.[2] – Since the growth of stored energy in irradiated graphite is so strongly dependent on temperature, a knowledge of the reactor graphite temperature is vital to a proper assessment of the state of the reactor. Temperature measurements are being compiled from all parts of the ORNL Graphite Reactor so that a complete temperature distribution will be obtained, and, at the present time, some important data are available.

For orientation purposes, it should be recalled that the reactor cooling direction is east to west, parallel to the slug rows. Traverses were made transverse to this direction (N-S) at the center of the reactor, 6 ft east of the center, and 6 ft west of the center; all three traverses were within 1 ft of a horizontal center plane (Fig. 58).

The measurements were made during January and February 1958, when the inlet air temperatures varied between −7 and +8°C, and all the temperatures were normalized with respect to an 85°C value from the continuously monitored position in the center traverse. The inlet air temperature is recorded at +8°C when the continuously monitored position is at 85°C. Higher temperatures in the south half of the reactor are due mainly to the location of the air inlet at the lower right-hand corner of the east face and, secondarily, to a complex flow pattern in the south half of the reactor.

[2] All graphite temperatures, scrapings, and corings were secured by C. D. Cagle and L. E. Stanford of the Operations Division.

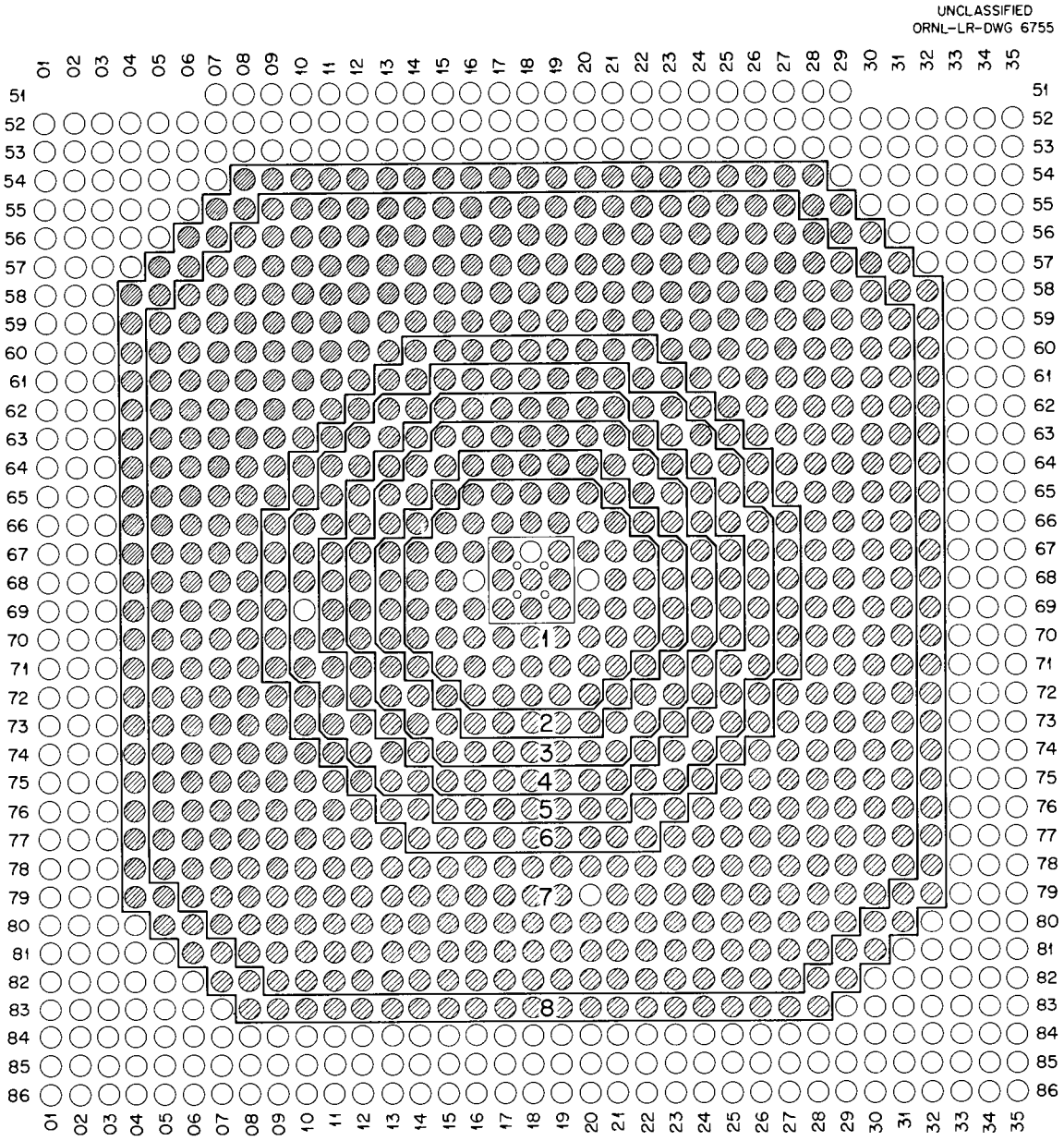

ZONE	NUMBER CHANNELS	NUMBER SLUGS
1	60	41
2	26	45
3	42	51
4	38	51
5	58	54
6	54	54
7	438	54
8	114	47

Fig. 55. Diagram of the East (Loading) Face of the Graphite Reactor.

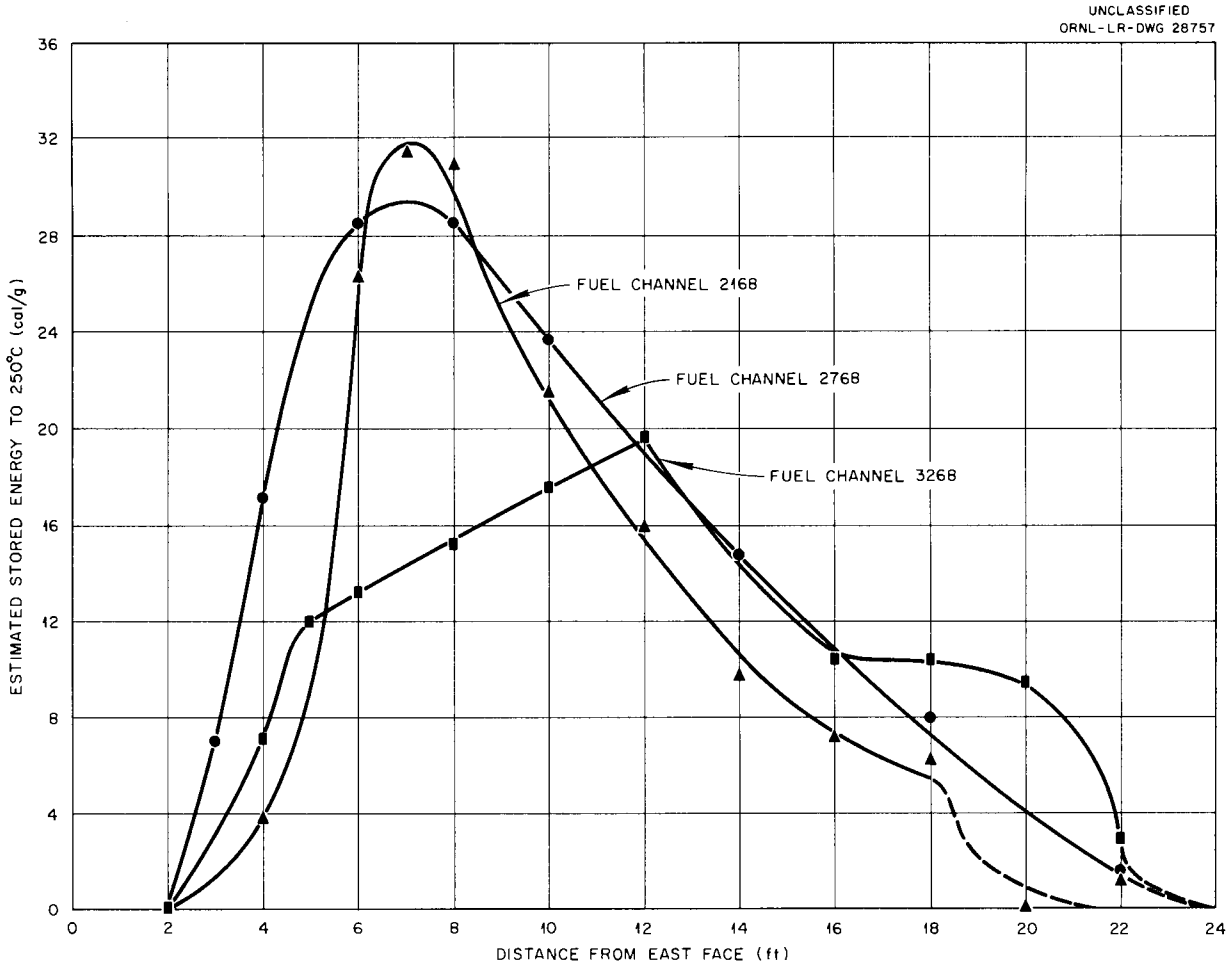

Fig. 56. Distribution of Stored Energy As Estimated from X-Ray Measurements.

It should be emphasized that the temperatures shown in Fig. 58 depict the coldest operating conditions in the reactor and that during the summer months these values are as much as 50°C higher for several positions. Temperature records reveal that on hot summer days with inlet air at 32°C the temperature in the continuously monitored center position reaches levels as high as 138°C, 53°C higher than that shown for a February recording in Fig. 58. This rise, which is considerably larger than the maximum seasonal variation of inlet air temperature, is due to the fact that the reactor power is maintained constant year around (3.4 Mw), and this level is based on the maximum allowable fuel element temperatures during the hottest summer days. The deviation of these temperatures from normal seasonal variations is due to the change in density of air with seasonal temperature changes (as well as to change in specific heat). Also, the volume and flow pattern of coolant air are altered because of the characteristic operational limits of the fans. For several weeks during the summer months, then, a considerable portion of the west half of the graphite lattice is operated at temperatures in excess of 100°C, and the growth of stored energy in that region is greatly diminished. It is observed that the very lowest temperatures are recorded on the north and south edges of the graphite stack, but this effect is

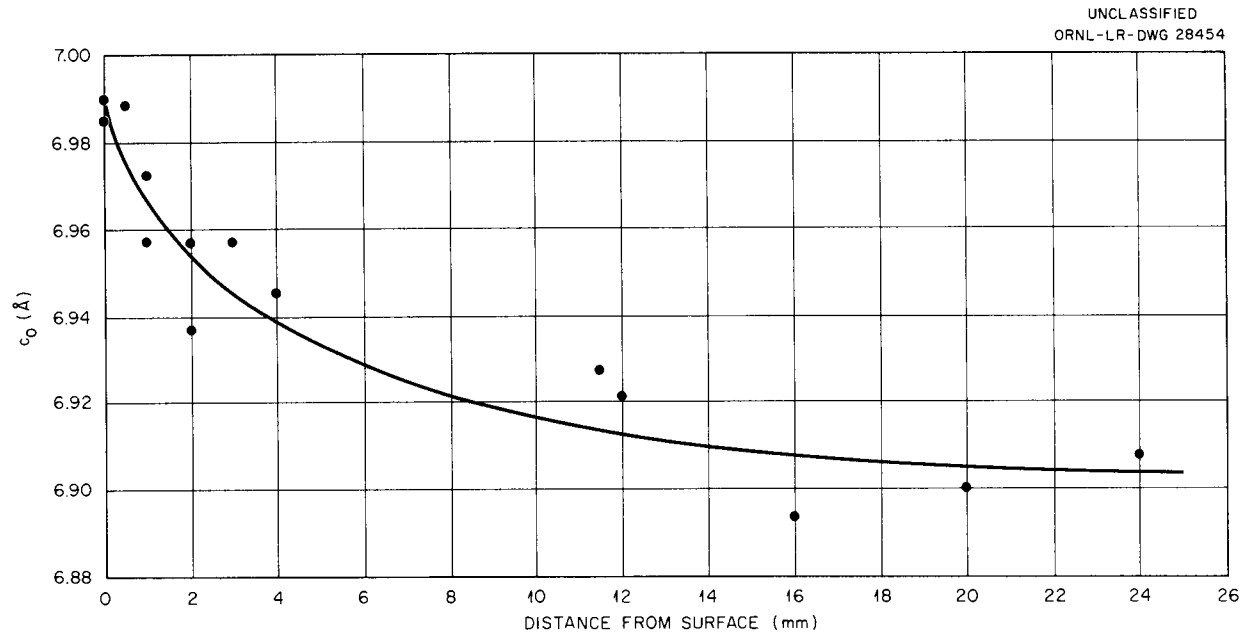

Fig. 57. Lattice Spacing vs Distance from Surface of Fuel Channel.

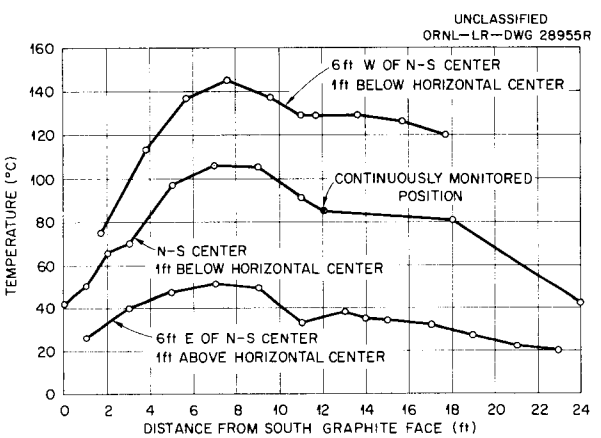

Fig. 58. North-South Graphite Temperature Traverses (Winter).

compensated for, in so far as stored energy is concerned, by the diminished flux (cosine distribution) on the edges of the stack.

Measurements at National Bureau of Standards

Heat of Combustion Measurements. – Total heats of combustion were measured by the thermochemical section[3] of the National Bureau of Standards. These heats include the normal heat of unirradiated graphite plus any increase in internal energy induced by irradiation. For purposes of establishing a standard heat of combustion for graphite from the ORNL Graphite Reactor, corings from the edge of the stringer removed in 1953 were given to the Bureau. The heat of combustion of this graphite was found to be within the limits of error of the determinations for other standard graphites from Hanford and Brookhaven.

As was mentioned previously, cores were sectioned to separate the more highly damaged surfaces from the bulk of the specimens for statistical estimates. Since the Bureau requested samples with masses of 4 to 5 g (although each determination consumes only 1 g), it was impossible to secure from each core a large enough sample that contained only highly damaged surface material. This means that the "top portions" (nearest to fuel element, Fig. 54) of the cores contained only a small percentage (<20%) of highly damaged surface graphite, but the "bottom portions" (farthest portion of core from fuel element, Fig. 54) were more clearly representative of the average condition of fuel channel graphite in the most heavily damaged region of the reactor.

[3] D. D. Wagman, National Bureau of Standards.

Three kinds of specimens were submitted to the National Bureau of Standards: (1) unannealed, (2) annealed to 254°C, and (3) annealed to 400°C. Although the annealing schedule is not directly related to a hypothetical reactor annealing schedule, it furnishes some useful information and will be described briefly.

1. Sectioned samples were drilled and tapped to accommodate a thermocouple in a snug fit at the approximate geometric center of the sample.
2. The samples were contained in stoppered tubes in air and were placed in an oil bath at constant temperature (150°C) for 16 hr.
3. The sample temperatures were monitored and did not exceed this temperature during the interval.
4. In successive stages, the oil-bath temperature was increased 10°C, at a rate of 0.5°C/min, and maintained at these levels for a period of 20 min before proceeding. These steps included stops at 160, 170, 180, and 190°C.
5. The sample temperatures were continuously monitored, and at no time did they exceed the bath temperatures.
6. When the sample temperatures reached 200°C, the tubes were removed from the oil bath and placed in a salt bath at constant temperature (254°C). The rise in sample temperatures was monitored, and the samples were removed when they reached 254°C, in approximately 3 min.
7. Those samples annealed to 400°C were taken from the 254°C bath and inserted in a second salt bath at 400°C, from which they were similarly removed.
8. At no time during these annealing runs were any temperature excursions observed.

The results of the National Bureau of Standards measurements are shown in Table 3. Included in

Table 3. National Bureau of Standards Heat of Combustion Measurements

Standard: unannealed, unirradiated ORNL graphite; heat of combustion, 7839 cal/g

NBS Sample No.	Fuel Channel	Distance from East Face of Graphite Stack	Sample Portion	Annealing Temperature (°C)	Heat of Combustion (cal/g)	Stored Energy Above Anneal Temperature (cal/g)	Stored Energy Below Anneal Temperature (cal/g)
1	1368	6'-2"	Bottom	254	7957	118	Av = 26
2	1368	6'-2"	Top	254	7977	138	
10	1368	6'-2"	Top and bottom	Unannealed	7993	154	
3	1466	6'-8"	Top and bottom	254	7970	131	Av = 31
8	1466	6'-8"	Top and bottom	254	7962	123	
4	1466	6'-8"	Top	Unannealed	7997	158	
7	1566	6'-8"	Bottom	400	7938	99	Av = 59
9	1566	6'-8"	Bottom	400	7940	101	
5	1566	6'-8"	Top	Unannealed	7998	159	
6	1566	6'-8"	Top and bottom	Unannealed	7998	159	
C-2	1666	6'-8"	Top and bottom	401	7940	101	68
C	1666	6'-8"	Top and bottom	Unannealed	8008	169	

Av* stored energy of five unannealed samples = 160 cal/g
Av stored energy to 254°C of four samples = 32 cal/g
Av stored energy to 400°C of three samples = 60 cal/g

*Obtained by taking the combined averages of the residual stored energies for specimens annealed at designated temperatures and subtracting from the combined average for all the unannealed specimens.

the tabulation are the results from fuel channel 1666 which were obtained earlier. Only a few observations concerning these data are necessary at this point, since the results are essentially self-explanatory. Only in the sections from fuel channel 1368 were wide variations found over the length of the core which would confirm the previously described x-ray observations. It was probably fortuitous that 1368-2 was sampled by the National Bureau of Standards in a manner which resulted in a higher proportion of highly damaged surface material than for the other samples. It is also of interest to note that the stored energy above 400°C did not vary by more than 2 cal/g in three measurements and that approximately 100 cal/g remains above 400°C.

Powder samples for c_0 spacing measurements were annealed in the same manner as the cores sent to the National Bureau of Standards, and the results are shown in Fig. 59. It is seen that annealing to 254°C reduces c_0 by only 0.02 Å, just 10% of the preannealed expansion. With an actual reactor annealing, it would be unfeasible to determine exactly what temperatures had been reached for known times in all parts of the reactor; therefore c_0-stored energy correlations following such a reactor anneal would have no meaning. Further, no data are available on the behavior of c_0 under irradiation following such a partial annealing. Consequently, it is clear that x-ray measurements cannot be confidently used to predict stored energy content in an annealed reactor.

Measurements at Brookhaven National Laboratory

Stored Energy and Adiabatic Rise Measurements. – Measurements at Brookhaven National Laboratory[4] were conducted in a double vacuum calorimeter in which the heating conditions are predetermined. A constant heat input is supplied to the system, which has negligible heat losses, so that the furnace temperature rises at the slow rate of 2°C/min and near-adiabatic conditions are achieved. The stored energy and the adiabatic rise were measured in a 7.5-g core, removed from fuel channel 1468 at a distance of 6 ft 2 in. from the east face of the graphite stack. The stored energy to 270°C was found to be 33 cal/g, and the adiabatic rise (105°C) occurred over the temperature span 165 to 270°C (Fig. 60). It was

[4] R. A. Meyer, Brookhaven National Laboratory.

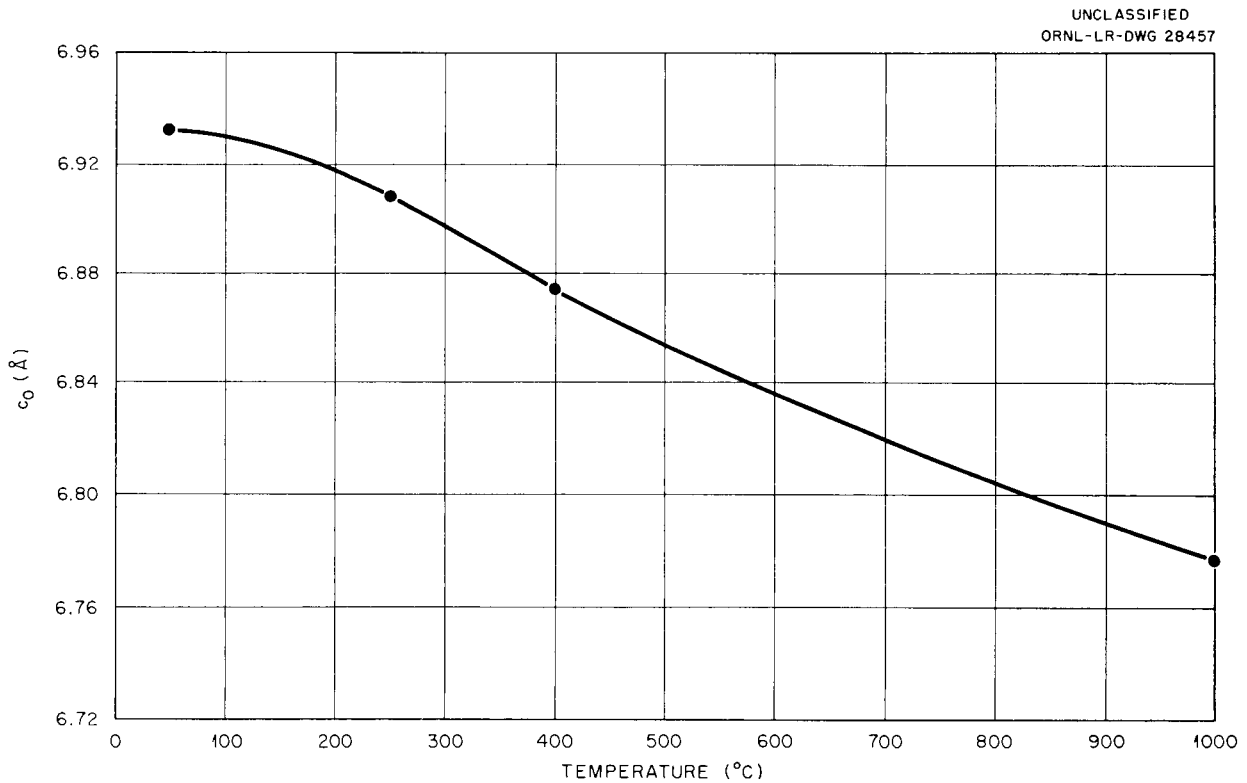

Fig. 59. Effect of Annealing on Lattice Spacing of Irradiated Graphite.

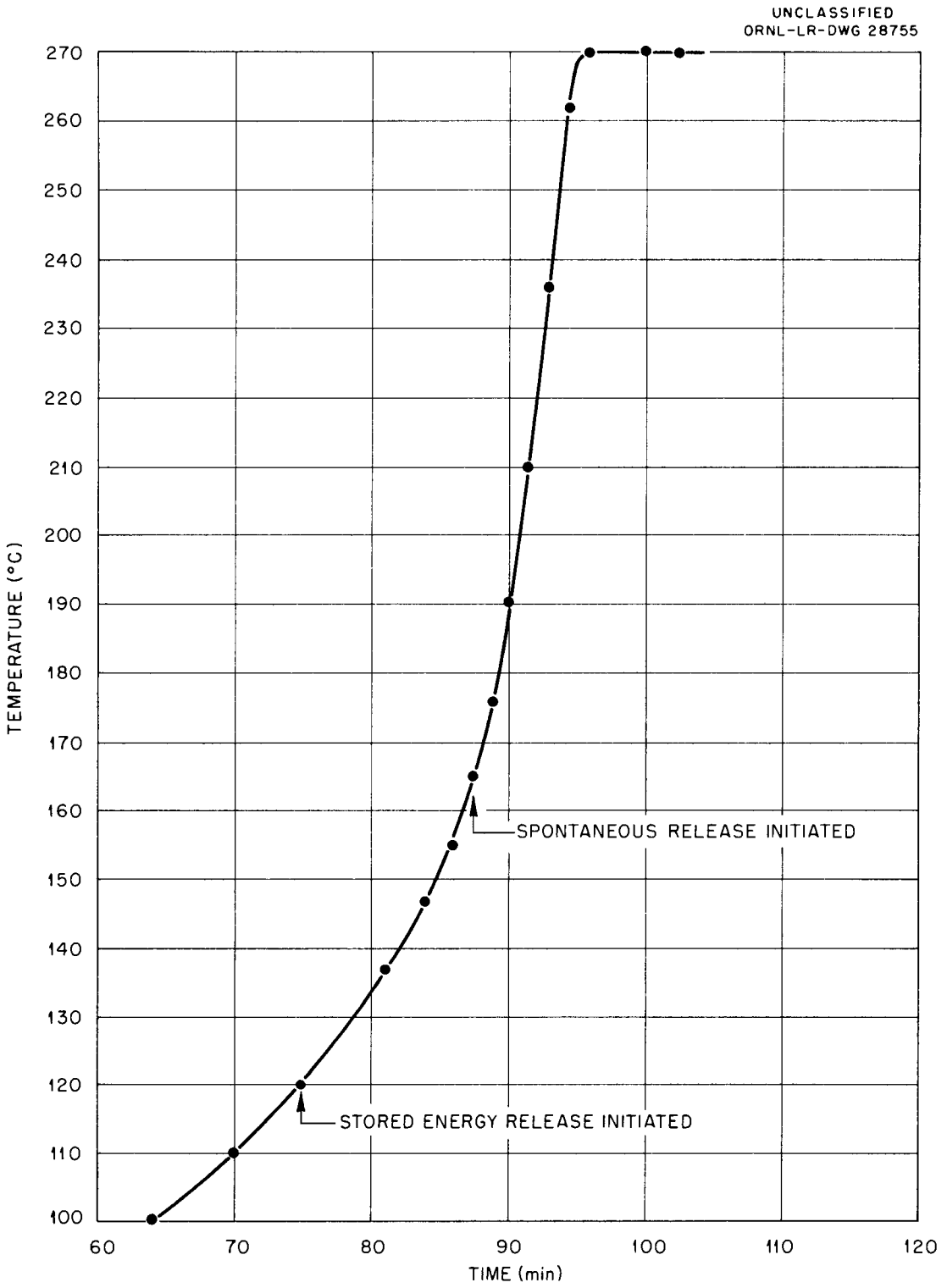

Fig. 60. Release of Stored Energy from Irradiated Graphite (Brookhaven Measurements).

also estimated that the stored energy between 400 and 800°C was about 40 cal/g.

Discussion

From these data it is evident that the ORNL Graphite Reactor is reasonably safe with respect to stored energy content. The favorable agreement of the various kinds of measurements indicates that the recent stored energy estimates from x-ray data are substantially correct and that the growth of stored energy since 1953 is reasonable. Since this growth of the low-temperature peak is only about 2 cal/g per year at the present time, no feeling of emergency should exist, and it is suggested that in any decision to anneal the reactor this margin of safety should be considered. The proposed new fuel loading of the reactor is of primary significance in any consideration for annealing the reactor. For this reason the final decision on new fuel loading should weigh heavily in any decision as to whether, when, and how the reactor should be annealed.

Of somewhat more academic interest is the "reconstructed" release spectrum which is fitted from all the experimental data (Fig. 61). First, it should be noted that the amount of energy above the specific heat curve is small (about 3 cal/g). In addition, the stored energy between 250 and 400°C is considerably higher than that usually exhibited in spectra of graphite irradiated at 30°C. In fact, this reconstructed spectrum has a shape similar to that for graphites from reactors that have been annealed to 250 or 300°C leaving the higher-temperature energy to grow still further. This is *not* to imply that the ORNL Graphite Reactor has been annealed in the past but simply to indicate that this reactor has been favored by higher-temperature operation, especially during the summer months. An inevitable conclusion is that even at temperatures as low as 30 to 60°C

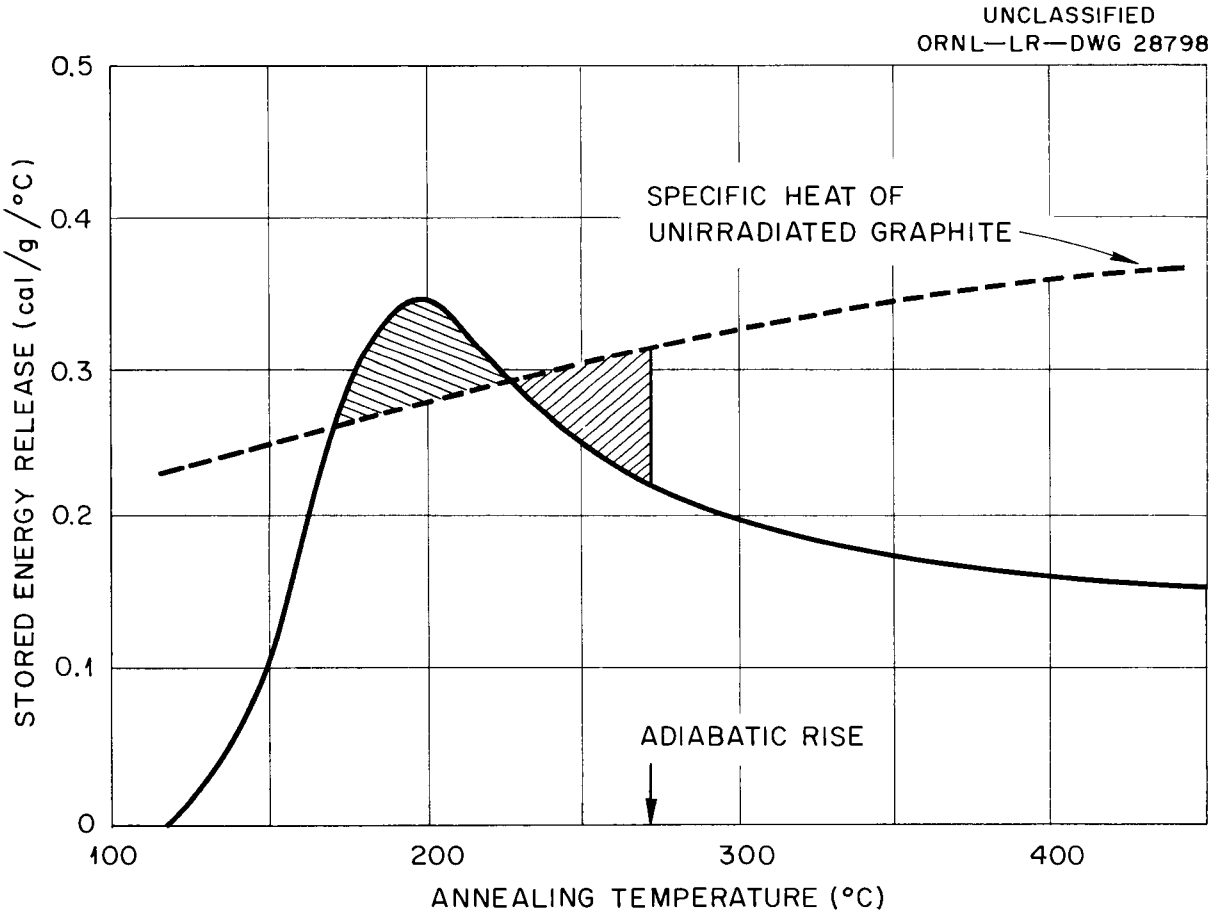

Fig. 61. "Reconstructed" Release Spectrum of Stored Energy.

the growth of stored energy is retarded by only small increases in temperature. Examination of extensive Hanford data in this temperature range reveals that the total stored energy is reduced by about 1% for each 1°C rise in temperature for irradiations similar to that in the ORNL Graphite Reactor.

This conclusion can be confirmed by comparing the ORNL data with data from Hanford,[5] Harwell,[6] and Windscale graphite. Figure 62 shows a comparison of ORNL data with Hanford data for a 30°C irradiation. The significant points to be noted are the small amount of energy above the specific heat curve and the greater amount of stored energy above 350°C in the ORNL sample.

[5]W. K. Woods, L. P. Bupp, and J. F. Fletcher, *Proc. Intern. Conf. Peaceful Uses Atomic Energy, Geneva, 1955* 7, 455 (1956).

[6]G. H. Kinchin, *Proc. Intern. Conf. Peaceful Uses Atomic Energy, Geneva, 1955* 7, 472 (1956).

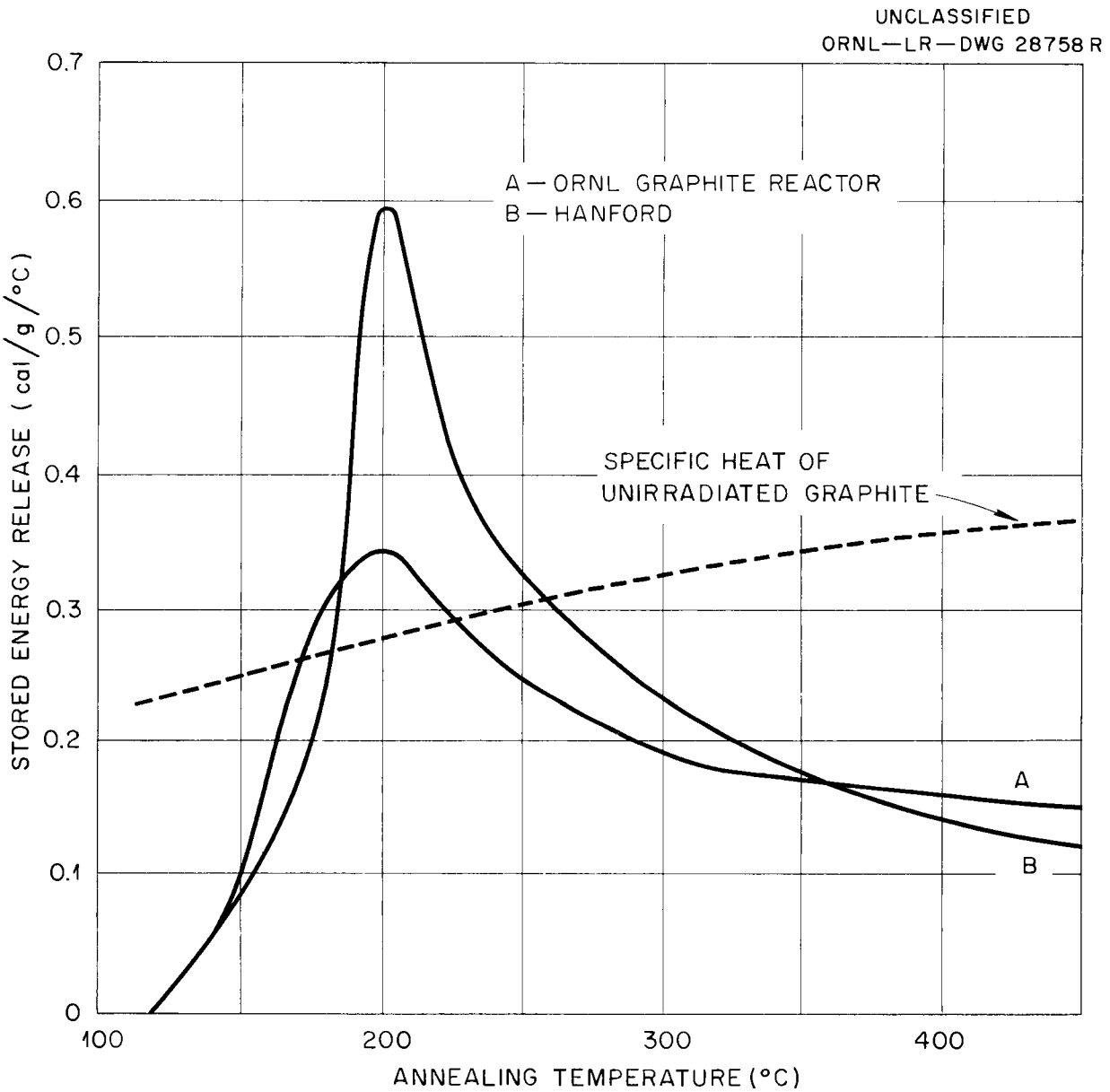

Fig. 62. Comparison of Stored Energy in ORNL and Hanford Graphite.

These can also be seen in Fig. 63, which shows the stored energy retained after various anneals for a Hanford sample irradiated at 30°C and for the ORNL sample. A greater amount of energy is retained above 500°C in the ORNL sample despite the fact that, before annealing, the Hanford sample had about 50 cal/g more total stored energy. Similar results are even more strongly exhibited by comparing Harwell and Windscale data (Figs. 64, 65, and 66). It is therefore clear that temperatures, even in the low range of 30 to 100°C, strongly affect the low-temperature (200°C peak) stored energy in irradiated graphite.

Questions often arise concerning high-temperature stored energy, released at temperatures above 400°C and up to 1800°C. Frequently, the high values associated with these stored energies are misleading, and they are meaningful only when they are referred to release spectra for known heating rates and to the specific heat curve for unirradiated graphite. Fortunately, between 400 and 1000°C the energy release spectrum

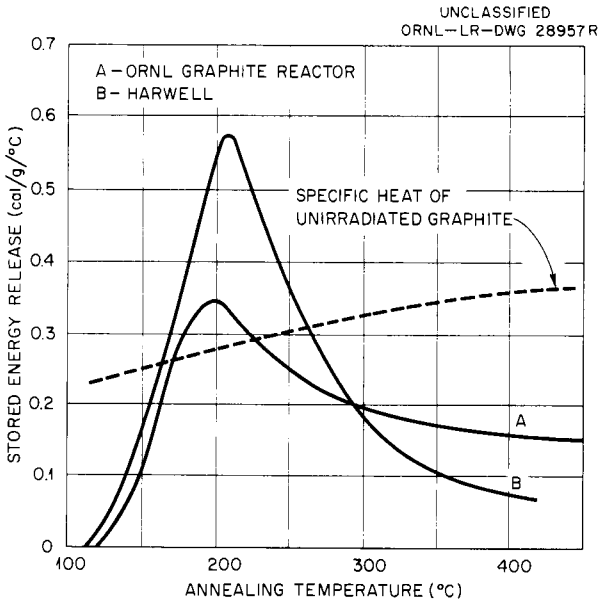

Fig. 64. Comparison of Stored Energy in ORNL and Harwell Graphite.

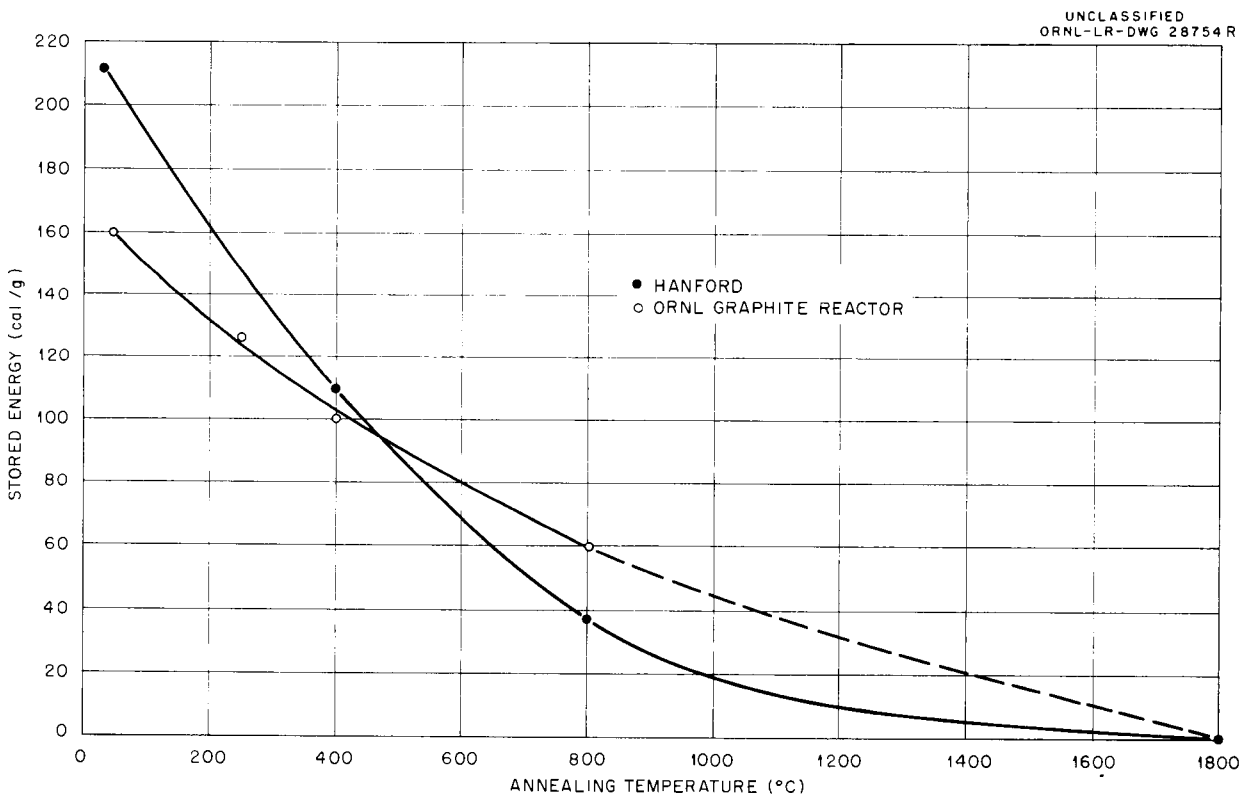

Fig. 63. Stored Energy Retained After Annealing of ORNL and Hanford Graphite.

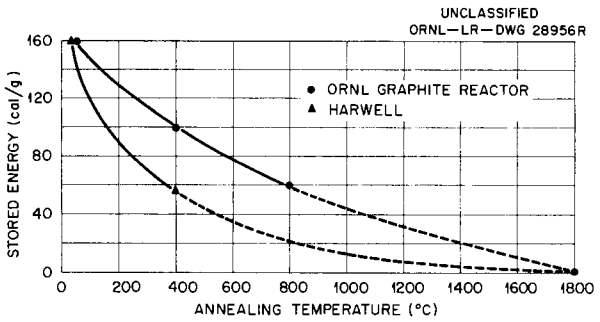

Fig. 65. Stored Energy Retained After Annealing of ORNL and Harwell Graphite.

is a rather smooth, shallow function that falls further away from the specific heat curve of unirradiated graphite with increasing temperature. This means that dangerous, spontaneous releases at these high temperatures cannot occur without violation of the second law of thermodynamics. In speaking of reactor safety, then, the concern should be with the energy release spectra in the low-temperature region (200°C), where energy may be released adiabatically. The fact that ORNL graphite contains 40 cal/g from 400 to 800°C and 60 cal/g from 800 to 1800°C is of no consequence to the safety of the reactor, and

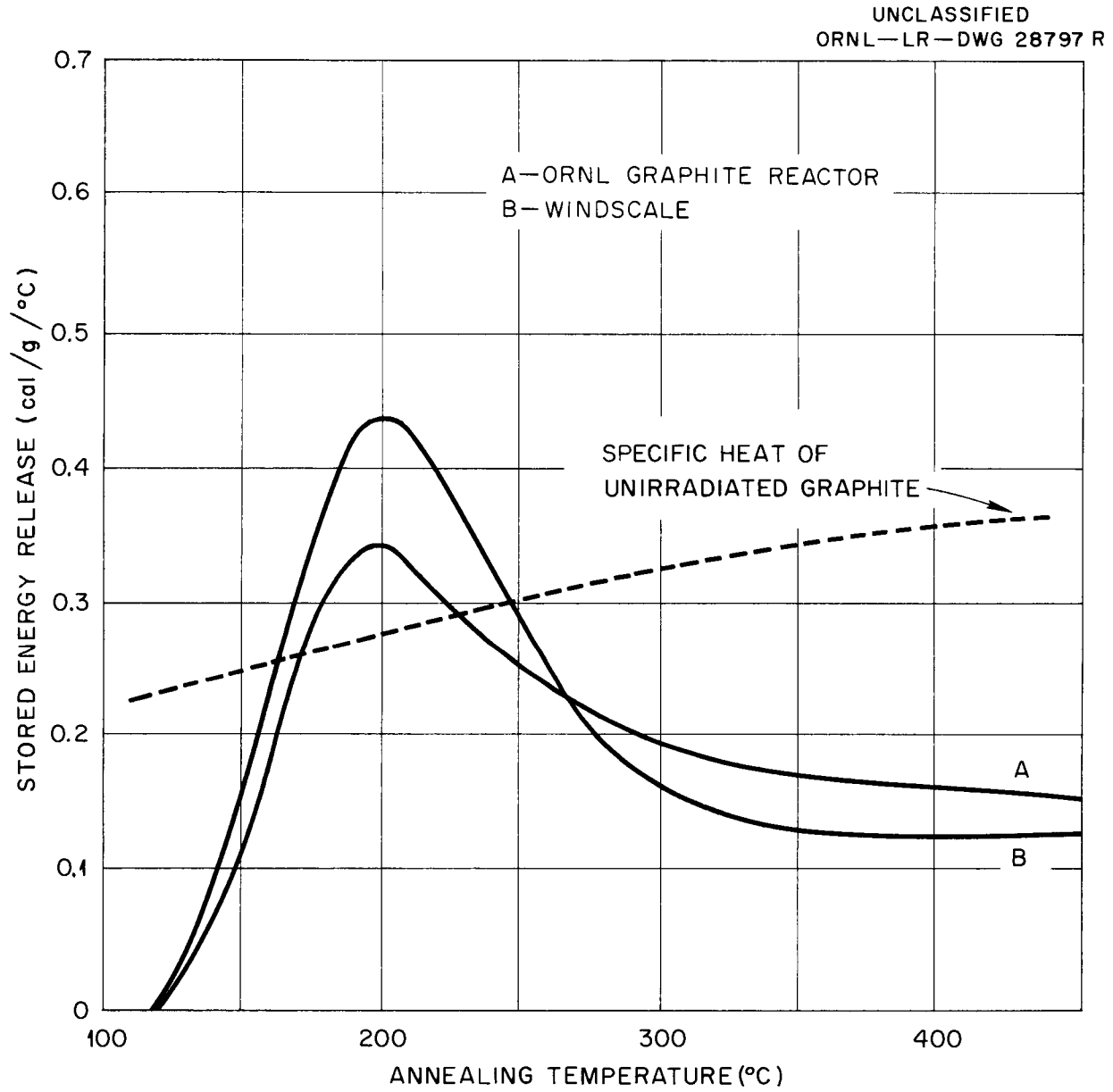

Fig. 66. Comparison of Stored Energy in ORNL and Windscale Graphite.

measurements of total stored energies should be considered in this light.

In order to determine the effect of a rather low-temperature anneal for potential reactor annealing procedures, a sample was annealed at 165°C for 18 hr, the temperature being monitored continuously, and the stored energy to 220°C was remeasured. It should be noted that during the 18-hr anneal no temperature excursions were observed. The resultant spectra are shown in Fig. 67 and indicate that higher-temperature anneals, say in the vicinity of ~225°C, would be necessary to reduce the hump that approaches the specific heat curve. Estimated regions of the graphite stack that contain negative specific heat are shown in Fig. 68. The boundary conditions used in this estimate are (1) integrated neutron flux greater than 2×10^{20} *nvt* and (2) maximum graphite temperatures of 50°C. From

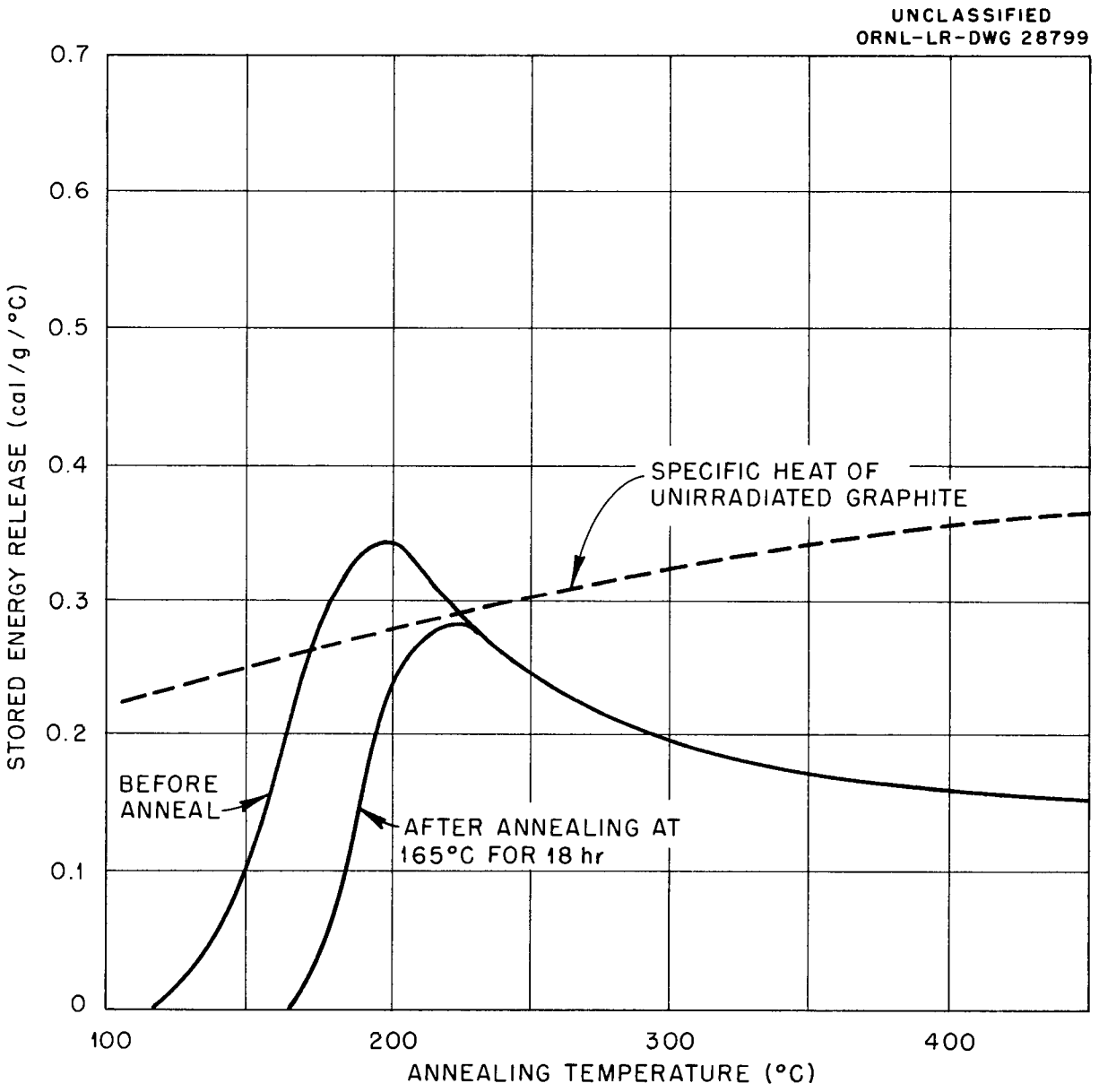

Fig. 67. Effect of Annealing on the Stored Energy Release Spectrum.

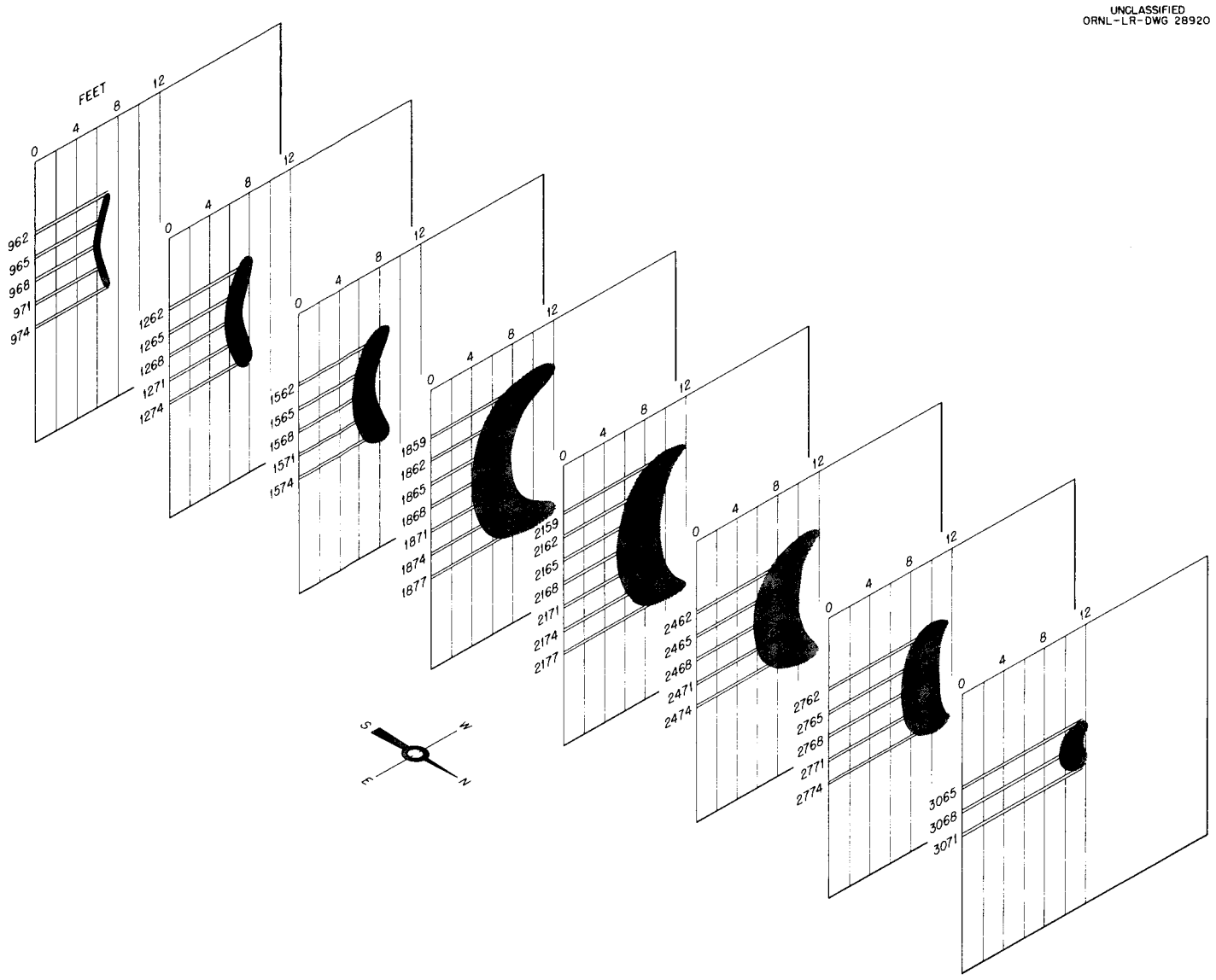

Fig. 68. ORNL Graphite Reactor Sections Containing Estimated Regions of Negative Specific Heat.

this approximation it appears that only about 5% of the stack is damaged to the extent that a spontaneous energy release could be propagated.

The results of this investigation clearly show that the stored energy content of the ORNL Graphite Reactor presents no hazard and that a safe condition exists. It is also clear that operating temperatures, even lower than 100°C, are important in affecting the growth of the 200°C stored energy peak.

YOUNG'S MODULUS AND INTERNAL FRICTION STUDIES

D. O. Thompson D. K. Holmes

During the past year studies of the Bordoni peak structure[1-5] in copper have been more or less completed, at least for the present. The results of the experiments have been rather gratifying in that it is felt that some advancement toward an understanding of the role of dislocations in the internal friction process has been made. These results will soon be presented in the open literature, so that only a short summary will be given here.

It has been found that it is possible to divide the experimental internal friction vs temperature curve of lightly cold-worked crystals into two parts, namely, a relaxation part which is dominant below about 125°K and a background part which is dominant above this temperature to room temperature. There is, of course, some overlap of the two parts about this temperature. The theoretical details of a single dislocation relaxation process have been studied by Seeger and Donth. In the present work it is shown that the low-temperature Bordoni relaxation spectrum is probably considerably more complex than originally thought. There seem to be at least four principal relaxation processes in the low-temperature range, and probably more which increase with added cold work. This result is in contrast with earlier results in which it was thought that there were two principal processes. The present results alleviate the obvious difficulties of Seeger's theory. A tentative identification of the relaxation peaks with the different types of dislocations can be suggested, but it is subject to revision pending further results, both theoretical and experimental. Further confidence in the decomposition of the Bordoni spectrum, which has been attempted for lightly worked single crystals, is gained when the sum curve of all the relaxation processes is compared with a Bordoni peak measured from a hard-drawn polycrystalline sample. The sum curve reproduces the polycrystalline curve in a fairly satisfactory manner. It is interesting to note that the smallest Peierls force obtained in these measurements is about the same as the critical shear stress for copper of the same nominal purity obtained by Blewitt.[6]

The background component of the internal friction and Young's modulus, as separated out in the present work, seems to be intimately related to the relaxation process. In the first place, it seems to become important at temperatures just slightly higher than the afore-mentioned relaxation processes, and second, the activation energy as determined from a rather simple theory is about twice the kink energy obtained from the relaxation processes. This may be a significant result. The background internal friction seems to be associated with a dislocation motion which can be described by Koehler's string model;[7] however, no details as yet can be given as to how the formation of kink pairs merges into a bowing-out process.

It should be pointed out that neutron irradiation has essentially made these studies possible, for it provides a means by which the dislocation component can be quenched. The sample can then be

[1] P. G. Bordoni, *Ricerca Sci.* 19, 851 (1949).

[2] P. G. Bordoni, *J. Acoust. Soc. Am.* 26, 495 (1954).

[3] D. H. Niblett and J. Wilks, *Phil. Mag.* [8]1, 415 (1956).

[4] A. Seeger, H. Donth, and F. Pfaff, *Discussions Faraday Soc.* 23, 19 (1957).

[5] H. Donth, *Z. Physik* 149, 111 (1957).

[6] T. H. Blewitt, *Phys. Rev.* 91, 1115 (1953).

[7] J. S. Koehler, in *Imperfections in Nearly Perfect Crystals*, p 197, Wiley, New York, 1952.

measured without any appreciable effective dislocation content.

In addition to the above results, bombardments at liquid nitrogen temperature upon copper crystals have been made. These experiments are yet in their early stages, but the results appear promising. A reduction in damping at liquid nitrogen temperature has been observed, in contrast with results reported by Barnes and Hancock.[7] In addition, evidence for a radiation-produced defect mobility has been obtained for the –30 to –40°C temperature interval.

It is presently planned to extend the cold-working studies to some of the body-centered cubic metals during the next year. This problem may be of importance, for it is thought that these metals should exhibit much larger Peierls forces than the face-centered cubic group. In addition, it is planned to continue the bombardments at liquid nitrogen temperature.

[7] R. S. Barnes and N. H. Hancock, *Phil. Mag.* [8]3, 527 (1958).

NEUTRON DAMAGE EFFECTS IN METALS AT LOW TEMPERATURES

T. H. Blewitt[1] R. R. Coltman, Jr. C. E. Klabunde
D. K. Holmes J. K. Redman

The low-temperature group has continued in its efforts to obtain a basic understanding of the mechanisms by which reactor neutrons change the properties of metals.

Earlier work by Blewitt *et al.* has clearly established that there is a very strong temperature dependence of the critical shear stress for neutron-irradiated copper crystals.[2] These results were obtained from measurements made in baths at various fixed temperatures, including liquid helium and nitrogen, dry ice and acetone mixture, and liquid Freon. A somewhat more detailed examination of this temperature dependence between the liquid nitrogen point (78°K) and the liquid helium point (4.2°K) is of particular interest from a theoretical standpoint. To obtain this information the critical shear stress of a high-purity copper single crystal irradiated at reactor ambient temperature to a flux of 1×10^{18} *nvt* was measured at several temperatures between 8 and 260°K. The resulting curve is shown in Fig. 69. The temperature was monitored by a copper-constantan thermocouple soldered to the free end of the single-crystal tensile specimen. A vacuum jacket was placed around the tensile rig so that it could be thermally isolated from the liquid helium bath. To cool the tensile rig and specimen, helium exchange gas was introduced into the vacuum jacket and later pumped out. A small resistance heater was used to warm the specimen and tensile rig to a given temperature after the initial lowest temperature measurement and the removal of the helium exchange gas.

The measured values for the critical shear stress as a function of temperature are shown in Fig. 70, in which an attempt at fitting the data with a theoretical curve is also shown. The theoretical form is obtained[3] by assuming that for yielding, dislocation lines must break through barriers introduced

[1] T. H. Blewitt is presently on leave for a year in Harwell, England.

[2] T. H. Blewitt *et al.*, in *Creep and Recovery*, p 84–110, American Society for Metals, Cleveland, 1957.

[3] T. H. Blewitt *et al.*, *Solid State Ann. Prog. Rep. Aug. 31, 1957*, ORNL-2413, p 9.

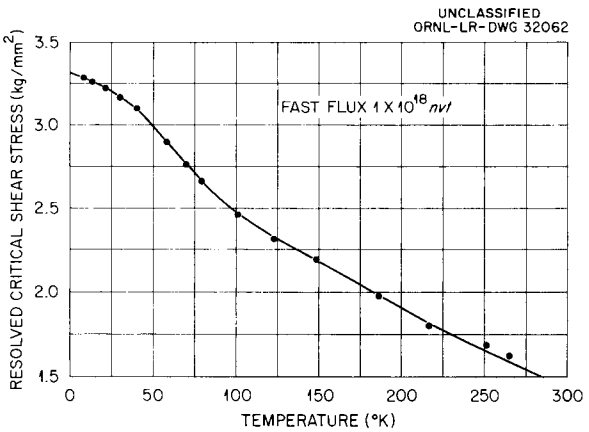

Fig. 69. Plot of Yield Stress vs Temperature for Irradiated Copper Single Crystal.

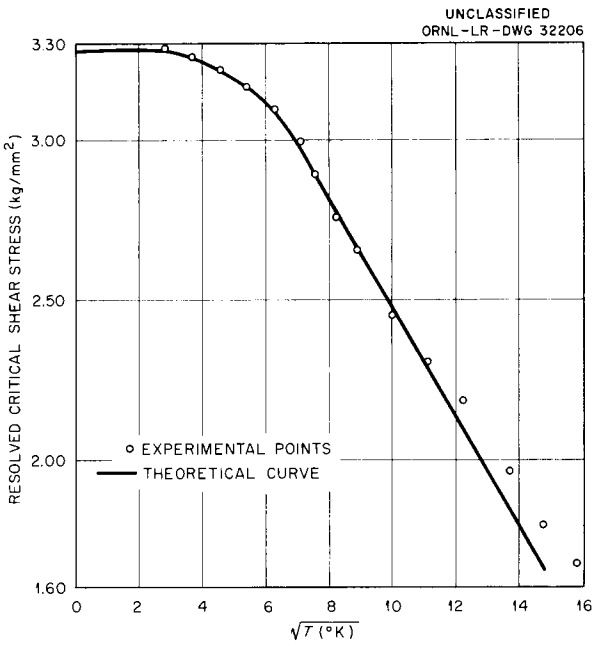

Fig. 70. Plot of Yield Stress vs $\sqrt{T}$ for Irradiated Copper Single Crystal.

by the neutron irradiation. On an average basis it may be imagined that a barrier can withstand a force from the dislocation up to a value F_0, at which force the dislocation breaks through the barrier. The critical shear stress is obtained by equating the barrier strength, F_0, to the sum of the applied force and the extra force due to the thermally induced oscillations of the dislocation line,

$$F_0 = F_\sigma + F_T \quad . \tag{1}$$

If L is the average spacing between barriers,

$$F_\sigma = \sigma b L \quad , \tag{2}$$

where b is the Burgers vector of the dislocation. From Leibfried's analysis[4] we have

$$F_T = \sqrt{\overline{F^2}} = \left[\sum_{n=1}^{M} \left(\frac{\hbar\omega_n}{2} + \frac{\hbar\omega_n}{e^{\hbar\omega_n/kT} - 1} \right) \right]^{1/2} , \tag{3}$$

where

$M = L/a$,

a = the lattice parameter,

$\omega_n = (n\pi/L)\sqrt{M/2\rho}$,

ρ = density.

The average force squared, $\overline{F^2}$, has the following limited forms:

$$\overline{F^2} \cong \begin{cases} (\mu b)\, kT & \text{at high temperatures} \\ (\mu b)\,(0.14)\, k\Theta & \text{at low temperatures} \end{cases} , \tag{4}$$

where μ is the shear modulus and Θ is the Debye temperature. Solving Eq. 1 for the critical shear stress, we obtain

$$\text{CSS} = \sigma = \frac{F_0}{bL}\left(1 - \frac{\sqrt{\overline{F^2}}}{F_0}\right) . \tag{5}$$

The theoretical fit shown corresponds to the following values of the parameters:

$$F_0 \cong 2 \times 10^{-5} \text{ dyne} \quad ,$$
$$L/a \cong 100 \quad .$$

Earlier work by the group had established a fast-neutron damage rate at low temperatures (15 to 20°K), as measured by changes in electrical resistivity, for high-purity beryllium and magnesium. Additional measurements have been made on these materials which are in good agreement with the earlier data. In addition, complete isochronal annealing data have been obtained from 20 to 300°K. The experimental techniques used to obtain these data are described elsewhere.[5] The results obtained from the beryllium sample are shown in Fig. 71, and those from the magnesium sample are shown in Fig. 72. The beryllium results

[4] G. Leibfried, in *Dislocations and Mechanical Properties of Crystals; an International Conference Held at Lake Placid, Sept. 6–8, 1956*, p 495, Wiley, New York, 1957.

[5] R. R. Coltman, T. H. Blewitt, and T. S. Noggle, *Rev. Sci. Instr.* 28, 375–80 (1957).

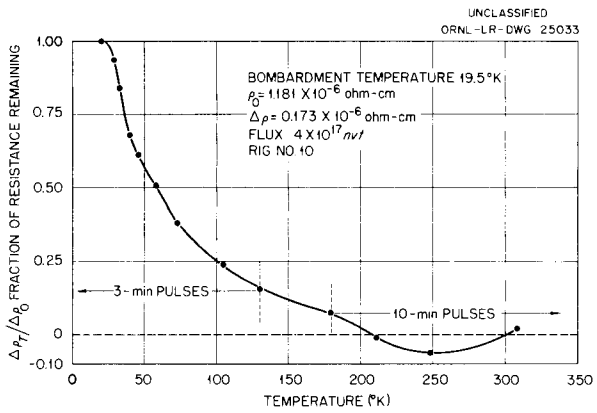

Fig. 71. Isochronal Annealing of Beryllium.

are particularly interesting since the recovery becomes complete below room temperature. This has not been found in any other neutron-irradiated metallic element. Also, these results differ widely from those found in copper,[6] where a large annealing peak is observed between 30 and 50°K followed by a very gradual and incomplete recovery up to room temperature. Typical annealing results for an annealed copper crystal can be seen in Fig. 73. It should be noted that the damage rate of beryllium is about 30 times that of copper, as measured by changes in residual resistivity. The decrease of the resistivity below the pre-bombardment value during recovery is believed to be real, but it is not understood.

The annealing of irradiated high-purity magnesium differs from that of beryllium and copper in that no pronounced annealing peaks occur. A small peak at 40°K and one between 100 and 150°K may be present, but these could be difficult to separate from the continuous recovery which seems apparent and which is found in copper above 50°K. As in the case of beryllium, the recovery at room temperature is almost complete. The damage rate of magnesium is about ten times that of copper.

Earlier studies by the group[6] have been made to examine the difference in damage rate and subsequent annealing between annealed and cold-worked copper crystals bombarded at 15 to 20°K. Measurable differences in damage rates were observed, but these differences were attributed to the fast-flux ripple believed to exist in the reactor. Since the fuel elements of the Graphite Reactor run horizontally on 8-in. centers, and since the low-temperature irradiation facility runs vertically, it was suspected that different damage rates would be found depending upon the elevation of any particular specimen in the cryostat. To measure this flux ripple in terms of damage rate, a piece of 0.025-in.-dia magnet wire 16 in. long was folded into a U-shaped specimen 8 in. long. Potential leads were soldered along both legs of the specimen, making four subspecimen intervals on one side and five on the other. The two legs were $\frac{1}{4}$ in. apart. The specimen was then mounted in a copper can with helium exchange gas, and the damage rate, as measured by changes in residual resistivity of each subspecimen, was measured at 17°K. Magnet wire was chosen as a suitable material for this experiment since it was believed that a small length taken from a large spool would be quite uniform. This is believed to be true, since the maximum deviation in residual resistivity of each subspecimen before bombardment was 8%. It should be noted that the differences in residual resistivity between some of the annealed and cold-worked copper crystals to be discussed below are as high as two orders of magnitude. The results of this experiment show that the damage-rate ripple in the hole 12 cryostat is less than 4% and probably less than 2% (as none of the observed variations fit a pattern ascribable to ripple). Differences in damage rates as large as 35% have been observed between annealed and cold-worked

[6] T. H. Blewitt *et al.*, *J. Appl. Phy.* **28**, 639–44 (1957).

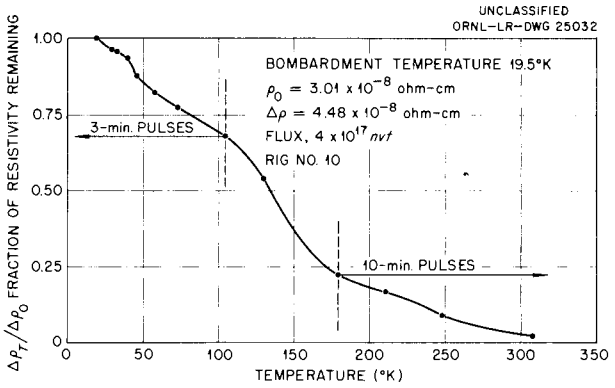

Fig. 72. Isochronal Annealing of High-Purity Magnesium.

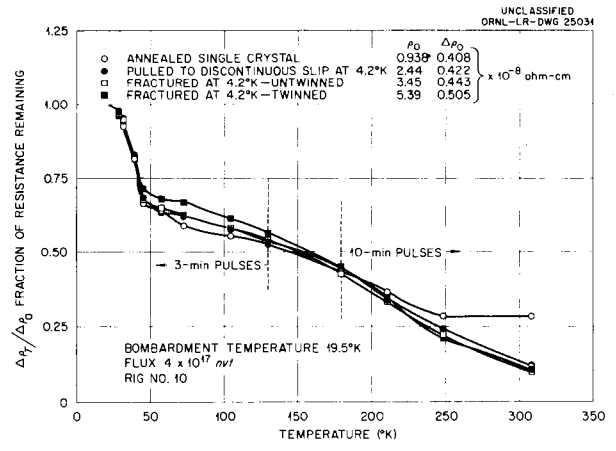

Fig. 73. Isochronal Annealing of Various High-Purity Copper Specimens.

copper crystals. Recent data shown in Fig. 73 on the damage rate and subsequent isochronal annealing of various high-purity copper crystals bombarded at the same time are in substantial agreement with earlier data.[6] It can be noted that the increase in resistivity due to bombardment, $\Delta\rho_0$, is greater for the cold-worked crystals. Although the sharp annealing peak in the 30 to 50°K range is quite similar for all specimens, measurable differences exist from 50 to 300°K, the cold-worked crystals showing more recovery at room temperature than the annealed crystals. Additional evidence supporting the above result that cold-worked copper damages at a faster rate than annealed copper was obtained from the second bombardment at liquid helium temperature, which is discussed later in detail. It was found that a cold-worked copper crystal at the same elevation in the cryostat and separated by a distance of $\frac{1}{8}$ in. from an annealed crystal (each specimen was about 0.035 in. in diameter and 1 in. long) damaged 35% faster at 4.17°K than the annealed specimen.

Recently a helium liquefying system has been installed in the hole 12 cryostat, enabling bombardments to be made near 4°K. The details of this system are described elsewhere in this report. Although reliable annealing data are not available at this time, accurate damage rate data as measured by changes in residual resistivity are shown in Table 4. All the damage rate curves for the materials shown in this table were linear within the precision of the experiment. All samples were at the same elevation in the reactor and were mounted in fence-post style on a $\frac{3}{16}$-in.-dia circle. The bombardment was made at 4.17°K for 154 hr and the samples received a flux of 4×10^{17} *nvt*. In a previous run a lead sample bombarded at 4.38°K to a flux of 1×10^{17} remained in the superconducting state throughout the bombardment.

During the past five years the low-temperature group has measured the residual resistivity of several hundred high-purity copper single crystals. It has been found that the resistivity of these specimens varies over two orders of magnitude from 3×10^{-10} to 3×10^{-8} ohm-cm. This result and the effect of residual resistivity upon work-hardening effects in copper crystals have been reported by Blewitt *et al.*[7]

[7] T. H. Blewitt, R. R. Coltman, and J. K. Redman, *Defects in Crystalline Solids. Report of the Conference on Defects in Crystalline Solids Held at the H. H. Wills Physical Laboratory, University of Bristol, July 1954*, p 369, Physical Society, London, 1955.

Table 4. Neutron Damage Rates of Various Elements at 4.17°K

Fast neutron flux = 6×10^{11} neutrons·cm^{-2}·sec^{-1}

ρ_0 = residual resistivity before bombardment

$\Delta\rho$ = total change in residual resistivity due to 4×10^{17} *nvt*

$d\rho/dn$ = damage rate

Specimen	ρ_0 (ohm-cm)	$\Delta\rho$ (ohm-cm)	$d\rho/dn$ (ohm-cm/neutron)
	$\times 10^{-9}$	$\times 10^{-9}$	$\times 10^{-26}$
Copper crystal, annealed*	0.62	3.79	0.95
Copper crystal, cold worked**	4.76	5.16	1.29
Silver	4.54	5.70	1.42
Gold	44.1	5.35	1.34
Zinc	9.61	33.9	8.48
Platinum	382	10.3	2.58

*Single crystal annealed 1 hr at 900°C in poor vacuum (20 μ of air) according to procedure described in the text.

**Single crystal pulled in liquid helium to fracture (about 130% elongation).

It has been the practice of many experimenters in preparing high-purity (99.999%) copper specimens for study to anneal their specimens at high temperatures in a hard vacuum to remove traces of cold work. Recently it has been found that annealing high-purity copper crystals in a poor vacuum of 10 to 20 μ of air at 900°C for 1 to 2 hr lowers the residual resistivity of the crystal by as much as a factor of 20. Values as low as 4×10^{-10} ohm-cm have been obtained in this fashion. Subsequent annealing in a hard vacuum at 1000°C for 2 hr with the specimen placed on a graphite boat raises the resistivity nearly to its original value. Smart *et al.*,[8] making room-temperature measurements of the resistivity of high-purity copper, have found earlier (1941) that the resistivity tended to decrease upon annealing in the presence of oxygen. They have suggested that the oxygen precipitates out impurities as oxides. To account for the large changes that occur in residual resistivity, the precipitates formed by the oxygen annealing process must be quite large in order that the effective scattering of impurity atoms be reduced. If precipitation does occur, then one is led to believe that large regions of very high-purity material exist in a specimen following an oxygen anneal. A rough estimate of the bulk purity (purity of the regions between precipitates) can be made by assuming that 1 at. % of impurity contributes about 1×10^{-6} ohm-cm to the residual resistivity. A sample having o resistivity of 5×10^{-10} ohm-cm then would have a bulk impurity concentration of 0.0005 at. %. This estimate is probably high, since the measured resistivity includes both the bulk resistivity and the contribution of the precipitates. The results also indicate that the amount of oxygen remaining in the samples must be quite small. It is possible that in the preparation of copper specimens annealing treatments carried out in the presence of oxygen may produce more desirable specimens.

[8] J. S. Smart, Jr., A. A. Smith, Jr., and A. J. Phillips, *Trans. Am. Inst. Mining Met. Engrs.* 143, 272–83 (1941).

REACTOR BOMBARDMENTS NEAR 4°K

R. R. Coltman, Jr. C. E. Klabunde J. T. Howe W. E. Busby

During the past year the construction, testing, and installation of a helium liquefying system used in conjunction with the present cryostat facility[1] in hole 12 of the Graphite Reactor have been completed. Two bombardments have been made in the reactor, one for 80 hr at 4.38°K and one for 160 hr at 4.17°K with the reactor at full power. The behavior of the liquefier circuit seems quite stable when minimum-temperature equilibrium conditions are reached, and flow characteristics show little change when the reactor is turned off or on. With the reactor off, the sample chamber, located at the center of the reactor, reaches about 3.75°K.

A circuit diagram of the liquefier is shown in Fig. 74. High-pressure (180 to 225 psig) room-temperature helium gas is taken from the main compressors of the large hole 12 refrigerator system. This gas enters a commercial Collins heat exchanger, where it is cooled by returning gas to some unknown low temperature. The gas then enters a section of Joy tube heat exchanger, where it is further cooled by the output gas of the main helium refrigerator. The temperature at this point may be variable depending upon how well the main refrigerator is operating, but is generally between 12 and 15°K. The gas then enters a Joule-Thomson heat exchanger and is further cooled by returning gas. One half of this exchanger is located outside the reactor, the other half inside the reactor in the upper 7 ft of the sample chamber of the original cryostat. The exact temperature of the cold end of this heat exchanger is unknown, but is probably around 6 to 7°K. At this point the gas enters a Joule-Thomson expansion valve located just above the reactor graphite. A portion of the gas is liquefied by the Joule-Thomson process, and the pressure is reduced to near atmospheric. The gas-liquid mixture is then transported by thin-walled stainless steel tubing to a thin-walled stainless steel receiving vessel at the center of the reactor. It is then returned in like manner to

[1] R. R. Coltman, T. H. Blewitt, and T. S. Noggle, *Rev. Sci. Instr.* 28, 375–80 (1957).

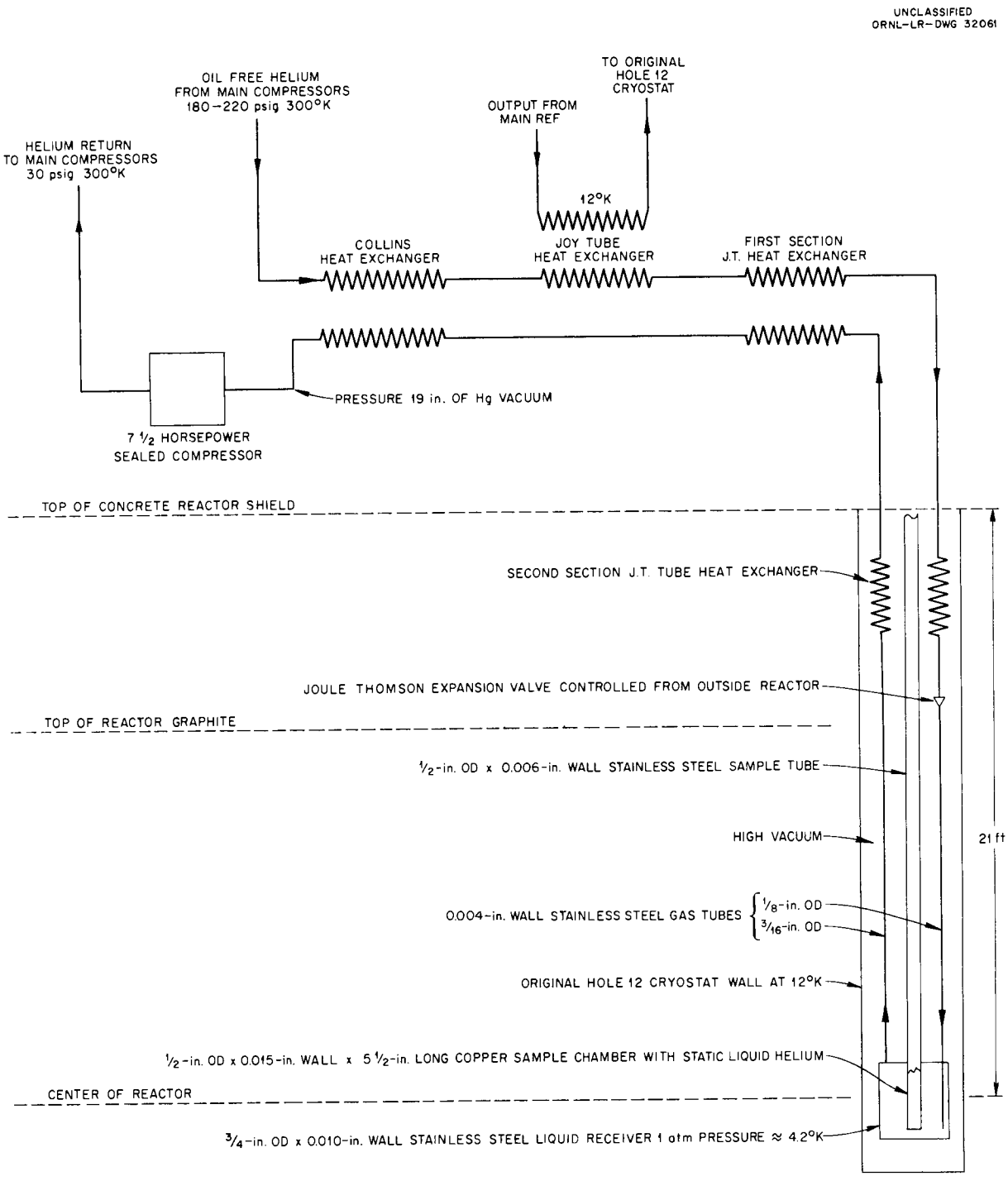

Fig. 74. Schematic Diagram of Hole 12 Helium Liquefier.

the low-pressure side of the Joule-Thomson heat exchanger, then directly into the Collins heat exchanger, out of which it emerges at room temperature and about 19 in. Hg vacuum (when minimum-temperature operating conditions have been reached). From here the low-pressure gas enters a hermetically sealed $7\frac{1}{2}$-hp compressor, where the pressure is raised to 30 psig. The gas is then returned to the low-pressure side of the main refrigerator compressor section, which also operates at 30 psig. The liquefier system, then, is a closed helium circuit which operates continuously.

The mass flow of helium through the liquefier circuit at minimum-temperature conditions is 30 scfh, or the equivalent of about 1.2 liters of liquid helium per hour. Tests show that mass flows as high as 180 cfh can be maintained. Although higher mass flows undoubtedly mean more refrigeration capacity in the liquefier, this is at the expense of a small temperature rise in the receiver. This comes about from the fact that a higher mass flow increases the suction pressure of the compressor, and hence the vapor pressure over the helium that has been liquefied is also raised. It has been found in this particular circuit that a high mass flow of 180 cfh can be maintained with the helium in the receiver being below the critical temperature (5.2°K) and critical pressure (18.5 psig). This illustrates the fact that in a circuit of this type the operating temperature (when below 5.2°K) is very strongly dependent upon the pumping speed of the low-pressure side of the system.

In the original design of the liquefier, it was hoped that a refrigeration capacity of 0.75 w near 4°K could be achieved. This figure was based, first, on the amount of heat required to vaporize 1 liter of helium per hour, and the mass flow necessary to produce this much liquid would not appreciably affect the output of the main compressors supplying the hole 12 refrigerator. Second, the only important heat load is the gamma heating due to the reactor, since the original cryostat is serving as a low-temperature thermal shield for that portion of the liquefier which is lower in temperature than the output of the main refrigerator. (The thermal radiation heat load on those portions of the liquefier circuit which operate above the output temperature of the main refrigerator does not appreciably affect the operation of the liquefier. This heat load is in fact absorbed by the main refrigerator, since at one point the temperature of the liquefier is forced down to the output temperature of the main refrigerator by means of the Joy tube heat exchanger.) It was felt that the smallest feasible facility that could be constructed and placed in the active lattice of the Graphite Reactor would have to weigh about 150 g. This includes the lower 12 ft of the inlet and outlet gas tubes, the receiving chamber, the sample chamber, the helium, and the samples to be bombarded. Since the gamma heating in the Graphite Reactor is 5×10^{-3} w/g, 150 g will vaporize a liter of helium per hour. Tests indicate that the heat capacity of the liquefier may be as high as 3 to 4 w at or below 5.2°K.

From Fig. 74 it can be noted that the sample tube leading to the sample chamber is a separate system from the liquefier. Helium can be supplied to the sample chamber in a measured quantity and liquefied to a depth sufficient to cover the samples. Samples are bombarded in static liquid helium, whose vapor pressure measured outside the reactor may be easily converted to sample chamber temperature. If too much helium is introduced into the sample chamber, the liquid level will probably rise into the sample tube and a vertical temperature gradient will exist in the liquid. The vapor pressure will correspond to the temperature of the liquid at the top of the column, and samples at a lower elevation will be at a lower temperature. In any event, as long as the vapor pressure is below the critical pressure, liquid must be present in the sample chamber. The height of the liquid level can be controlled by careful metering of the quantity of helium introduced into the sample chamber.

HOLE 50 LIQUID NITROGEN CRYOSTAT

J. T. Howe W. E. Busby R. R. Coltman

A cryostat, shown in Figs. 75, 76, and 77, has been built for hole 50 of the ORNL Graphite Reactor. This cryostat utilizes a machined heat exchanger, such as the one on the hole 12 cryostat, and coiled helium lines, such as those used on the hole 52 cryostat to provide for differential expansion between the helium lines and the sample chamber.

It was decided to build a new compressor and heat exchanger system, the experience gained in building and operating the other cryostats being utilized to simplify and improve the design. A schematic diagram of the new circuit is shown in Fig. 78.

A tank of sufficiently heavy material to hold a vacuum was found at the salvage yard and was modified to serve as the receptacle for the liquid nitrogen pot, which will be surrounded by a radiation shield. The counterflow heat exchanger will be installed in a straight aluminum tube to permit use of a high vacuum and a radiation shield also. Both radiation shields will be wrapped with aluminum foil and will be cooled by the off-gas from the nitrogen pot.

Control of the cryostat temperature will be made by means of a bypass valve which will adjust the amount of gas flowing through the cryostat system.

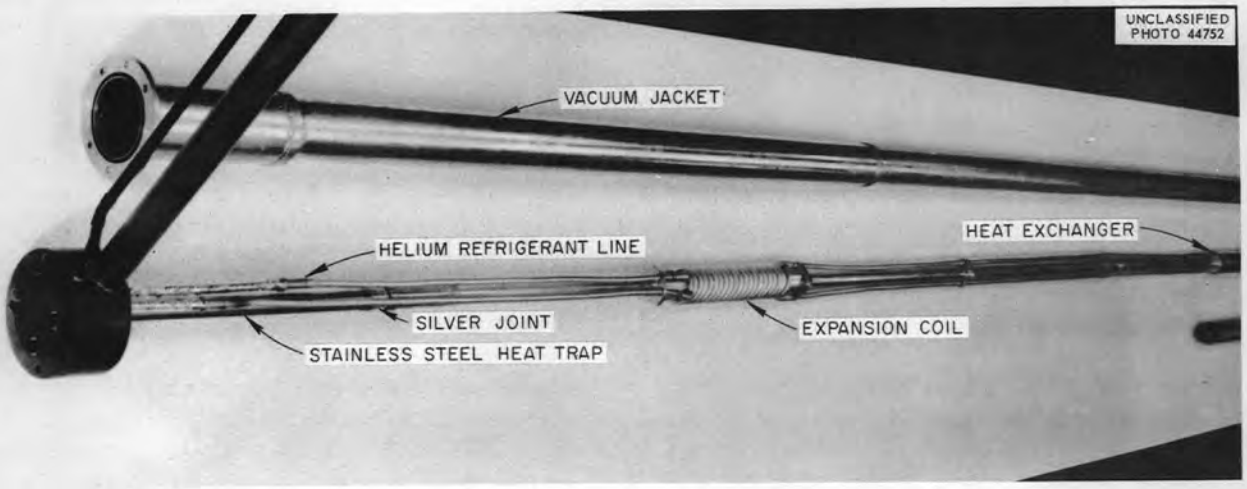

Fig. 75. Assembled Cryostat and Vacuum Jacket for Hole 50, ORNL Graphite Reactor.

Fig. 76. Expansion Coil for Hole 50 Cryostat.

Analysis of the hole 52 cryostat system, which is built on somewhat the same principles, indicates that there is a heat loss of about 75 w in the lines from cold case to cryostat, another 75-w loss in the cryostat itself, and (based on a nitrogen consumption in excess of ten 20-liter cans of nitrogen per day) more than 225 w loss in the cold-case system, which has lost considerable insulation efficiency since it was installed early in 1952. The cold case is a 55-gal drum which is filled with Santocel; it is not completely air-tight and has accumulated some moisture over the years. Both the nitrogen pot and the counter-flow exchanger are located within the drum.

The new hole 50 installation should virtually eliminate the losses from the external system so that the total load on the new system, cryostat included, is estimated at not more than 150 w, corresponding to about four cans of nitrogen per day.

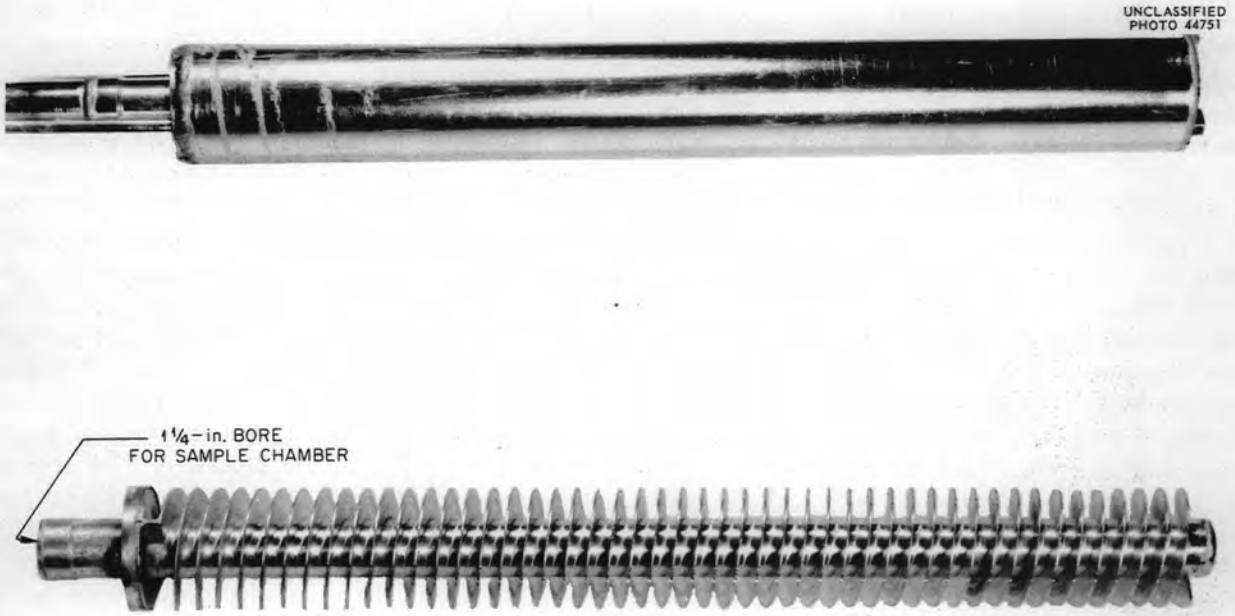

Fig. 77. Hole 50 Cryostat Heat Exchanger Before and After Casing.

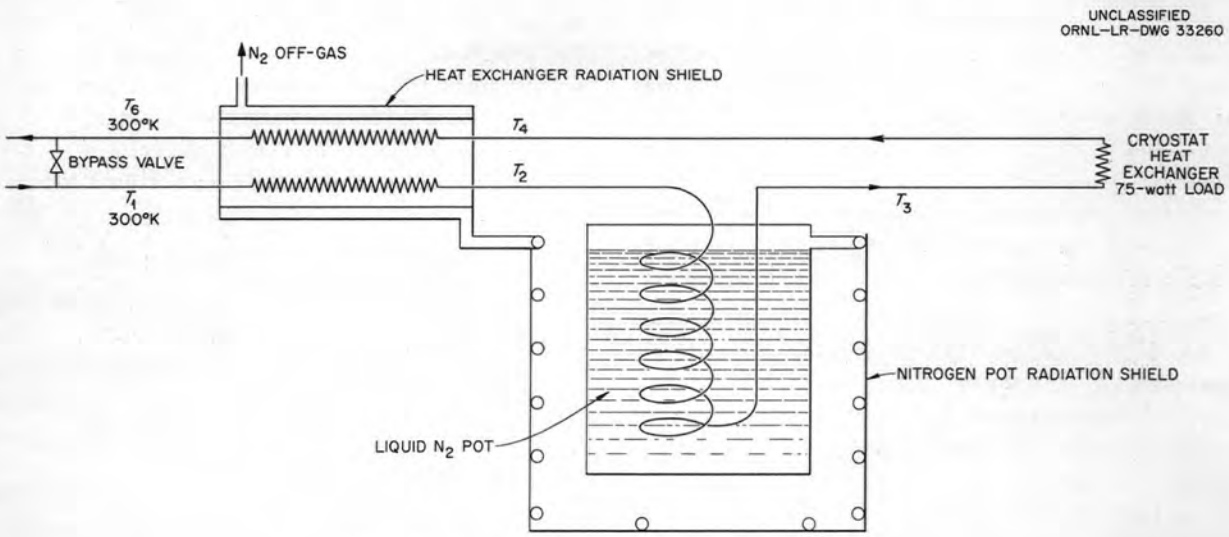

Fig. 78. Schematic Diagram of Hole 50 Cryostat.

CHEMCIAL PROPERTIES OF METAL SURFACES

F. W. Young, Jr. L. H. Jenkins

It is well established that the rate of chemical reaction on metal surfaces is dependent on the crystal face which is reacting. It has also been observed more recently that the reaction rate is generally not uniform over any one crystal face. This latter fact has led to investigations of the effect of imperfections in crystals on the chemical reactions at surfaces. In the studies of this group on oxidation and on dissolution of metals in aqueous solutions, particular emphasis has been placed on determining the role of imperfections in the metal on these reactions.

Observation of Dislocations as Etch Pits

In order to study the chemical properties of dislocations in metal crystals, it is necessary to have some method of locating the dislocations. A method for locating the dislocations as electrolytic etch pits in copper which was doped with tellurium was devised. To show that these etch pits did correspond to dislocations and to investigate the movement of dislocations in copper as a function of temperature, a study was made of the polygonization of copper. This work has been published,[1] and the following is an abstract of the paper:

Polygonization of Copper.[1] F. W. Young, Jr. – It has been demonstrated that dislocations can be revealed as etch pits in copper crystals doped with a small amount of Te. The progress of polygonization of such copper after bending was followed with etch pits and x-ray diffraction. It was found that climbing occurred at 500°C and that polygonization was complete after 2 hours at 1000°C. In similar experiments with three samples of nominally 99.999% copper, the one which was probably purest did not polygonize, while the other two did so. This indicates that if impurity is necessary for polygonization, only a very small amount is required.

While it is interesting to study the properties of dislocations in copper doped with tellurium, it would be more interesting to study the properties of dislocations in pure copper. If some method were available for detecting clean dislocations, the role which dislocations play in the mechanical deformation of copper could be investigated in detail. Also, it might be possible to determine the chemical potential of dislocations. Therefore a program of etching copper in a variety of solutions is in progress with the goal of detecting clean dislocations as etch pits.

It is possible that the following factors govern the formation of etch pits at clean dislocations. Dislocations which have impurities segregated at them obviously have a markedly different chemical potential at the dislocations as compared with other points on the surface. In contrast, it seems probable that the chemical potential at a clean dislocation is not very different from the potential at other sites on the surface. The implication from this small difference in potential is that in order to form etch pits at clean dislocations the energy of the etching reaction must be of the same order of magnitude as the difference between the energies of the two types of sites. A second factor which must be considered is that in order for a pit to be observed it must be large in atomic dimensions. Therefore, the dissolution rate parallel to the surface must be about the same as the rate normal to the surface. To effect this balance in dissolution rates, it may be necessary to poison the step which is formed when a pit is nucleated so that the step does not move a large distance away from the dislocation site before a second step is nucleated.

Sufficient information on the etching of metals is not available for preparing a suitable etchant for the formation of pits at clean dislocations. As a corollary to the studies of the dissolution of copper crystals in aqueous salt solutions, a methodical investigation of etching solutions which appear to meet the requirements outlined above is in progress.

Oxide Nuclei and Dislocations

Since the discovery that thin oxide films on metals are not of uniform thickness but rather have nuclei of oxide in them which are thicker than the base film,[2] there has been much speculation as to the cause of this phenomenon. It has

[1] F. W. Young, Jr., *J. Appl. Phy.* **29**, 760 (1958).

[2] J. Bardolle and J. Benard, *Rev. met.* **49**, 613 (1952); E. A. Gulbransen and W. R. McMillan, *J. Appl. Phy.* **24**, 1416 (1953); W. W. Harris, F. L. Ball, and A. T. Gwathmey, *Acta Met.* **5**, 574 (1957); K. R. Lawless, F. W. Young, Jr., and A. T. Gwathmey, *J. chim. phys.* **53**, 667–74 (1956).

been suggested that there might be a correspondence between oxide nuclei and dislocations in the metal. Regular arrays of dislocations can be introduced into copper crystals by appropriate bending and annealing. The formation of arrays of oxide nuclei corresponding to such arrays of dislocations would establish a correlation between oxide nuclei and dislocations. A study has been made of the correspondence between oxide nuclei and dislocations, and a paper is being prepared for publication. A summary of this work follows.

Single crystals with the orientation shown in Fig. 79 were grown of 99.999% copper and of 99.999% copper with tellurium, tin, or silicon added as impurities. These crystals were bent about the $[\bar{1}\bar{1}2]$ direction so as to obtain slip in the $[1\bar{1}0]$ direction on the (111) plane and annealed so as to cause polygonization, thereby arranging the dislocations introduced by bending in well-defined rows.[1] The dislocations could be observed as electrolytic etch pits in the crystals of copper doped with tellurium; in the 99.999% copper and in the copper doped with tin or silicon, the dislocations could not be revealed as etch pits. However, it has been shown by x-ray diffraction that such crystals can polygonize,[1] and thus one of these polygonized crystals should have dislocations in arrays similar to those shown to exist in copper doped with tellurium.

The bent and polygonized crystals were oxidized in purified oxygen by the different techniques according to which oxide nuclei have been formed.[2] For copper doped with tellurium, oxide nuclei were formed at the dislocation sites. By photographing the oxide nuclei, then electropolishing and etching the sample and photographing the etch pits, and comparing the two photographs, it was established that the correspondence between oxide nuclei and etch pits was one-to-one. Photomicrographs of an area on $(\bar{1}\bar{1}2)$ after oxidation and after subsequent electropolishing and electroetching are shown in Figs. 80 and 81. The small differences in position of the subboundaries between the two photographs are due to the fact that $\sim 10\ \mu$ of copper was removed by the electropolish. For copper doped with tin there was some enhancement of oxidation at the polygon boundaries when the crystal was oxidized by one of the techniques. For 99.999% copper and for copper doped with silicon, there was no evidence of enhanced oxidation at the dislocation sites. Oxide nuclei which were not related to the dislocations were also formed on all the crystals under the proper conditions of oxidation. The experimental results are summarized below:

Composition	Oxide Nuclei at Dislocations	Oxide Nuclei
99.999% Cu	No	Yes
Cu + 0.01% Te	Yes	Yes
Cu + 0.05% Sn	Yes	Yes
Cu + 0.1% Si	No	Yes

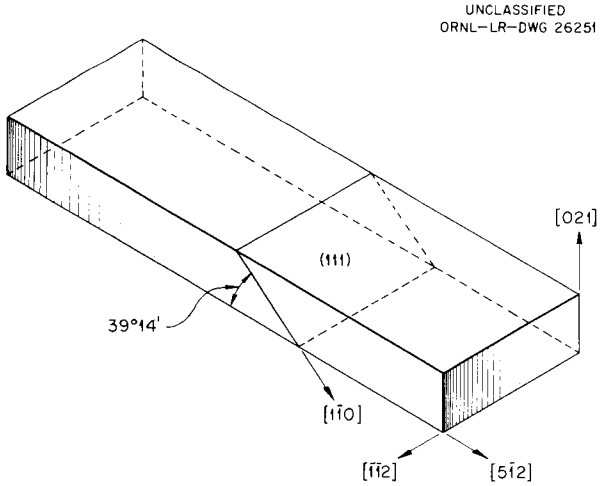

Fig. 79. Orientation of Crystal Before Bending.

The formation of oxide nuclei at dislocations only if the copper crystals were doped with certain impurities indicates that the dislocations act as a line source of the impurity atoms and that these impurity atoms are responsible for increasing the rate of oxidation in the immediate vicinity of the dislocation. Further, the chemical potential of the dislocation sites for clean dislocations does not appear to be sufficiently different from that of other points on the surface to change the rate of oxidation appreciably.

It should be emphasized that the impurity content of the crystals used in this study was low. For example, the crystals of copper doped with tellurium were 99.99% copper, which has generally been considered high-purity copper by investigators of the rate of oxidation of metals. The fact that the rate of oxidation is increased at dislocation sites in slightly impure copper obviously has practical significance.

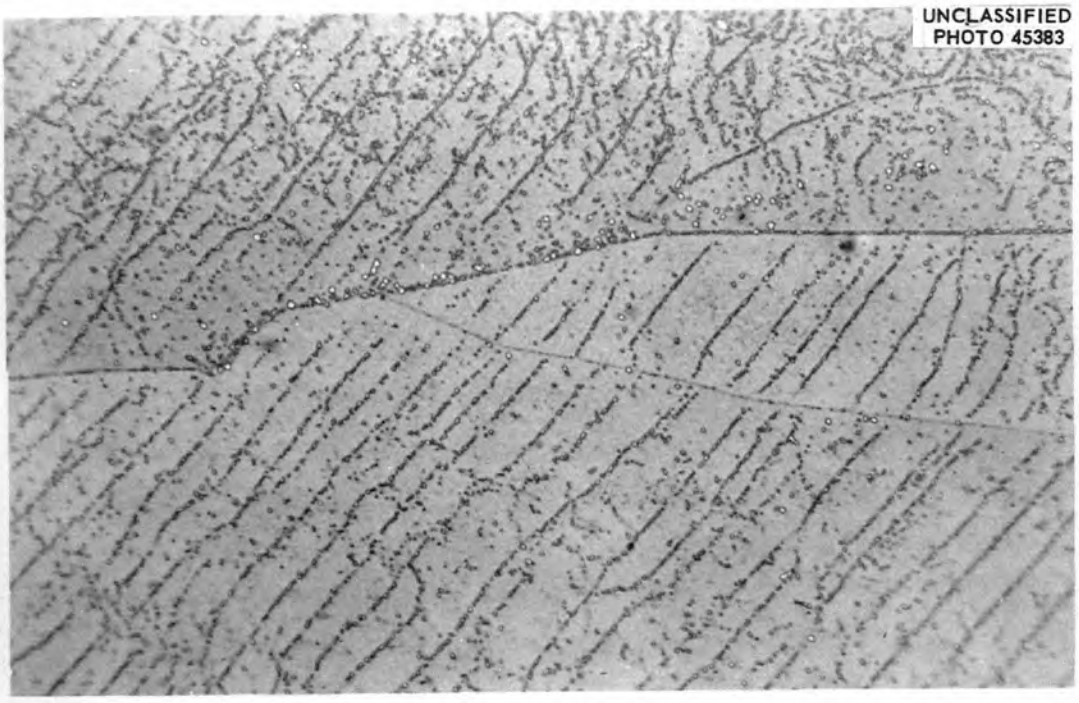

Fig. 80. Oxide Nuclei on $(\bar{1}\bar{1}2)$ Face. 500X.

Fig. 81. Electrolytic Etch Pits on Same Area as Fig. 80. 500X.

Dissolution of Copper in Aqueous Media

In an attempt to understand the effect of crystal face on the dissolution of copper in aqueous solutions the following reaction has been investigated:

$$(1) \quad Cu^0 + H_2O + xCN^- \rightleftharpoons Cu(CN)_x^{1-x} + OH^- + \tfrac{1}{2}H_2$$

Earlier stages of the work consisted of observing the etch patterns produced on single-crystal hemispheres of pure copper (99.999%) exposed to aqueous KCN. In all cases it was observed that the major poles were less reactive than other areas of the sphere. Figure 82 illustrates typical results which were obtained. Regardless of the concentration of cyanide employed, the degree of attack on the major poles was in the order (110) > (100) > (111).

Fig. 82. (110) Pole of Copper Hemisphere Etched in 0.5 *M* KCN for 45 min. 500X.

During these investigations of dissolution rates and etching processes the role of dislocations in forming etch pits in pure copper has been considered an allied problem. The foregoing results indicated that, in addition to the other problems involved in attempting to reveal dislocations as etch pits, the orientation of the etched surface is a major problem. This fact was clearly demonstrated when a bent copper crystal which had been polygonized[1] was repeatedly etched in KCN. Invariably, etch pits, which did not correspond to dislocations, were produced on the (210) face but not on the (112) face of the crystal. In addition to the effect of orientation, the following factors, some of which were discussed in a previous section, affecting the production of etch pits have been and are being studied: (1) reaction rates (slow vs fast reactions), (2) poisoning the surface during etching by the formation of insoluble compounds, and (3) variations in concentration of etching reagent and pH of the solution.

Reaction rates of copper (99.999%) single-crystal plates in dilute aqueous KCN were studied.[3] Analysis of the data showed that at least three reactions (1, and also 2 and 3 below) were involved:

$$(2) \quad 2Cu + \tfrac{1}{2}O_2 \rightleftharpoons Cu_2O$$

$$(3) \quad Cu_2O + H_2O + 2xCN^- \rightleftharpoons 2Cu(CN)_x^{1-x} + 2OH^-$$

A large portion of the past year has been spent in developing a system which permits removal, as nearly as possible, of all dissolved oxygen from the solution employed and which allows such solutions to be transferred to the reaction apparatus under an inert atmosphere that is maintained during the course of the reaction. Kinetic data on the attack of deaerated aqueous KCN on copper platelets are now being gathered.

It has been reported[4] that for the reaction

$$(4) \quad Cu^0 + Cu^{++} \rightleftharpoons 2Cu^+$$

the equilibrium constant is 1×10^{-6} at 20°C. Since this reaction is important in both dissolution studies and electrode potential measurements, the reaction between metallic copper and deaerated dilute ($\sim 10^{-4}$ *M*) $CuCl_2$-HCl solutions was studied. Complete removal of dissolved oxygen is probably unobtainable, and therefore the results of these experiments are somewhat inconclusive. However, the data indicated that in these dilute solutions the only Cu^+ ion measurable results from oxidation of metallic copper by oxygen followed by dissolution of Cu_2O by HCl. Also, it was definitely shown that if reaction 4 does proceed to any extent the equilibrium constant for the reaction is less than 10^{-6}.

The dissolution rate of copper single-crystal platelets in dilute ($\sim 10^{-4}$ *M*) HCl exposed to air was also investigated. The over-all reaction is of zero order. Therefore the reaction rate must be

---

[3] F. W. Young, Jr., and L. H. Jenkins, *Solid State Ann. Prog. Rep. Aug. 31, 1957*, ORNL-2413, p 25.

[4] F. Fenwick, *J. Am. Chem. Soc.* 48, 860 (1926).

controlled either by a diffusion process or by the rate of oxidation of copper by oxygen.

The reaction between metallic copper and aqueous $Cu(H_2NCH_2CH_2NH_2)_2SO_4$ was observed. In the presence of oxygen Cu^+ was found in solution, but in the absence of oxygen no reaction occurred. Again the process seemed to be the dissolution of Cu_2O, by ethylenediamine in this case, rather than oxidation of metallic copper by bivalent copper ions.

Other reagents are being investigated for information concerning reaction rates and etching characteristics, but at this time the results are inconclusive.

MIGRATION OF DEUTERIUM IN COPPER

M. T. Robinson
R. L. Tanner[1]
A. L. Southern
W. R. Willis[2]

The migration rate of hydrogen in metals is of general metallurgical and physical interest, although very few measurements have been reported. The experiments described here were performed to assess the possibilities of employing a beam of moderate-energy deuterons as the source of diffusing deuterium and, at the same time, as the probe for monitoring the migration rate. The neutron counting rate resulting from the $D(d,n)He^3$ reaction is related to the concentration of diffusing deuterium in a target according to:

$$(1) \qquad P(t) = \alpha' \int_0^\infty \sigma[E(x)](x,t)\, dx \ ,$$

where $P(t)$ is the measured counting rate, x is the distance into the target measured normally to the irradiated surface, $E(x)$ is the deuteron energy, $\sigma[E(x)]$ is the $D(d,n)He^3$ cross section, and (x,t) is the concentration of diffusing deuterium. The proportionality constant, α', contains counter efficiency and geometry factors, as well as the deuteron beam current. The limit of integration in Eq. 1 may be taken as infinite, since the nuclear reaction cross section becomes exceedingly small before the beam particle density in the target differs appreciably from that in the incident beam.

Experiments similar to the present ones have been reported by Fiebiger[3] and by groups at the University of Arkansas[4] and at Vanderbilt University.[5] Fiebiger used neutron detection, as did the Vanderbilt group in their earlier work, while in later work they counted protons from the $D(d,p)T$ reaction. The Arkansas group also counted protons. All these investigators show curves of the neutron counting rate[6] against time which appear to saturate in reasonable times. Unfortunately, Fiebiger's papers contain no experimental points, and so no real assessment of his saturation values can be made. The low counting rates which he observed (about 225 neutrons/sec for copper, about 1% of the values which we have obtained) make it possible that experimental uncertainties concealed continued small increases in the counting rate. The Arkansas data are confusing in that the neutron yields observed are claimed to be independent of beam current. Since, as will be shown below, the steady-state yields should depend on the *square* of the current, it seems likely that the target temperature depended strongly on the current. The high current and voltage (600 μa at 400 kv) make this appear quite reasonable. Fiebiger reported no loss of deuterium from his targets when they stood in a vacuum for a week, but Arnold did find such losses to occur.

In the present experiments, attention has been given primarily to determining whether or not the

[1]Department of Physics, Memphis State University, Memphis; summer employee at ORNL, 1958.

[2]Department of Physics, West Virginia Wesleyan College, Buckhannon; consultant to Solid State Division.

[3]K. Fiebiger, *Z. angew. Phys.* 9, 213–23 (1957); *Z. Naturforsch.* 11a, 607 (1957).

[4]R. W. Fink *et al.*, *University of Arkansas Annual Progress Report*, U.S.A.E.C. Contract AT-(40-1)-277 (March 1, 1958).

[5]R. T. Arnold, thesis, Vanderbilt University, 1955; C. D. Curtis, private communication.

[6]Where proton counting is done, the neutron datum can be deduced by using nuclear reaction cross-section data.

curves for buildup of the neutron counting rate can be regarded as indicative of diffusion and to the possibility of deducing diffusion coefficients of deuterium from such data.

Experimental Procedure

The deuterons employed in the experiments were extracted from a conventional radio-frequency ion source, accelerated to 176 kev by a Cockcroft-Walton generator set, and magnetically analyzed to select a beam of D^+ (and H_2^+) ions. The analyzed beam was focused on the target by an electrostatic lens. A liquid-nitrogen-cooled section was provided in the drift tube to prevent collection of pump oils on the target surface. The general layout is shown in Fig. 83. The deuteron current was measured by making the target part of a Faraday cage, the collected charge being passed to ground through an electronic current integrator or, in later work, through a recording microammeter. The latter procedure was required in order that small and comparatively rapid variations in the beam current could be measured. A typical current trace is shown in Fig. 84. The Faraday cage was provided with a guard ring maintained at about −250 v to prevent escape of secondary electrons. Measurements of current as a function of the negative guard-ring bias showed 60 v to be adequate to suppress the electron current.

The neutron detector consisted of a 20-in. cube of paraffin contained in an aluminum can. Three 1-in.-dia by 5-in.-long proportional counters were

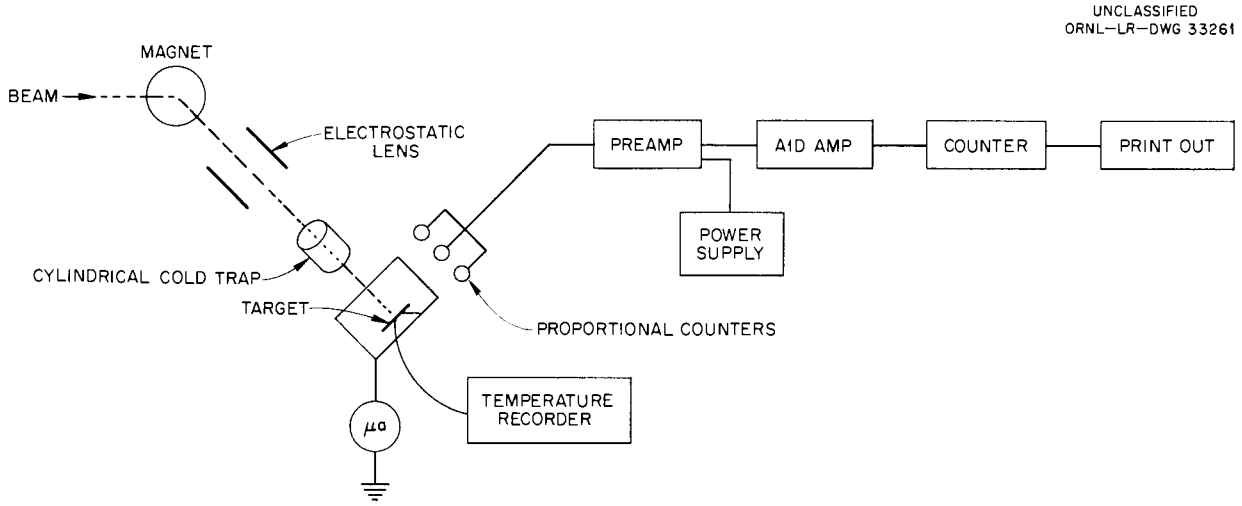

Fig. 83. Experimental Arrangement.

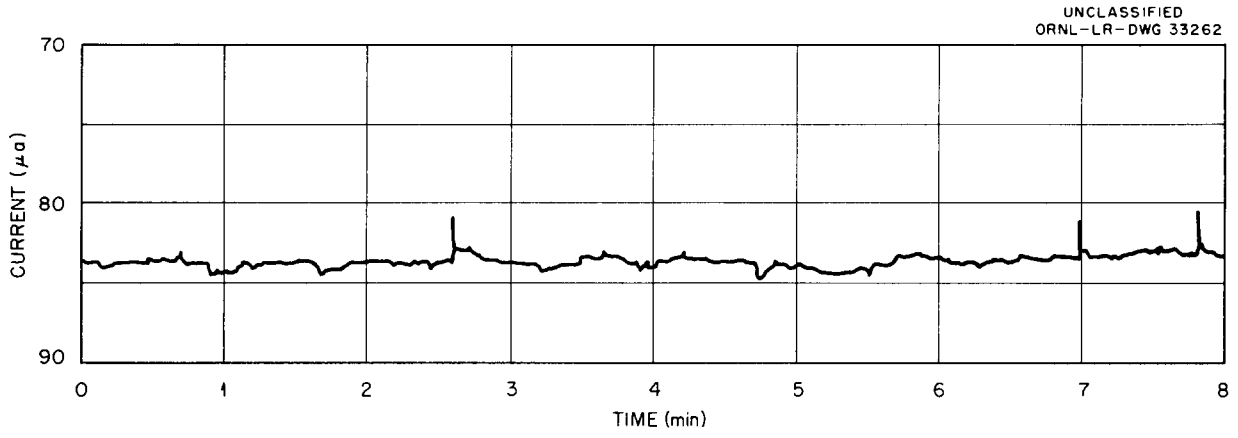

Fig. 84. Typical Current Recording.

located on 3-in. centers in a plane 2 in. below the top surface of the paraffin. The counters were filled to 71 cm Hg pressure with $B^{10}F_3$. The three counters were connected in parallel through an AlD preamplifier and an AlD linear amplifier to a Berkeley model 7350 timer-scaler. The output of the scaler was recorded on adding machine tape by a Berkeley model 1452 digital print-out unit. The scaler could be programed to count for a specified interval of time, at the end of which the accumulated count was recorded and the scaler was cleared to wait the start of the next cycle. In most of the experiments, counting periods of 1 to 10 sec were used with delay intervals of 10 to 1 sec.

The neutron detector was shielded from background by surrounding it with a wall of borated paraffin. The largest source of background appeared to be in the analyzing magnet, where the rejected ions (H^+, HD^+, D_2^+, etc.) were allowed to strike the drift-tube walls, although neutrons also originated at other points in the system. The background of neutrons from cosmic rays and from other accelerators in the ORNL High Voltage Laboratory was generally low enough to be ignored.

Before the liquid-nitrogen-cooled trap was installed in the drift tube, considerable difficulty was encountered with the accumulation of carbon deposits on the target. These appeared to result from radiolysis (or possibly pyrolysis) of diffusion pump oils which condensed on the target. The deposits were eliminated by use of the trap.

Three types of target holders have been used. In the first, which proved to be unsatisfactory, a thin metal foil was clamped against a water-cooled block. Adequate target cooling could not be maintained in this system because of failure of the target to conform to the surface of the cooled block. In the second unit, shown in Fig. 85, the holder and target were combined. Cooling water flowed within $\frac{1}{16}$ in. of the irradiated surface, and a ring of five thermocouple wells extended to within $\frac{1}{32}$ in. of this surface. The third holder, Fig. 86, was arranged so that cooling water could be sprayed on the back of the target, which was cut from a thin sheet of metal. The temperatures were measured by copper-constantan thermocouples soldered directly to the target. Figure 87 is a typical temperature record showing the changes occurring as the beam is turned on the target.

Two methods have been used to prepare copper targets for irradiation, neither appearing especially advantageous over the other. In one method the surface of the target was burnished with a fine crocus cloth and then cleaned with xylene. In the other method the target was washed with soap

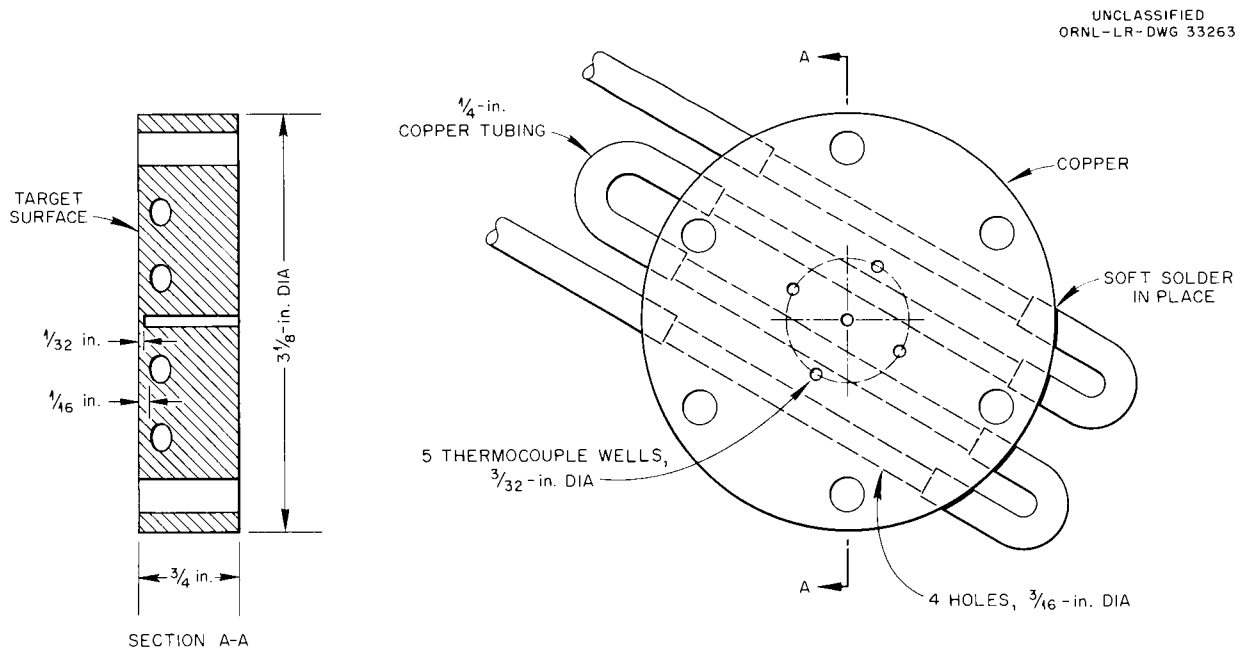

Fig. 85. Copper Target with Cooling Lines and Thermocouple Wells.

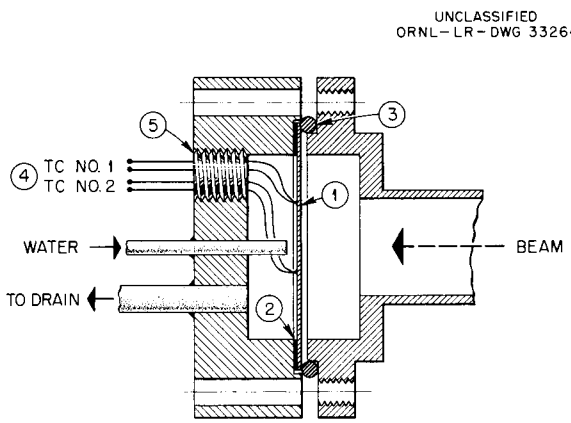

(1) COPPER (0.032-in. THICK x $2^{9}/_{32}$-in. DIA)

(2) NEOPRENE (0.032-in. THICK x $2^{9}/_{32}$-in. DIA)

(3) LEAD O-RING ($^{1}/_{8}$-in. MATERIAL)

(4) THERMOCOUPLE, 24 GAGE TYPE "T", SOFT SOLDER IN PLACE

(5) CONAX TG-24-A4

Fig. 86. Target Holder Assembly.

and water, heated by dipping in hot water, etched briefly in 50% nitric acid, then rinsed in 5% nitric acid and distilled water.

Experimental Results

Figure 88 shows plots of the observed neutron counting rate for four successive runs made on target 34, shown in Fig. 85. It is clear from the data that no steady-state counting rate is reached up to the limit of the figure. In fact, the final run in this series was extended to about 3 hr (1.08×10^4 sec) without any evidence for saturation of the neutron counting rate. It is also clear that the deuterium content of the target – at least near the irradiated surface – dropped sharply when the beam was turned off. The drop was greater when the beam was off for longer periods. The sharp drop occurring in the data from run 4 is believed to be associated with an accidental excursion of the target temperature. After completion of this run, a microhardness traverse was made across this target.[7] A region of distinctly softer metal (about 20–25% lower diamond pyramid hardness) was found where the beam struck the target. This softening, which we have not been able to duplicate on other targets, is believed to be associated with the drop in counting rate. It was noted that the curves of Fig. 88 could be made to coincide by appropriate changes in the origin. In particular, the long-time portions can be made to agree very well with one another. Qualitatively, the results obtained on this target are in agreement with what one expects for a diffusion-controlled process.

Data have been obtained on a number of other copper targets and are in general qualitative agreement. The counting rates are found to be moderately strong functions of the beam current. No steady states have been observed, although if the beam current density is low enough, the slope of the long-time data is difficult to detect.

Interpretation of Experiments

If it is assumed that the target is infinitely thick,[8] the appropriate solution to the one-dimensional diffusion equation is

$$(2)\quad (x,t) = \alpha' t^{1/2}\left[e^{-(x-R)^2/4Dt} - e^{-(x+R)^2/4Dt}\right] -$$

$$-\frac{\alpha}{2R}\,|x-R|\,\operatorname{erfc}\frac{|x-R|}{2(Dt)^{1/2}} + \frac{\alpha}{2R}\,|x+R|\,\operatorname{erfc}\frac{(x+R)}{2(Dt)^{1/2}},$$

where the source is assumed to be planar at a distance R (the deuteron range) below the irradiated surface. This result is inconvenient for our purpose, since the integration over the space variable required by Eq. 1 cannot be carried out readily. The following device has been used: The diffusion equation is solved with the condition that the flux of deuterium at $x = R$ is given by

$$\frac{\alpha}{2}\left[1 + \operatorname{erfc}\frac{R}{(Dt)^{1/2}}\right]$$

as required by Eq. 2. The solution sought will be the one for which the space and time variables are separated. It is assumed that there is no

[7] We are indebted to E. J. Manthos for these measurements.

[8] A good approximation in our work, since the range of 176-kev deuterons in Cu is only about 2.2 μ compared with target thicknesses of 25 to 750 mils.

UNCLASSIFIED
ORNL-LR-DWG 33265

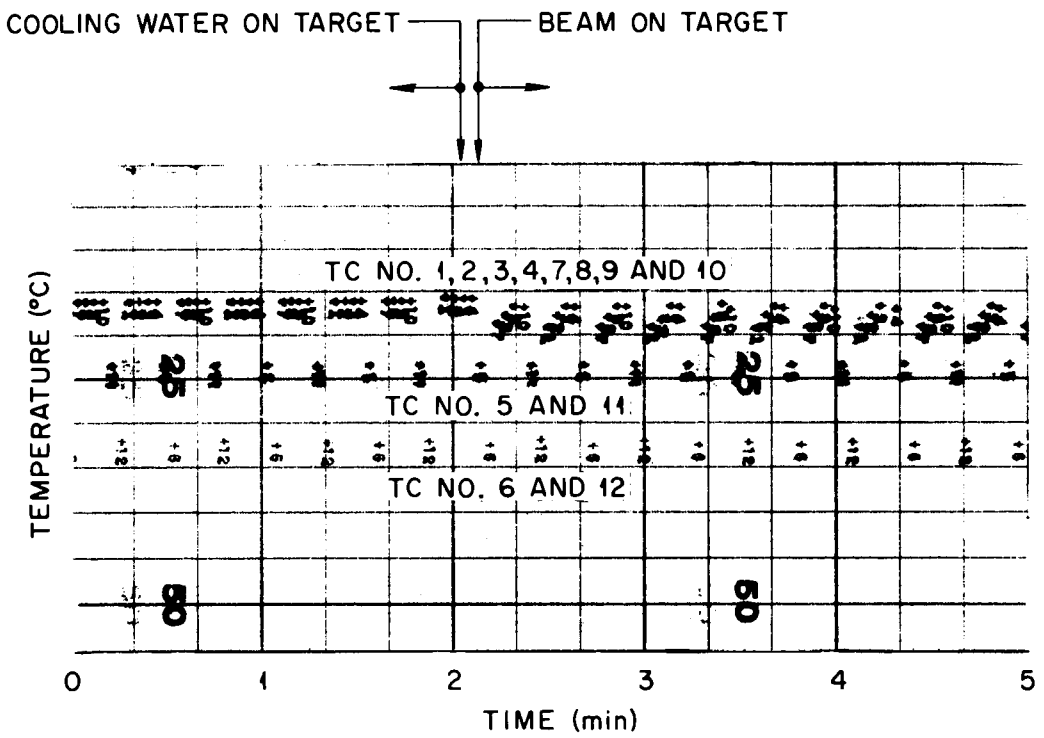

THERMOCOUPLE NO. 1 AND 7 CENTER OF TARGET
THERMOCOUPLE NO. 2 AND 8 — 1/4 in. FROM CENTER AT ZERO DEGREES
THERMOCOUPLE NO. 3 AND 9 — 1/4 in. FROM CENTER AT 120 DEGREES
THERMOCOUPLE NO. 4 AND 10 — 1/4 in. FROM CENTER AT 240 DEGREES
THERMOCOUPLE NO. 5 AND 11 ROOM TEMPERATURE
THERMOCOUPLE NO. 6 AND 12 RECORDER TEMPERATURE

Fig. 87. Temperature Trace (°C) of Target Thermocouples – 5-min Duration.

resistance to escape of deuterium from the irradiated surface. The result may be written as

$$(3)\quad (x,t) = \alpha \sum_{k=0}^{\infty} \frac{(-1)^k}{(2k+1)^2\pi^2} \sin\frac{(2k+1)\pi x}{2R} \times \left[1 + \operatorname{erfc}\frac{R}{\sqrt{Dt}} - \Phi_{k+\frac{1}{2}}\left(\frac{R}{\sqrt{Dt}}\right)\right],$$

where

$$(4)\quad \Phi_k(z) = \frac{2z}{\sqrt{\pi}} \int_0^1 e^{-(zv)^2} \cos 2k\pi v \, dv \ .$$

Hence, using Eq. 1, we may write:

$$(5)\quad P(t) = A \sum_{k=0}^{\infty} \beta_k \left[1 + \operatorname{erfc}\frac{R}{\sqrt{Dt}} - \Phi_{k+\frac{1}{2}}\left(\frac{R}{\sqrt{Dt}}\right)\right] \ ,$$

where

$$(6)\quad \beta_k = \frac{(-1)^k}{(2k+1)^2} \int_0^{\infty} \sigma(x) \sin\frac{(2k+1)\pi x}{R} dx \ .$$

The β_k's are functions only of the deuteron energy and may be computed from available data on the slowing-down of charged particles in matter and on the $D(d,n)He^3$ cross section. Hence the neutron counting rate, $P(t)$, is determined by the two

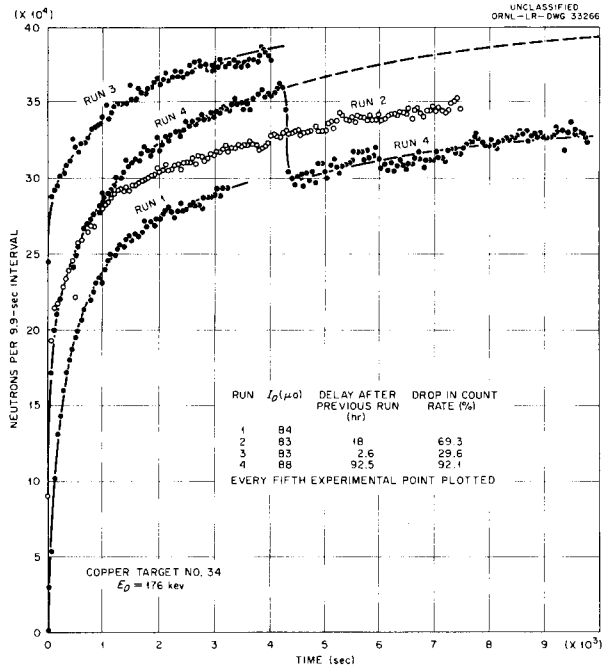

Fig. 88. D-D Neutron Counting Rate.

parameters A, a scale factor, and D/R^2, the scaled diffusion coefficient. For long times, Eq. 5 predicts that $P(t)$ will vary as

$$P(t) \approx A'\left(1 + \operatorname{erfc} \frac{R}{\sqrt{Dt}}\right) . \tag{7}$$

The portions of Fig. 88 for $t > \sim 3000$ sec fit this relationship very nicely. Based on a rough fit of the data, the values obtained are:

$$D/R^2 = 1.21 \times 10^{-3} \text{ sec}^{-1} ,$$

$$D = 3 \times 10^{-11} \text{ cm}^2/\text{sec} .$$

A least-squares fit of the data of run 1 of target 34 (Fig. 88), *in which the time dependence of the flux at* $x = R$ *was ignored*, yielded $D = 7 \times 10^{-11}$ cm^2/sec. In each case the deuteron range was taken to be 1.62 μ.

At the present time a program is being written for the evaluation of Eq. 5 on the Oracle so that an existing least-squares code can be utilized to derive diffusion coefficient values from our data.

The solution of Eq. 6 above for the space-dependent function β_k requires a knowledge of cross sections as a function of penetration. Further, the solution of Eq. 5 will yield values of D/R^2, so that the range must be known to compute the diffusion coefficient. A final solution then requires a knowledge of the range and the variation of beam energy with penetration.

There is no satisfactory theory of stopping power in this energy range. The calculations of Aron *et al.*,[9] which are extrapolations of high-energy relationships, do not agree with experimental data on the stopping power of copper.

A range-energy graph for deuterons in copper has been constructed by graphic integration of experimental values of the stopping power of copper for protons. The data from the critical compilation of Allison and Warshaw[10] were extrapolated to zero energy by using a relationship formally like the Fermi-Teller equation:

$$-\frac{dE}{dx} = k\sqrt{E} .$$

Here k was evaluated to give a smooth fit to the data.

[9] W. A. Aron, B. G. Hoffman, and F. C. Williams, *Range-Energy Curves*, AECU-663, UCRL-121, Second Revision (April 20, 1950).

[10] S. K. Allison and S. D. Warshaw, *Revs. Modern Phys.* 25, 779 (1953).

A graphic integration of this curve to 20 kev and evaluation of the integral

$$-\frac{1}{k}\int_0^{20}\frac{dE}{\sqrt{E}}$$

leads to values of the range of protons in copper for energies from 0 to 400 kev. The deuteron ranges were found from:

$$R_d(2E) = 2R_p(E) \ .$$

Figure 89 shows these values.

From the above results, values of cross section as a function of penetration (Fig. 90) were found by

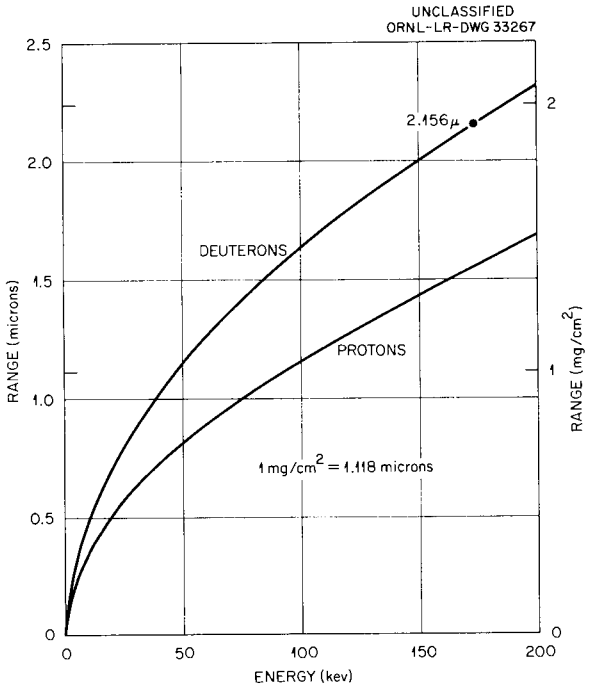

Fig. 89. Range vs Energy for Protons and Deuterons in Copper.

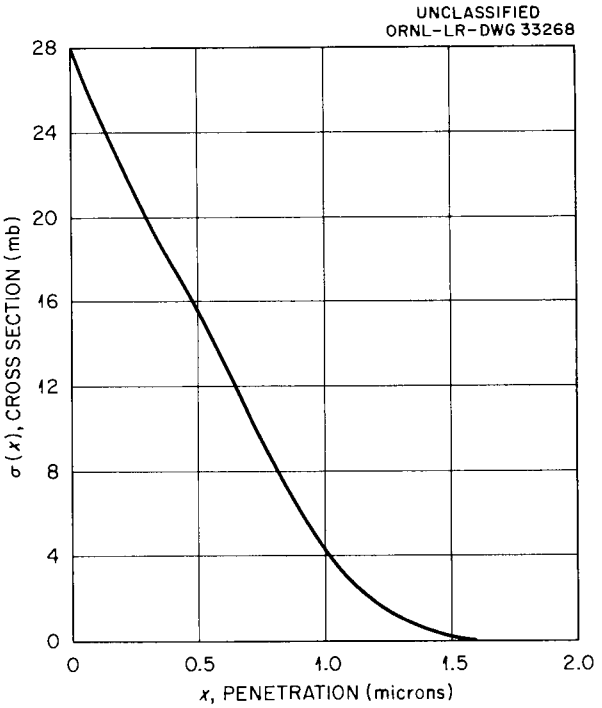

Fig. 90. Cross Section vs Penetration for Deuterons in Copper. Initial energy, 174 kev.

using the values of cross section as a function of energy reported by Arnold[11] and Wenzel.[12]

The values of β_k were found from Eq. 6 by graphic integration, since no simple analytic function could be found to express $\sigma(x)$. Due to the rapid decrease in β_k as k rises and to the fact that the time-dependent functions of Eq. 5 saturate rapidly for moderate k values, four terms of the summation were found to be adequate.

[11] W. R. Arnold *et al.*, *Phys. Rev.* 93, 494 (1954).

[12] W. A. Wenzel and W. Whaling, *Phys. Rev.* 88, 1153 (1952).

IRRADIATION AND QUENCHING EXPERIMENTS ON COPPER-ALUMINUM ALLOYS

M. S. Wechsler R. H. Kernohan

An aspect of irradiation effects that is of fundamental and practical importance is the way in which diffusion-controlled processes in solids are affected by the radiation. An example of a diffusion-controlled reaction that is accelerated or triggered by neutron bombardment is the process that causes the resistivity of certain alloys to decrease upon neutron irradiation.[1] The effect is particularly striking in Cu-Al and Cu-Zn. Upon neutron irradiation at ambient reactor temperatures, Cu-Al alloys show a sharp decrease in resistivity (Fig. 91). As the irradiation proceeds, the resistivity reaches a minimum at $0.5–1.0 \times 10^{18}$ neutrons/cm^2, followed by a linear increase. The magnitude of the decrease in resistivity increases with aluminum content, and no decrease is observed for pure copper. The process responsible for the decrease in resistivity is very likely diffusion-controlled.

[1]Some of these effects were described qualitatively in the previous progress report (R. H. Kernohan and M. S. Wechsler, *Solid State Ann. Prog. Rep. Aug. 31, 1957*, ORNL-2413, p 19); a detailed discussion of these experiments will be given by M. S. Wechsler and R. H. Kernohan, "Neutron Irradiation Effects on Cu-Al Alloys," *J. Phys. Chem. Solids* (to be published).

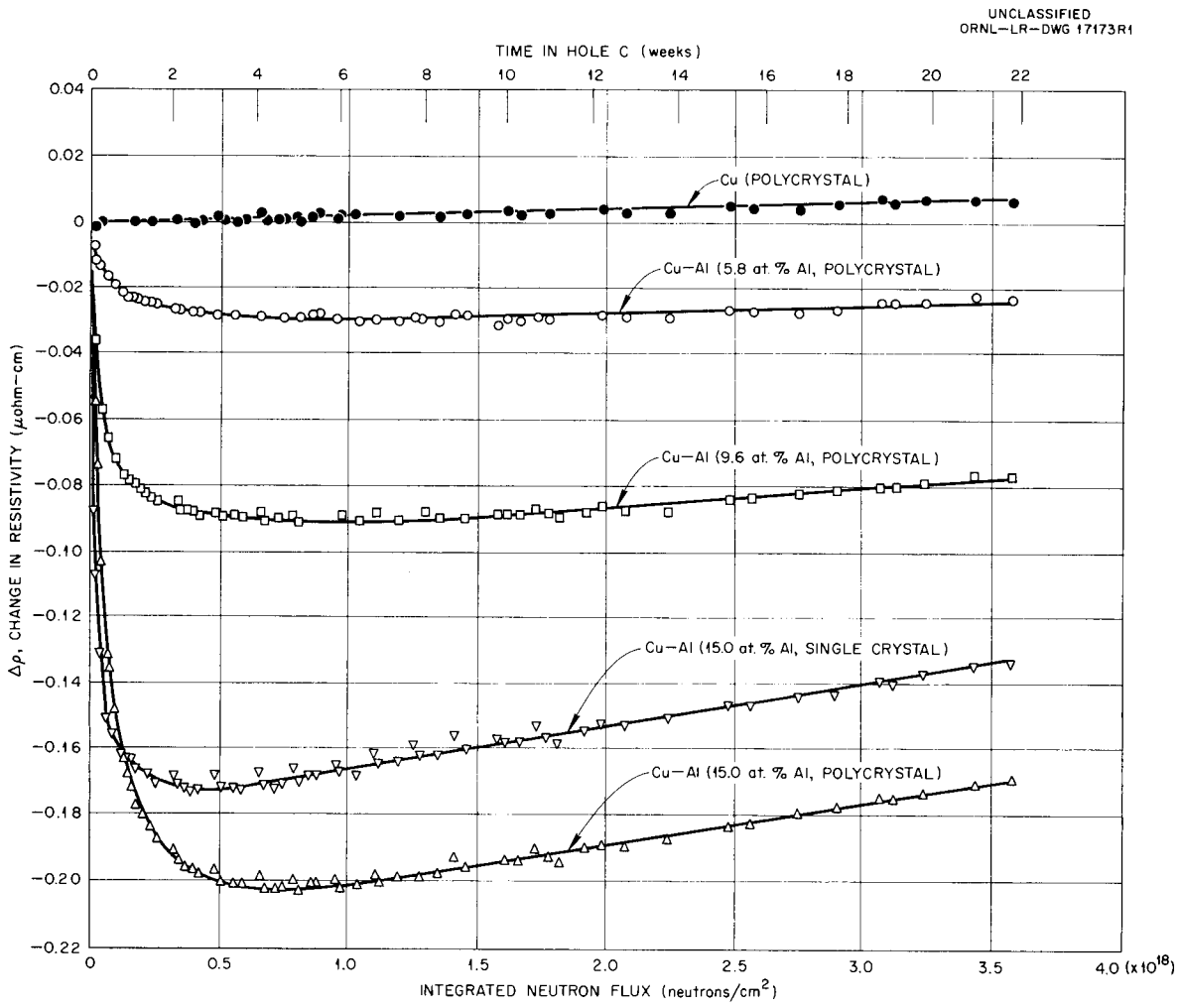

Fig. 91. Change in Resistivity (Corrected to 20°C) vs Exposure in Hole C at Ambient Reactor Temperature (~35°C).

This is indicated by the observation that no decrease in resistivity takes place when the irradiation is carried out at −120°C (Fig. 92). Figure 92 also shows that, when the sample is warmed above −50°C after irradiation at −120°C, the resistivity decrease will set in. This feature facilitates the study of the kinetics of the process.

Isothermal annealing curves at 0–34°C are shown in Fig. 93 for a number of Cu-Al samples that were previously irradiated for three weeks at −120°C. These curves were normalized, and a parameter f was calculated as a function of time at each temperature; f represents the fractional amount that the process departs from completion. The time τ corresponding to a given value of f was found to be given by an expression of the type:

$$\tau = \tau_0 \exp \frac{\epsilon_M}{kT} , \quad (1)$$

as can be seen in Fig. 94. The activation energy ϵ_M for the carrying out of the process is found to increase as the process progresses. In Fig. 95, ϵ_M is plotted vs f. An extrapolation of the curve to $f = 1$ indicates that the process starts with an activation energy close to zero. When the process is 50% completed, ϵ_M is about 0.8 ev, and the final value appears to be approximately 1.0 ev.

In general, it is felt that the alloy is in a metastable state in its preirradiated condition and that the irradiation endows the material with the ability to proceed to thermal equilibrium with an attendant decrease in resistivity. There are two possibilities as to the nature of the metastability. First, in its unirradiated state, the alloy may possess less than the equilibrium amount of order. In this event, it must be specified that the order is local, since no superstructure has been observed for these alloys. The irradiation may then be thought to introduce lattice vacancies, which enhance mobilities and permit the appropriate atomic rearrangements to take place at lower temperatures than they can in the absence of the irradiation. Unfortunately, no clear correlation is known to exist

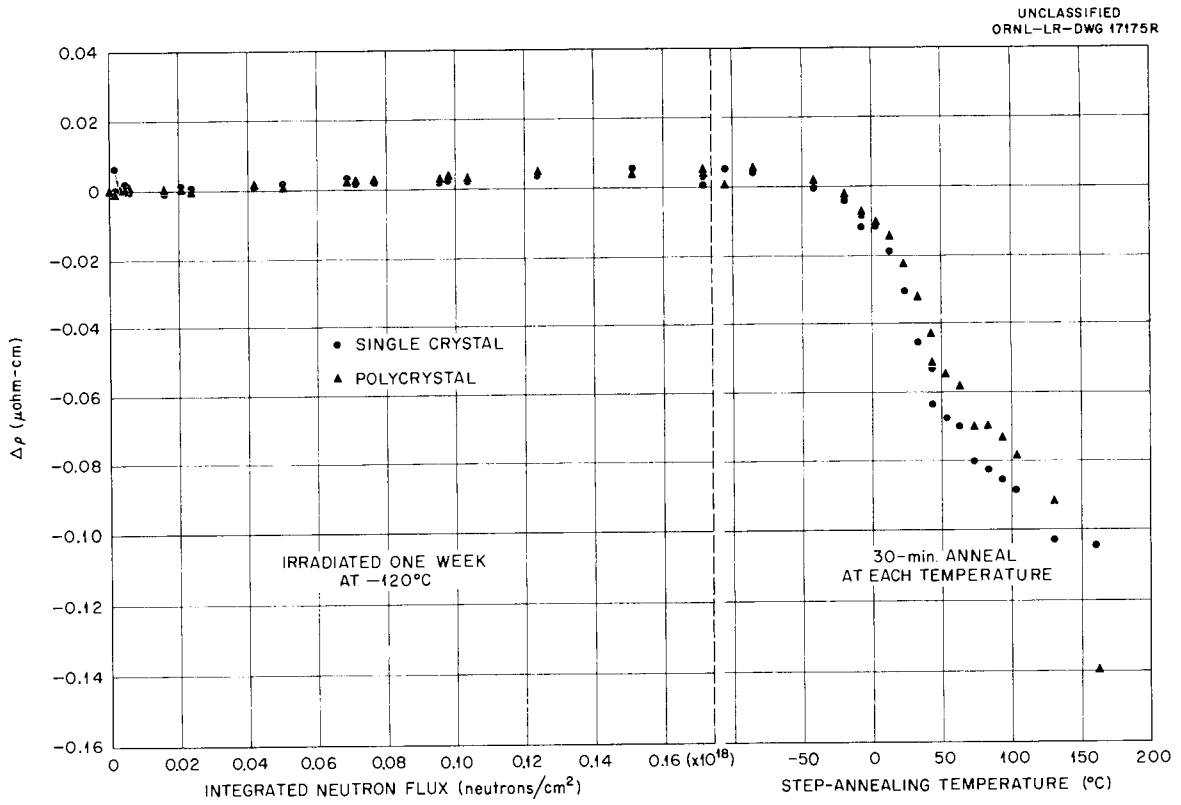

Fig. 92. Change in Resistivity of Cu-Al (15.5 at. % Al) vs Exposure at −120°C in Hole 52, Followed by Step-Annealing Measurements at −120°C.

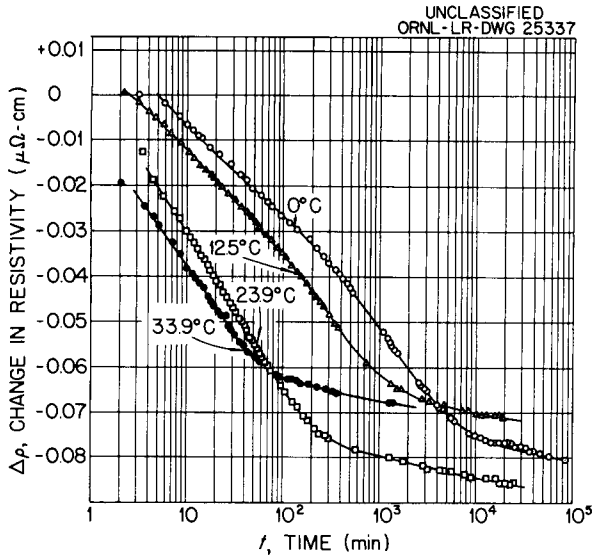

Fig. 93. Isothermal Annealing of Cu-Al (14.8 at. % Al) Samples Previously Irradiated for Three Weeks at −120°C.

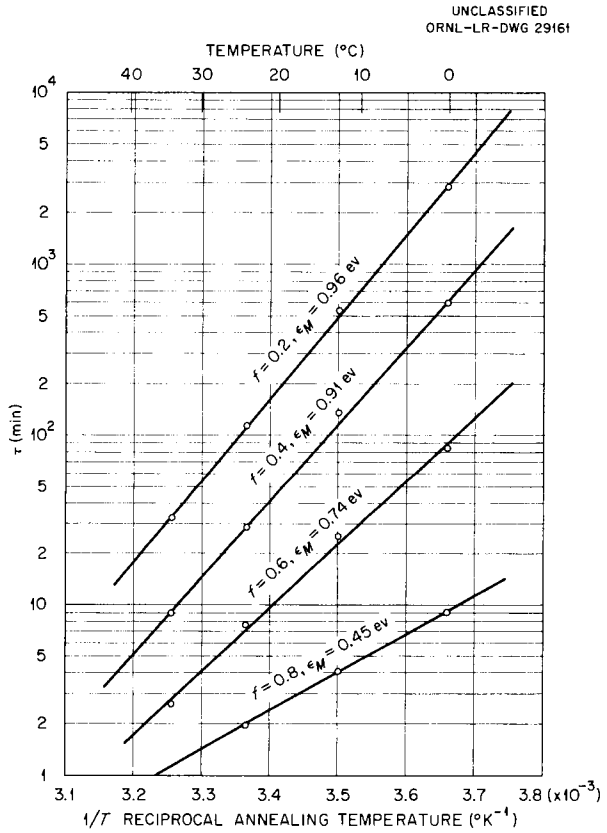

Fig. 94. Activation Energy Plot for Annealing After Irradiation for Three Weeks at −120°C. Cu-Al (15 at. % Al).

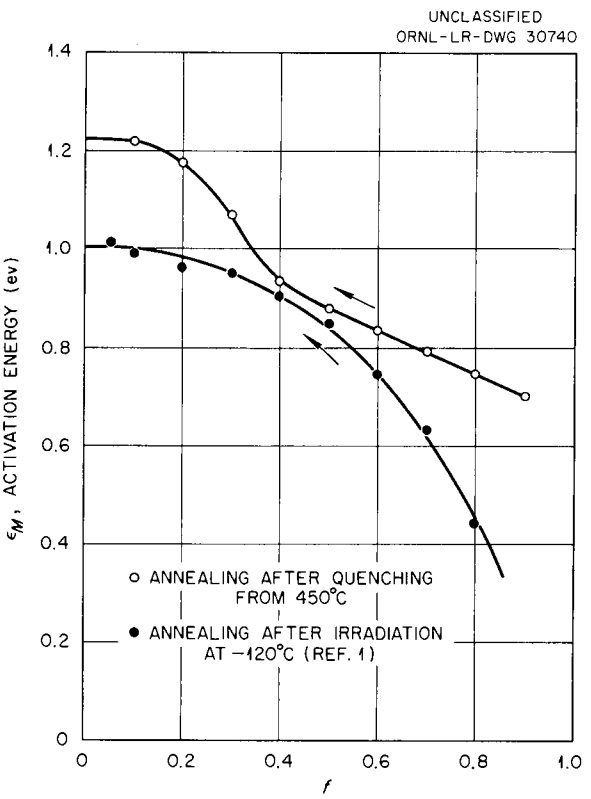

Fig. 95. Activation Energy vs *f* for Annealing After Quenching from 450°C. The data for annealing after irradiation at −120°C are shown for comparison. The process goes from *f* = 1 to *f* = 0 as indicated by the arrows.

between changes in short-range order and resistivity. A second point of view is that the metastability is due to a nonequilibrium concentration of lattice vacancies. In this case the neutron bombardment may introduce special sites at which the annihilation of the excess vacancies may take place. The details of this mechanism are rather complicated, however. For one thing, it must be postulated that the irradiation-produced vacancies agglomerate into voids and have a negligible effect on the resistivity.

In the event of either of the above-mentioned approaches to an explanation of the decrease in resistivity of Cu-Al alloys upon irradiation, it is suggested that a nonequilibrium configuration is established in the normal preparation of the alloys. This situation can result from the circumstances illustrated schematically in Fig. 96. If it were possible to maintain equilibrium during cooling, the

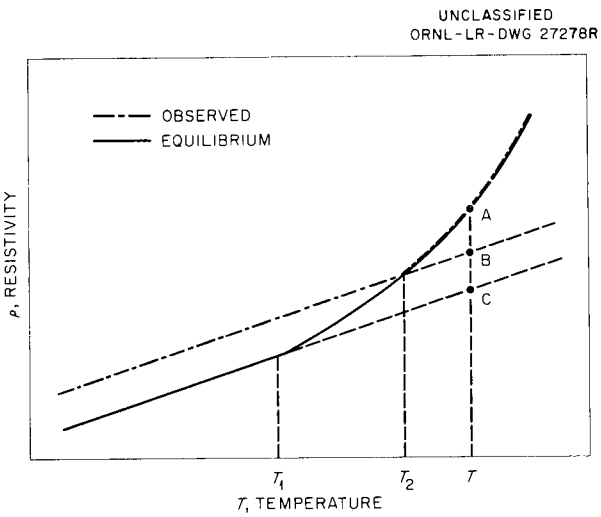

Fig. 96. Schematic Illustration of the Effect of Incipient Quenching.

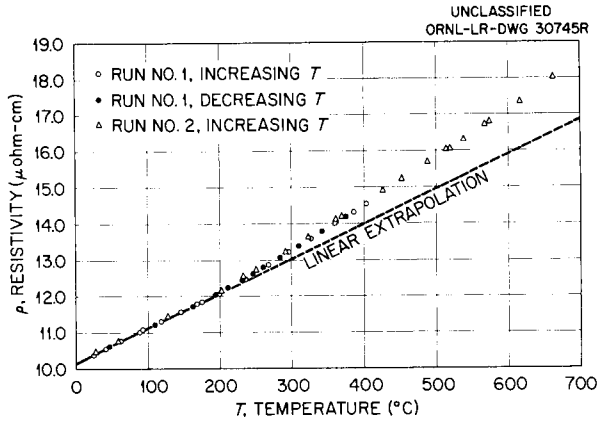

Fig. 97. Static Measurements of Resistivity vs Temperature.

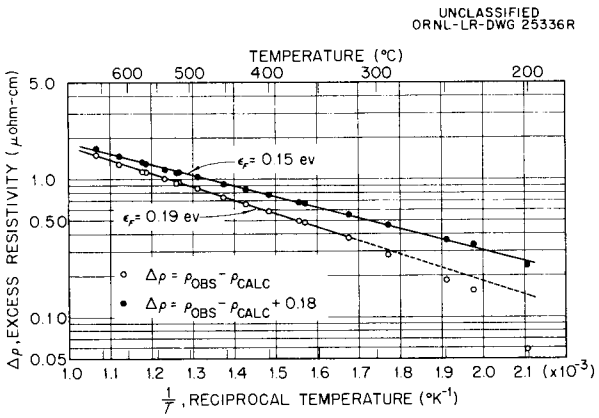

Fig. 98. Excess Resistivity from At-Temperature Measurements. Cu-Al (14.8 at. % Al).

resistivity would follow the full curve. However, at a temperature above T_1 the atomic mobilities become so low that it is impossible to avoid freezing-in the configuration characteristic of temperature T_2. Thus, at lower temperatures an amount of excess resistivity corresponding to BC is retained. Hence BC also represents the decrease in resistivity that takes place upon irradiation at ambient reactor temperatures. At-temperature measurements have been made that show this type of behavior. In Fig. 97 it is seen that the resistivity is a linear function of the temperature between room temperature and 200°C. However, above 200°C the observed values lie above a linear extrapolation of the measurements made below 200°C. It may be assumed that this deviation is due to the introduction of disorder or defects at the higher temperatures. Furthermore, if a single activation energy is associated with the formation of this higher-energy configuration, the excess resistivity is expected to be governed by the relation

$$\Delta\rho = A \exp \frac{-\epsilon_F}{kT} . \qquad (2)$$

The validity of this expression may be tested by plotting the difference between the observed and extrapolated points in Fig. 97 on a logarithmic scale vs reciprocal absolute temperature. This is shown by the open-circled points in Fig. 98. Equation 2 is well satisfied between 320 and 660°C with the value ϵ_F = 0.19 ev, but at lower temperatures the open circles fall lower than is predicted by Eq. 2. This behavior may be understood by reference to Figs. 96–98. The data in Fig. 97 correspond to the curve labeled "observed" in Fig. 96 with T_2 = 200°C. However, the irradiation experiments indicate that at lower temperatures the unirradiated alloy departs from equilibrium by an amount corresponding to BC in Fig. 96. If we assume that the irradiation facilitates the return to complete equilibrium, then we may take BC = 0.18 μohm-cm, since this is the decrease observed for the 15 at. % Al alloy upon irradiation at ambient

reactor temperatures.[2] For $T > T_2$, the excess resistivity is not given by AB in Fig. 96 but by $AB + BC$. Therefore, the $\Delta\rho$ values plotted in Fig. 98 should be increased by $BC = 0.18$ μohm-cm. When this is done, Eq. 2 is satisfied over the entire range of temperatures with a value of 0.15 ev for ϵ_F.

The discussion in the preceding paragraphs has indicated that, even upon slow cooling, it is extremely difficult to avoid retaining at low temperatures the disorder or defects characteristic of about 200°C. If this is the case, it should be possible to retain larger resistivities by increasing the cooling rate. The resistivity of Cu-Al (15 at. % Al) was measured as a function of air-cooling (~5 deg/sec) and water-quenching (~4×10^3 deg/sec) from various temperatures. The results of the measurements upon air-cooling are shown in Fig. 99, in which it can be seen that there is a slight tendency for the resistivity to decrease upon holding between 150 and 200°C but that when the air-cooling is done from temperatures above 200°C the resistivity is increased. However, when the air-cooling is done from temperatures above 310°C, the retained resistivity once again decreases. A similar behavior above 450°C was observed upon quenching into water. These measurements are shown in Fig. 100, where the results of the static (Fig. 98) and air-cooling (Fig. 99) experiments are also shown for comparison. Larger retained resistivities are observed for quenched samples than for air-cooled samples. The maximum quenched-in resistivity was observed at 450°C. The decrease in retained resistivity that occurs upon air-cooling from above 310°C and upon quenching from above 450°C indicates that the nature of the annealing process is affected by the temperature from which the sample is cooled. An increase in this temperature apparently causes the annealing during cooling to be accelerated, so that when the cooling is done from increasingly higher temperatures more and more annealing occurs during the cooling.

The annealing kinetics after water-quenching from 450°C have been studied. Figure 101 shows the normalized isothermal annealing curves for temperatures between 45 and 100°C. The time, τ, for various fractional amounts of completion of the process is plotted in Fig. 102 vs reciprocal

[2]The curves in Fig. 91 are considered to represent the superposition of a saturating decrease and a linear increase in resistivity. When this separation is made for the data of the single-crystal 15 at. % Al sample, the saturation value is −0.18 μohm-cm.

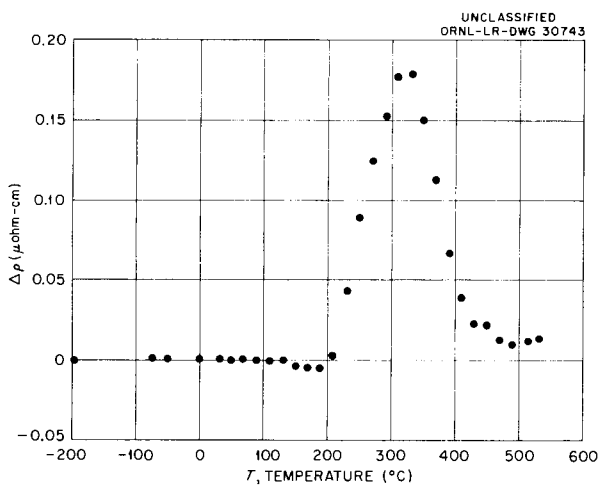

Fig. 99. Change in Resistivity Upon Air-Cooling. The sample was held at each T for 30 min. For $T > 30$°C, the sample was cooled in air to room temperature prior to insertion in liquid nitrogen. All measurements were made in liquid nitrogen.

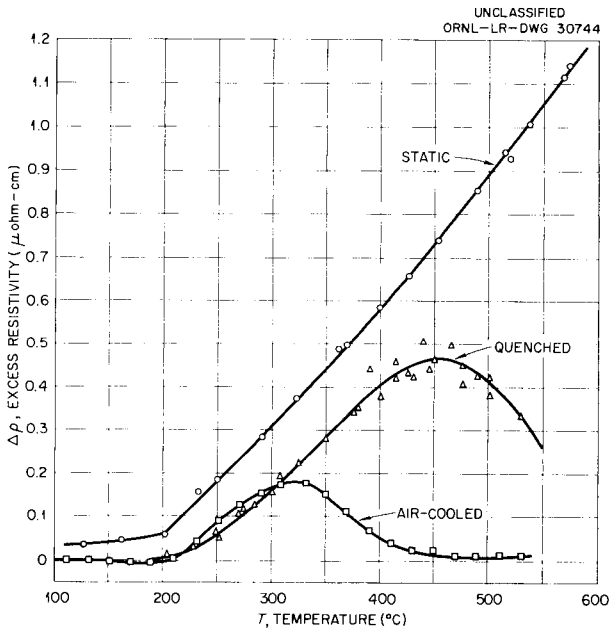

Fig. 100. The Quenched-In Resistivity as a Function of Quenching Temperature. The results of the static measurements (run 2) and the air-cooling measurements are shown for comparison.

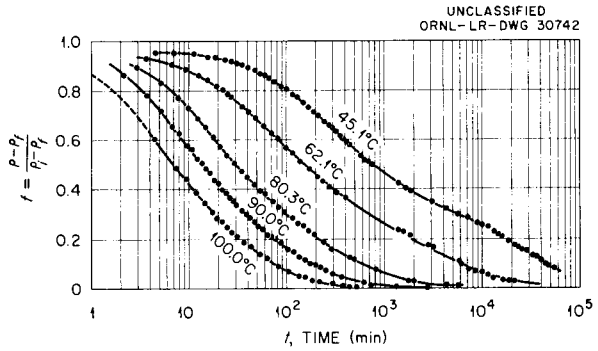

Fig. 101. Normalized Isothermal Annealing Curves After Quenching from 450°C.

annealing temperature. It is seen that Eq. 1 is fairly well satisfied at each value of f but that the value of ϵ_M increases as the annealing process proceeds (i.e., as f decreases). The variation of ϵ_M with f is plotted in Fig. 95, where a comparison is made between the annealing characteristics of the alloy after quenching and irradiation. In both cases the activation energy is lower at the earlier stages of the annealing. This indicates that the annealing may take place over a range of activation energies. At the outset, the lower-energy annealing modes predominate. But these apparently become exhausted. In order to continue the annealing, higher-energy barriers to the annealing must be surmounted. The irradiation appears to enable the annealing to proceed with a lower activation energy, particularly in the earlier portion of the annealing.

On the sole basis of the experiments described above, it is difficult to conclude whether an ordering reaction or the annealing of defects gives a more reasonable explanation for the effects. Experiments[3] are now in progress that offer the possibility of a more direct determination of the atom movements that are a consequence of the

[3]This work is being done in collaboration with B. S. Borie and C. J. Sparks of the Metallurgy Division.

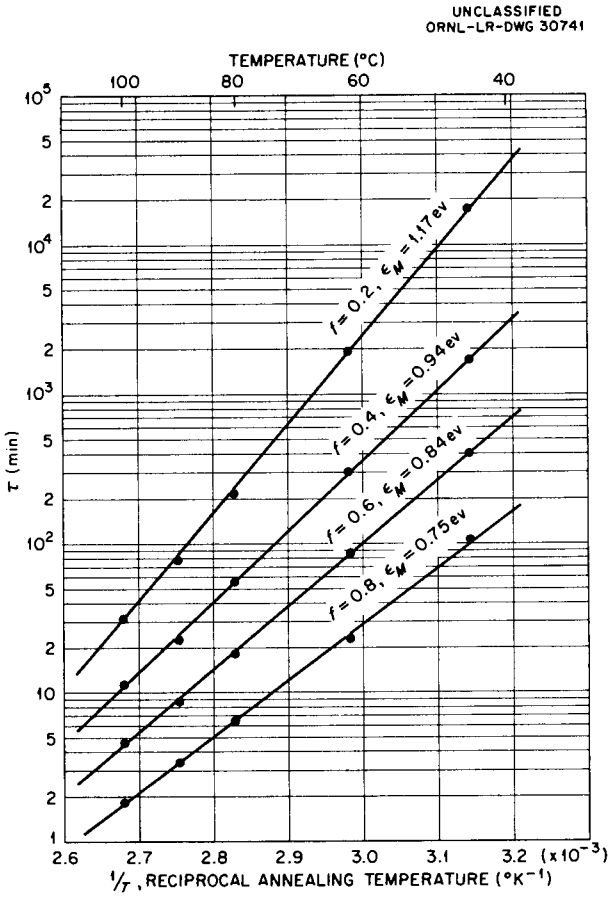

Fig. 102. Activation Energy Plot for Annealing After Quenching from 450°C.

irradiation and quenching treatments. The x-ray diffuse scattering from a single crystal of Cu-Al (15 at. % Al) is being examined in the $(hk0)$ plane of reciprocal space. A characteristic short-range-order diffuse scattering from the annealed crystal has been observed, which is different from that previously reported in the literature for other alloys. The corresponding measurements on irradiated and quenched samples have not yet been made.

MISCELLANEOUS SMALL-ANGLE X-RAY SCATTERING STUDIES OF Al-Ag

R. E. Jamison

The taking of small-angle x-ray scattering data from Al-Ag has been discontinued; the purpose of this article is to summarize the work and a large part of the analyzed data which has not been reported previously. Some of the data are well refined and are a confirmation of data reported elsewhere,[1,2] but part of the data is strictly preliminary in nature and is presented only for use by those who might continue such work.

Early difficulties in the experiment were overcome in large part without having to change the basic technique, described earlier[3] as a simple double-slit adaptation for a commercial diffractometer. The worst difficulties in order of magnitude were with inhomogeneities of silver content, variation in sample thickness, and variations in x-ray intensity. The latter two difficulties tended to spoil attempts to determine relative numbers of zones per unit volume.

The variation in x-ray intensity was overcome in part by adding a milliampere stabilizer to the x-ray unit and, at times, checking the intensity by use of a standard sample chosen for its unusual homogeneity.

Early in the experiment the undesirable variations in sample thickness and silver content were partly overcome by taking a large amount of data from quite a few samples to improve the results statistically. The important effects seen in these data are reviewed below:

1. The normal process of zone growth was retarded as a result of previous fast-neutron irradiation.

2. The normal ring-type scattering pattern was partly annihilated during early heat treatment following irradiation. This effect was never seen in nonirradiated samples and was seen most frequently in samples with previous irradiation of 5×10^{18} *nvt*. Data from only one pair of samples indicated that this effect possibly increases with initial zone size.

3. Unexplainable but definite lack of retardation was observed in one irradiated sample which was, in all obvious respects, like those samples which showed pronounced retardation.

The most interesting and consistent effect was the zone growth retardation, and when it seemed certain that this was real, effort was concentrated on several samples which were chosen by chemical analysis for uniform silver content (20 ± 1 wt %) and by x-ray analysis for uniform zone size and number of zones per unit volume. At about the same time, the counting technique was improved considerably by the addition to the apparatus of a commercial counting-rate computer. This computer allows continuous use of the x-ray source, thereby multiplying the data per man-day by a factor of 3.

After further study of the retardation in the selected samples, effort was concentrated on one pair of samples (unirradiated and irradiated, taken from adjacent positions in the parent foil following quench) which were unusually homogeneous with respect to x-ray scattering measurements. Figure 103 shows data taken from this pair of samples during early heat treatment. The reason for concentrating effort in only one pair of samples is

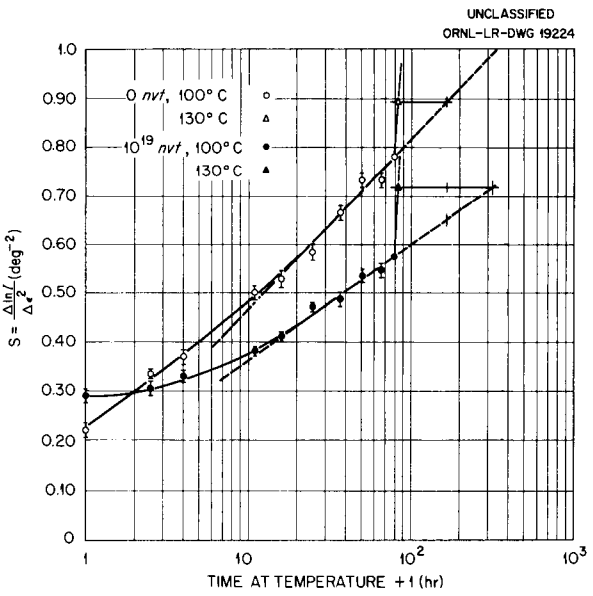

Fig. 103. Slopes of Scattering Curves vs Time at Temperature for Al-Ag.

[1] R. E. Jamison, *Solid State Semiann. Prog. Rep. Feb. 29, 1956*, ORNL-2051, p 41.

[2] R. E. Jamison, *Bull. Am. Phys. Soc.* 2, 151 (1957).

[3] R. E. Jamison, *Solid State Semiann. Prog. Rep. Feb. 29, 1956*, ORNL-2051, p 39.

obvious when it is realized that each point in this figure represents several days of nearly continuous x-ray measurements. It was impossible with existing facilities to obtain data for such a careful analysis from more than a few samples in a reasonable period of time.

Figure 103 shows plots of the slopes of the scattering curves vs time at temperature for a normal and a previously irradiated sample. The slopes are proportional to the square of the radii of gyration of the zones.[4] It can be seen that the rate of zone growth in the irradiated sample is nearly zero at zero time, indicating a very pronounced retardation due to previous fast-neutron bombardment. The initial difference between the irradiated and the unirradiated samples is what would be expected considering the temperature (~35°C) and duration (six months) of bombardment. Data not shown here indicate that with further heat treatment at higher temperatures the irradiated sample recovers, with its slope eventually exceeding that of the unirradiated sample. From x-ray photographs showing the streak pattern after onset of the true precipitation of Ag_2Al platelets, there is a scarcely perceptible indication that the onset of true precipitation is enhanced.

The tangents indicated in Fig. 103 at change of aging temperature after 78 hr at 100°C are the tangents used to determine "activation energies" for the process of zone growth. The "activation energy" for the unirradiated sample was found to remain nearly constant at about 26 kcal/mole, whereas that for the irradiated sample appeared to decrease from a nearly infinite value through the value 34 kcal/mole after 78 hr at 100°C and eventually decreased at higher aging temperatures to values less than those for the unirradiated sample.

At several points during the aging of this pair of samples, careful determinations of the relative x-ray intensities were obtained. Figure 104 shows the results of assuming that only one zone size is represented in each predominant slope of the scattering curve, extrapolating this slope to zero angle, and determining the intercept intensity. This intensity divided by the slope to the third power is a number proportional to the number of zones per unit volume.[4] The points in each set, 1 to 4, were selected because of nearly equal predominant slopes; so this plot is independent of time at temperature. As aging progresses from points 1 to 4 through the interval in which the plot of slope vs time at temperature for the irradiated sample falls below the same plot for the unirradiated sample (Fig. 103), the points indicating the number of zones per unit volume (Fig. 104) for the previously irradiated sample are seen to fall consistently above those for the unirradiated sample. With respect to time at temperature, point (3, normal) corresponds to a point about halfway between point (2, irradiated) and point (3, irradiated). Figure 105 shows a similar analysis when it is assumed that more than one zone size is represented in the predominant slope, and the same conclusion is reached with regard to the numbers of predominant zones per unit volume.

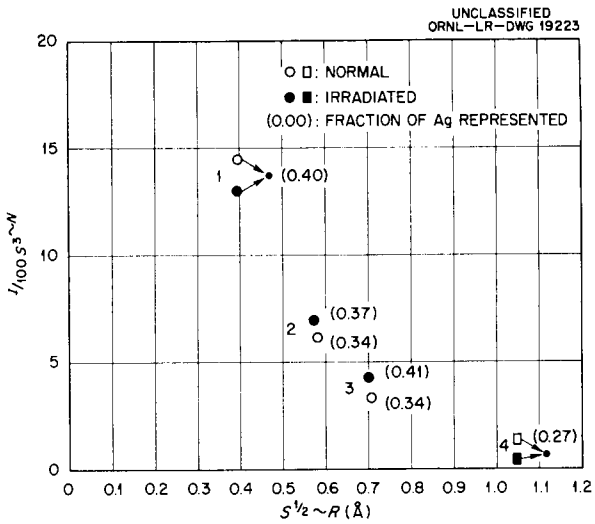

Fig. 104. Plot of I/S^3 vs $S^{1/2}$. Only one zone size assumed to be represented in each predominant slope.

Figure 106 shows some miscellaneous effects, including annihilation of the ring-type scattering pattern after very short aging time following irradiation. The intensity of the plot from the parent strip is not reliable, but the shape of the plot near zero angle is, and it appears that the reactor temperature of 35°C has caused a detectable partial annihilation.

Also seen in Fig. 106 is the apparent inability of this alloy to return to its original as-quenched condition when annealed for 17.5 hr at 525°C and requenched without cold-working. To the

[4] A. Guinier and G. Fournet, *Small Angle Scattering of X-Rays*, tr by C. B. Walker, Wiley, New York, 1955.

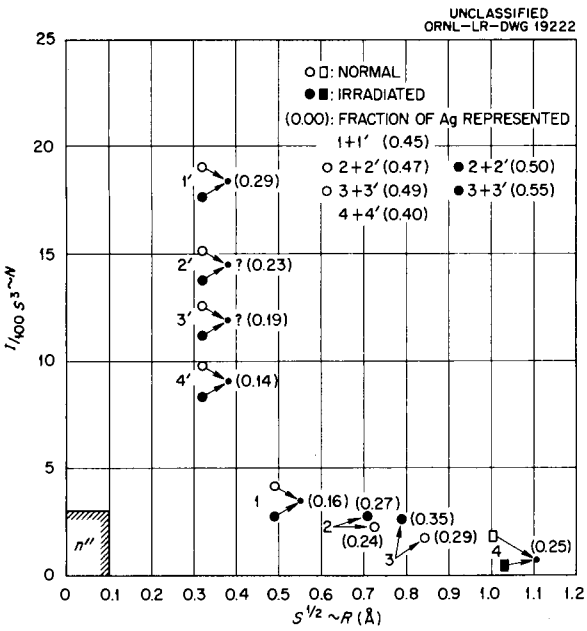

Fig. 105. Plot of I/S^3 vs $S^{1/2}$. More than one zone size assumed to be represented in each predominant slope.

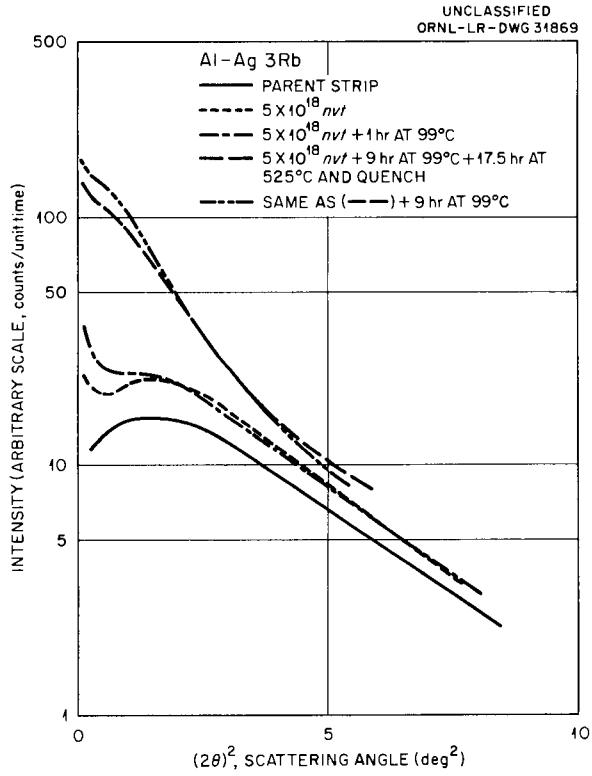

Fig. 106. Effects of Irradiation and Aging on Scattering Pattern. Sample 3Rb.

author's knowledge this effect has not been reported in the open literature even though it occurs in unirradiated as well as in previously irradiated samples. It possibly occurs to different degrees, depending on the amount of previous irradiation, and this might be interesting to examine in future work.

In an attempt to overcome the problem of sample inhomogeneities, various sample-forming techniques were attempted. Figure 107 shows data taken from an Al-Ag foil sample formed by compressing, sintering, rolling, and heat-treating mixed powders of aluminum and silver. Here again, the intensity indicated for the as-formed sample is not reliable, but an important effect on irradiating and aging is observed. After irradiation and ½ hr at 100°C there is a detectable partial annihilation of the already faint ring-type pattern. During the same time there is no detectable change in the predominant slope as there is in unirradiated similar samples during the same time. With an additional hour at 100°C, annihilation is nearly complete and the slope has increased considerably. This is assumed to be a rather direct observation of silver diffusing into the silver-poor shell surrounding each silver-rich zone[5] and then, after further heat treatment, actually enlarging the zone.

[5]C. B. Walker and A. Guinier, *Acta Met.* 1, 568 (1953).

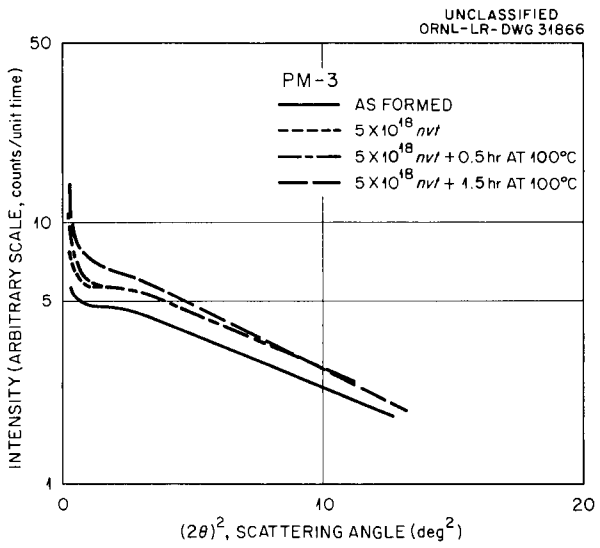

Fig. 107. Effects of Irradiation and Aging on Scattering Pattern. Sample PM-3.

The ring annihilation shown in both Fig. 106 and Fig. 107 has never been observed in unirradiated samples of any type. It has appeared in some samples formed in the regular manner, by melting aluminum and silver together in proper proportions, but mostly in those with only 5×10^{18} *nvt*. It has appeared in all the samples formed by the powder technique and given the same irradiation. It should be noted that the latter samples, as formed, would be expected to include a large number of microscopic voids and oxide inclusions. Nothing more can be said about the relative states of the samples formed by the two techniques with respect to the degree of lattice distortion or microscopic gradients in the silver concentration.

Another sample-forming technique which was tried was to clad pure silver foil with pure aluminum foil, roll the combination, sinter, roll again, hold for a time at solution temperature, and quench. Figure 108 shows scattering curves from such a sample, taken after various times at solution temperature, compared with a standard sample formed by the melting technique. Although a positive conclusion cannot be reached, because of assumed lack of reproducibility of the quenches, it appears that the ring diameter continues to increase with time at solution temperature while the increase in the predominant slope saturates. This technique, although resulting in a rather complex distribution of silver, seems to offer good possibilities for use in diffusion studies.

A rather unusual result of the very careful counting technique used late in the experimentation on Al-Ag is shown in Fig. 109. The use of the counting-rate computer allows measurements of intensities differing by a factor of 10^2, and multiple predominant slopes are seen in the scattering from aged Al-Ag samples. This could result from spurious scattering, but data from other samples showing various relative values of the predominant slopes indicate that it does not. The sample is not particularly homogeneous, and it is suspected that the various slopes result from an irregular range of zone sizes within the sample. Another and more interesting possibility is that the slopes correspond to different dimensions of nonspherical zones uniform in silver content. An irradiation of 10^{19} *nvt* seems to have very little if any effect on a similar sample. The most carefully taken data from the irradiated sample have not been

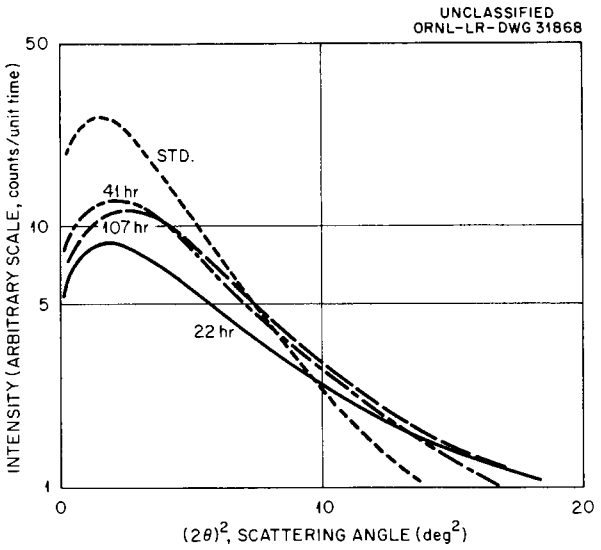

Fig. 108. Scattering, After Various Times at 520°C, from Sample Prepared by Cladding Foils.

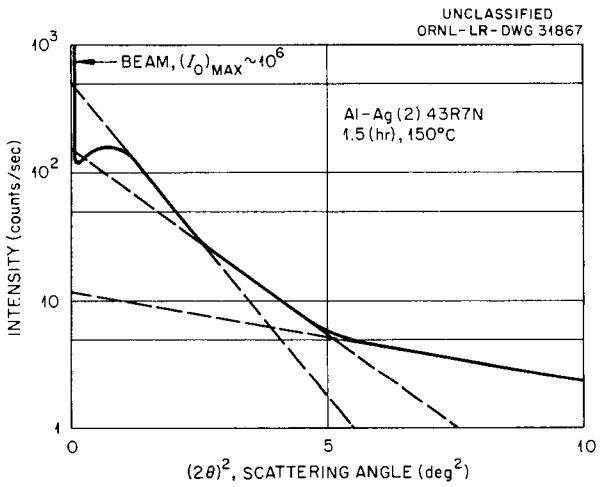

Fig. 109. Scattering from Sample Al-Ag (2) 43R7N.

analyzed, but it can be concluded that there is not the pronounced redissolving of silver in the large zones that might be expected, assuming the existence of thermal or displacement spikes. In fact, there appears to be a slight change in the opposite direction but with a slight increase in the number of zones per unit volume. A corresponding increase in slope by thermal treatment would result in a decrease in the number of zones per unit volume as seen in Fig. 104. The anomaly could result from radiation-induced true precipitation, although this is not observable in x-ray photographs of the irradiated sample.

SOME MECHANICAL YIELD PHENOMENA IN UNIRRADIATED AND FAST-NEUTRON-IRRADIATED PURE COPPER SINGLE CRYSTALS

R. E. Jamison

Introduction

A qualitative study of the nature of mechanical yielding in irradiated copper was undertaken following the observation of yield points and slip-line structures in fast-neutron-irradiated pure copper single crystals similar to those seen in α-brass.[1] The object was to look for dependencies in the nature of the yield phenomena on amounts of previous irradiation as well as on temperatures and times between various interrupted and alternated extensions at 78 and 300°K. Recent interest and the reporting of similar data by others have encouraged the author to describe in this report some of the work performed early in 1953, which, partly because of the rather unusual results and relatively sparse data, has been withheld from publication. Haasen and Kelly[2] have recently reported results from a very similar and thorough study of mechanical yielding in aluminum and nickel single crystals. They point out that a yield point, shown schematically in Fig. 110 and characterized simply by a positive value for $\Delta\sigma$, is of general occurrence in single crystals of pure face-centered cubic metals deformed at low temperatures. The results from copper described here are compared with the results of Haasen and Kelly from nickel, and the effects of previous neutron irradiation on values of $\Delta\sigma$ are emphasized. The irradiation effects may contradict the explanation of the yield-point phenomenon favored by Haasen and Kelly.

[1] R. E. Jamison and T. H. Blewitt, *Phys. Rev.* 86, 641 (1952).

[2] P. Haasen and A. Kelly, *Acta Met.* 5, 192 (1957).

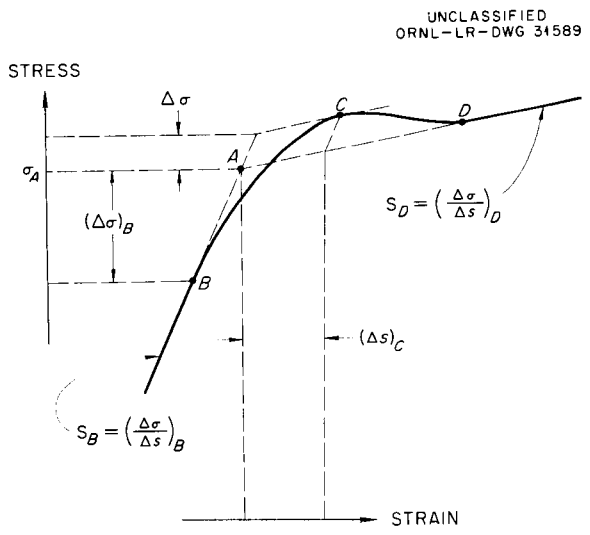

Fig. 110. Schematic of the Mechanical Yield Phenomenon Showing Various Parameters Which May Be Determined from the Load-Elongation Curve.

Experimental Details

Single-crystal tensile specimens of nearly pure copper were prepared and deformed by the same techniques as those described by T. H. Blewitt.[3] The following four main types of tests were carried out in various orders on each specimen:

Test 1. The specimen was strained a few per cent at either 78 or 300°K, unloaded for a time, and then further strained at the same temperature.

Test 2. The specimen was strained a few per cent at 78°K, unloaded and annealed in place at 300°K, and then further strained at 78°K.

Test 3. The specimen was strained a few per cent at 300°K, unloaded for a time, lowered to 78°K, and then further strained at 78°K.

Test 4. The specimen was strained a few per cent at 78°K, unloaded and annealed in place at 300°K, and then further strained at 300°K.

In most of the tests, values of the various parameters associated with the re-straining and indicated in Fig. 110 were easily determined from the automatically recorded load-elongation curves. This article is concerned mainly with values of $\Delta\sigma$, which is a measure of the maximum divergence of the curve from the extrapolation of the nearly linear portion beyond point D.

Results

The results from two samples of like original orientation are summarized in Fig. 111. The values from the irradiated sample were more erratic than those from the unirradiated sample and are shown here somewhat idealized. The samples

[3] T. H. Blewitt, *Phys. Rev.* 91, 1115 (1953).

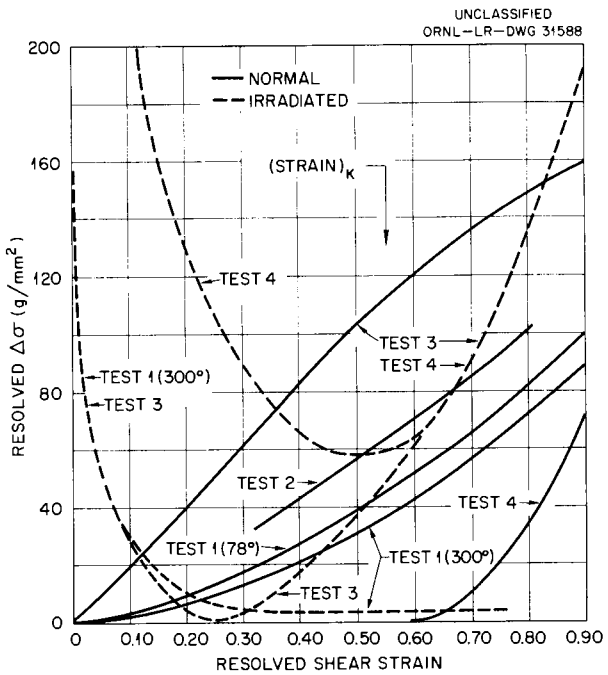

Fig. 111. Resolved $\Delta\sigma$ vs Resolved Shear Strain from Various Tests for Two Copper Single Crystals of the Same Orientations, One with 1.5×10^{19} *nvt*. The original angles between the three nearest [100]-type poles were 44.5, 47.5, and 78.5°.

were calculated to be in single slip for all the data represented in this figure. The approximate strain beyond which there is very little difference in values of σ_A between the irradiated and unirradiated samples[4] is indicated by $(\text{strain})_K$. As discussed elsewhere,[4-6] σ_A and the temperature dependence of σ_A are increased with previous fast-neutron irradiation, while the rate of hardening is reduced for strains less than $(\text{strain})_K$. This should be remembered when comparing these plots of $\Delta\sigma$ vs strain with the plots by Haasen and Kelly of $\Delta\sigma$ vs σ_A.

As Haasen and Kelly found for nickel, $\Delta\sigma$ is increased for test 2 over that for test 1 and is independent of time at 300°K for times greater than a few minutes. However, the ratio of the value for test 2 to that for test 1 at 78°K is not nearly so high here as that for nickel. This might be partly accounted for by the difference in orientation. It is assumed that a large portion of the data from nickel (perhaps for values of $\sigma_A > 7$ kg mm^{-2}) is taken from the sample in double slip. Also, it should be noted that the strain rate used here is $\sim 2.2 \times 10^{-4}$ sec^{-1}, which is at least two times that used by Haasen and Kelly.

The only other noteworthy difference between the results from nickel and those from unirradiated copper is in test 3: Haasen and Kelly reported a wide scatter in the values from nickel, whereas there is no such scatter in the values from unirradiated copper. It might be assumed that the scatter observed by Haasen and Kelly resulted from the relatively high concentrations of impurities in the nickel used. This seems particularly plausible in view of the effects of irradiation on the results of test 3 on copper.

The pronounced effect of irradiation in various tests on copper is rather spectacular. For strains less than ~0.30 the effect on $\Delta\sigma$ in Fig. 111 is masked by the superposition of a radiation-induced yield point, larger in magnitude than the deformation-induced yield point. Beyond this strain, it is seen that (1) there is a pronounced decrease in values of $\Delta\sigma$ from tests of types 3 and 1 at 300°K, (2) there is a pronounced increase in values of $\Delta\sigma$ from tests of type 4, and (3) neither of these effects is apparently correlated with the effects of irradiation or temperature on σ_A.

Particularly interesting are the results shown in Fig. 112 from a slightly irradiated sample with an original orientation such that it is in double slip during a large portion of its deformation. All the pulls shown are at 300°K and, except for No. 1, are of test 4 type, having been just previously strained at least 3% at 78°K before releasing, aging at 300°K, and reloading. The following effects are very pronounced:

1. The radiation-induced yield point which appears on the first pull decreases in magnitude as deformation proceeds, until in pull 9 there is no apparent superposition of a radiation-induced effect.
2. The deformation-induced yield point is easily distinguishable from the radiation-induced yield point, the former increasing in magnitude until double slip is calculated to occur, while the latter decreases in magnitude to zero (pulls 1, 4, 6, and 9).
3. There is a sharp discontinuity in the plots of $\Delta\sigma$ vs strain and $(\Delta s)_C$ vs strain. From the results shown in Fig. 111 it can be assumed that

[4] R. E. Jamison and T. H. Blewitt, *Phys. Rev.* **91**, 237 (1953).

[5] T. H. Blewitt and R. R. Coltman, *Phys. Rev.* **82**, 769 (1951).

[6] D. K. Holmes *et al.*, *Bull. Am. Phys. Soc.* **1**, 130 (1956).

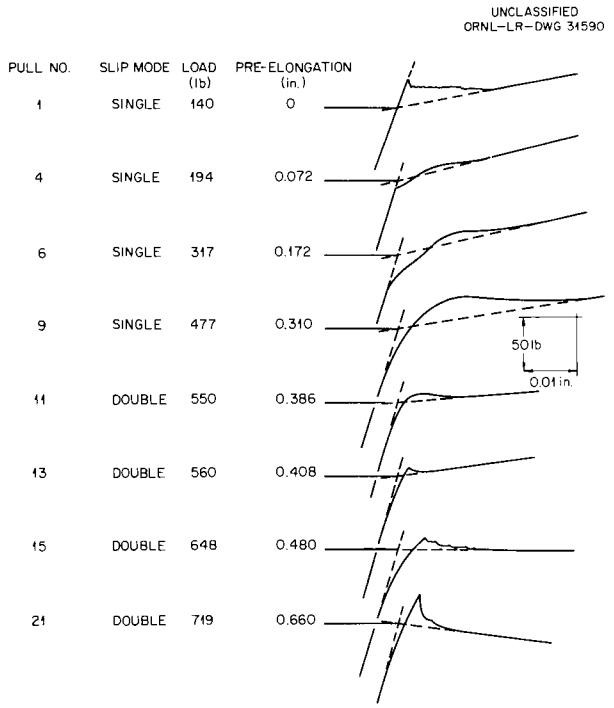

Fig. 112. Portions of Load-Elongation Curves at Mechanical Yielding for a Copper Single Crystal with 5×10^{17} *nvt*. The original angles between the crystal axis and the three nearest [100]-type poles were 40, 57.5, and 69°. The original gage length was 1.44 in.

this discontinuity is at least accentuated by the previous irradiation.

4. After the observed discontinuity, a third and entirely new type of yield point develops, apparently related to the amount of previous double slip, becoming larger in magnitude as double slip proceeds.

The remaining data from this sample indicate among other things that while the results of test 4 are apparently orientation-dependent as shown, the results of test 1 are not.

Various miscellaneous results were obtained from irradiated and unirradiated copper, as follows:

1. Radiation-induced yield points or superposition of yield points occurs on early pulls at both 78 and 300°K. The superposition of a radiation-induced yield point is particularly pronounced at room temperature and carries throughout the data shown in Fig. 111.

2. As would be expected, a decrease in S_B (Fig. 110), which is usually seen on reducing the temperature of the strain (test 3), is not so pronounced where there is indication of a superimposed radiation-induced yield point.

3. When the load is released before point D (Fig. 110) is reached, the characteristics of the load-elongation curve on reloading are very different from those of the regular curves.

4. Zero values of $\Delta\sigma$ from test 4 in unirradiated copper are generally accompanied by relatively large values of $(\Delta\sigma)_B$.

Discussion

Possibly the most important results described here are the three distinct types of yield-point phenomena (seen in pulls 1, 9, and 15 of Fig. 112). To date, there has been some confusion because of considerable use[7] of the term "yield point" to describe various effects in metals and alloys and irradiated metals without differentiation of the various types of mechanical yield which may be generally describable as "yield-point phenomena." The dependence of the yield type, as well as the magnitude of the yield point, on sample history might, in fact, account for the difference of opinion between Haasen and Kelly and T. H. Blewitt about proposed mechanisms. Blewitt's results[3] for test 2 were taken from a sample definitely in double slip, whereas Haasen and Kelly's conclusion that the yield point was not a strain-aging effect could possibly have resulted from observations of samples only in single slip.

The mechanism proposed by Haasen and Kelly, described as an irreversible process occurring during unloading which results in a rearrangement of dislocations, does not seem to be supported by the data from irradiated copper. For example, it seems difficult, at least with a simple argument, to explain by use of the irreversible unloading mechanism the simultaneous decrease in values of $\Delta\sigma$ for test 3 and the increase in values of $\Delta\sigma$ for test 4 resulting from previous irradiation.

---

[7] J. C. Fisher, in *Dislocations and Mechanical Properties of Crystals; an International Conference Held at Lake Placid, Sept. 6–8, 1956*, p 513, Wiley, New York, 1957.

HRP RADIATION METALLURGY

J. C. Wilson
R. G. Berggren F. M. Grizzell J. T. Humphries[1]

The HRP radiation metallurgy program is mainly concerned with evaluating the effects of fast-neutron irradiation on steels and welds used in pressure vessel construction.[2] Most of the effort of the last year went into carrying out a number of irradiation experiments in the MTR, the procurement of alloys, and machining of specimens. On the order of 1300 specimens were irradiated during the year and testing is still in progress, with a backlog of several hundred untested specimens. The objectives sought in the irradiation program were to determine the effects of elevated irradiation temperature, to evaluate the effect of specimen size (by comparing full-size Charpy V-notch specimens with the subsize Izods used before), and to irradiate larger quantities of specimens so that the effect of different irradiation and testing variables could be investigated in a selected number of steels.

Notch-Impact Properties

Because annealing of the radiation effects is to be expected at the operating temperature of power reactors, it is necessary to determine the effect of irradiation temperature. Much of the information on irradiation effects has been obtained in the range from 100 to 200°F because of the difficulty of irradiating large numbers of specimens at controlled elevated temperatures in high-flux reactors. An apparatus for irradiating approximately 300 tensile and impact specimens was successfully used in the MTR.[2] Gamma-ray heat was used to obtain the range of temperatures desired. Figures 113 and 114 show the notch-

[1] Co-op student, University of Tennessee.

[2] J. C. Wilson, R. G. Berggren, and F. M. Grizzell, *Solid State Ann. Prog. Rep. Aug. 31, 1957*, ORNL-2413, p 75.

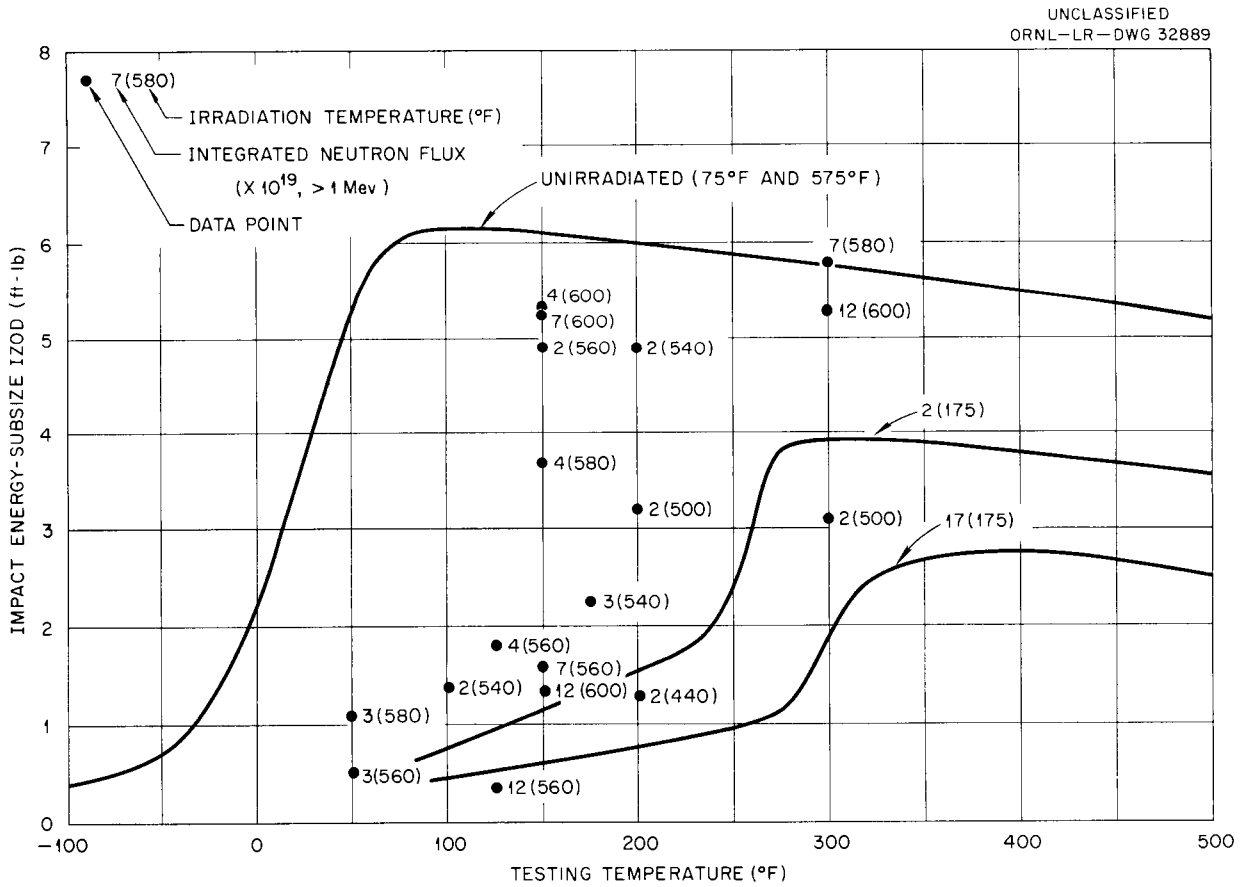

Fig. 113. Subsize Notch-Impact Results for Irradiated ASTM A-212 Grade B Carbon Steel Plate.

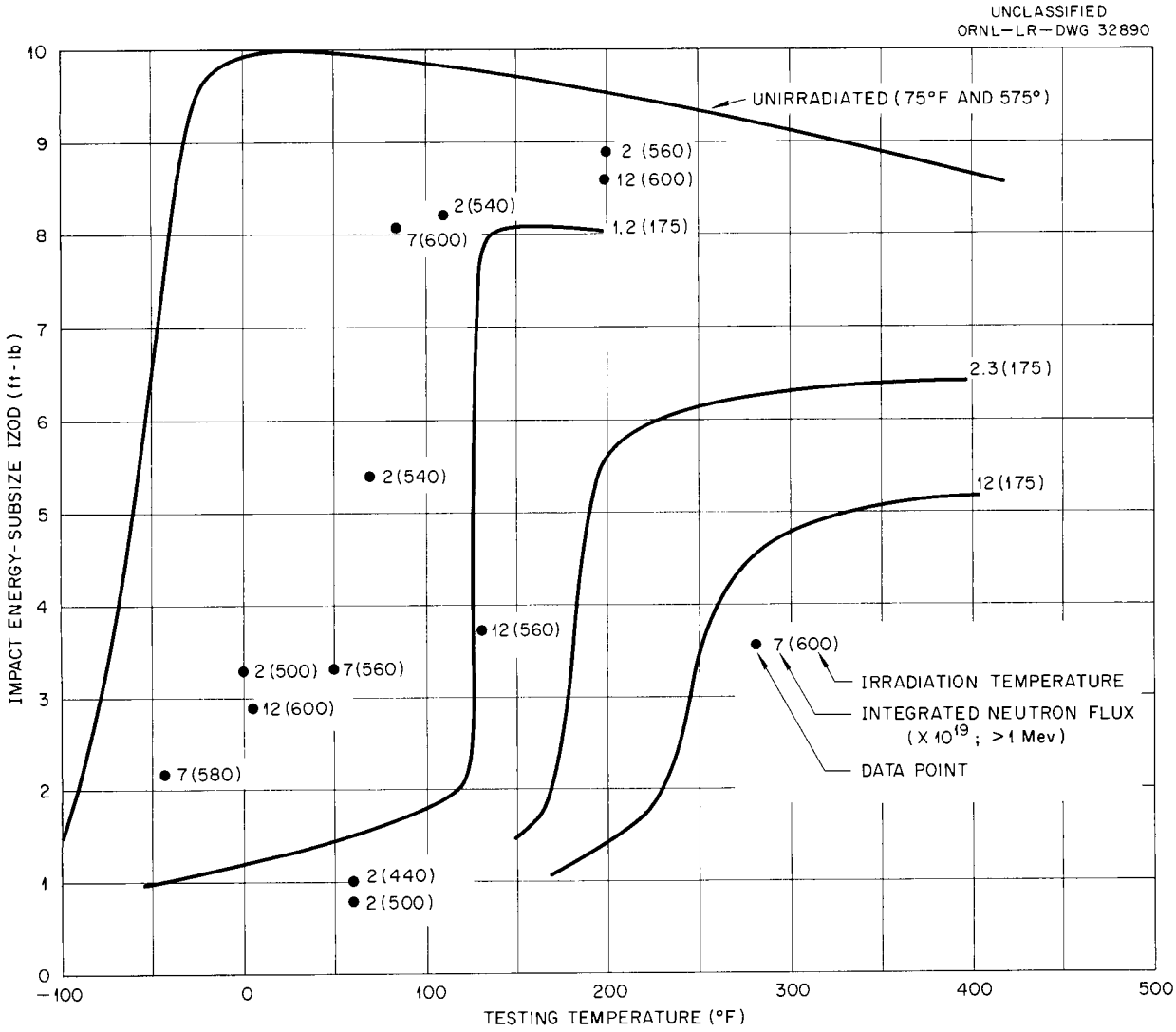

Fig. 114. Subsize Notch-Impact Results for Irradiated Carbon-Steel Weld (E-7016 Rod) (Item 65W).

impact results for a wrought steel and a corresponding weld metal. The full curves show the earlier results at lower irradiation temperatures; the individual points give both irradiation temperature and dose. From these data points it is possible to outline the temperature and flux dependence of the transition-temperature shift in these materials, Figs. 115 and 116. Similar data on several other steels have been obtained, and the results fall within the limits shown in Figs. 115 and 116. The most striking feature of these curves is that the transition-temperature shift is extremely sensitive to fast-neutron dose and irradiation temperature, particularly at the lower doses. The amount of reduction in radiation effects seen in Figs. 115 and 116 for a given irradiation temperature is not the same.

Doses up to 10^{19} fast neutrons/cm^2 and irradiation temperatures between 500 and 600°F are typical for water- and gas-cooled power-reactor vessels. It is easily seen that careful estimation or determination of fast-neutron doses and service temperatures will be required to evaluate the effects of irradiation in reactor vessels.

The effect of irradiation temperature was determined in a number of steels in both normalized and hot-rolled conditions with Charpy V-notch

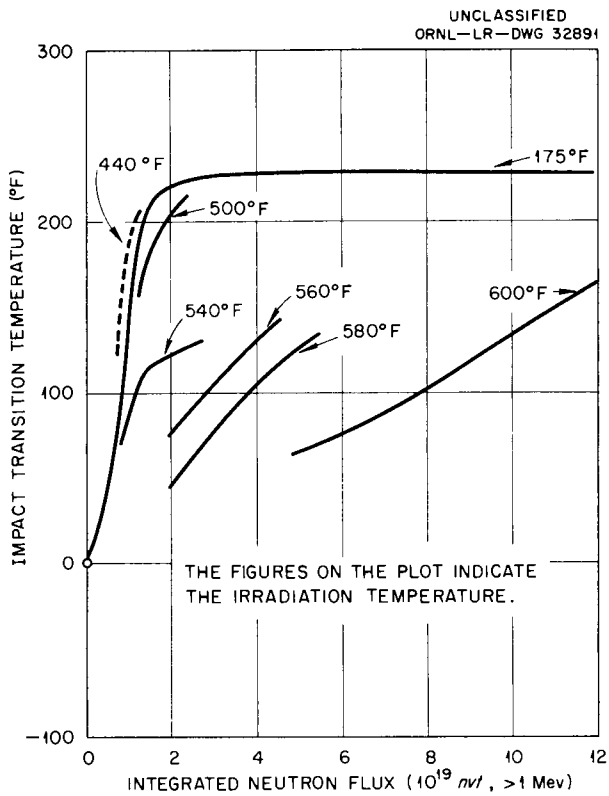

Fig. 115. Estimated Impact Transition Temperatures of Irradiated ASTM A-212 B High Tensile Strength Carbon-Silicon Steel; Subsize Izod Test, 4-in. Plate, Hot-Rolled (Item 65).

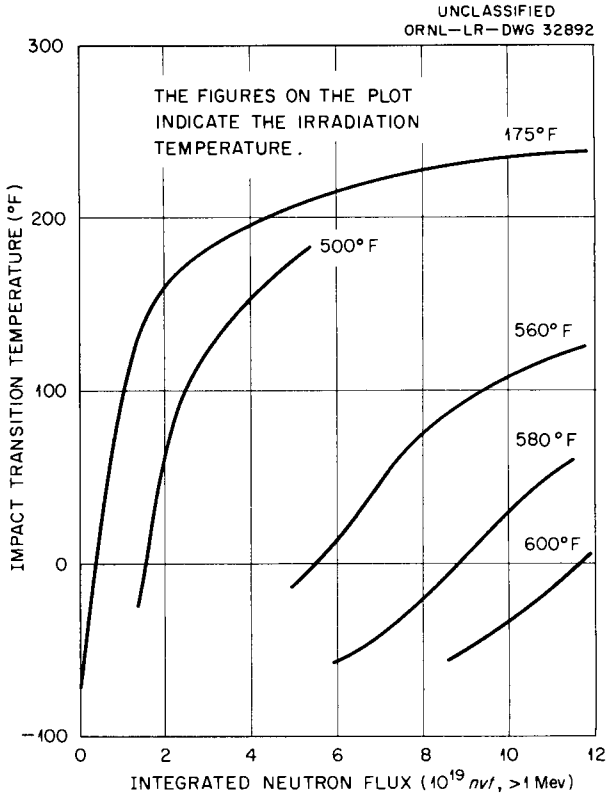

Fig. 116. Estimated Impact Transition Temperature of Irradiated Carbon-Steel Weld Metal; Subsize Izod Test, 4-in.-Thick Multipass Butt Weld, E-7016 Electrode, Stress Relieved (Item 65W).

specimens. Doses of 1 and 5 × 10^{18} fast neutrons/cm^2 were employed at irradiation temperatures of 175 and 575°F. Two of the curves are shown in Figs. 117 and 118; in one case the effects are decreased by the higher irradiation temperature as much as they are decreased by a factor of 5 reduction in dose, but in the other case (Fig. 118) there is little beneficial effect of the higher irradiation temperature. Apparently there are slight differences in the effects of a given irradiation temperature, even in steels of similar types. This conclusion is of course confirmed in Figs. 115 and 116. The transition-temperature shifts for the Charpy specimens are shown in Table 5.

High-purity iron and a high-purity iron alloy containing 0.14% carbon have been studied to determine the effects of purity. The analyses

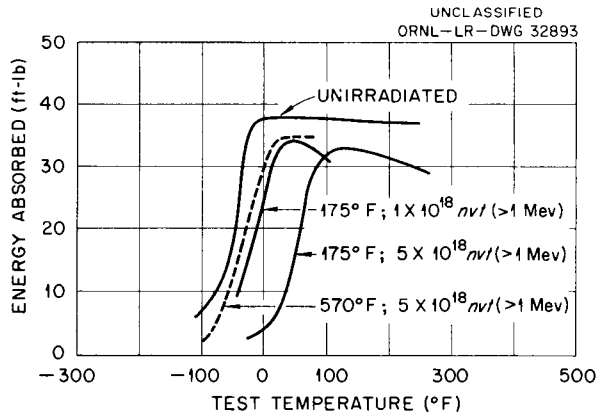

Fig. 117. Charpy V-Notch Impact Strength of Irradiated ASTM A-212 B High Tensile Strength Carbon-Silicon Steel; $\frac{5}{8}$-in. Plate, Normalized from 1700°F (Item 43).

are listed in Table 6. Two different grain sizes were produced in the iron by subcritical and supercritical anneals. Figures 119 and 120 show the results. The shifts in transition temperature for the same dose are much less than those observed in steels: a typical steel might show a transition-temperature increase of 300°F at the higher doses at which the high-purity iron and iron-carbon alloys show increases of 70 to 180°F. The alloy with 0.14% carbon also shows very little change as compared with steels of the same carbon content. Apparently the large radiation-induced transition-temperature shift in steels is not a characteristic (as had been thought) of the carbon-containing body-centered cubic lattice. Another peculiarity of the irradiated high-purity iron and iron-carbon alloys is that no appreciable drop in energy absorption occurs above the transition temperature. In steels a drop of the order of 30 to 50% is observed at high doses. It is not yet known why the high-purity materials have such different properties from the steels. Possibly the annealing temperature for radiation-produced defects is lower in the higher purity materials. This does not seem likely in view of the data on annealing of iron and steels by Kunz and Holden[3] and by Mehan and Baldwin.[4] It is quite surprising that the least change in the high-purity iron alloys was seen in the coarse-grained

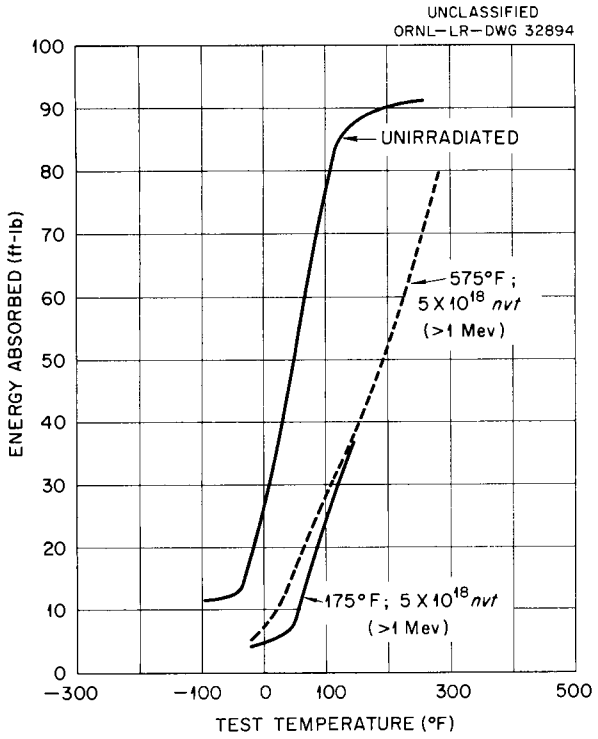

Fig. 118. Charpy V-Notch Impact Strength of Irradiated ASTM A-212 B High Tensile Strength Carbon-Silicon Steel; 6-in. Plate, Normalized and Stress Relieved (Item 115).

[3] F. W. Kunz and A. N. Holden, *Acta Met.* **2**, 816 (1954).

[4] R. L. Mehan and E. E. Baldwin, *Effects of Neutron Radiation on Notched Bend and Tensile Properties of ASTM A-201A Carbon Steel*, KAPL-1874 (Nov. 9, 1957).

Table 5. Charpy V-Notch Impact Transition Temperatures of Several Irradiated Steels

Material	15-ft-lb Transition Temperature (°F)			
	Irradiation*			
	None	1×10^{18} n/cm², 175°F	5×10^{18} n/cm², 175°F	5×10^{18} n/cm², 575°F
ASTM A-212 grade B, hot-rolled ¾-in. plate	−85	−30	25	−40
ASTM A-212 grade B, normalized ¾-in. plate	−65	−20	55	−30
ASTM A-212 grade B, normalized 6-in. plate, ¼ thickness	−30		70	35
ASTM A-285 grade A, hot-rolled ¾-in. plate	40	105	200	125
ASTM A-285 grade A, normalized ¾-in. plate	10	60	150	115
ASTM A-301 grade B, furnace-cooled from 1675°F, ¾-in. plate	15	70	170	110

*Flux values are integrated neutron flux > 1 Mev.

Table 6. Chemical Analyses of Iron and Iron-Carbon Alloy

Element	High-Purity Iron (%)	Iron-Carbon Alloy (%)
Carbon	0.004	0.138
Oxygen	0.0038	0.0023
Nitrogen	0.000073	0.00066
Nickel	0.0028	0.01
Silicon	0.009	0.02
Phosphorus	0.001*	0.002
Sulfur	0.003*	0.006
Other metals	<0.005*	<0.005*
Others	<0.002	<0.002

*Indicates typical values – elements not analyzed for in these heats.

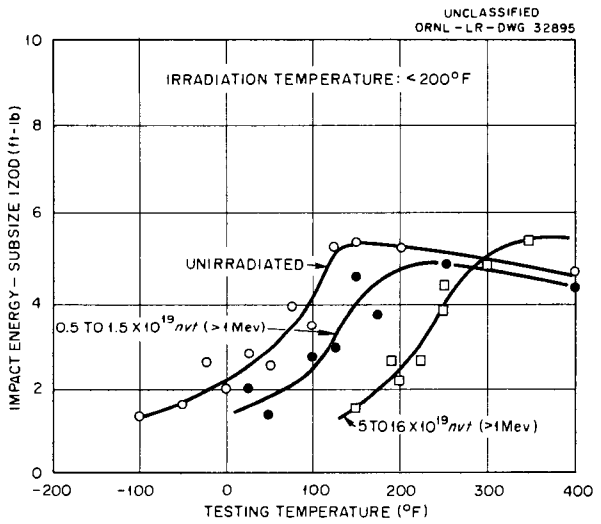

Fig. 119. Subsize Notch-Impact Results for Irradiated High-Purity Iron, Subcritical Anneal (1150°F) (Item 25).

(0.1 to 1.0 mm grain size) iron. The fine-grained material in Fig. 119 (subcritical anneal, grain size 0.02 to 0.06 mm) would be expected to have a lower transition temperature than the coarse-grained iron, but it does not, and the increase of transition temperature with irradiation is much greater.

Earlier data have indicated that a fine grain size was not sufficient to assure the maximum

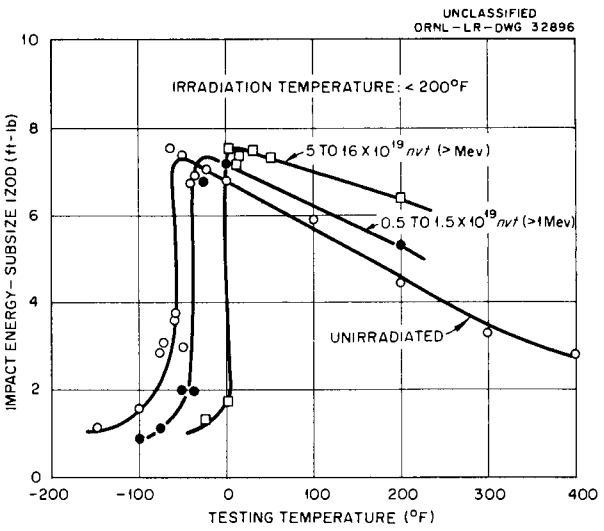

Fig. 120. Subsize Notch-Impact Results for Irradiated High-Purity Iron, Supercritical Anneal (1705°F) (Item 25).

protection from brittle fracture. Two steels of almost identical composition (with one aluminum-killed to yield a fine grain size) were tested.[5] It was concluded that there was some advantage to using the finer grain size, and this conclusion seems valid from an engineering standpoint since the difference in grain size was obtained as it would be in commercial practice. It is well known that preparation of two samples of different grain size in the same material by working, heat treatment, etc., often introduces differences other than grain size; and a great deal more study is necessary to clarify the grain size effects.

Tensile Properties

The tensile properties of the various irons and steels have been studied concurrently with the notch-impact properties. Irradiation temperatures between 550 and 800°F were obtained in 12 carbon and stainless steels in the apparatus from which the elevated-temperature impact data were obtained. Because of the geometry of the tensile specimens the temperatures were generally higher than for the corresponding notch-impact specimens irradiated at the same time. Table 7 lists some representative values. Apparently a higher irradiation temperature is required to anneal out

[5] R. G. Berggren and J. C. Wilson, *Recent Data on the Effects of Neutron Irradiation on Structural Metals and Alloys*, ORNL CF-56-11-1 (Jan. 30, 1957).

Table 7. Tensile Properties of Irradiated Steels

Alloy	Dose (fast neutrons/cm^2)	Temperature of Irradiation (°F)	Yield Strength (psi)	Tensile Strength (psi)	Uniform Elongation (%)
			$\times 10^3$	$\times 10^3$	
A-106, fine-grain, 0.24% carbon	0		40	76	18
	2×10^{19}	580	81	102	8
	2×10^{19}	680	55	87	11
	2×10^{19}	760	48	82	12
	8×10^{19}	580	79	106*	6
	8×10^{19}	780	47	79	11
	1×10^{20}	175	97	102	4
A-106, coarse-grain, 0.24% carbon	0		46	80	14
	2×10^{19}	580	93	115	8
	2×10^{19}	680	67	98	9
	2×10^{19}	760	43	84	14
	7×10^{19}	580	87	103*	3
	7×10^{19}	780	64	94	11
	1×10^{20}	175	116	121	2
A-212, 0.2% carbon	0		40	75	25
	2×10^{19}	175	92	98	6
	2×10^{19}	560	76	102	9
	2×10^{19}	680	61	90	12
	2×10^{19}	760	56	84	14
	6×10^{19}	700	82	105*	6
	6×10^{19}	780	59	81	13
	1×10^{20}	175	109	116	4
E-7016	0		59	73	16
	5×10^{18}	175	69	78	11
	5×10^{18}	600	61	77	17
	2×10^{19}	175	108	108	0
	6×10^{19}	700	83	94	12
	6×10^{19}	740	77**	85	12
	6×10^{19}	780	69	77	15
	1×10^{20}	175	115	115	0

*Broke without necking; work-hardening rate greater than for unirradiated specimen.
**2.0 per minute testing rate; all others 0.05 per minute.

the radiation-induced increase in yield strength than the notch-impact transition-temperature shift. In all cases where irradiations were carried out below 200°F the rate of work-hardening (immediately after yielding) has been lower than in the unirradiated metal. Several specimens irradiated at elevated temperatures had work-hardening rates equal to or greater than those of the unirradiated metal in spite of the increased yield stress; three of these specimens broke without appreciable necking after several per cent uniform elongation. In contrast, all specimens irradiated at lower (< 200°F) temperatures showed appreciable necking, and in general the uniform elongation (before necking) was more sharply reduced.

The shapes of the stress-strain curves are often remarkably altered by irradiation. Figure 121 shows stress-strain curves at several neutron doses for a high-purity iron and an iron–0.14% carbon alloy. In high-purity iron an intermediate dose (*a* in Fig. 121) raises the yield up to almost the tensile strength; on running the test at a higher strain rate (by a factor of 40) the yield strength is increased until it is above the tensile strength, and the uniform elongation is much reduced. Both fine-grained (subcritical anneal) and coarse-grained iron (normalized from critical temperatures) behave in a similar manner although the loss of uniform elongation with increasing strain rate is greater in the fine-grained material. Somewhat the same behavior is noted in high-purity iron–0.14% carbon alloys (*b* in Fig. 121) when in the hot-rolled condition, but in the normalized condition (*c* in Fig. 121) the material behaves more like steel. In mild steel with the usual yield point,[4] irradiation tends to reduce the prominence of the yield point, reduce the uniform elongation, and change the necking elongation but little until doses of the order of 10^{20} fast neutrons/cm^2 are reached.

The structures are not the same in the high-purity iron–0.14% carbon alloy, although the grain

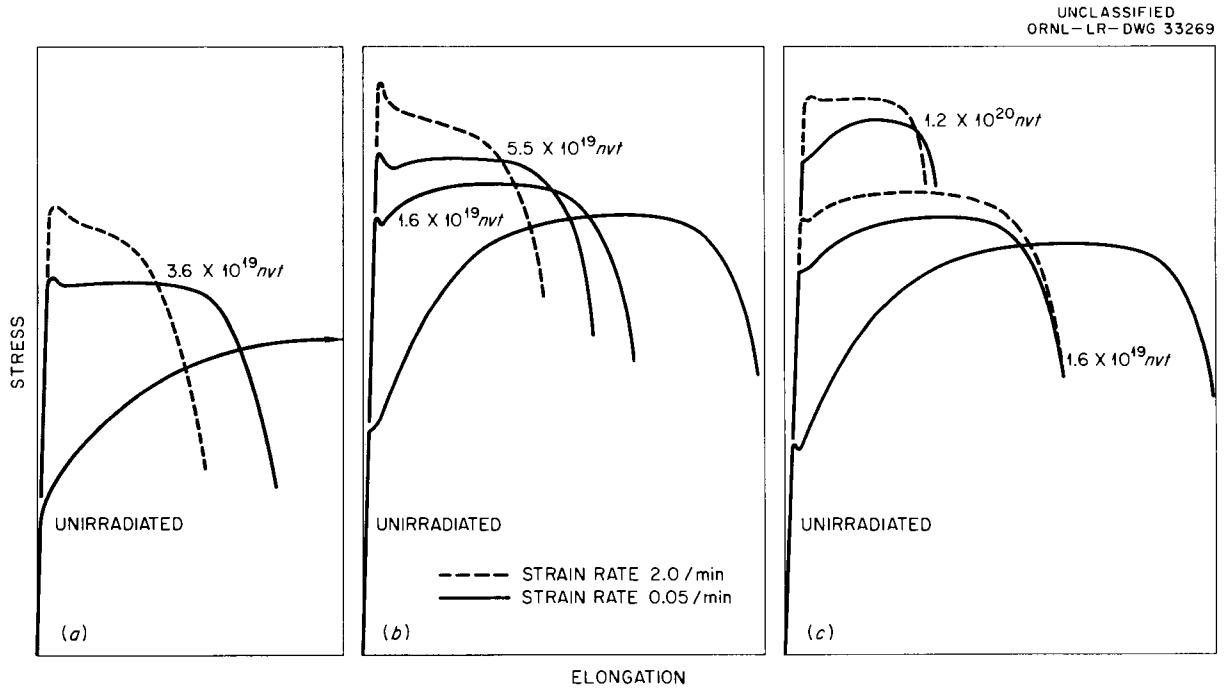

Fig. 121. Effect of Irradiation on Stress-Strain Curves. (*a*) High-purity iron; typical of both fine- and coarse-grained material. The change of uniform (and total) elongation with strain rate is large. The uniform elongation tends to be reduced more at lower doses in the fine-grained material. (*b*) High-purity iron–0.14% carbon alloy, hot-rolled. The elongation is reduced by irradiation and high strain rates in a manner similar to that for iron. The yield point is slightly more prominant. (*c*) High-purity iron–0.14% carbon alloy, normalized. The normalized material is not so sensitive to loss of uniform elongation with increased irradiation or strain rate.

sizes are not greatly different. In the normalized material the pearlite is present as large, thin irregular volumes rather than in equiaxed grains as in the hot-rolled metal. After irradiation the amount and distribution of pearlite appear to have a strong influence on the work-hardening capabilities.

In both cases (high-purity iron and high-purity iron–0.14% carbon) the normalized material is superior in retaining uniform elongation after irradiation. The notch-impact data also showed the normalized material to be superior, particularly in the case of the iron.

High strain rates have little effect on the uniform elongation in steels (mostly of more than 0.1% carbon) thus far tested.

Discussion

From observations on strain rate and uniform elongation, one would expect that the notch-impact properties would be less affected in the steels than in the irons. Apparently this is not so: the notch-impact data from the iron and the iron-carbon alloy indicate that less change occurs than in most of the steels. Apparently, then, the manner of yielding and the uniform elongation (as observed in conventional tensile tests) are not important in determining notch-impact properties. The uniform elongation must be important in ductile fracture (since it determines the strain at which necking will begin) and it may influence the initiation of brittle fracture.

The reasons for the loss of notch ductility upon irradiation are not evident. The Charpy data indicate that large changes in transition temperature can be produced with little accompanying change in tensile properties. Temper embrittlement was thought to be a possible cause, but limited examinations showed some grain-boundary fracture, not, however, in predominance.

The varied strain-rate dependence of the various alloys and the variety of stress-strain curves obtained suggest that the manner of initial yielding, as indicated by the stress-strain curves, is not helpful, because none of the various phenomena correlate with notch-impact behavior. The delay time for initiation of plastic deformation may be changed by irradiation, and indeed one interpretation of the slow descent of the stress-strain curve from the upper yield point might be that the breakaway of pinned dislocations is proceeding very slowly (as compared with the few milliseconds required for carbon-pinned dislocations at room temperature), but the delay times so suggested would be very long. If this were true, the transition temperature would be expected to change much more than was observed in iron.

It is possible that a delay time, either for dislocation breakaway or for dislocation motion after breaking away, is responsible for the transition-temperature shift. Cottrell[6] has correlated the properties of carbon-pinned dislocations in iron with the observed delay times for plastic deformation; he shows, however, that the increase in transition temperature should be a function of the strength increase (as by irradiation). No such correlation has been observed in our data.

In summary the work of the year has shown the magnitude of the beneficial (and occasionally increased damaging) effects of elevated-temperature irradiations. The variation in radiation-induced property changes with composition or structure shows clearly that, in principle at least, an improved degree of resistance to deleterious radiation effects can be produced in pressure vessel steels.

Miscellaneous

During the year specimen production has been expedited (with a large reduction in cost) by having an outside contractor do the work. Several thousand specimens are on hand ready for irradiation or auxiliary tests. Irradiation techniques have improved so that much larger numbers of specimens may be subjected to a wider variety of irradiation and test conditions. Much of the specimen material is now being prepared from 3- to 8½-in.-thick plates of steel. The effects of position in the plate (and thus structure) are being studied. Emphasis will shift from subsize Izod to Charpy V-notch specimens as the more capacious facilities in the ORR are used. Increased emphasis on high-purity alloys of iron and carbon and other alloying elements is expected in order to determine the reason for the superiority of the high-purity alloys over steel.

[6] A. H. Cottrell, *Trans. Met. Soc. Am. Inst. Mining Met. Engrs.* 212, 192 (1958).

The delay time for the initiation of plastic deformation and the effects of strain rate on work-hardening will be thoroughly studied.

Hot-cell testing facilities have continued to operate well: ample spare parts (including a complete spare impact machine), supplies, and improved construction have greatly reduced maintenance and down time.

Design of ORR facilities, apparatus, and instrument installation is well under way.

A complete summary of all data obtained on this program is being compiled for publication.

RADIATION METALLURGY

J. C. Wilson

W. E. Brundage W. W. Davis N. E. Hinkle J. C. Zukas

Effect of Irradiation on Creep

A series of tube-burst tests has been operated in facility HB-3 of the MTR to determine the effect of neutron bombardment at the highest available flux density on the stress-rupture life of Inconel at 1500°F. For comparison, the stress-rupture life of the material was determined in the absence of irradiation, with all other conditions the same.

Experiment 1 contained eight specimens at stresses of 3000 to 5000 psi in a helium atmosphere. The rupture lives of the in-pile specimens were a factor of 3 to 5 shorter than those of the control specimens, Table 8, but rupture lives for both in-pile and control tests were considerably shorter than reported by the Metallurgy Division for this material. These results are attributed to thermocouple errors, possibly caused by contamination of the helium atmosphere. Thermocouple tests were conducted to study the contamination of the atmosphere and are reported below. Postirradiation strain measurements have been completed and are tabulated in Table 8. The strain at fracture was 0.7 to 1.2% for the in-pile specimens, a factor of 5 reduction in ductility for this material. Figure 122 shows the localized failure that occurred in in-pile specimens, and Fig. 123 shows the large number of voids and the grain-boundary separation typical of the more ductile control specimens.

The in-pile phase of experiment 2 has been completed, and disassembly of the apparatus is in progress. The six in-pile tube-burst specimens in this test contained a coaxial cold finger to remove excess gamma heat with high-velocity air flow. This design was very successful in improving the temperature control, whereas in experiment 1 the specimens tended to overshoot 1500°F (without electric heat) under certain conditions of reactor operation. Figures 124 and 125 show specimen details and the experiment assembly, respectively. The experiment was operated at stresses of 3000 to 5000 psi with an air atmosphere to minimize effects of environment on the thermocouples. The rupture lives of the in-pile specimens are a factor of 3 to 5 shorter than those of the control specimens, Table 9, and the control-test results were comparable with data obtained by the metallurgy Division. The greatest reduction in rupture life occurred at the highest stress levels in both in-pile experiments. The rupture life and the total strains of a number of specimens tested in air and stressed with helium internal pressure are tabulated in Table 9. These results compare favorably with data obtained by the Metallurgy Division.

During in-pile operation of experiment 2, the routine operation included repressurization of a specimen when rupture was indicated (by a sharp decrease in stressing pressure) to determine whether the specimen had failed or whether some fitting, external to the apparatus, had leaked. Specimens 64 and 65, when repressurized, were observed to maintain pressure for a considerable time before rupture was again indicated. Specimen 68, repressurized a few weeks after rupture, maintained pressure for about 10 hr. Specimen 76 did not hold pressure at any time after initial rupture, and specimen 71 was never repressurized.

All the control specimens, except 41 and 44, exhibited this behavior to some degree sometime after the initial rupture. The original stress was maintained until rupture was again indicated only

Table 8. Effect of Neutron Bombardment on the Rupture Life of Inconel Tubing at 1500°F in Helium – Experiment 1

Specimen Number	Wall Thickness (mils)	Stress (psi)	Irradiation*	Rupture Life (hr)	Total Strain** (%)
21	30	3000	MTR	78	0.74
22	30	3000	MTR	78	0.67
29	30	3000	None	300	3.1
33	30	3000	None	144	3.9
1	50	4000	MTR	23	0.85
3	50	4000	MTR	29	0.97
34	50	4000	None	115	7.5
36	50	4000	None	105	7.5
16	30	4000	MTR	33	0.72
20	30	4000	MTR	17	1.14
27	30	4000	None	78	4.4
31	30	4000	None	100	5.0
17	30	5000	MTR	13	1.2
24	30	5000	MTR	19	1.0
25	30	5000	None	103	5.2
30	30	5000	None	55	5.0

*Irradiation in HB-3 of the MTR – fast flux >1 Mev, 2×10^{13} neutrons·cm^{-2}·sec^{-1}.
**From diameter measurements after test.

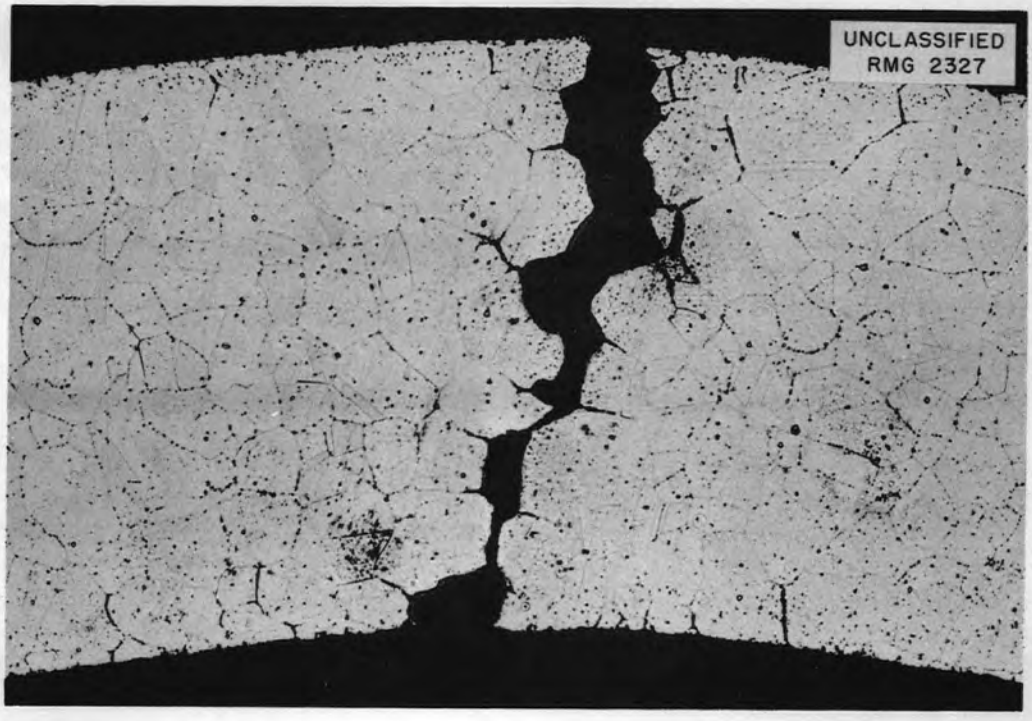

Fig. 122. Transverse Section at the Fracture of an Inconel Tube-Burst Specimen Tested In-Pile at 1500°F in Helium. The stress was 4000 psi and the rupture time was 33 hr. 100X.

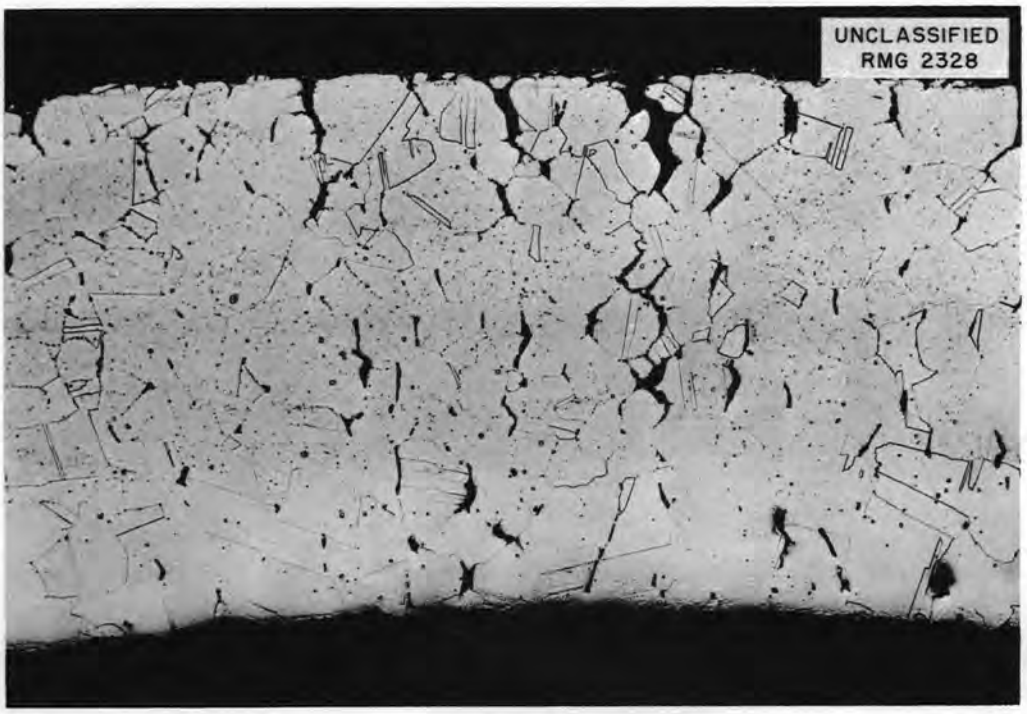

Fig. 123. Transverse Section near the Fracture of an Inconel Tube-Burst Control Specimen Tested at 1500°F in Helium. The stress was 4000 psi and the rupture time was 100 hr. 100X.

for control specimens 35, 43, and 45. This rupture-sealing phenomenon is thought to occur when sufficient oxide forms on the fracture surfaces to seal the ruptured specimen.

Apparently the oxide formed in the rupture fissures has a strength (and cohesion to the metal) of the same order as that of the metal. Shahinian and Achter have studied the atmosphere dependence of the creep-rupture properties of two nickel-base alloys;[1,2] of the several mechanisms they suggest that may lead to the observed greater strength in air[2] is the formation of strengthening oxide in cracks. The above data on resealing of specimens support this conclusion. The rupture times listed in Table 9 are for the first observation of rupture. The specimens that were repressurized for a considerable time are designated in Table 9; the total strain for these specimens probably includes the strain until first rupture (fracture strain) plus postfracture strain occurring while the specimens were repressurized and stressed after the original rupture had sealed.

While the apparatus containing the control specimens for experiment 1 was being disassembled, it was observed that the thermocouple wires were extremely brittle. As a result of this and of the abnormally short rupture lives recorded in experiment 1, two experiments were performed to find the cause of the thermocouple wire brittleness. An Inconel tube was used to contain Chromel-Alumel and iron-constantan thermocouples and the materials used in the stress-rupture experiment in a helium atmosphere. The emf of these thermocouples was compared with the emf of thermocouples located in air on the outside of the Inconel tube. The first test, which contained structural metals and ceramic electrical insulators, indicated no emf errors from 1500 to 1700°F. The second test, which also included fused quartz thermal insulation (used in experiment 1), was held constant at 1500°F by means of a thermocouple in air, and the Chromel-Alumel thermocouples in helium showed an emf decrease equivalent to

[1] P. Shahinian and M. R. Achter, *Temperature and Stress Dependence of the Atmosphere Effect on Nichrome V*, NRL-5037 (Oct. 23, 1957).

[2] P. Shahinian and M. R. Achter, *The Effect of Atmosphere on Creep-Rupture Properties of a Nickel-Chromium-Aluminum Alloy*, NRL-5133 (May 6, 1958).

Fig. 124. Parts for In-Pile Apparatus of Experiment 2. At the top is the assembled tube-burst specimen with the capillary pressure tube at the left end and the cold finger tube at the right end of the specimen. The bottom two parts are the unassembled parts of the cold finger. Approximately 1 cfm of air is blown through the cold finger to provide cooling during reactor operation. The air enters from the in-pile end of the specimen, where the gamma heating is more severe. At the in-pile end, conductive cooling from the specimen to the cold finger takes place; along the gage length of the specimen, cooling is by radiation to the cold finger.

100°F during 200–250 hr of operation. The iron-constantan emf remained constant after an increase equivalent to 50°F in the first 48 hr. Temperature control of the test was then changed to a Chromel-Alumel thermocouple in helium; the Chromel-Alumel thermocouple in air and the iron-constantan couples in helium indicated that the temperature of the apparatus rose at an increasing rate for the duration of the test. Posttest examination revealed brittle thermocouple wires from the second test but not from the first test. These data indicate that the fused quartz (or some contaminant in it) used in helium is disturbing the atmosphere in such a way as to cause Chromel-Alumel thermocouple calibration changes. These data also indicate that short rupture times in experiment 1 and its controls were at least partially due to thermocouple errors.

ORR Creep Experiments

Tube-burst experiments similar to experiments 1 and 2 will be performed in lattice position F-3 of the ORR. The fast flux should be higher than in the MTR, and the geometry should allow simultaneous irradiation of a larger number of specimens. All essential features of the MTR experiments will be retained in the ORR apparatus, since excellent temperature control was achieved at the MTR in spite of the high and variable level of gamma-ray heating. The necessary modifications to the MTR design (because of the different magnitude and orientation of the gamma-ray gradient) are being bench-tested.

The pool-side facility of the ORR will be utilized for more basic experiments on the effect of neutron bombardment on the creep rate. Some of the variables to be studied include temperature, flux density, and state of the test material. These experiments will be designed to determine the conditions of maximum sensitivity to irradiation and whether the results of the above experiments are due to changes of creep rate, fracture mechanism, or both.

The major obstacle to successful in-pile creep measurements is the extensometer. The MTR experiments showed that good temperature control could be achieved. Presently, the emphasis is on development of pneumatic gaging that appears to be insensitive to neutron and gamma-ray bombardment. Until an acceptable extensometer is available, creep tests of the before-after measurement type will be performed. The first ORR creep experiment will probably be a stress-relaxation-type test, consisting of a number of springs with a preset tensile strain in order to study a variety of materials and stress conditions.

The design of the general facilities for these experiments is nearing completion, and fabrication of the instrumentation has begun. The prototype of the pool-side-facility experiment can is built and will be hydrostatically tested before final design is completed.

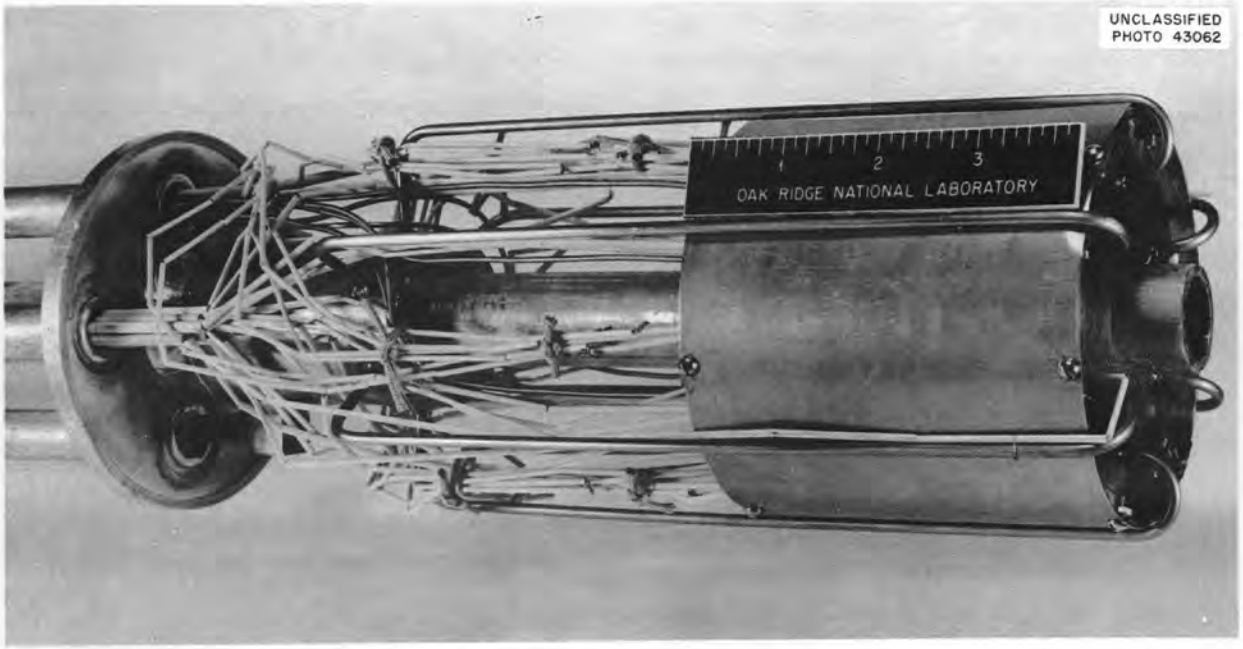

Fig. 125. Assembled In-Pile Apparatus for Experiment 2. The tube-burst specimens are located inside the cylindrical container at the right. Each specimen has its own furnace. The six outside tubes carry air to the cold fingers. The central tube carries water for cooling the in-pile plug.

Measurements of Neutron Flux

Flux measurements are necessary to correlate the results of in-pile tests in different facilities. The most commonly used monitors for such measurements are cobalt for thermal flux and sulfur for fast flux (energy greater than 2.8 Mev). The neutron fluxes in reactor facilities used or to be used by the Radiation Metallurgy Group (HB-3 in LITR, HB-3 in MTR, F-1, C-8, and pool-side facility in ORR) have been measured, and it is common practice to include cobalt and sulfur monitors in each experiment that is irradiated. Counting and computations are performed by G. W. Leddicotte's group.

Counting of cobalt samples (taken to have a cross section of 36.7 barns and a half life of 5.3 years) having a disintegration rate of less than 2×10^5 d/min is done in a gross-gamma scintillation counter employing a sodium iodide crystal. For samples with higher activities, a gamma ion chamber is used and the results are compared with a standard cobalt sample having a known disintegration rate. For sulfur the same gamma ion chamber is used. The reaction $S^{32}(n,p)P^{32}$ is used for fast-neutron measurements. A threshold of 2.8 Mev is assumed; the cross section used is 0.37 barn and the half life 14.3 days. The bremsstrahlung arising from the beta decay of P^{32} is compared with a known standard.

LITR. – Experiments irradiated in HB-3 of the LITR are sealed in a stainless steel water jacket having a nominal water thickness of $\frac{1}{4}$ in. The front of this jacket is positioned in the hole $2\frac{1}{4}$ in. from the reactor core tank at the center line of the hole. Monitors were placed at the points where flux is to be measured. The following tabulation gives the apparent neutron flux approximately 4 in. from the reactor core tank near the center line from six different experiments:

Sample	Apparent Neutron Flux (neutrons·cm^{-2}·sec^{-1})	
	$S^{32}(n,p)P^{32}$	$Co^{59}(n,\gamma)Co^{60}$
	$\times 10^{11}$	$\times 10^{12}$
1	1.1	6.8
2	4.4	7.7
3	6.2	5.7
4	5.4	6.1
5	5.2	8.5
6	4.5	7.0

Table 9. Effect of Neutron Bombardment on the Rupture Life of Inconel Tubing at 1500°F in Air – Experiment 2

Specimen Number	Wall Thickness (mils)	Stress (psi)	Irradiation[a]	Rupture Life (hr)	Fracture Strain[b] (%)
71	30	3000	MTR	784	
73	30	3000	MTR	>869	*c*
48	30	3000	None	>2850	9.6[c]
64	30	4000	MTR	343	*d*
65	30	4000	MTR	279	*d*
43	30	4000	None	801	13.8[d]
44	30	4000	None	797	10.7
68	30	5000	MTR	94	
76	30	5000	MTR	96	
35	50	5000	None	473	11.2[d]
41	30	5000	None	487	8.4
45	30	6000	None	145	17.3[d]
46	30	6000	None	165	11.4
47	30	7000	None	90	10.3
26	30	7000	None	119	10.8[e]
28	30	5000	None	410	5.7[e]
37	50	5000	None	429	*e*

[a]Irradiation in HB-3 of the MTR – fast flux >1 Mev, 2×10^{13} neutrons·cm^{-2}·sec^{-1}.

[b]Postirradiation strain measurements have not been completed.

[c]Creep strain; not ruptured.

[d]Fracture strain plus postfracture strain due to repressurizing.

[e]Tests conducted with helium inside and air outside the specimen.

The first three samples were irradiated in identical experiments and the last three were included in cans of metallurgical test specimens. The low value of fast flux for sample 1 cannot be accounted for at this time.

The fast flux above 0.6 and 1.5 Mev was measured in the HB-3 facility of the LITR by D. Binder. A special run of 10 min at a power level of 300 kw was made with Np^{237} and U^{238} by use of a special technique.[3] Sulfur monitors were used to measure the gradient in the hole. No water jacket was used. Figure 126 shows the flux pattern vs the distance from the reactor core tank along the center line of HB-3 as given by the sulfur for these conditions and the points from the Np^{237} and U^{238} measurements.

ORR. – The flux patterns in the C-8 and F-1 core positions and in the pool-side facility of the ORR were measured during early power runs. Cobalt and sulfur monitors were used in the core, whereas only sulfur was used in the pool-side facility. The reactor power level was 40 kw for 2 hr, with the fuel loaded in the expected permanent

[3]D. Binder, *Solid State Ann. Prog. Rep. Aug. 31, 1957*, ORNL-2413, p 122–24.

operating configuration.[4] Fluxes at design power should be 500 times the values listed below.

Figure 127 for C-8 shows that both the fast flux and the thermal flux peak at about 6 in. below the center line of the reactor, the fast at 4.39×10^{10} neutrons·cm^{-2}·sec^{-1} and the thermal flux at 2.3×10^{11} neutrons·cm^{-2}·sec^{-1}. At the top of the core the fast flux drops sharply to a value of 1.9×10^{9} neutrons·cm^{-2}·sec^{-1}. The thermal flux curve in this facility may show some change when longer periods of irradiation are used because the induced activity in the monitor samples at this power level was so low that counting became difficult.

Figure 128 for F-1 again shows the flux peak about 6 in. below the center line, with a value of 2.72×10^{10} neutrons·cm^{-2}·sec^{-1} for fast flux and a corresponding value of 3.0×10^{11} neutrons·cm^{-2}·sec^{-1} for thermal flux. This facility is presently being monitored, and the shape of the curve may differ with the shim rods in different positions.

[4] D. C. Cagle and R. A. Costner, Jr., *Initial Post-Neutron Measurements in the ORR*, ORNL-2559 (to be published).

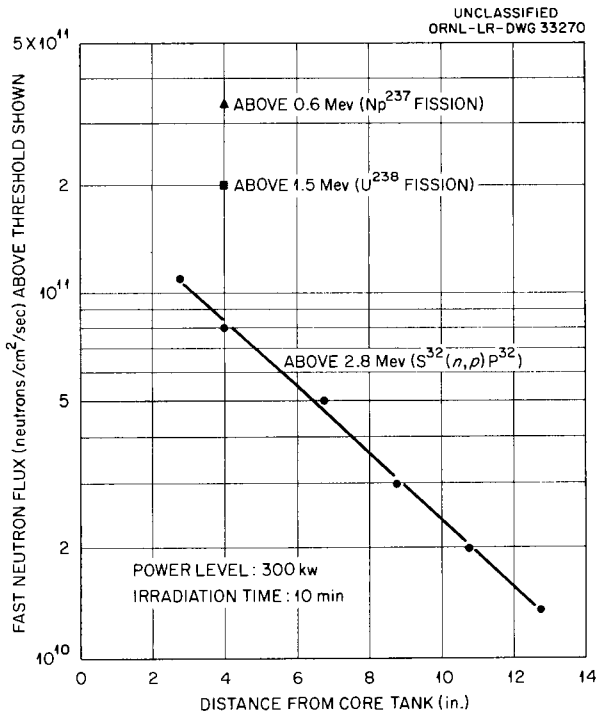

Fig. 126. Neutron Flux Distribution Along Center Line of Facility HB-3 of LITR.

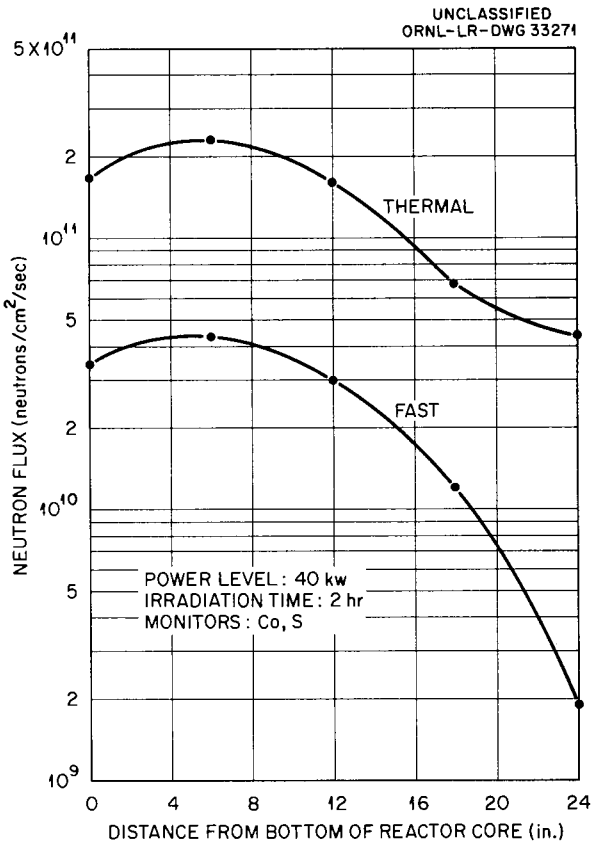

Fig. 127. Neutron Flux Distribution Across Facility C-8 of the ORR.

Forty-eight samples of sulfur were irradiated in an aluminum can in the pool-side facility to determine the spatial distribution of fast flux in a 1.5-ft^3 void. The water layer between this can and the flat face of the reactor vessel was about $\frac{1}{16}$ in. thick.

Over a 1-ft-square area in a plane $\frac{5}{8}$ in. from the reactor face a maximum flux (>2.8 Mev) of 10^{13} neutrons·cm^{-2}·sec^{-1} was measured, and the flux fell to about one-third of this value at the corners of the area measured. Along the center line (perpendicular to the reactor face) the fast flux fell to 6.5×10^{12} neutrons·cm^{-2}·sec^{-1} at 6 in. from the reactor face. The fast flux gradient is much less steep than in the usual beam hole.

The fluxes reported in the pool-side facility are estimated for 20-Mw operation by linear extrapolation of data obtained at 40 kw. At higher power the control rods will be farther out of the core, the temperature will be higher, and the xenon buildup in the center of the core will be higher.

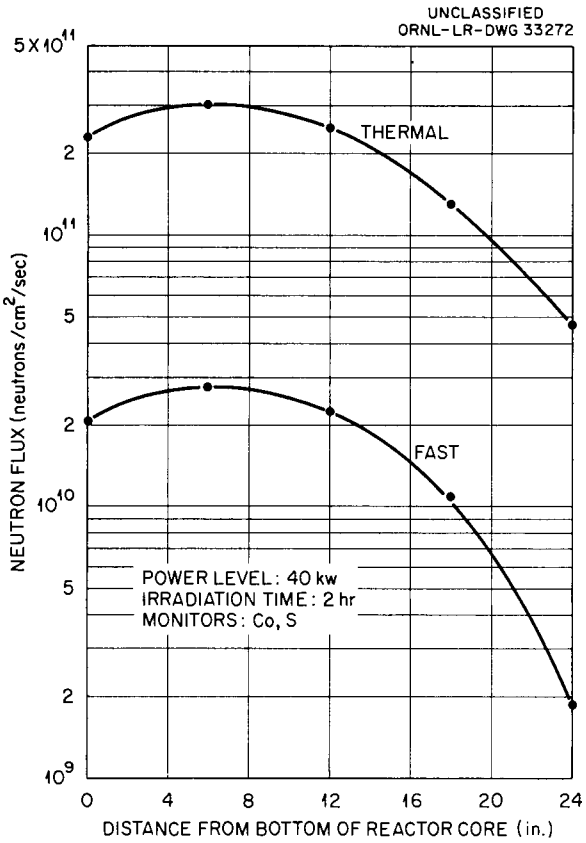

Fig. 128. Neutron Flux Distribution Across Facility F-1 of the ORR.

These factors may affect the flux distribution somewhat.

Flux monitoring will continue to be an integral part of all experiments where it is feasible.

ORR Facilities Engineering

The Radiation Metallurgy Group expects to operate five experiments in the ORR at the same time. Two of these will be located in the reactor core and the others located in the pool-side facility. Varied experiments are planned for these installations, ranging from specimens in contact with the reactor cooling water to pressurized specimens operating at 1500°F. A single system of terminal boxes, terminal and instrument panels, etc., is being engineered for joint use by any of the group's experiments.

Long leads will be required to connect the in-pile experiments to the instruments, because the center line of the reactor is 24 ft below the surface of the water, and space is not available for instruments at the top of the pool. Total length of the leads will run from 50 to 70 ft, depending on the installation. This length would be impractical to make in a single run, and so junction boxes just above the water level in the pool have been designed. One of these boxes will serve as a terminus for each experiment tube and will also provide hermetic sealing for the experiment for special atmospheres.

The section of experiment tube inside the reactor tank must be sufficiently rigid to support and position the experiment in the reactor core and to withstand vibration induced by the turbulent flow of reactor cooling water. This presents the problem of accurate bending of the tubing and assembly of the experiment. The use of the pool-side facility will simplify construction problems and permit the use of larger experiment cans but has the disadvantage of a lower neutron flux. This facility is constructed in the reactor pool on the west side of the reactor tank. The experiment cans are separated from the core of the reactor only by a 1-in.-thick aluminum plate that constitutes a flat side on the reactor tank. Three fuel elements are loaded in the core against this plate to give a region of relatively high fast flux about 9 in. wide and 24 in. high. The experiment cans may occupy a space up to 24 in. wide and may also extend any desired distance away from the reactor. Brackets have been installed which will permit the facility to be subdivided vertically by the experiment cans which can be fabricated in modular widths from 2 to 24 in. as required by the experiment.

The pool-side facility brackets were installed and measurements made from the brackets to the tank face before the reactor was critical to ensure that accurate positioning of the experiment cans would be possible. This was necessary since the reactor tank varied somewhat from the construction drawing dimensions and the "flat" face was bowed. The facility has been used to mount a 16-in.-wide, 17-in.-high, $10\frac{1}{4}$-in.-deep box constructed to permit flux measurements to be made, and gamma-heating measurements will follow. A thermocouple mounting bracket has also been used

in this facility by the Operations Division to measure the operating temperatures of the pool-side surfaces of the reactor tank.

In order to provide the maximum flexibility in changing from one type of experiment to another, the instruments for four of the five experiments have been grouped together. Permanent instrument, electrical, and gas leads from four of the junction boxes will end at a patch and terminal panel designed to permit ready connection of any of the instruments to any of the experiments.

Design of the permanent installation has been completed, and work orders for construction have been placed.

THE Np^{237} FISSION REACTION AS A RELATIVE MONITOR FOR DISPLACEMENT REACTIONS

D. Binder

In order to compare radiation damage experiments in different facilities of the same reactor (or different reactors), it would be desirable to have the neutron flux spectrum from 10 kev to several Mev. The in-pile measurement of this spectrum is made difficult by the lack of threshold detectors in the 1- to 600-kev range. The Pu^{239} fission reaction can be made to have a threshold of 1 kev with a large B^{10} shield, but this is inconvenient for small reactor holes and also leads to flux depression. At and above 600 kev, the Np^{237} fission reaction has an effective threshold of 600 kev, the U^{238} fission reaction a threshold of 1.5 Mev, and the $S^{32}(n,p)P^{32}$ reaction a threshold of 3.0 Mev.

While we are unable to measure the entire flux spectrum, it is possible that one of these reactions might serve as a good relative monitor. This would presuppose that there are no radical changes in flux spectra between facilities, or that the radiation damage process is such as to minimize these variations. In displacement reactions one minimizing process might be the ionization of the recoil atoms from collisions with neutrons of high energy. This ionization would lead to a negligible displacement of atoms, so that, above a certain energy, the increased energy of the neutron would be wasted. Thus the significant parameter would be the number of neutrons having more than a certain energy, rather than the spectrum, and one threshold reaction would serve as a good relative monitor.

The relative yields of the three threshold reactions were measured at various positions near and in the donut, or uranium converter, of hole 51N of the ORNL Graphite Reactor. Cadmium covers were used with the fission reactions, and the technique with Np^{237} was described previously.[1] The results are shown in Fig. 129, where the center of the donut is at the "distance" of 20 in. and the donut extends about 5 in. to either side of this center. At the distance of 19 in. the relative enhancement of the three reactions by factors of 2.9, 3.4, and 4.6 shows some change in neutron spectrum.

[1] D. Binder, *Solid State Ann. Prog. Rep. Aug. 31, 1957*, ORNL-2413, p 122.

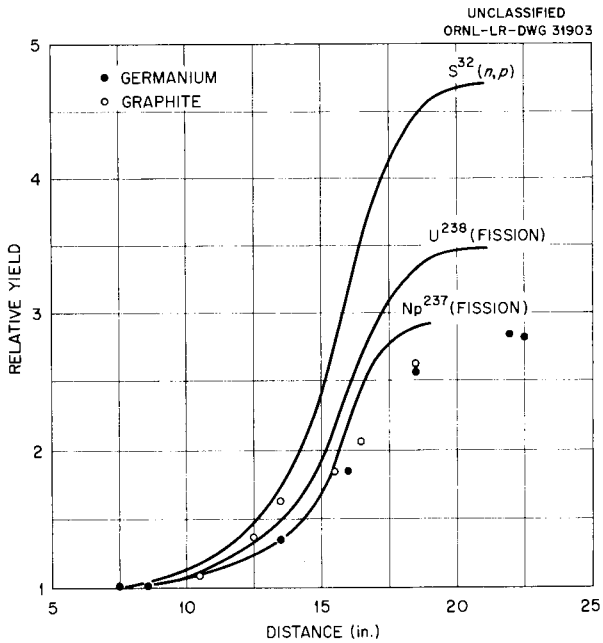

Fig. 129. Comparison of Relative Yields of Threshold Reactions with Radiation Damage in Hole 51N.

As examples of solid-state reactions caused by displacements, the conductivity changes in *n*-type germanium and graphite were chosen because they are fast reactions at room temperature and the materials differ in atomic weight by a factor of 6. Although there is some scatter in the graphite data in Fig. 129, the conductivity changes in the two solid-state reactions are in general agreement as far as yields relative to a position outside the donut are concerned. The threshold reaction with which they are in best agreement is the Np^{237} fission reaction, and the agreement is good to 20% except for one scattered graphite point.

Since Np^{237} was the most promising monitor, the measurements were extended to various holes in the Graphite Reactor. The values so obtained for the flux above 0.6 Mev are shown below:

Hole	Position	Flux (neutrons/cm^2) $\times 10^{11}$
51N	Center	3.6
1768	Center	2.4
A	Center	0.64 ± 0.09
52	Center	0.8
19	Center	1.0
19	32 in. from center	0.8

The flux-dependent part of the Cu-Al alloy reaction[2] changes 3.6 times as fast in hole C as in 1768. Holes A and C are in symmetrical positions, and the flux ratio between hole 1768 and hole A is 3.8 ± 0.6, in agreement with the Cu-Al data within experimental error.

[2] M. S. Wechsler and R. H. Kernohan, *J. Phys. Chem. Solids* (to be published).

COMPARISON OF REACTOR AND GAMMA IRRADIATION OF POLYMERS

D. Binder W. K. Kirkland R. L. Towns

The aim of the present investigation is to separate the effects of neutrons and gamma rays in reactor irradiations of polymers. The method is the comparison of the effects of pure gamma rays from a cobalt source and the neutrons and gamma rays from a reactor source. In the reactor the significant index for the effect of neutrons is assumed to be the hydrogen content. For a given neutron energy, the hydrogen recoils are 12 times more energetic than carbon recoils and the cross sections are comparable. Furthermore, the effects on polymers are by ionization and excitation, and the hydrogen recoils lose almost all their energy in this way, while the carbon recoils lose some of their energy in elastic collisions. The argument is even stronger for elements heavier than carbon.

The calorimetric measurements of Richardson[1] in the ORNL Graphite Reactor indicate that only 20% of the energy absorbed by graphite is from neutrons. If two polymers are irradiated, one containing hydrogen and the other with no hydrogen, the first will be affected by both neutrons and gamma rays, and the second mostly by gamma rays. The two polymer reactions first studied were the density change of Teflon and the viscosity change of polymethyl methacrylate. The polymers were irradiated in a 6.5×10^5 r/hr cobalt source and in a standard position of hole 19 of the Graphite Reactor. The reaction rate in the reactor was 0.3 times that in the gamma source for Teflon and 0.9 for methacrylate. The results are in the expected direction of an increased rate for the hydrogenous polymer, but the absolute magnitudes are a factor of 2 or 3 lower than Richardson's results for equivalent hydrogen contents. Since the irradiations were made in air, which is known to affect the two reactions, additional gamma irradiations of polymethyl methacrylate were made in a vacuum. The same results were obtained within 5%. No effect greater than 10% was observed on changing the intensity of the gamma source from 0.4 to 2.0×10^6 r/hr for polymethyl methacrylate, but there is some indication of an intensity effect at 10^7 r/hr. It is in the direction of a smaller

[1] D. M. Richardson, *Calorimetric Measurement of Radiation Energy Dissipated by Various Materials Placed in the Oak Ridge Pile*, ORNL-129 (Dec. 23, 1948).

effect for increased intensity. The dense ionization track of a hydrogen recoil may produce effects similar to those at a gamma intensity of 10^7 r/hr.

The investigation was widened to include polymer reactions resulting in an evolution of gas. The three polymers studied were polyethylene, nylon, and allyl diglycol carbonate. The samples were irradiated in a vacuum, and the gas not condensed by a liquid nitrogen trap was measured by its pressure in known volumes after transfer with a Toepler pump. The gas evolved was measured in the standard position in hole 19 and in a 2.0×10^6 r/hr cobalt gamma-ray source. The ratios observed (now relative to 2.0×10^6 r/hr) were 0.5 for allyl diglycol carbonate, 0.7 for nylon, and 0.7 for polyethylene. These values were in closer agreement with Richardson's work than the ratios for Teflon and polymethyl methacrylate, although the results are still 20 to 40% too low. The remaining difference may very well be due to the facts that the measurements were taken in different holes in the reactor and that the polymer effects were studied at a position 6 ft from the center of hole 19.

Bopp and Towns have made calorimetric measurements 6 ft from the center of hole 19, but on the other side of the reactor (see "Energy Absorption in the Reactor by Calorimetry," this report). The discrepancy between these measurements and the polymer ratios is smaller than with Richardson's values, but this comparison is based on the assumption that the hole is symmetrical with respect to neutrons and gamma rays.

On comparison of the gassing reactions with the cleavage reactions in Teflon and polymethyl methacrylate, it seemed possible that the cleavage reactions resulted in a poorer efficiency for the neutron irradiation. To investigate this further, the decrease in the viscosity of poly-α-methylstyrene was measured both in the reactor and in gamma-ray sources. The decrease is much smaller than for polymethyl methacrylate per unit radiation, and the preliminary data show a large scatter. The results do group, however, with the gassing reactions.

The ratio of the effects of the reactor and an arbitrary gamma-ray source of 1.0×10^6 r/hr (assuming no intensity effects) is summarized for the five polymers in Fig. 130. The abscissa is the ratio of the number of hydrogen atoms n_H to the number of electrons n_e in the polymer. Also plotted are the two calorimetric measurements of Bopp and Towns at the appropriate hydrogen contents of the two materials used. If the polymer reactions went as the energy absorbed, the points would plot along a straight line which would go through the calorimetry points. The three gassing reactions and the methylstyrene reaction agree with the dotted line drawn through the two calorimetry points to within 15%. There is a factor of 2 discrepancy between this line and the Teflon and Lucite reactions. If the results are stated in terms of efficiencies, these two reactions have a lower efficiency by a factor of 2, per unit energy absorbed in the reactor, than the other four reactions. The cause for this different efficiency is at present unknown.

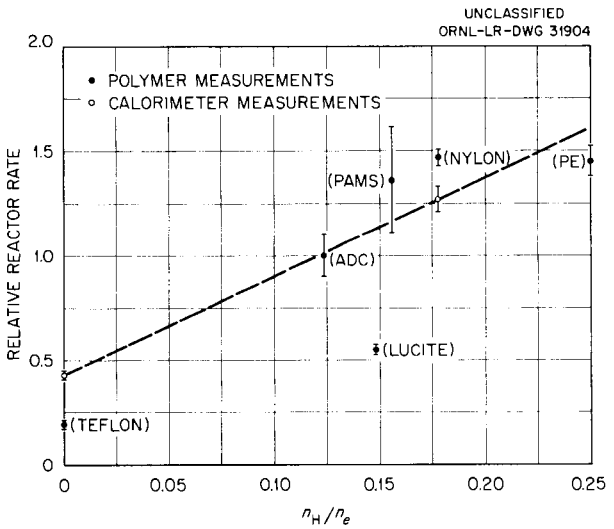

Fig. 130. Ratio of the Effects of Reactor and Gamma Radiation on Polymers. ADC, allyl diglycol carbonate; PAMS, poly-α-methylstyrene; PE, polyethylene. Lucite is the trade name of polymethyl methacrylate.

EFFECTS OF RADIATION ON PLASTICS AND ELASTOMERS

W. W. Parkinson W. K. Kirkland
O. Sisman W. C. Sears[1]
J. E. White[2]

Infrared Studies of Plastics and Elastomers

The changes produced by radiation in the molecular structure of plastics and elastomers, as indicated by infrared absorption spectra, are under continuing investigation.[3] Significant changes had previously been observed in the absorption peaks arising from various isomeric arrangements of the olefin (C=C) groups. In order to determine the concentrations of these species, two parallel efforts are being made to establish quantitative absorption coefficients for the spectrophotometer used in the spectral measurements.

Measurements had been made earlier of the absorption at characteristic frequencies by carbon disulfide solutions of hydrocarbon standards. Absorptivities conventionally determined at low concentrations were found to be inapplicable to solid film samples of polymers.[3] Equations are now being derived by the method of least squares for the curves of absorption vs concentration for the hydrocarbon standards. It is hoped that absorptivities from these equations can be applied to the solid films at the concentration level of the olefin groups in the films.

The second effort to obtain useful absorption coefficients is being made on polybutadiene standards having known content of the various C=C species. Measurements of absorption at the characteristic frequencies have been made on thin films deposited from solutions on salt plates. Early measurements were inconsistent because of nonuniformity of thickness. Techniques have since been developed for preparing films of uniform, known thickness.

Influence of Physical Properties on the Effects of Radiation

It has been proposed that the motion of molecular segments and fragments affects the processes taking place in polymeric materials during irradiation. The arrangement of polymer molecules in crystalline regions places large constraints on the motion of molecular segments. The effect of crystallinity of polyethylene on radiation-induced cross-linking has received attention recently but has not been resolved.[4,5] Orientation of polymer chains in glassy materials would be expected to impose a lesser constraint than crystallization upon molecular motion. Only the usual glassy restraints upon translational and rotational motion exist, but the spatial relations of polymer molecules in an oriented glass lie somewhere between the precise array of the crystalline state and the random arrangement of the ordinary glass. To investigate the effect of orientation on the behavior of polymeric materials, biaxially oriented samples of polystyrene, which cross-links, and polymethyl methacrylate, which cleaves, have been irradiated. The radiation-induced process studied was the change in molecular weight by cross-linking or scission.

The oriented material available for irradiation was in the form of sheets which had been stretched to about three times their original dimensions in both length and width. The oriented condition of the sheets was investigated by dimensional measurements and x-ray diffraction photographs before and after allowing samples to relax at elevated temperature. After 3 hr at 100 to 105°C the dimensional changes appeared to be completed. It was found for both the polystyrene and polymethyl methacrylate that the ratio of the relaxed to the original long dimension or "machine direction" was about 0.3, while the same ratio for the width was about 0.4. The x-ray diffraction photographs showed differences between the stretched and relaxed material which have not yet been analyzed.

The specimens were sealed in glass or quartz tubes after being evacuated to 2 μ for 20 hr.

---

[1] Consultant, University of Georgia.

[2] Summer research participant, Lafayette College, Easton, Pa.

[3] W. W. Parkinson, W. C. Sears, and O. Sisman, *Solid State Ann. Prog. Rep. Aug. 31, 1957*, ORNL-2413, p 83.

[4] E. J. Lawton, J. S. Balwit, and R. S. Powell, paper presented at the 131st Meeting of the American Chemical Society, Miami, Florida, April 7–12, 1957.

[5] W. P. Slichter and E. R. Mandell, *J. Phys. Chem.* 62, 334 (1958).

Unoriented samples were sealed in the tubes with the oriented samples in an alternating arrangement to ensure equal radiation exposure to each type of material. The unoriented or randomized specimens were obtained by the relaxation treatment described above, so that the composition of the two types of material was identical. Viscosity measurements showed that the average molecular weights were unaffected by the heat treatment.

The specimens were irradiated in two Co^{60} gamma sources and in hole 19 of the Graphite Reactor as listed in Tables 10 and 11. After irradiation the molecular weights of the specimens were determined from measurements of the viscosities of dilute solutions of the polymers. The number of cross links or scissions per gram was calculated from the change in the number of molecules per gram and is listed along with the energy required per cross link or scission in Tables 10 and 11.

It is significant that the energy required per cross link in polystyrene is altered by orientation of the molecules, while the energy per scission

Table 10. Molecular Weight Changes Produced by Irradiation of Oriented and Random Samples of Polymethyl Methacrylate

Condition	Source		Final Molecular Weight	Scissions per Gram	Exposure (ev/g)	Energy per Scission
	Type	Intensity (r/hr)				
		$\times 10^6$	$\times 10^5$	$\times 10^{17}$	$\times 10^{20}$	
Oriented	None	None	1.36			
Random	None	None	1.36			
Oriented	Co^{60}	0.61	1.31	3.2	0.361	113
Random	Co^{60}	0.61	1.31	3.2	0.361	113
Oriented	Co^{60}	9.6	1.22	9.6	2.27	236
Random	Co^{60}	9.6	1.22	9.6	2.27	236

Table 11. Molecular Weight Changes Produced by Irradiation of Oriented and Random Samples of Polystyrene

Condition	Source		Final Molecular Weight	Cross Links per Gram	Exposure (ev/g)	Energy per Cross Link (ev)
	Type	Intensity (r/hr)				
		$\times 10^6$	$\times 10^5$	$\times 10^{17}$	$\times 10^{20}$	
Oriented	None	None	2.57			
Random	None	None	2.57			
Oriented	Co^{60}	9.6	2.74	2.8	4.31	1540
Random	Co^{60}	9.6	2.70	2.2	4.31	1960
Oriented	Co^{60}	9.6	2.93	5.5	7.91	1440
Random	Co^{60}	9.6	2.87	4.7	7.91	1680
Oriented	Reactor	1.5	4.62	20	13.5	682
Random	Reactor	1.5	4.04	16	13.5	828

in polymethyl methacrylate is unaffected. It has not been established whether the effect in polystyrene is due to alignment of the polymer chains or whether diffusion and subsequent reaction of radiation-produced molecular fragments are enhanced by voids introduced in the specimen by the mechanical work of the orienting process. The latter possibility will be investigated by accurate density measurements of oriented and randomized samples. Enhanced diffusion of reactive species would have a more marked influence at the higher rates of energy absorption, and so further examination of this hypothesis is planned by irradiating oriented and randomized materials in sources of widely differing intensities.

The variation of the energy required per event at different doses is probably caused by a departure from the relation between viscosity and molecular weight, which was established empirically for the unirradiated polymer but which was used for calculation of all molecular weights.

Miscellaneous Polymer Studies

Apparatus has been designed to study the stress-strain and the stress-relaxation properties of plastics and elastomers during irradiation. By measurement of these properties it is hoped to separate the effects of simultaneous cross-linking and cleavage. The rack for stressing the specimens has been assembled and tested. It was found that the linear ball bearings in the guides imposed excessive friction. Revision of the apparatus to minimize friction is planned.

It has been proposed that the crazing of polystyrene under stress proceeds by the development of cracks between parallel segments of polymer chains. Cross-linking between chains, then, should retard crazing. Square rods $\frac{1}{2}$ in. on edge and 4 in. long were made up from stock polystyrene sheet. Half of these samples were irradiated in sealed aluminum cans in hole 19 of the Graphite Reactor for two weeks (6×10^8 rads or 6×10^{10} ergs/g). A portion of the irradiated samples was set aside for aging in air, since oxygen is reported to form peroxy cross links with the free radicals in irradiated hydrocarbons. The remaining irradiated specimens were fixed, along with unirradiated control samples, in a flexural loading fixture. After 20 hr under load there was extensive crazing of the unirradiated controls while there was no visible crazing of the irradiated specimens.

At higher loadings, the irradiated specimens broke before appreciable crazing developed in the unirradiated samples. Furthermore, it was observed that, for all loadings, the irradiated samples broke shortly after they first began to craze even though the radiation exposure was too low to affect the tensile strength as measured in the conventional test. Time-to-rupture tensile tests are planned to explore this difference in behavior of irradiated and unirradiated plastics.

The aged specimens were exposed to air for periods of three and four months, during which time the deep brown color produced by irradiation was almost completely bleached out. The irradiated specimens developed crazing at about the same rate as unirradiated controls under flexural loads. Apparently, exposure to air for long periods destroys, rather than enhances, the craze resistance of irradiated polystyrene.

RADIATION STABILITY OF CERAMIC MATERIALS

C. D. Bopp

It is expected that the temperature coefficient of the Young's modulus may prove a more sensitive indication of radiation changes than the absolute value of the modulus, since the temperature coefficient is not altered by chipping or corrosion which may occur during the radiation exposure. (In order to measure the absolute value of the modulus, it is necessary to employ accurately machined specimens.) It has been found necessary to take particular care with respect to the design of the vibration exciter and to the mounting of the specimen (Fig. 131). The original exciter design, which employed a long nickel tube, has been found unsuitable since resonances of the long tube interfered with the detection of the resonances of the test specimen. The original exciter was replaced with a solid nickel rod, of $\frac{1}{8}$-in. dia and 1-in. length, the same size as previously employed for room-temperature measurements.[1] The specimen is pressed against the supports and against the driver by the weight of the clamp. Guides are used to position the specimen before clamping. It was found necessary to remove the guides after clamping since temperature-induced dimensional changes caused the guides to press against the specimen and alter the mode of vibration. The mode of vibration is also affected by the positions of the driver and supports, since nodes tend to be formed at each of the points of contact of the driver and the supports with the specimen. The effect of the temperature-induced change in position of the driver with respect to the supports is minimized when the free length of the specimen above the driver is large (as is the case for long specimens). For short specimens of $\frac{3}{4}$-in. length it is necessary to correct for the effect of temperature on the driving position. The apparatus correction is less than 10% for $\frac{3}{4}$-in.-long type 347 stainless steel specimens, but the correction is about half the uncorrected value for plate glass and silica glass, since the temperature coefficient is an order of magnitude less for ceramic materials than for metals. The size of the correction is is reduced for longer specimens. The apparatus correction is determined by measuring the temperature coefficients of "standard" specimens made from materials with known values of the temperature coefficient.

This technique has been employed to study the effect of an irradiation of 6×10^{20} *nvt* epithermal neutrons on a specimen of plate glass. The specimen was so corroded through contact with the reactor cooling water that it was not possible to obtain a sensitive measurement of the absolute value of the modulus. The increase in density[2] and Knoop hardness[3] have already been reported. The Knoop hardness number was increased more than threefold. It was determined that the temperature coefficient of the modulus was unchanged by irradiation within about ±7%. The measurement was made at 1000 cps in the temperature range from −50 to 0°C. The insensitivity of the temperature coefficient of the modulus as compared with the Knoop hardness indicates that the change in Knoop hardness is not caused by a change in

[1] C. D. Bopp, O. Sisman, and R. L. Towns, *Solid State Semiann. Prog. Rep. Feb. 29, 1956*, ORNL-2051, p 29.

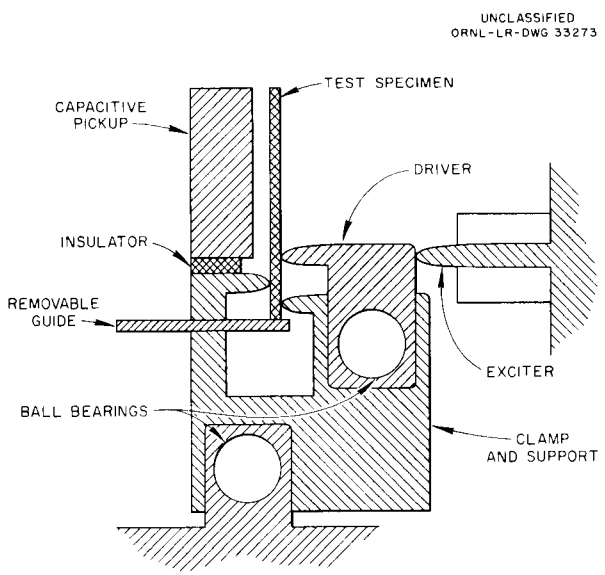

Fig. 131. Vibration Apparatus.

[2] O. Sisman, C. D. Bopp, and R. L. Towns, *Solid State Semiann. Prog. Rep. Aug. 31, 1957*, ORNL-2413, p 81.

[3] *Ibid.*, p 82.

the elastic constants. This conclusion is in agreement with results obtained for another specimen exposed to 2×10^{19} *nvt* epithermal neutrons, whose dimensions were not altered so much as to prevent the measurement of the absolute value of the modulus. For the shorter exposure the modulus remained constant within ±5% although the Knoop hardness increased 20%.[3]

ENERGY ABSORPTION IN THE REACTOR BY CALORIMETRY

C. D. Bopp O. Sisman R. L. Towns

It is desirable to know the energy absorption from fast neutrons and gamma radiation in comparing the relative efficiencies of light and heavy particles in damaging materials sensitive to ionizing radiation (e.g., organic polymers). The energy absorption in graphite and nylon was measured calorimetrically in hole 19 of the Graphite Reactor. The total energy absorption in each of these materials was apportioned into the components from fast neutrons and gamma radiation for carbon and hydrogen, as listed in Table 12. From the results for carbon and hydrogen the absorption by other elements may be estimated.[1] Since most of the energy absorbed by hydrogen comes from fast neutrons and the energy absorbed by carbon is primarily from gamma radiation, the energy absorption is a measure of the fast neutron flux and the gamma flux.

The nylon and graphite were in the form of hollow cylinders $\frac{3}{4}$ in. in length and $\frac{1}{2}$ in. in diameter. In order to minimize energy degradation of the neutron energy spectrum, the nylon cylinder was only $\frac{1}{8}$ in. in wall thickness. The cylinders were wrapped with 10-mil copper sheet and were insulated from an outer aluminum container by a $\frac{3}{16}$-in. air film. Foamed polystyrene spacers separated the cylinders from each other and centered them in the aluminum can. Copper-constantan-copper (No. 36 wire) differential thermocouples measured the temperature gradients between the copper sheets and the aluminum can. The temperature gradients were calibrated in terms of heat flux by supplying energy to the cylinders electrically. For this purpose graphite

[1] D. M. Richardson, A. O. Allen, and J. W. Boyle, *Proc. Intern. Conf. Peaceful Uses Atomic Energy, Geneva, 1955* 14, 209 (1955).

Table 12. Energy Absorption in the Graphite Reactor

Material	Energy Absorption* ($cal \cdot g^{-1} \cdot sec^{-1}$)			
	From Gamma Radiation	From Fast Neutrons	From the Decay Radiation from Thermal Neutron Reactions	Total
	$\times 10^{-4}$	$\times 10^{-4}$	$\times 10^{-4}$	$\times 10^{-4}$
Calorimeter 1 (nylon and copper)	2.2	5.2	1.0	8.4
Calorimeter 2 (graphite, copper, and insulation)	2.1	0.8	0.5	3.4
Carbon	2.1	0.7	<0.1	2.8
Nylon	2.3	6.7	<0.1	9.0
Hydrogen	4.2	61	<0.1	65

*Measured in hole 19, $5\frac{1}{2}$ ft from the center of the reactor, at a reactor power of 3500 kw. The hydrogen content of the nylon was taken as 9.7%; the thermal flux, as about 7×10^{11} neutrons·cm^{-2}·sec^{-1}.

resistors were mounted in holes drilled into the cylinders. In order to minimize heat losses, the lead wires were placed in thermal contact with the cylinders and were insulated from convection currents.

The calorimeter was tested in a 2.00×10^6 r/hr Co^{60} source. Both calorimeters checked the value from cerous sulfate dosimetry within about 1.5% (the error involved in positioning samples in the source). The calibration curve of the calorimeter in terms of temperature gradient vs electrical power was linear below 10^7 r/hr. (It was not attempted to calibrate the calorimeter for higher fluxes.) In hole 19 of the Graphite Reactor, readings showed more scatter than in the gamma source owing to fluctuation in the ambient temperature of the cooling water for hole 19. Rapid changes in the ambient temperature of only a few tenths of a degree caused displacements in the calorimeter indication for periods as long as 15 min. In order to obtain the best readings, the calorimeter differential thermocouples and the ambient temperature were followed with a recording potentiometer and readings were taken only when the ambient temperature was most constant. The reproducibility of the reactor readings was about ±2%.

The method for apportioning the total energy absorption into the components from fast neutrons and gamma radiation was described by Richardson.[1] In order to calculate the energy absorption values of Table 12 it was necessary to correct for the energy absorption by the copper sheets in the calorimeter. The copper sheet is 28% of the weight of the nylon calorimeter and 15% of the weight of the graphite calorimeter. Energy absorption from gamma radiation by the copper sheet is 15% of the total for the graphite calorimeter and 13% of the total for the nylon calorimeter.

Uncertainty in the correction for thermal neutron absorption by the copper (owing to uncertainty as to the value of the thermal flux) is of the same order as scatter in readings from ambient temperature fluctuations.

Energy absorbed by the nylon owing to the production of chemical unsaturation is of the same order as the uncertainties already mentioned and is therefore neglected.

GAS-COOLED REACTOR FUELS

O. Sisman J. G. Morgan

Since ORNL has assumed complete responsibility for the fuel element for the Gas-Cooled Reactor prototype, major effort for the next year will be placed on radiation-effects studies directly related to the design of this fuel element. Long-range studies will also continue on more advanced fuel materials for future high-temperature gas-cooled reactors.

The basic criteria for the GCR prototype fuel element are that it will contain slightly enriched UO_2 canned in type 304 stainless steel and be cooled with helium. The UO_2 pellet size has been tentatively set at 0.705 in. OD and 0.50 in. long. Helium pressure outside the canned pellets will be 400 psi.

Radiation damage studies are being carried out on canned UO_2 which simulate the conditions of the reactor fuel element as nearly as can be presently envisioned. Release of fission gas and integrity of the fuel element and UO_2 pellet are being studied under conditions of varying power density, burnup, temperature, and pellet geometry, as well as several less important conditions. The experiments are designed primarily to answer the questions of gas pressure buildup in the fuel can and temperature increase in the UO_2 and to furnish the basis for a choice of UO_2 pellet shape between a solid pellet, a pellet with a central hole, and a pellet with a ceramic bushing in the central hole.

Prototype UO_2 Capsule Experiments

M. T. Morgan D. Pratt

A series of experiments on stressed UO_2 fuel element prototypes is planned for operation in the LITR and other reactors. The first of these experiments was terminated on August 6, 1958, due

to failure of a gas seal. This test was composed of 12 hollow cylinders of UO_2 sealed in purified helium in a type 304 stainless steel can (see Fig. 132). A steel spring was loaded to apply a stress equal to that of a full-size fuel element, about 2.75 lb. Heat, generated in the UO_2 during irradiation, was transferred to the outside jacket, which is cooled by the reactor water, through a 0.020-in. annulus of helium at 400 psi pressure. A rack and pinion mounting allowed vertical positioning of the experiment so that predetermined temperatures (measured by Chromel-Alumel and platinum vs platinum–10% rhodium thermocouples) could be maintained during operation.

The UO_2 samples were prepared by the Ceramics Laboratory[1] of the Metallurgy Division. Ammonium diuranate was precipitated from UO_2F_2, and the UO_2 was recovered by successive calcinations and prepressed at 15,000 psi. After the pellets were formed at 7500 psi, they were statically pressed at 35,000 psi and sintered for 1 hr at 3180°F in an atmosphere of 7 parts of nitrogen to 3 parts of hydrogen.

The samples are 0.705 in. OD, 0.250 in. ID, and 0.500 in. long, weigh approximately 27.5 g each, and have a density of 10.4 g/cc. The U^{235} content is 1.91%, and the U:O ratio, by stoichiometric analysis, is 1:2.005.

Spectrographic analysis showed traces (less than 0.1% by weight) of Al, B, Be, Ca, Cr, Cu, Fe, Mg, Mo, Ni, Si, and Ti. A chemical analysis for fluorine showed less than 10 ppm.

Experimental Conditions. – The experiment was operated for 330 hr at full reactor power. A gas pressure of 400 psi was maintained on the outside of the canned UO_2. Cladding temperatures of 950°F were reached with the center UO_2 temperature at 1850°F. The can will be examined in the hot cell for dimensional changes. Very important information on a first experiment of this type was obtained which verified the heat transfer calculations used in the design.

Miniature UO_2 Capsule Experiments

M. T. Morgan M. F. Osborne

The retention of fission gases by the canned fuel elements is an important factor in GCR fuel

[1]A. J. Taylor, private communication, Aug. 12, 1958.

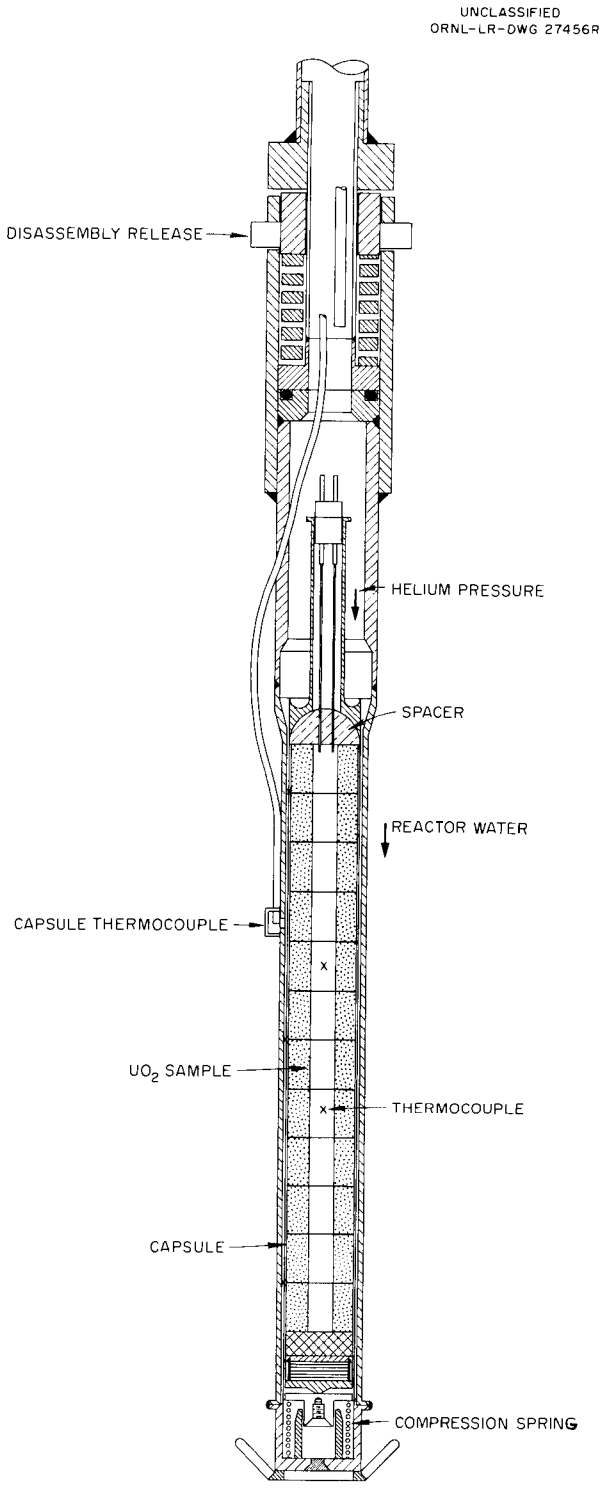

Fig. 132. Fuel Element Experiment.

element design, since the release of gas can cause distortion or swelling by a buildup of pressure in the can and tends to increase the temperature of the fuel by diluting the helium in the can.

Fission gas release is considered mainly the result of solid-state diffusion.[2] Normally, diffusion is affected by temperature, concentration, total surface area, and time. The total surface area available for adsorption of gas, as measured by the Brunauer-Emmett-Teller method (using krypton instead of nitrogen for high-density UO_2), is a function of density. This series of UO_2 experiments was designed for measurement of the fission gas retention of UO_2 with different densities considered usable for GCR fuel elements and for examination of the fracturing of the UO_2 which is expected to occur as a result of high thermal stress. The capsule is shown in Fig. 133. Nominal clearance between the samples and the inner wall of the sealed capsule is 2 mils. The capsule is sealed in a helium atmosphere and contains a titanium sponge getter to remove residual oxygen.

The UO_2 was prepared by the Ceramics Laboratory of the Metallurgy Division. Ammonium diuranate was precipitated from UO_2F_2, calcined to UO_2, and prepressed at 15,000 psi. The UO_2 was crushed through a 35-mesh screen, formed at 23,000 psi, and sintered at 3180°F for 1 hr in an atmosphere of 7 parts of nitrogen to 3 parts of hydrogen.

The specimens were hollow cylinders, each measuring 0.156 in. OD × 0.078 in. ID × 0.250 in. long (see Fig. 134). In the first test of the series the specimens had an average density of 10.52 g/cc, or 96% of theoretical. Other sample properties were as follows:

U/O ratio by stoichiometric analysis	1:2.008
U^{235} content	15%
Gas surface area	0.002 m^2/g or 3 times the geometric area
Spectrographic analysis	Less than 0.01% by weight of Al, B, Ca, Cr, Cu, Fe, Mg, Mo, Ni

[2] J. D. Eichenberg *et al.*, *Effects of Irradiation on Bulk UO_2*, WAPD-183, p 25 (Oct. 1957).

Irradiation. – The capsule was irradiated in the LITR for 1829 hr at 3000 kw reactor power. Conditions of the test are tabulated below:

Burnup	4.5% U^{235}
Integrated flux (thermal)	6.6×10^{19} neutrons/cm^2
Power dissipation	730 w/cc
Inside temperature	1770°F
Outside temperature of UO_2	1670°F
Thermal stress	13,000 psi

A bench test was made to determine the variation in actual temperature of the shell from that indicated by the thermocouples. These thermocouples were spot-welded to the shell in the annular space required for the cooling air stream. The bench test was conducted with power generation, temperatures, and air flow that simulated operating conditions in the reactor. Temperatures were recorded on a Brown recorder and checked with an optical pyrometer. The total variation was less than 10°F, which is less than the error that may be expected with this equipment, and therefore can be disregarded.

The second of the air-cooled experiments was inserted in the LITR on June 24, 1958. The design was changed to allow two sets of samples to be irradiated at the same time. This experiment is in facility C-46, which has a neutron flux of 4×10^{13} neutrons·cm^{-2}·sec^{-1}, or twice that of the first test. The sample properties are the same as those used in the first air-cooled experiment. The following temperatures are being maintained:

	Inside	Shell
Top	1770°F	1150°F
Bottom	2000°F	1380°F

Results – After irradiation, fission gas samples were taken by puncturing the capsule in the Solid State Division hot cell with a tube piercing valve. The gas was allowed to flow into an evacuated system from which an aliquot was valved off into a glass bulb. The gas samples were analyzed with an NaI gamma-ray scintillation spectrometer. These results are compared below with the total

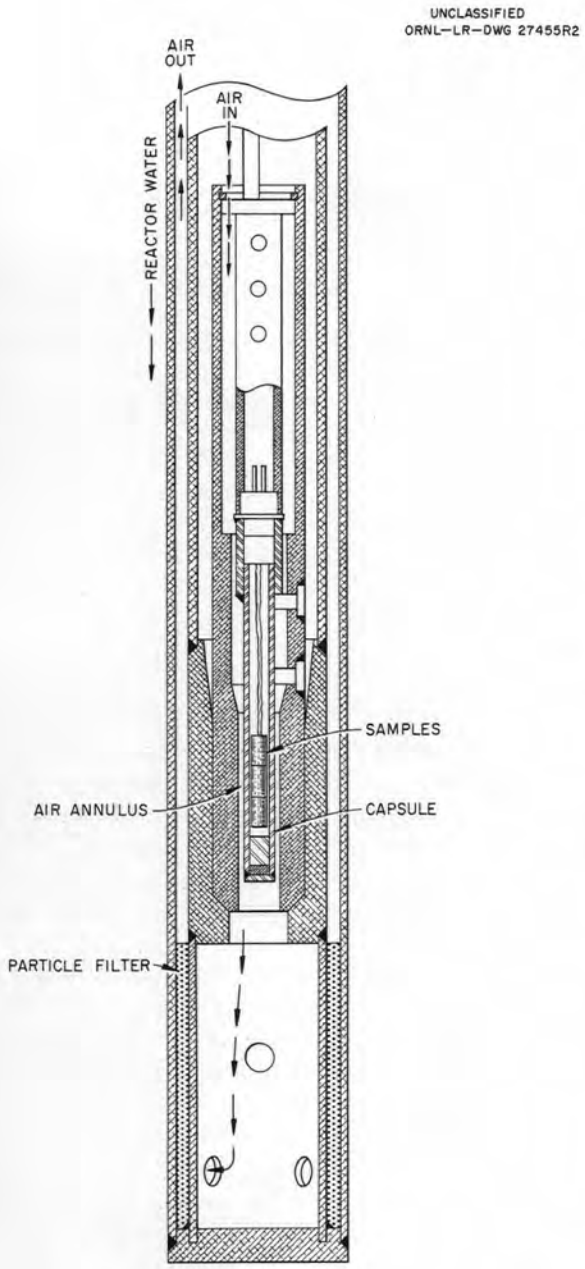

Fig. 133. Air-Cooled Irradiation Facility.

amount of each isotope existing at the time of sampling:[3]

	Kr^{85m}	Xe^{133}	Xe^{135}	I^{131}
Gas in the capsule (cc)	8×10^{-8}	3×10^{-5}	3×10^{-7}	3×10^{-7}
Total gas existing (cc)	4×10^{-6}	4×10^{-3}	2×10^{-5}	4×10^{-4}
Gas released (%)	<2	0.7	0.2	0.1

Fig. 134. Specimens of UO_2 for Measurement of Retention of Fission Gases.

Further examination of the capsule is being delayed pending arrangements for a hot cell which can handle plutonium contamination.

High-Temperature Ceramic Fuels

J. G. Morgan M. T. Morgan

Chromium-Al_2O_3. – Two samples of 70% Cr–30% Al_2O_3 were irradiated in evacuated quartz containers cooled by the reactor water. This material had a density of 5.91 g/cc and an average heat capacity from 25 to 1000°C of 0.171 $cal \cdot g^{-1} \cdot (°C)^{-1}$. The samples, $\frac{1}{4}$ in. in diameter and 1 in. long, were examined for structural changes after irradiation (1×10^{20} *nvt*, thermal). No evidence of changes was found. Figure 135 illustrates a typical specimen of this type before and after irradiation. The Knoop hardness number (3-kg load) showed an increase from 472 to 675 as the result of irradiation.

A UO_2 fuel plate, $\frac{1}{8} \times \frac{1}{2} \times 1\frac{1}{2}$ in., clad with Cr-Al_2O_3 was irradiated in the LITR C-42 vertical facility for a total of 2800 hr at 3000 kw reactor power. The plate generated 150 w/in.^{2} fission heat. The average plate surface temperature was

[3]Calculated by using values obtained from graphs given by J. O. Blomeke and M. F. Todd, *Uranium-235 Fission-Product Production as a Function of Thermal Neutron Flux, Irradiation Time, and Decay Time*, ORNL-2127.

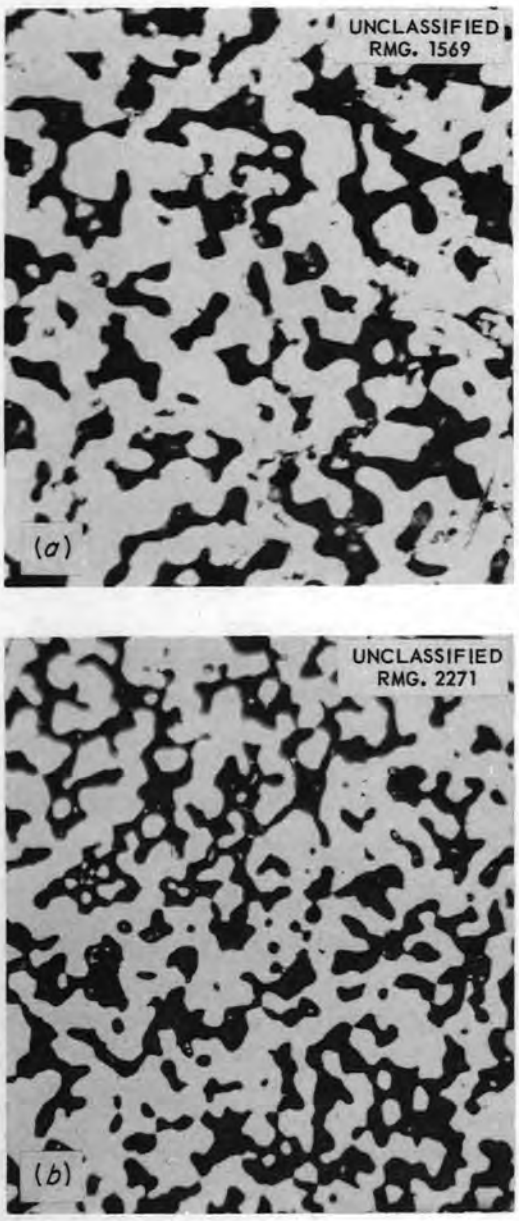

Fig. 135. Specimen of 70% Cr–30% Al_2O_3. (*a*) Unirradiated, 750X; (*b*) irradiated, 500X.

1000°C, with a maximum of 1050°C. Burnup was calculated to be 14.7% U^{235} at a neutron dosage of 2.5×10^{20} *nvt*, thermal. Construction of the experiment capsule is shown in Fig. 136. The experiment was conducted to determine irradiation effects on the structure and to measure fission gas retention of the cladding.

The typical appearance of the unirradiated fuel plate is shown in Figs. 137 and 138. The irradiated specimen was characterized by a high degree of stringered voids which were distributed in halo-type patterns around, but removed from, the fuel-

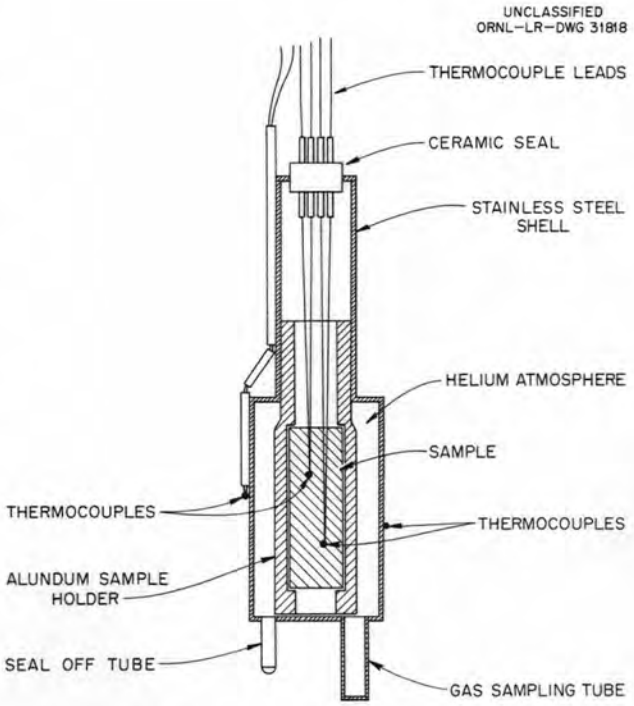

Fig. 136. High Temperature Capsule.

bearing portion of the specimen (see Fig. 139). This pattern was positioned eccentric to the location of the fueled area, being displaced toward one end of the plate. An area showing this porosity at higher magnification is seen in Fig. 140. It may be significant that these voids are characterized by a region containing only chromium which always appears toward the interior side of the porosity halo. Figure 141 shows the UO_2 particle before and after irradiation. The increase in the size of voids within the UO_2 particle as the result of irradiation is typical of dispersion-type fuels at this burnup. There was evidence of slight diffusion between the UO_2 and Al_2O_3 particles as a result of irradiation. The exterior surfaces of the irradiated fuel specimen showed a 2-mil oxide layer identified as Cr_2O_3. The physical measurements are given below and the fission gas release data are given in Table 13.

	Preirradiation	Postirradiation
Alpha activity (counts/min)	13	
Weight (g)	8.8215	9.0625
Density (g/cc)	5.84	5.39
Length (in.)	1.495	1.504
Width (in.)	0.498	0.510
Thickness (in.)	0.125	0.149

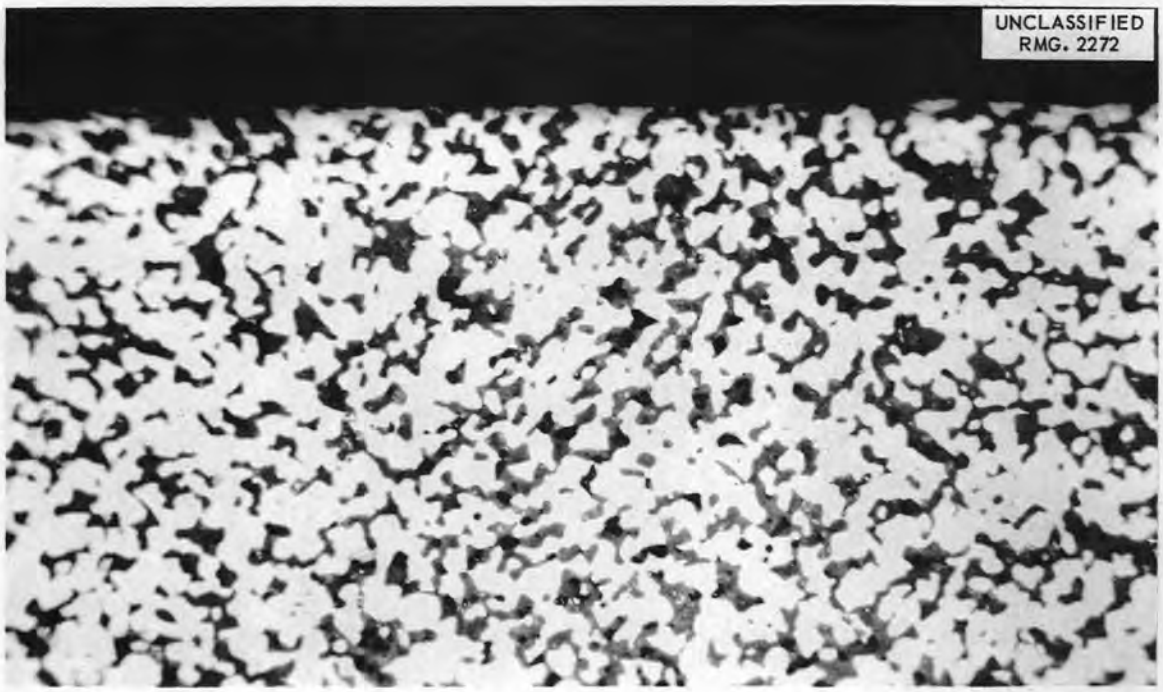

Fig. 137. Exterior Surface of UO_2 Fuel Plate Clad with Cr-Al_2O_3. 500X.

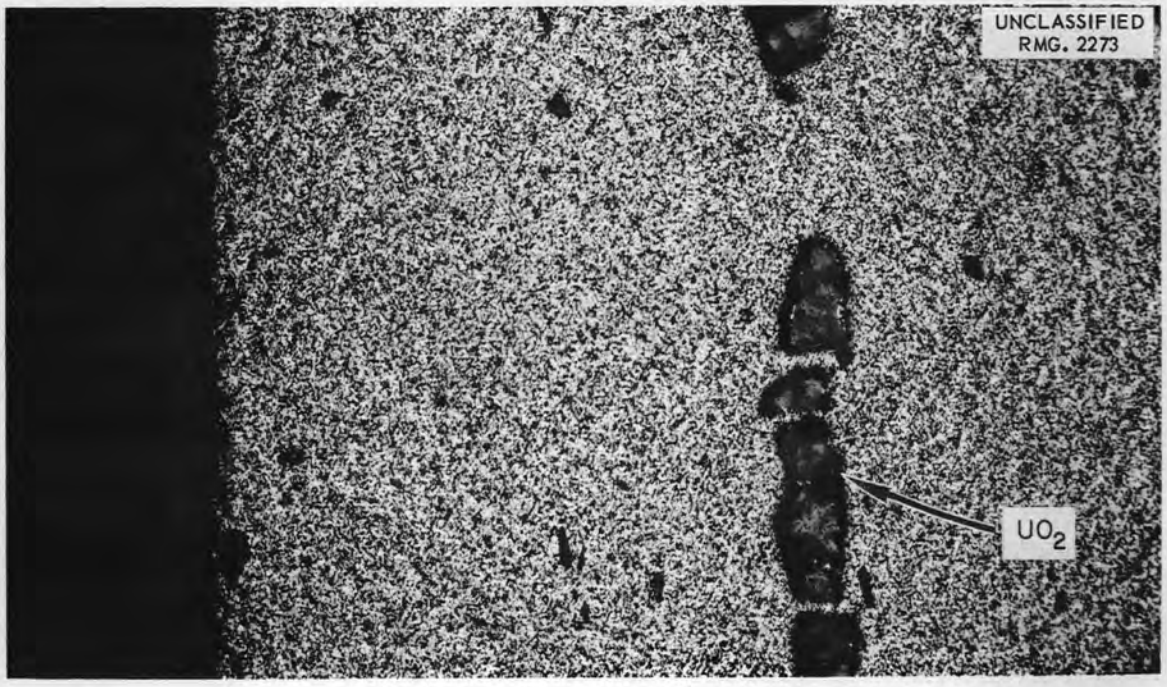

Fig. 138. Sectioned Fuel Plate. 55X.

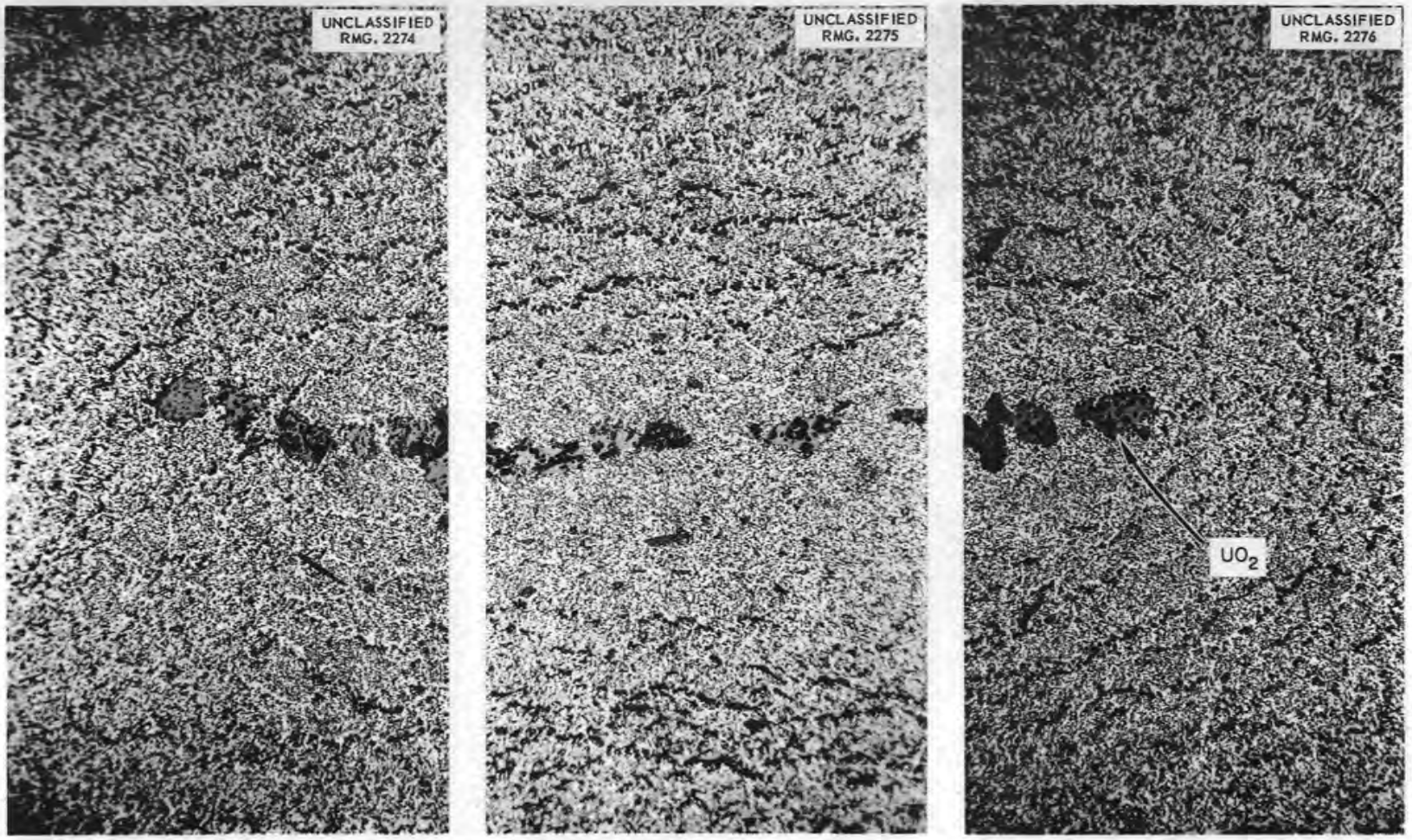

Fig. 139. Irradiated Fuel Plate. 55X.

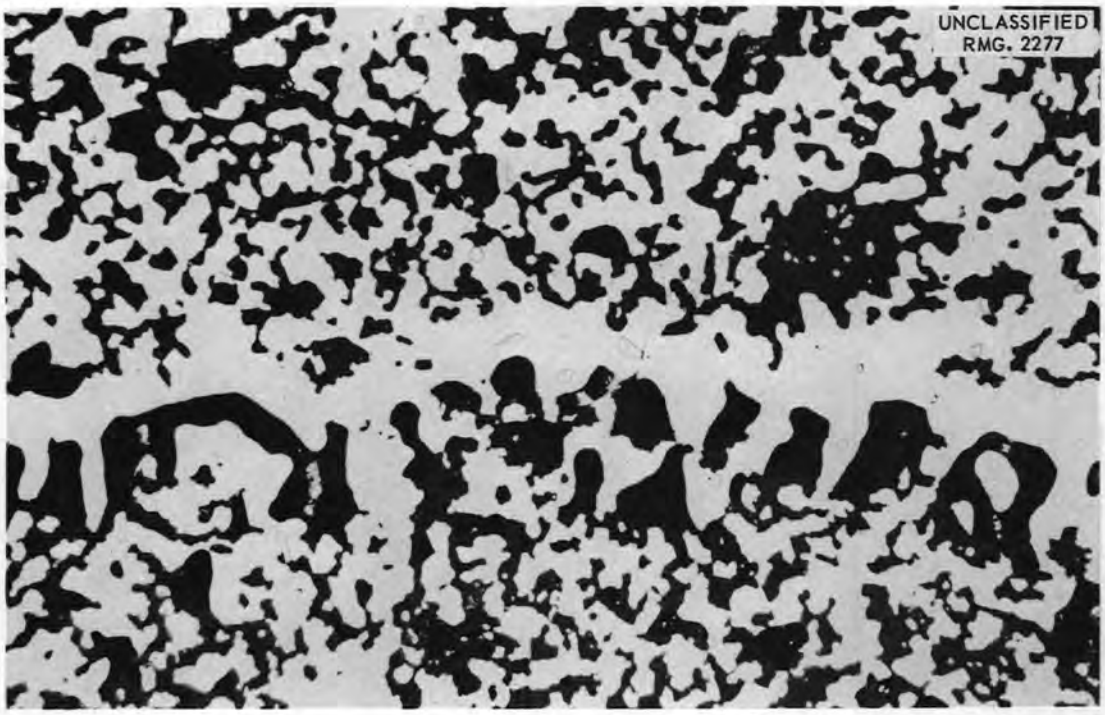

Fig. 140. Porosity in Cladding. 500X.

Table 13. Fission Gas Evolution

	Xe^{133}	Xe^{135}
Fission gas measured (cc)	9×10^{-9}	26×10^{-9}
Fission gas total* (cc)	17×10^{-3}	28×10^{-5}
Gas escaped through cladding (%)	5×10^{-5}	9.3×10^{-3}

*Total isotope existing at time of sampling based on graphs in ORNL-2127 (see ref 3).

Fission Gas Retention Studies on High-Temperature Coatings

R. M. Carroll

A prerequisite for certain fuel materials is the ability to retain gaseous fission products. A reactor experiment is planned to test the ability of graphite coated[4] with SiC-Si to retain gaseous fission products at high temperatures and high heat fluxes. The sample will be heated by its own fission heat to the desired temperatures and the evolved fission gases analyzed. The initial tests will be made with unclad fuel (ThO_2-UO_2) to establish the rate and amount of gaseous evolution as a function of time, burnup, and temperature. Subsequent tests will be made with ceramic fuel clad in high-density graphite and graphite with an SiC-Si coating.

The temperature of the sample will be controlled by controlling the position of the fuel sample in the reactor. To facilitate this operation, a hydraulic positioning mechanism has been designed and constructed. This device will provide the added advantage of being an experiment safety control, since an approach to a dangerous situation will result in an automatic withdrawal of the sample from the high-flux region of the reactor.

Evolved fission gases will be continuously analyzed by a gamma-ray spectrometer. A stream of helium swept over the surface of the fuel sample will carry the fission gases to the spectrometer for analysis within 5 min of evolution.

An air cooling system will be used to transport the heat from the sample. The experiment is expected to attain a heat flux of 200,000

[4]The coatings were developed and made by J. R. Johnson of Minnesota Mining and Manufacturing Corporation.

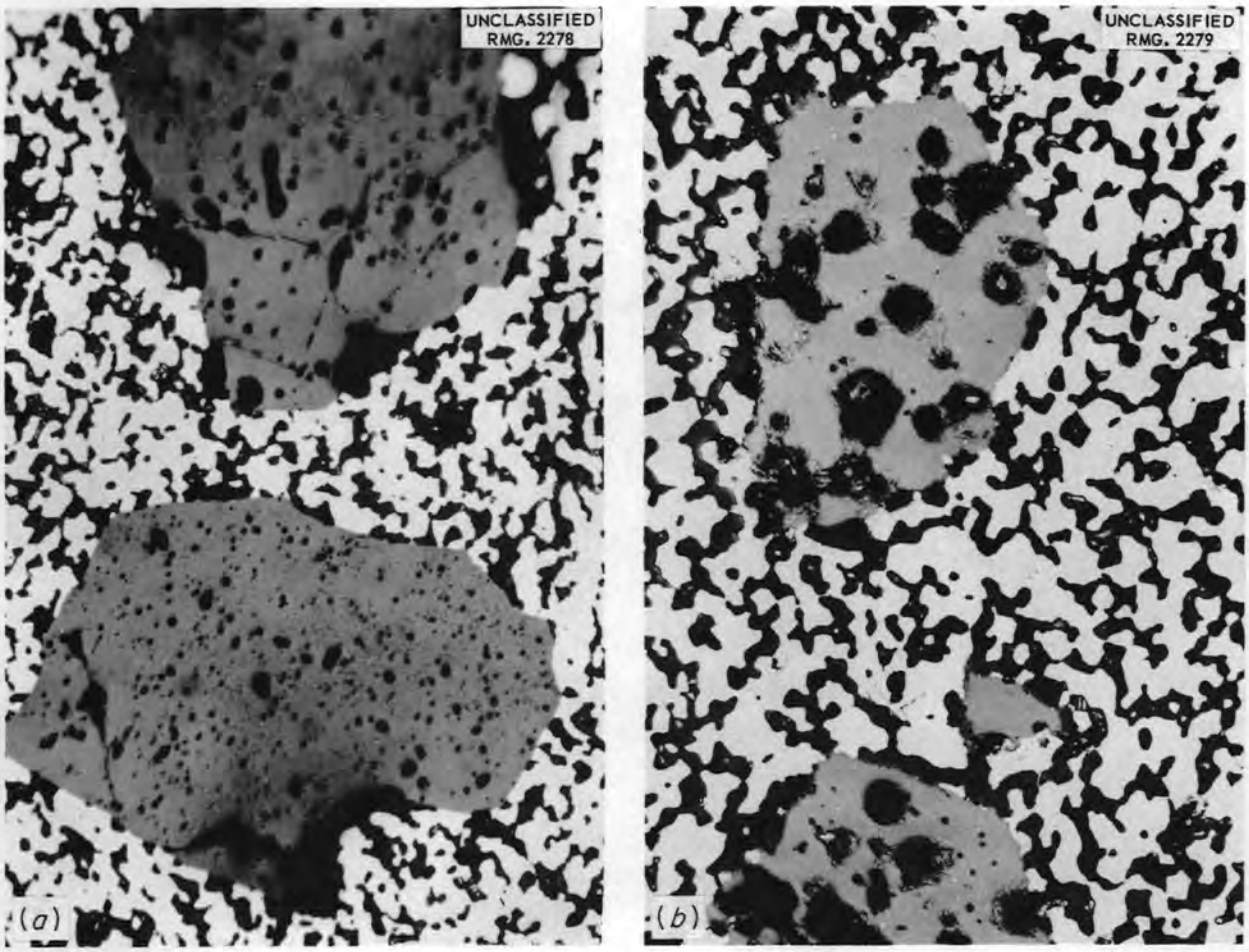

Fig. 141. Particles of UO_2 in Fuel Plate Core. (*a*) Before irradiation; (*b*) after irradiation. 500X.

$Btu \cdot hr^{-1} \cdot ft^{-2}$ with a 2000°F fuel surface temperature. The facility to be used is C-1 in the ORR.

SiC-Si Cladding for High-Density Graphite

R. M. Carroll

The development of a moderator capable of withstanding high temperatures in oxidizing atmospheres is of great importance for a gas-cooled reactor. For this reason, SiC-Si cladding for graphite is being examined for oxidation and erosion resistance outside the reactor in preparation for subsequent experiments to be done in the reactor. Four different samples of graphite coated with SiC-Si have been subjected to bench tests.

The first experiment was primarily designed to act as a destructive erosion test. The experiment consisted of a needle-point blast of air directed at one portion of the sample (see Fig. 142). The specimen was 0.75 in. long and 0.75 in. in diameter and contained a cylindrical sample of UO_2. The air blast impinged on a surface at 1830°F with a near-sonic velocity. Because of the small area of the jet, erosion at this point could be compared with the surrounding surface of the sample. After 1000 hr of testing, the only observed change was a slight discoloration at the point of impact.

The sample was periodically weighed, and a gradual weight increase was noted (see Fig. 143). When the sample was weighed, it was removed directly from the furnace and cooled in an air blast. No evidence of cracking, spalling, or any thermal shock damage was observed.

The experiment was terminated after more than 1000 hr of testing when a platinum thermocouple was inadvertantly placed in direct contact with the specimen. The Pt-Si reaction that resulted formed

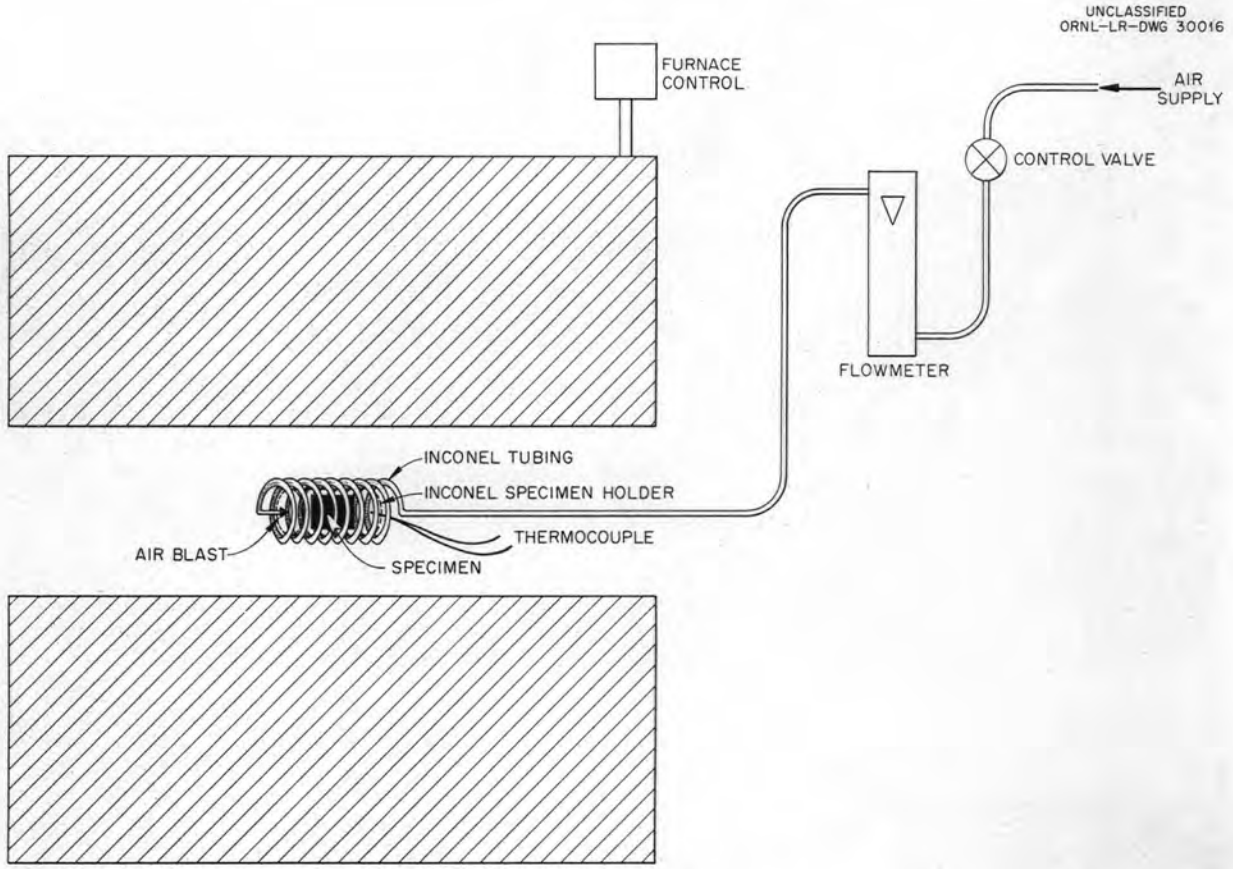

Fig. 142. Erosion Test for Coated Graphite.

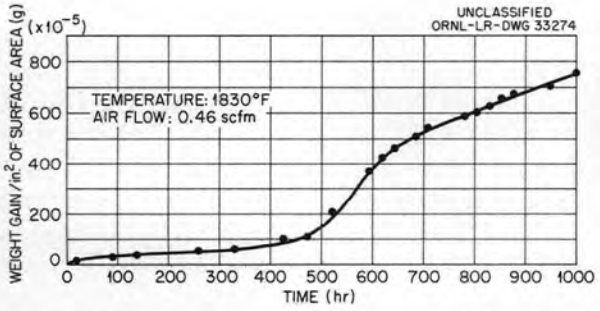

Fig. 143. Weight Gain of Coated Graphite in Air Blast Test.

a porous section in the SiC-Si coating, and the graphite oxidized beneath the coating, leaving only a hollow shell in the vicinity of the Pt-Si reaction area (see Fig. 144). The sample was sectioned and examined metallographically. For comparison, a sample of graphite container that had not been subjected to this treatment (shown in Fig. 145) was also sectioned and examined metallographically. The tested sample is shown in

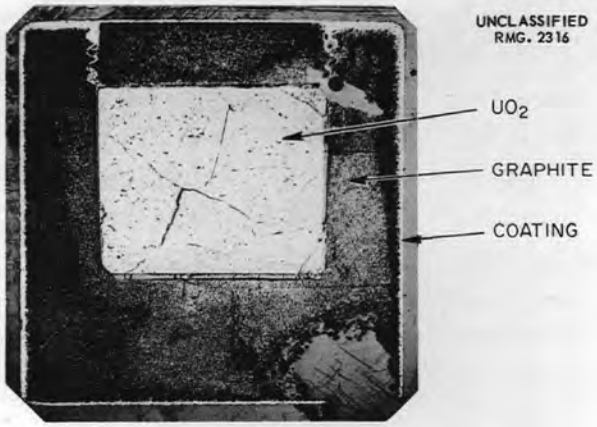

Fig. 144. Sectioned Test Sample After Failure of Cladding at Lower Right Corner. Air blast was directed on upper end, against the lid surface.

Fig. 146, in which the darker gray area of the cladding is the SiC phase, also found next to the graphite. The thicker layer of SiC in the comparison container (Fig. 145) is probably due to

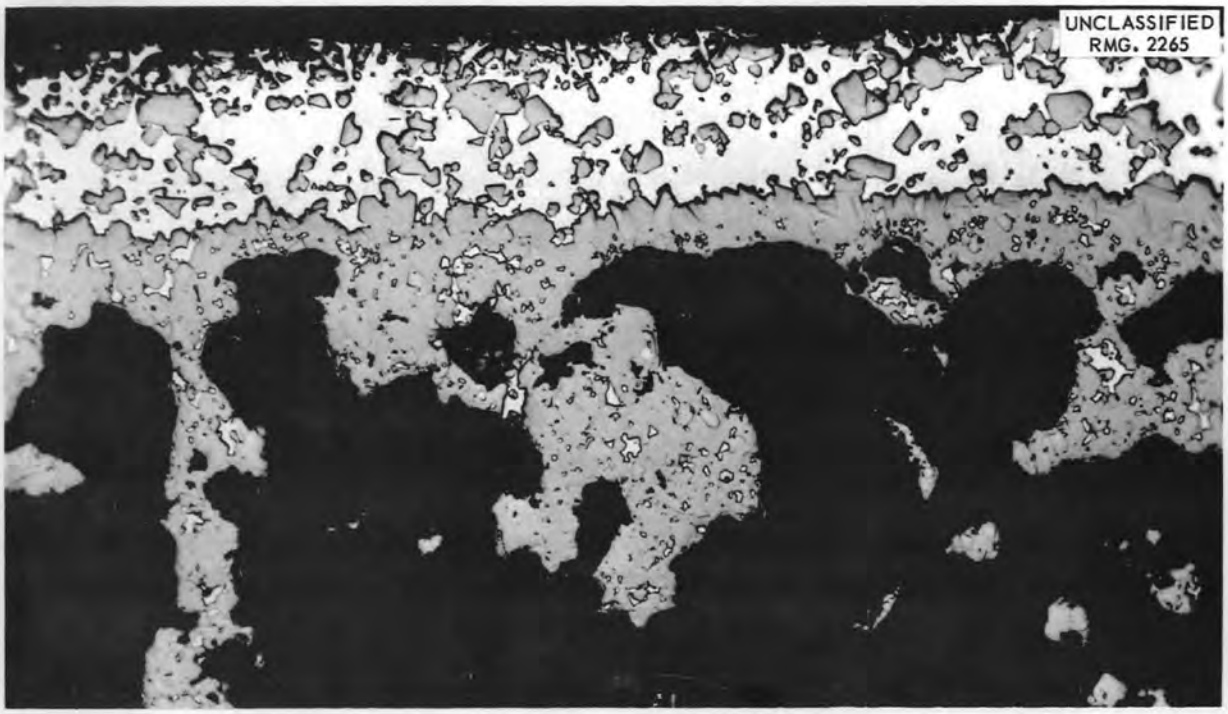

Fig. 145. Sectioned Graphite Container Clad with SiC-Si, As Received. 250X.

Fig. 146. Sectioned Test Sample of Graphite Clad with SiC-Si After 1000-hr Air Blast Test. 250X.

the method of application of the coating,[4] which is still an experimental operation. The over-all thickness of the cladding is about the same.

The second experiment, currently in progress, was designed primarily as an oxidation test. Three graphite specimens coated with SiC-Si, each $\frac{1}{4}$ in. in diameter and 1 in. long, are placed in an Inconel holder and inserted into an Inconel tube in a furnace. Air is forced through the tube and over the specimens (see Fig. 147). Because of the excellent resistance of the first specimen to oxidation, the temperature was increased to 2000°F and the average velocity of the air stream past the specimens was increased.

The air velocity past the surface of the specimens is 140 fps with a volume flow of 0.95 scfm. To date, after 335 hr of operation, two of the specimens have exhibited no detectable change in weight or appearance; however, one of the specimens evidently had, or has developed, a small hole in the cladding. A weight loss of 11.9% has resulted, although there has been no change in external appearance. This defect became apparent only after more than 30 hr of testing.

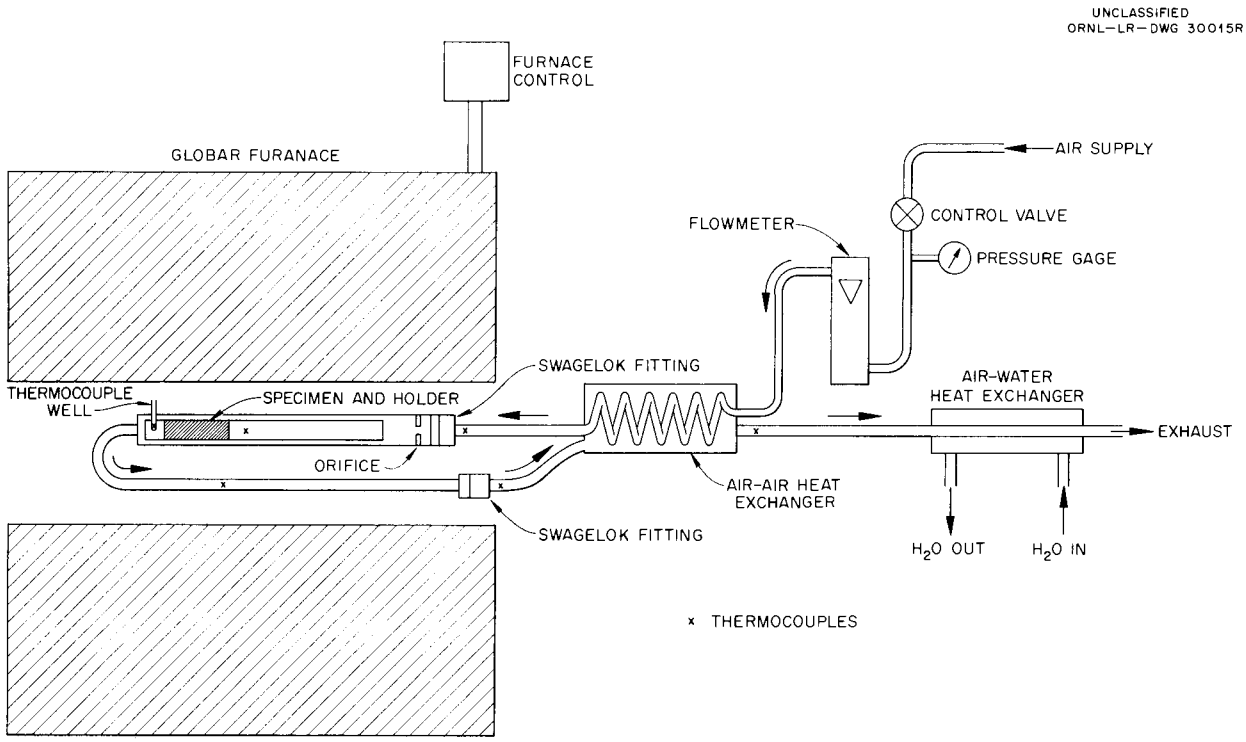

Fig. 147. Oxidation Test for Coated Graphite.

A high-temperature oxidation-irradiation test is proposed to evaluate the integrity of the SiC-Si cladding under actual reactor conditions. This experiment can be divided into two tests. The first test, which will be a phase of the fission gas retention studies, will be the evaluation of the SiC-Si as a fuel element cladding, with the cladding operating much hotter than the cooling gas stream. The second test will be to evaluate the SiC-Si as a moderator cladding, with the cladding only slightly hotter than the coolant gas stream. This can also be performed in conjunction with the fission gas retention tests by mounting clad graphite specimens in the cooling gas stream just below the fuel sample.

Gas-Cooled In-Pile Loop for Ceramic Fuels Studies

P. E. Reagan

An experiment is being constructed to study radiation effects on ceramic fuels at high temperatures. The portion of the loop in the active core of the ORR is illustrated in Fig. 148, and the location of both in-pile and auxiliary components is shown in Fig. 149.

The design consists of concentric in-pile tubes containing a removable test capsule cooled by recirculated gas. These concentric tubes enter the reactor tank at V2 flange and extend downward with a 17-in. horizontal offset into the reactor lattice B-9 position. A flux of approximately 0.7×10^{14} thermal neutrons$\cdot$cm$^{-2}\cdot$sec^{-1} is expected at 20 Mw reactor power. The gas to be used in the first tests will be nitrogen; however, air or other gases could be used as a coolant. The entire loop contains 160 ft^3 of gas, which is forced through the in-pile tubes by a 30-hp oil-free compressor. The compressor and other auxiliary components are located within a shielded compartment in the reactor basement. Coolant lines between this compartment and the reactor pool are also shielded.

In general, density changes and dimensional stability will be studied, but specific studies will be done on fission product retention. To determine fission product leakage rates during the test, a spectrometer is located in the exhaust leg of the loop. Two series of ceramic fuel tests are presently scheduled for this loop. The first series will be Cr-Al_2O_3 bodies containing enriched UO_2, and the second series will be Si-SiC bodies containing

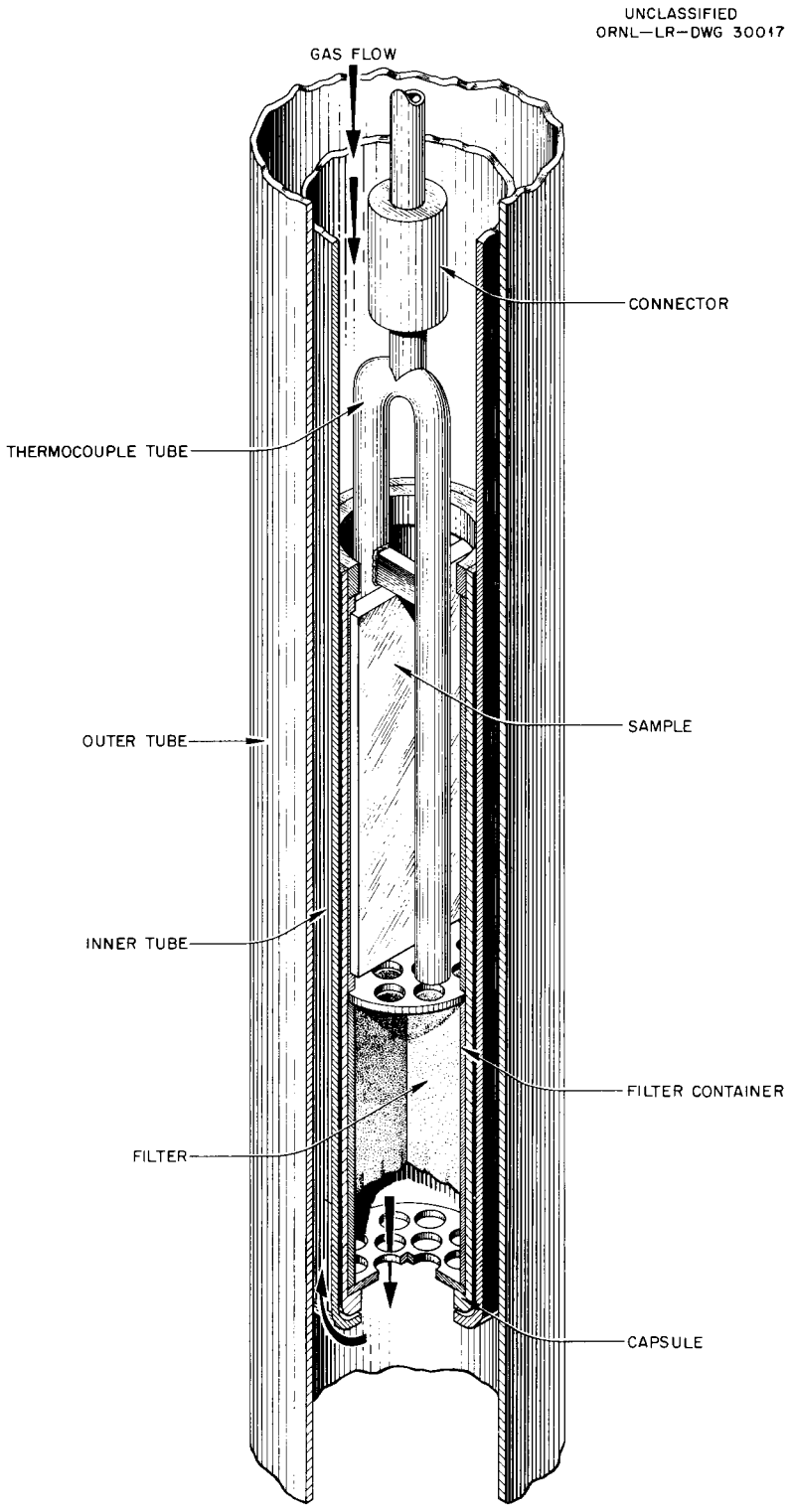

Fig. 148. Gas-Cooled In-Pile Loop.

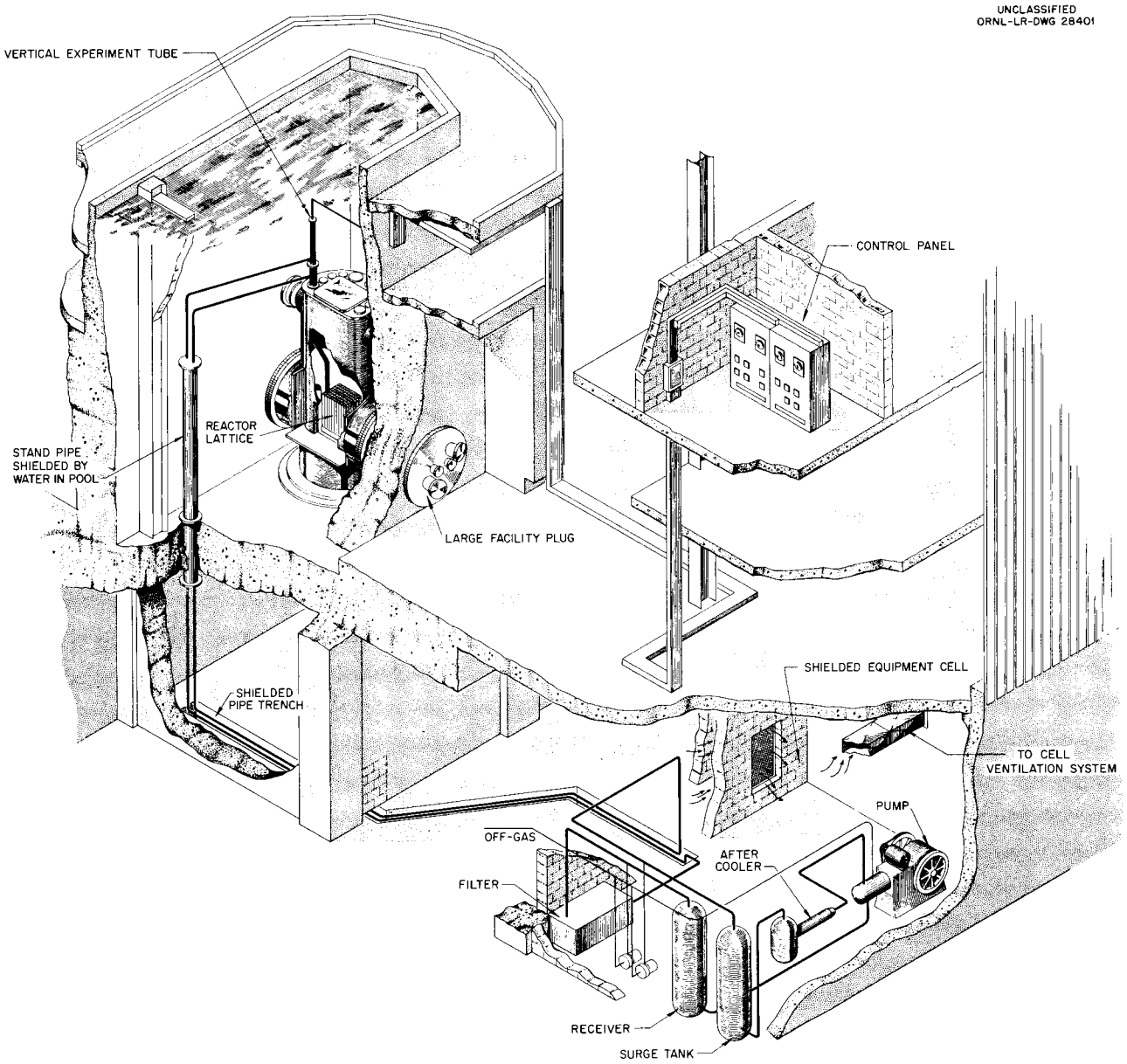

Fig. 149. Vertical Loop Experiment Showing Provisions for Shielding Piping and Equipment.

enriched UO_2. Each series will operate at 2000–2500°F fuel sample surface temperature with fuel samples generating up to 500,000 $Btu \cdot hr^{-1} \cdot ft^{-2}$.

The experiment has been approved by the Experiment Review Committee, and basic components have been purchased and are scheduled for completed installation in October. The instrumentation, except for a wireway being installed for common use, will also be completed by this date, and fuel sample tests are expected to begin in December.

Temperature Measurement in the Gas-Cooled Loop

M. T. Morgan

The irradiations planned for the ORR in which a cermet-clad fuel plate is placed in a high-velocity air stream are at temperatures beyond the melting point of all commercial thermocouple wire except platinum vs platinum-rhodium. Platinum, however, reacts with the cermet at high temperatures; so at present there is no known means of measuring the

temperature with thermocouples. A radiation pyrometry method is being investigated. Deterrents to such a design are small available space, high gamma heating, and irradiation damage.

By the use of electrically opposed double elements, one of which is exposed to the sample and the other enclosed, it is possible to cancel the effects of gamma heat. Such an arrangement will be calibrated by bench tests before operation. This design is shown in Fig. 150. An electrically heated system for bench tests has already been made, and construction of the pyrometer will begin soon.

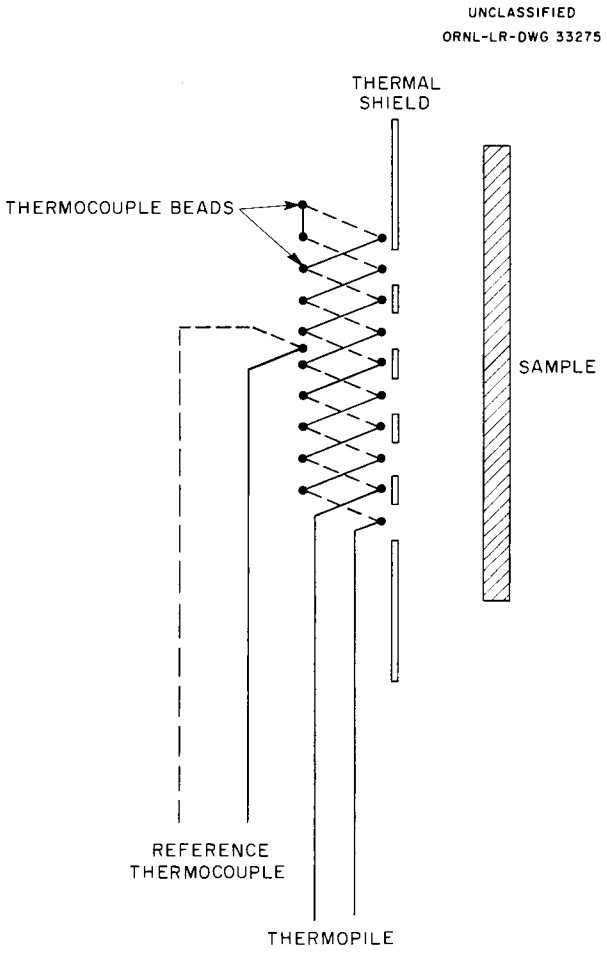

Fig. 150. Radiation Pyrometer for ORR Experiment.

Thermocouple Irradiation Studies

C. D. Baumann

Ceramic fuel element studies are being made at temperatures requiring noble-metals thermocouples. The noble-metals thermocouples in common usage at ORNL are platinum vs platinum–10% rhodium or platinum vs platinum–13% rhodium. Rhodium has a rather large thermal neutron absorption cross section (150 barns), and so for reasonable exposure periods there may be appreciable rhodium burnups (e.g., $1\frac{1}{2}\%$ per 10^{20} *nvt*). Rhodium burnup may seriously affect the thermocouple calibration. It is the purpose of this study to measure the effect of neutron exposure on the calibration of Pt vs Pt-Rh and Chromel-Alumel thermocouples.

Bare and ceramic-insulated platinum vs platinum–10% rhodium and Chromel-Alumel thermocouples have been inserted in a water-cooled hollow beryllium piece in the C-47 location adjacent to the active core in the LITR. The thermocouples are about 18 in. long and are encased in $\frac{3}{8}$-in.-OD aluminum tubes (see Fig. 151). After being irradiated for the desired period, the tube is removed from the active lattice and short-time activity allowed to decay before the thermocouples are calibrated.

To date only the bare platinum vs platinum–10% rhodium thermocouples have been calibrated, because the remaining wires are too radioactive to be handled outside the hot cells. The measurements have been made by the standards laboratory of the Instrument Department using the routine method and equipment for calibrating plant platinum vs platinum-rhodium thermocouples. This is essentially the method recommended by the National Bureau of Standards in NBS Circular 590. Techniques for adapting this method to hot cell manipulation are being developed and will be used to calibrate the remaining couples and all the couples to be irradiated in the ORR.

Three sets of platinum vs platinum–10% rhodium couples have been calibrated. The results are shown in Figs. 152 and 153.

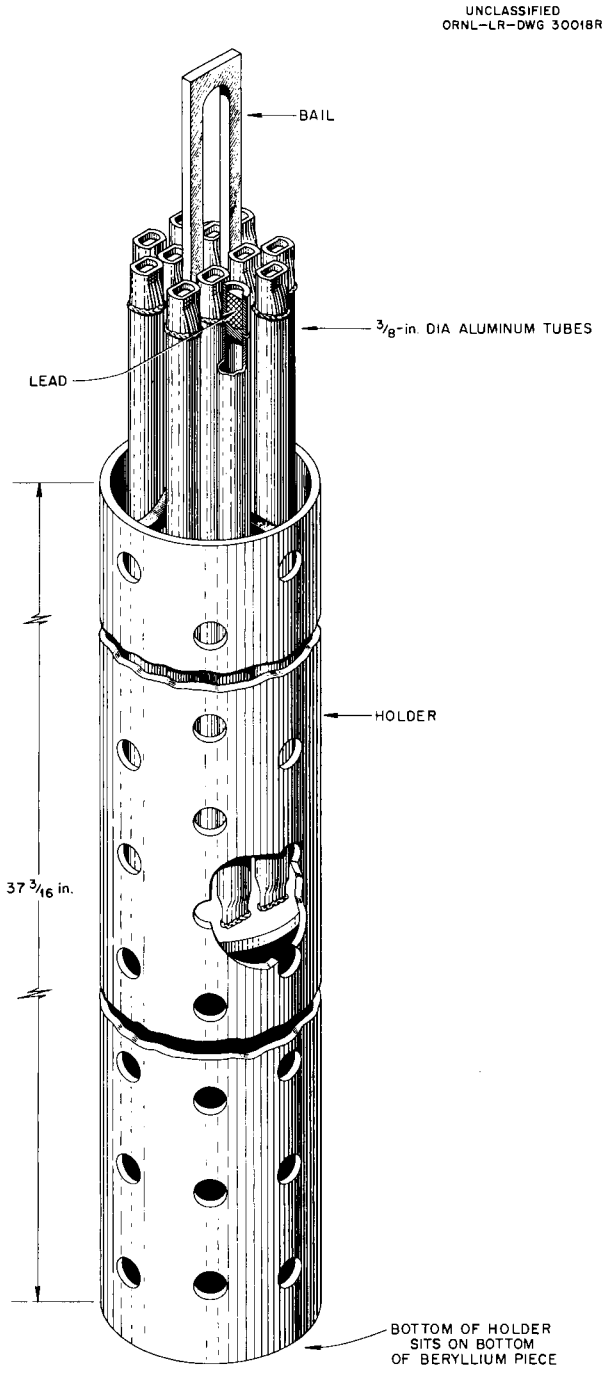

Fig. 151. Thermocouple Irradiation Test.

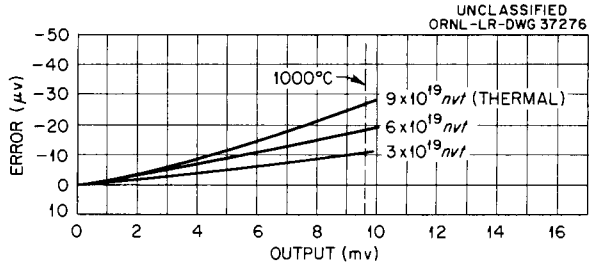

Fig. 152. Effect of Irradiation on Platinum vs Platinum–10% Rhodium Thermocouple. Bishop wire. Microvolts difference from an unirradiated thermocouple of the same wire.

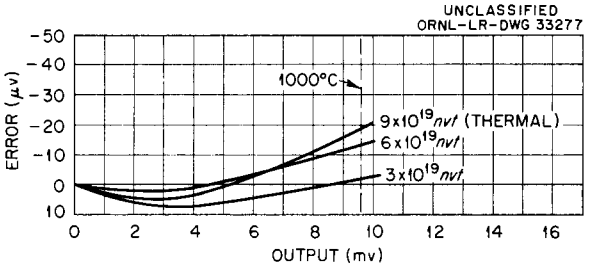

Fig. 153. Effect of Irradiation on Platinum vs Platinum–10% Rhodium Thermocouple. Sigmund Cohn wire. Microvolts difference from an unirradiated thermocouple of the same wire.

Supplementary measurements indicate that most, if not all, of the difference between irradiated and nonirradiated couples occurs in the platinum–10% rhodium. It is apparent that there is a significant difference in performance in the wire from the two manufacturers. The Sigmund Cohn rhodium wire is very much more radioactive than the Bishop wire. A gamma-ray spectrum analysis made after several weeks of decay indicates most of the long-time activity in all wires to be due to Ir^{192}. Additional samples are being prepared to identify the short-lifetime components. Additional thermocouples are being irradiated in the ORR to measure effects at higher exposures.

HIGH-RADIATION-LEVEL EXAMINATION LABORATORY

O. Sisman S. Dismuke

The Solid State Division has assumed the responsibility for the design of a hot cell facility to be used by the entire Laboratory. The Laboratory was allotted $200,000 last year for the design of part I of this facility, which is to cost 3.5 million dollars. A preliminary design has been completed and is shown in Figs. 154–156. The location of this laboratory will be at the present site of the west end of Building 3550.

As shown in Figs. 154–156, the laboratory will consist of three banks of cells for the examination of highly radioactive materials, with space allowed for the construction of a fourth bank of cells. Attached to each two banks of cells will be a relatively large cell area which will be used exclusively for decontamination, remote maintenance, and loading and unloading of specimens. The laboratory will also include an area for work with materials of low-level radioactivity and a third area for equipment development and testing and for doing cold experiments which are associated with the hot cell work.

The work in this laboratory will be primarily of the metallurgical type rather than chemical. Major emphasis is placed on the necessity of performing work with materials which are highly alpha or beta radioactive in addition to having a high level of gamma activity. The cells have been designed under the new philosophy of complete containment and remote maintenance and manipulation, rather than the philosophy of depending upon ease of decontamination. These cells will contain no personnel entry because of the anticipation that it will not be necessary for personnel to enter these cells at any time. Radioactive equipment will be brought into the working cells through the maintenance cell. Radioactive waste will be removed from the working cells through the maintenance cells. Between the maintenance cell and the working cells will be an area in which remote decontamination may be done on equipment that is to be removed from the cells. An area will be provided directly above the cells for equipment that has been removed from the cells for temporary storage. Access to the storage cell will be accomplished through a roof plug above the decontamination cell. As in the main cells, personnel entry will not be required to the storage cells.

It is anticipated that a large fraction of the maintenance of contaminated equipment will be done remotely in the maintenance cell. However, the remote maintenance cell will be shielded from the remainder of the cell bank, and maintenance may be done through glove ports when the level of activity is low enough. Directly behind the glove port area will be an exclusion area in which final decontamination and maintenance may be performed in frogman suits if necessary.

It is important that all openings into the cells be tightly sealed so that absolutely no leakage of air will be possible to the adjoining areas. To this end, all services will be brought into the cells at the back wall, and they will be brought through gasketed shield plugs. When required, a shield plug will be ejected into the cell by a new plug which will replace it. Each shield door will be sealed by a separate seal door. Windows and manipulators will be installed so that they can be replaced without entry into the cell and without the escape of air from the cell.

Every piece of equipment in these cells will be completely portable, even the cell air movement units. If repairs are necessary, each unit of equipment may be unplugged and removed from the cell and replaced by a new unit while the old one is being repaired in the maintenance cell. Since entry to these hot cells is through the sides rather than the top, there is no need for a high-bay crane area. This leaves a second-story area, above the cells and exclusion areas, which may be used for low-level work in shielded dry boxes. Entry to this low-level area will be through the same change room that services the first-floor exclusion areas.

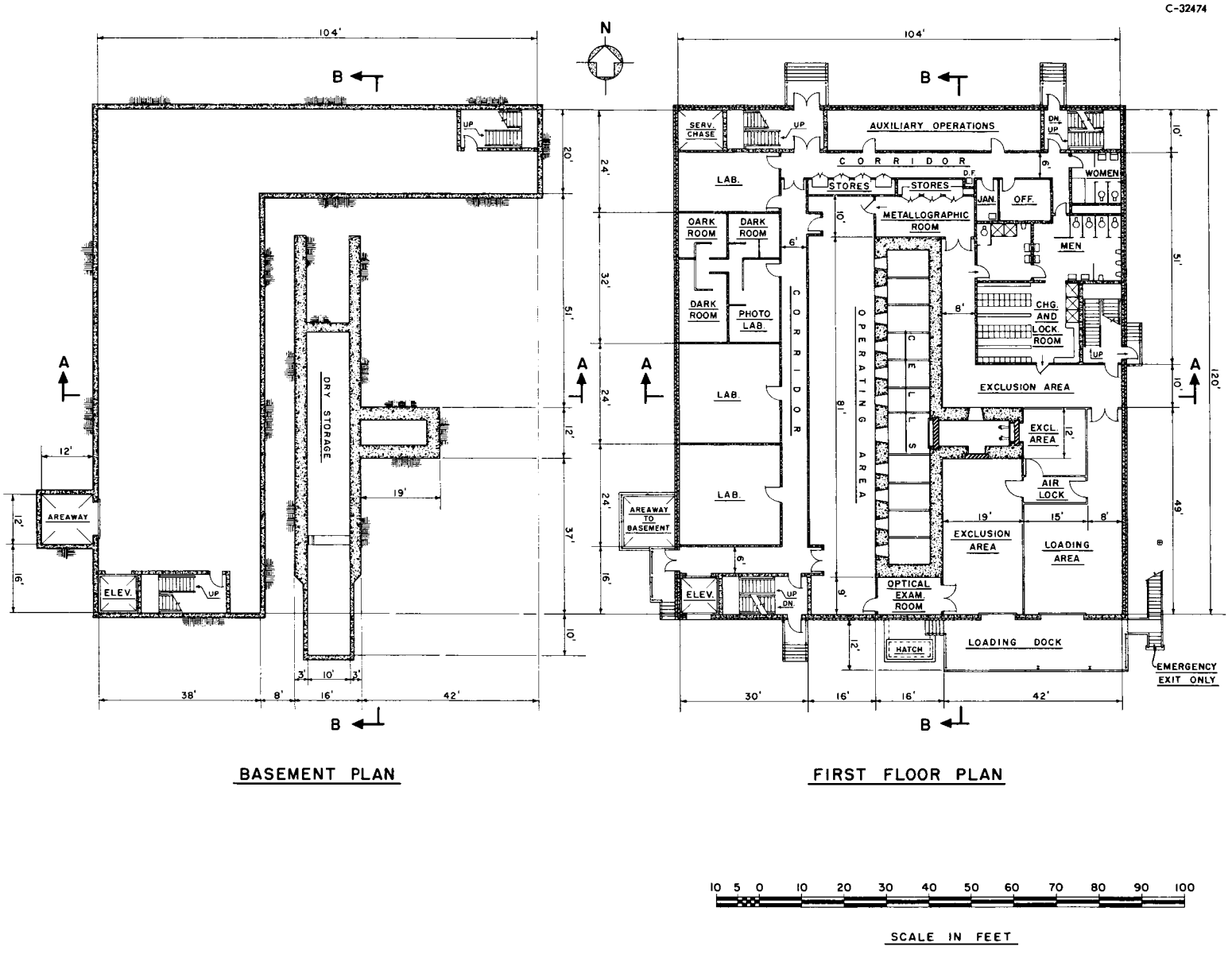

Fig. 154. Proposed High-Radiation-Level Examination Laboratory. Basement and first floor plans.

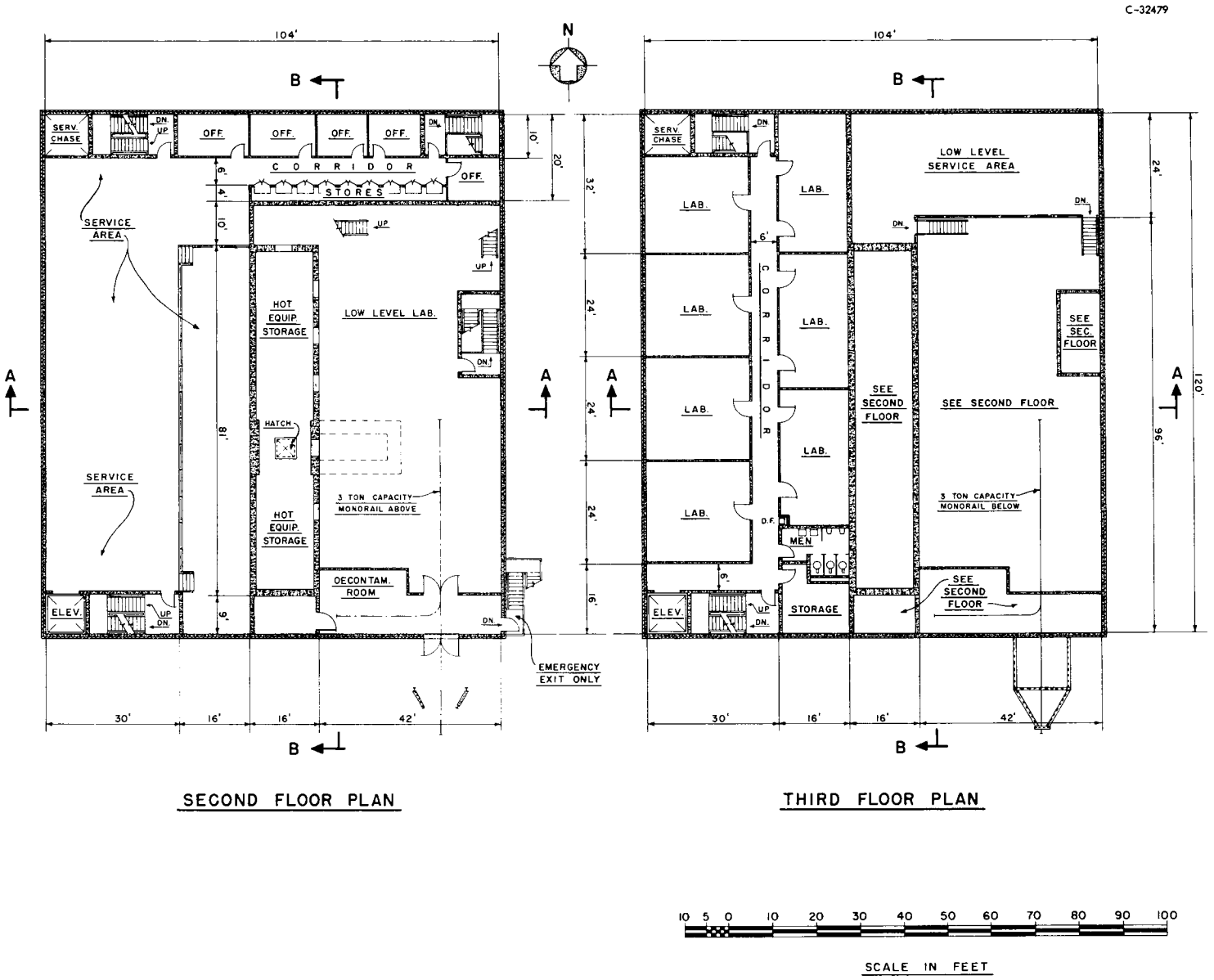

Fig. 155. Proposed High-Radiation-Level Examination Laboratory. Second and third floor plans.

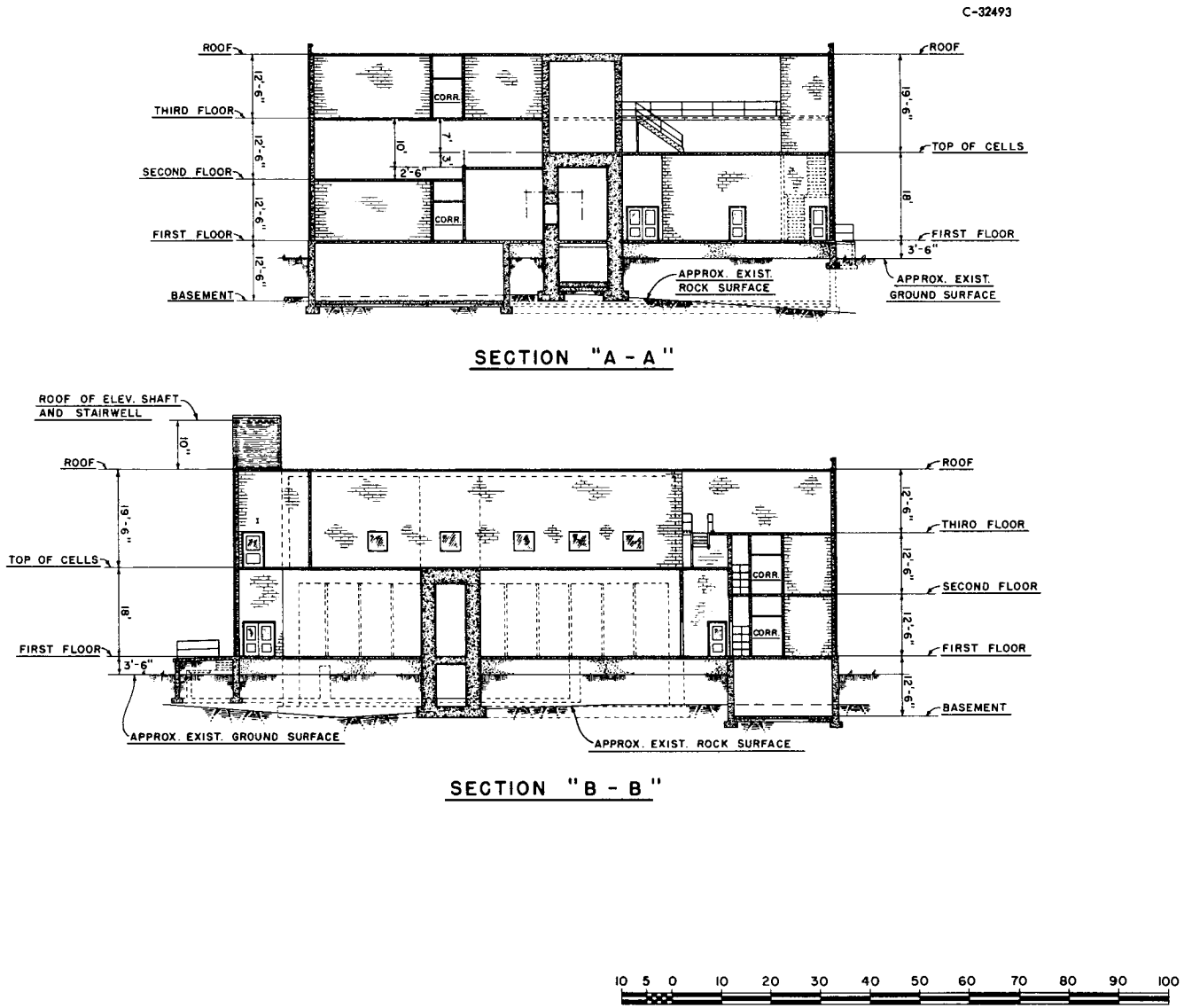

Fig. 156. Proposed High-Radiation-Level Examination Laboratory. Sections "A-A" and "B-B."

RECYCLING VISCOMETER

L. H. Jenkins C. C. Webster

Preliminary testing of the recycling viscometer (Fig. 157) has been completed. The tests were carried out with standard mixtures of water and glycerol of known viscosity. In order to make the solutions conducting, a small amount of KCl was added to each, but the effect on the viscosity of the solutions was negligible. Results obtained indicate that viscosities can be determined with an error no greater than ±1% in the range of 5 to 10 centipoises. No attempt was made to determine any values outside this range.

The following information about the instrument should be useful in future operations. All notations apply to instrument model Q-1852, serial 1.

Principles of Operation

Air (or helium) pressure is applied alternately to each leg of a U-tube (Fig. 158) which contains the fluid being tested and a magnetic ball. This alternating pressure causes the fluid and ball to flow in one direction for a time; then the flow is reversed. Flow reversal is controlled by two spark plugs with a 7-in. probe. The plugs are located at the top of each leg of the tube and are actuated when the fluid reaches a certain level. Both the fluid and magnetic ball are constantly flowing, but the direction of flow is periodically reversed. The test fluid must conduct electrically for the spark plugs to function.

Located on each leg of the U-tube is a 12-in.-long spacer. At each end of the spacers are coils of gold wire which serve as detectors for the magnetic ball. The information from the coils is fed to the bridge balancing circuit. From the bridge the information is relayed to a Berkeley Universal EPUT and timer which records the time of flight of the magnetic ball across the spacers on a Berkeley digital recorder. Two times are recorded for each cycle, the times required to traverse the spacer lengths on the down and up legs.

Operational Procedure

1. Place the magnetic ball and about 100 ml of fluid in the U-tube and replace all connections. The amount of fluid is critical, for if too much fluid is present the flow time in each direction will be too short for the ball to complete the full cycle. However, if it is desirable to use more than 150 ml of fluid, the spark plug tips could be shortened.

2. Connect the leads from the detector to the input side of the bridge balancing circuit. The top lead from each coil is connected to one of the four red terminals on the bridge breadboard connection. The four leads from the bottom of the coils are connected to the two black terminals on the board, two leads to each terminal.

3. Make the air supply connections and adjust the supply pressure to about 20 lb and the blanket pressure to 4 lb by means of the two valve controls located on the instrument panel.

4. Set the red indicator on flowmeter and chart to the desired flow rate. In the range of 5 to 10 centipoises settings between 35 and 80 are recommended.

5. Turn on the power switch of the viscometer, taking care that the unlabeled switch to the left of the power switch is in the down (off) position. The latter switch cuts out the solenoids and prevents fluid flow even though power and air pressure are being supplied to the controls.

6. Connect the output lead on the instrument panel to the input terminal of the Berkeley timer.

7. Balance the bridge circuit, using the coarse and fine adjustments, until the microammeter on the panel reads as near zero as possible. Balance is important in that the timing operation will be in error unless proper balance is obtained. When proper balance is obtained the null indicator on the panel will light up.

8. Start the fluid recycling by flipping the solenoid switch at the left of the power switch to the up (on) position. Ignore the first few cycles so that a steady state is obtained; then record the data for 15 to 20 cycles. Determine the average value for the down and up flight times.

9. Reset the flow controller and determine the average flight times at 5 to 10 different flow rates. If determinations are desired at flow rates greater than 80 on the scale, it is advisable to increase the blanket pressure to 5 lb.

10. If it is desirable to determine the time of the flow cycle, a combination cycle counter and timer is furnished. The outlet plugs for the timing

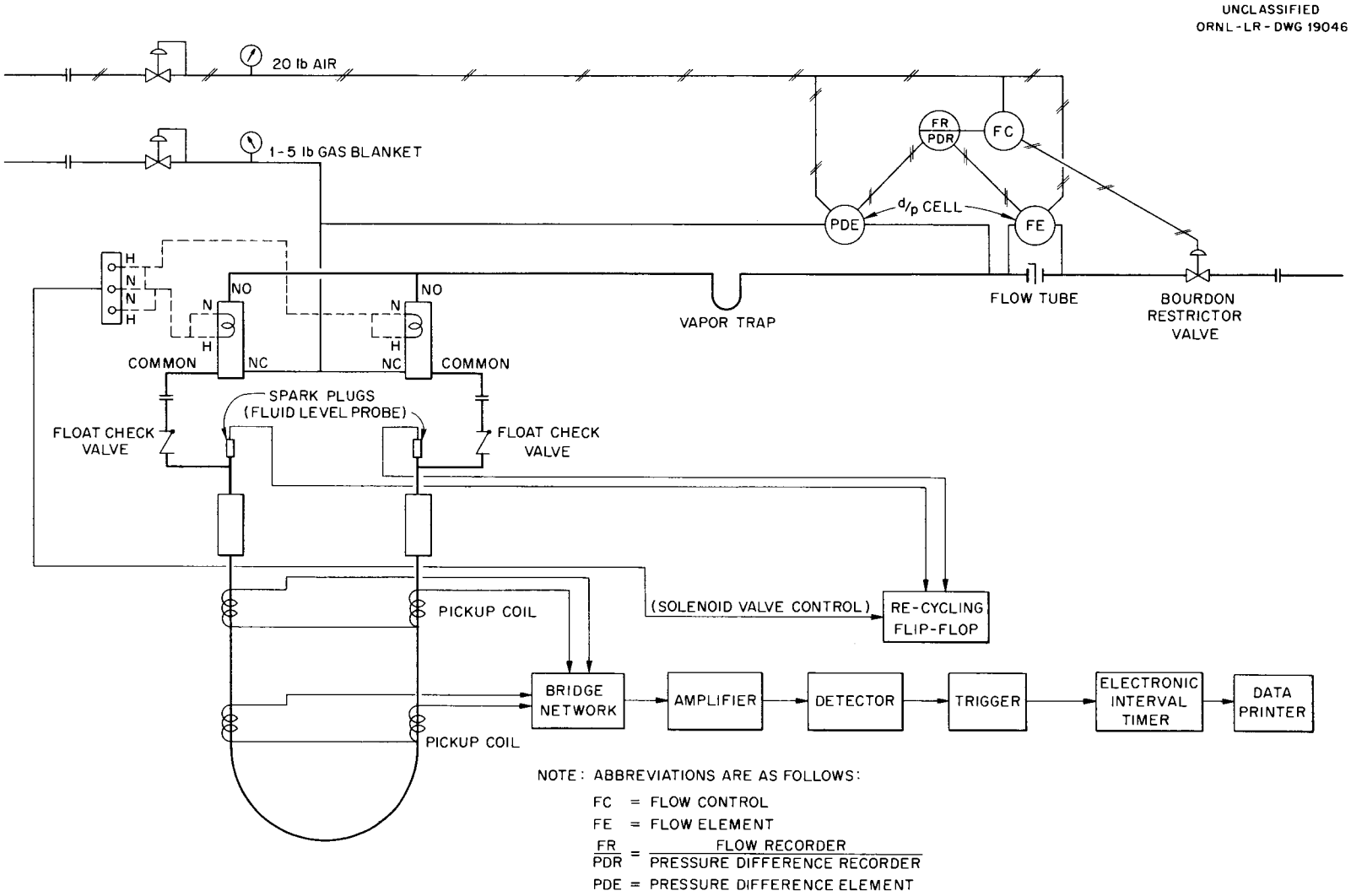

Fig. 157. Recycling Viscometer. Schematic diagram.

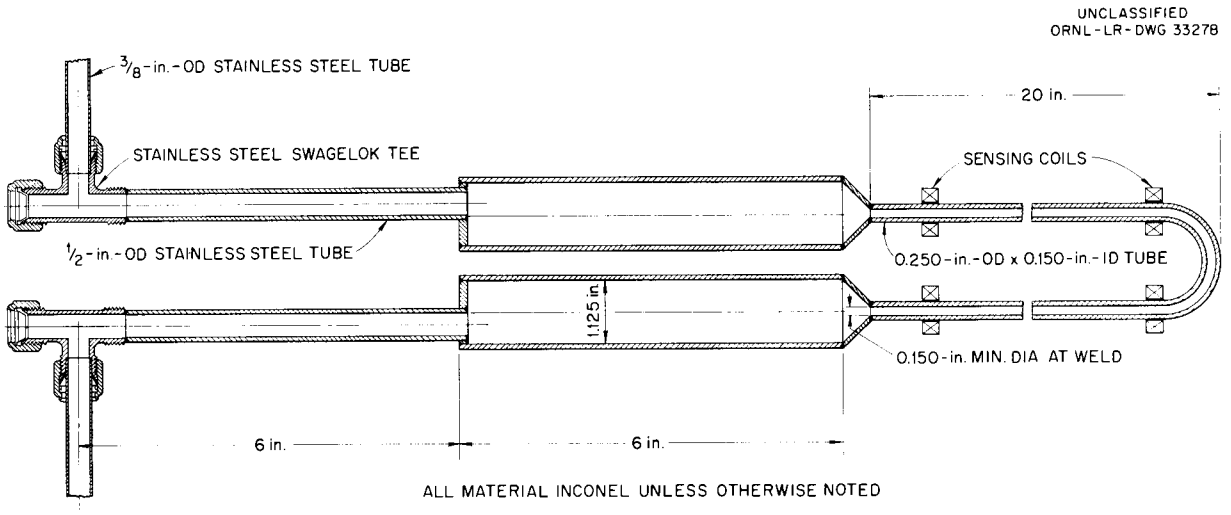

Fig. 158. Recycling Viscometer. Assembly.

device are located at the bottom of the instrument panel.

Treatment of Data

1. Determine the average value of the down (t_1) and up (t_2) flight times for several standard solutions of known viscosity at 5 to 10 different flow rates. Plot t_1 vs t_2 to obtain standard viscosity curves.
2. Determine t_1 and t_2 for the fluid under study at various flow rates and calculate the viscosity by interpolation with standard curves.

Uses and Limitations

1. The instrument is useful only as a secondary standard. The viscosity of an unknown can be determined only by comparison with that of a known standard.
2. Since wall effects are included in the measurements, no comparisons can be made between different U-tubes. Also, no comparison using a single U-tube is valid unless the horizontal and vertical alignment of the tube is exactly the same when data are gathered on fluids of known and/or unknown viscosity.
3. Since thermal expansion or contraction will change the distance between the detector coils, standard viscosities should be determined near the temperature at which the viscosity of the unknown will be studied. In some systems this would be a severe handicap if the viscosity of the fluid was reasonably temperature sensitive.
4. Since wall effects are not the same in each leg of the tubes, the effect of gravity cannot be canceled from the data by subtracting t_1 from t_2. Therefore no mathematical expression can be developed for the system.
5. Precision of the instrument is excellent. Individual values of t_1 and t_2 agree remarkably well with the average values. However, wide deviations are, of course, encountered if fluid flow is either very slow or very fast.

ELECTRODEPOSITION IN MOLTEN FLUORIDES

W. A. Brooksbank M. F. Osborne

The equipment for investigating electrodeposition in molten fluoride salts has been completed and satisfactorily meets the primary requirements for operation. The capacities for electrical heating and water cooling are ample, and the enclosed system assures maintenance of a relatively pure inert atmosphere.

The cylindrical enclosure (Fig. 159), 22½ in. in diameter by 42 in. long, is of welded stainless steel construction and is mounted vertically on

UNCLASSIFIED
ORNL-LR-DWG 33279

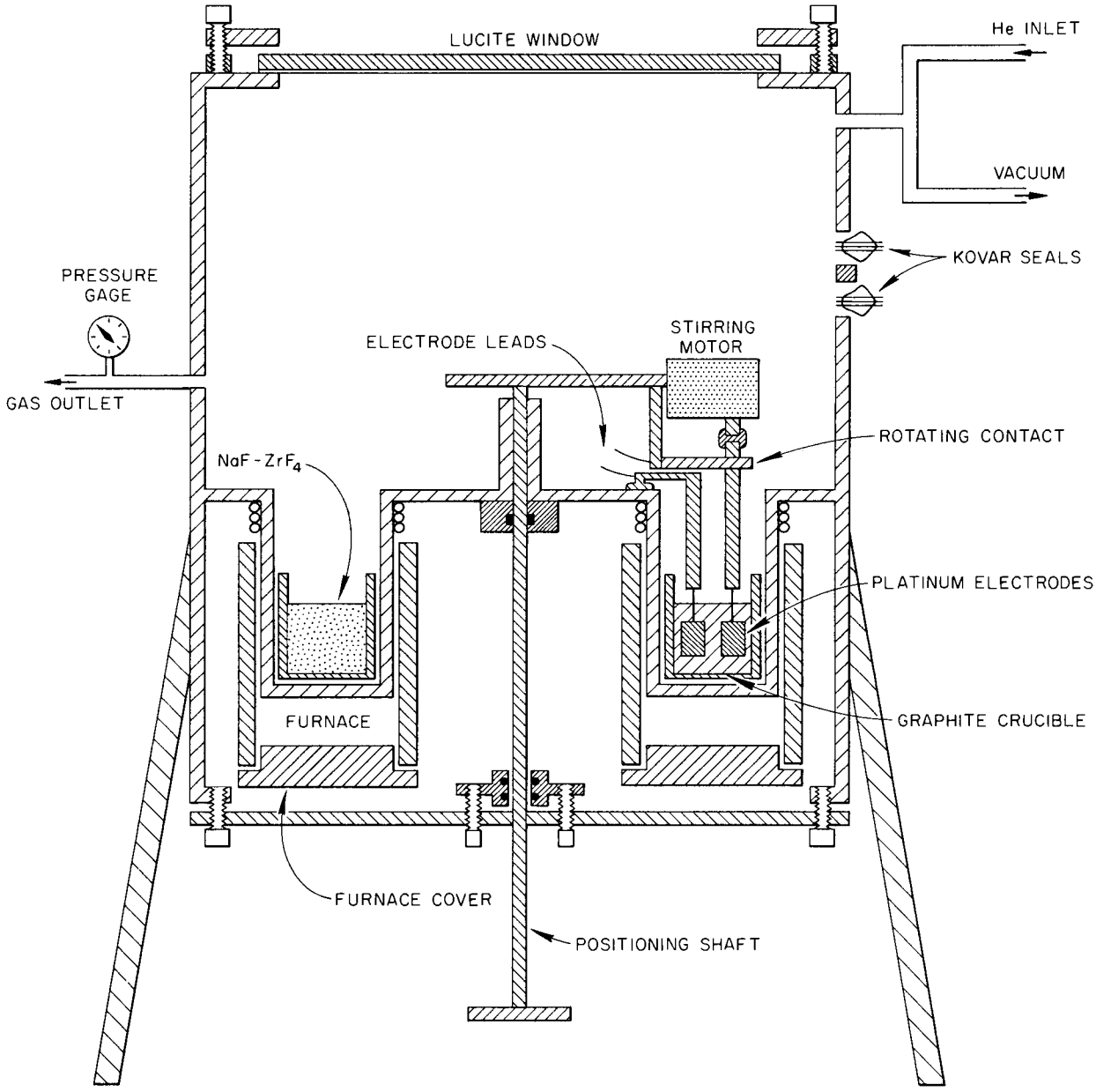

Fig. 159. Equipment for Study of Electrodeposition in Molten Fluorides.

four casters for mobility. At the top, 60 in. above the floor, a 14-in. Lucite window provides good visibility to the interior. Two crucible wells, $4\frac{1}{2}$ in. in inside diameter by 10 in. deep, accommodate the salt containers. Heavy-duty clamshell heaters are capable of heating these wells to a temperature of more than 800°C, and the surrounding cavity is packed with Rockbestos high-temperature insulation. A central shaft, capable of vertical and rotary motions, allows remote transfer of the stirrer and electrode between the two crucibles. Neoprene O-rings form the shaft seal, and a rubber gasket seals the Lucite window. Two large Kovar seals provide 16 electrical leads to the interior for electrodes, stirring motor, thermocouples, etc. Copper cooling coils are soldered to the shaft seal, to the flange supporting the window, and around the tops of the crucible wells for protection against excess heating of vulnerable components.

Graphite crucibles contain the electrolyte, which is a 50-50 mole % mixture of NaF and ZrF_4. These crucibles are isolated from ground by covered crucibles of fired Lavite. Platinum electrodes are mounted on long platinum tubes reinforced with $\frac{15}{64}$-in. steel drill rods. The rotating member serves as both a stirrer and a cathode, being turned by a small electric motor mounted on the central shaft crosspiece and driven by an external Variac. The cathode is insulated from the motor by a Teflon sleeve, and brushes of brass foil serve as the rotating contact. An Ag-AgCl reference electrode is suspended in the salt through a hole in the Lavite lid, which is aligned to receive the cathode through another hole. The stationary anode is mounted on a block of lead sitting on the floor of the vessel.

Such conventional gas purification equipment as a vacuum pump, an Arthur D. Little cold trap, and the necessary pressure gages is utilized for filling the vessel with purified helium.

Thermocouples are installed in the walls of the graphite crucibles for temperature indication and control. An instrument rack houses dual Wheelco temperature controllers and 20-amp Variacs which function quite well. Due to the poor thermal coupling between furnace and crucible there is extensive temperature lag and overshoot in the initial heating, but control is good after stabilization of temperature.

The source of power for electrodeposition is a regulated d-c power supply built by New Jersey Electric Corporation, with another choke coil and capacitor added to further reduce ripple. Ammeters with ranges of 0 to 100 ma, 0 to 1 amp, and 0 to 10 amp are connected in parallel for accurate current measurement. A high-resistance potentiometer, preferably of the continuously recording type, with a range of 0 to 1.5 or 0 to 20 v is needed. A converted Brown recorder should afford sufficient accuracy for these voltage measurements.

Although somewhat awkward physically, this equipment should prove adequate for a study of the electrical properties of molten fluorides or for other experiments requiring elevated temperatures and inert atmospheres.

FUSED SALT POLAROGRAPHY

R. J. Carter

The fused salt polarography program has been terminated, at least temporarily. At present, with very little further development work, the polarographic method could probably be used for qualitative and quantitative analysis of fused nitrate solutions containing not more than four or five reducible cations. However, adaptation of the method to analysis of fused fluoride solutions introduces several serious problems not encountered with fused nitrates. To solve these problems, although not impossible, would be so time-consuming that it is impractical to attempt to solve them at present. The following is a summary of the work that has been done, the difficulties that have been encountered, and recommendations for the course of future work should the program be reactivated at some later date.

Instrumentation

The polarograph was obtained from Y-12, where it had been built for a research project on the determination of corrosion products (iron, chromium, nickel) in fused fluorides. The instrument is similar to those used in aqueous polarography with

the exception that the high-resistance current-measuring circuit, common to aqueous instruments, has been replaced with a circuit of much lower resistance. Originally, a conventional single-variable recorder was used to plot the current passing through the polarographic cell, the assumption being made that the potential applied to the cell was a linear function of time. However, because of the relatively high conductivity of fused salts, it is virtually impossible, without using complicated circuitry, to vary the applied potential linearly with time. For this reason, the original recorder was replaced with a Moseley model 2 X-Y recorder. The single disadvantage in using this type of recorder, the performance of which is otherwise quite satisfactory, is its relatively low impedance when used for measuring potentials smaller than approximately 100 mv. Because of the low impedance, the recorder draws a small amount of current and records the sum of the current through the polarographic cell and the current which it draws itself. This difficulty can be overcome by adding to the circuit a compensating device which will produce a current equal in magnitude but opposite in direction to the current drawn by the recorder, thus canceling this current out of the polarographic current-voltage curve.

A 10-ohm, 10-turn Helipot, presently being used as a voltage divider to vary the potential applied to the polarographic cell, is unsatisfactory since its resistance, and therefore the applied potential, changes in small steps rather than in a continuous manner. This causes a broadening of the current-voltage curve along the voltage axis; for this reason, the Helipot should be replaced with a smooth 10-ohm, 10-turn slide-wire or similar voltage dividing device.

Tentative plans had been made for doing derivative polarography with fused salts by using a curve-following attachment in conjunction with the X-Y recorder. With such an arrangement, a current-voltage curve, traced over with specially prepared electrically conducting ink, could be scanned at a uniform rate along the X (voltage) axis, generating an output voltage proportional to the value of Y (current) on the current-voltage curve. This voltage would then serve as the input to a differentiating circuit, and the output, a voltage proportional to the first derivative of the current-voltage curve, would be plotted by a second recorder. Since the maximum on a plot of derivative vs voltage corresponds to the half-wave potential of the original current-voltage curve, a means of rapidly identifying the ion or ions involved is thus provided.

Microelectrodes

The microelectrodes used in the investigation of corrosion products in fused fluorides consisted of a Morganite (high-purity aluminum oxide) tube of fine bore, into which was fused a silver wire, forming a small silver bead at one end of the tube. This microelectrode was mounted concentrically in a nickel tube approximately $\frac{3}{8}$-in. in inside diameter, the end of the microelectrode being set even with the end of the tube. The unit was immersed in the fused fluoride, and helium was passed through the nickel tube at the rate of approximately one bubble per second. As each helium bubble formed and expanded, the microelectrode was momentarily out of contact with the fused salt and a current of zero was recorded. When the bubble became large enough to break away from the nickel tube and rise, the microelectrode came in contact with the fused salt. At the instant of contact, the microelectrode was completely unpolarized and the current flowing through the polarographic cell had its maximum value for the cycle; the current then rapidly decreased with a $1/\sqrt{t}$ dependence on time until a new helium bubble broke the contact and the current returned to zero. The actual peak current at the instant of contact could not be determined because of lag in the response of the recorder. It was decided that current-voltage curves obtained with this type of electrode were not true polarographic curves, since polarization of the microelectrode was always incomplete and a steady-state diffusion current was never actually attained. The use of helium bubbling was therefore discontinued, and stationary microelectrodes in continuous contact with the fused salts were used.

Both platinum and silver microelectrodes were investigated. They were made by the usual method of inserting a wire of the desired metal into a Morganite tube, melting the wire, and letting it solidify to a small bead in one end of the tube.

Approximately 15 to 20 of these electrodes, both silver and platinum, were tested in fused fluoride solvent (Flinak) containing traces of reducible cations, such as Ni^{++} (as NiF_2), at temperatures between 550 and 650°C. In only one or two instances was it possible to obtain current-voltage curves with characteristic shapes which were reproducible to a reasonable degree.

VOLATILITY PROCESS STUDIES

W. A. Brooksbank, Jr. R. J. Carter M. F. Osborne

In order to determine the behavior of fission products under conditions which occur in the Volatility Process, three experiments were carried out. The first was essentially a small-scale duplication of the actual processing of irradiated fuel. The second was a determination of the behavior of a short-lived fission product, Mo^{99}, during hydrofluorination, and the third was a study of the behavior of MoF_6 on a sodium fluoride adsorption column.

Activity data in these experiments were obtained by means of a gamma scintillation spectrometer, the crystal and photomultiplier tube of which were completely enclosed in a cylindrical lead shield mounted on a traversing mechanism. A $\frac{1}{8} \times \frac{1}{8}$ in. collimating slit in the shield immediately in front of the crystal made it possible to scan the different sections of the equipment and to follow the movement of volatile fission product activity.

In the first experiment, a small amount of six-month-cooled fluoride fuel from an in-pile loop, a piece of U-Zr alloy, and 100 g of 50-50 mole % $NaF-ZrF_4$ as solvent were placed in an Inconel hydrofluorination vessel and heated to approximately 650°C. The following operations were then carried out:

1. a 10-hr sparge with helium,
2. a 10-hr sparge with HF at 50 cc/min,
3. a 10-hr sparge with HF at 110 cc/min,
4. transfer of the melt to a fluorination vessel and fluorination of the melt, together with adsorption of volatilized material on a sodium fluoride column for 1 hr followed by a 4-hr desorption period.

Separate traps for HF, F_2, UF_6, and fission products were provided to prevent any of these substances from leaving the system. During the first three operations the spectrometer was positioned at the gas exit line of the hydrofluorination vessel. During the fluorination and absorption-desorption step it was placed at the exit line of the fluorination vessel.

At the conclusion of these operations, radiochemical analyses were made on the feed, waste salt, top and bottom of the sodium fluoride columns, the waste traps, and on the acid washes from the fission product trap and UF_6 trap. A porous nickel filter, present in the system to trap particulate matter, was examined with the gamma spectrometer and, when sufficient activity was present, by radioautography. Deposits on the filter were analyzed spectrographically. Uranium in the UF_6 traps, in the waste salt, and in the sodium fluoride columns was determined by fluorimetric methods.

For the activity measurements on the exit gas streams, the spectrometer was adjusted to count all gammas having energies greater than 50 kev. The activity level during the helium sweep remained constant, except for a burst of activity at about 3.6 hr after startup. This burst was so rapid that it could only have come from a particle of active material being swept by the gas stream. The activity was not identified. After a 4-hr induction period during the HF sweep the activity gradually increased from 46,000 to 54,000 counts/min. There was a 2-hr induction period during fluorination, after which the activity in the exit line from the fluorinator rapidly increased from 8000 to 39,000 counts/min. The activity buildup showed no leveling off, but continued to grow until the conclusion of the experiment. The radioactivity in the gas stream at the end of the fluorination was identified with the gamma spectrometer as Nb^{95}.

The filter was removed at the conclusion of each gas sweep and examined by mounting it on the

crystal of a 2 × 2 in. NaI(Tl) scintillation spectrometer in a low-background area. The following results were obtained:

Helium sweep	Zr^{95}-Nb^{95}, Ru^{103}, La^{140}, and probably Te^{129}
HF sweep	Very low activity; possibly U^{235}; data uncertain
Second HF sweep	Very low activity; possibly U^{235}; data uncertain
Fluorine sweep	Activity at least 100 times greater than helium sweep; spectrometrically pure Nb^{95}

A yellow deposit collected on the filter during the fluorination was shown by spectrochemical analysis to be mainly chromium and nickel. A radioautograph localized the Nb^{95} activity to the area of the deposit.

Radiochemical analysis failed to detect activity in the cold traps, the NaF columns, or the waste traps. The percentages of the fission products remaining in the waste salt in the reaction vessel were: Zr^{95}, 72%; Nb^{95}, 32%; total rare earths, 82%; Sr, 90%; and Cs^{137}, 100%.

As an indication of the tracer level involved, typical fission product activities in the feed were: Cs^{137}, 0.031 mc; Zr^{95}, 2.54 mc; and Nb^{95}, 2.79 mc. The uranium content was 230 mg.

The object of the second experiment was to study the behavior of molybdenum during hydrofluorination and subsequent fluorination. For this experiment, a gray wedge analyzer was added to the gamma spectrometer, permitting the recording, on photographic film, of a complete gamma spectrum in 15 sec. The spectrometer was adjusted to count all gammas with energies greater than 50 kev and was positioned at the gas outlet line of the reaction vessel.

A 10-mg molybdenum foil was irradiated at a high flux in the LITR for 60 hr to produce Mo^{99} tracer. The foil was then placed in the reaction vessel with a charge of NaF-ZrF_4 at 650°C and HF flow was started and continued for 24 hr at a flow rate of 10.6 g/hr. At the end of hydrofluorination, fluorine was passed through the melt for 7 hr, at which time a cold trap became plugged and the experiment was terminated. A plot of activity vs time is shown in Fig. 160. Gray wedge spectra taken on the peak at 13 hr were inconclusive since the actual activity increase was

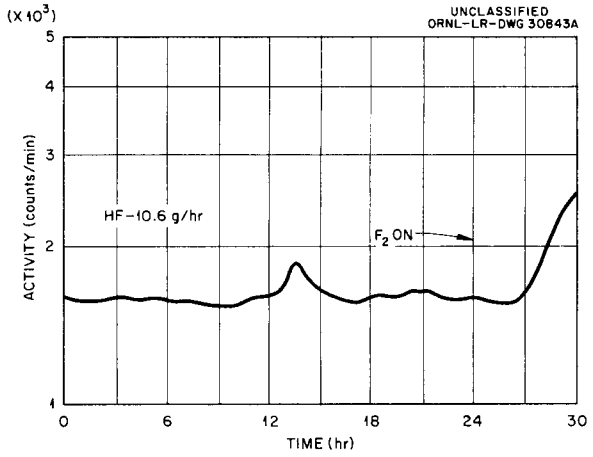

Fig. 160. Volatility of Mo^{99} from Fused Salt.

only one-fifth of background. Indications were that it was probably W^{187} which was induced in the molybdenum metal by neutron bombardment of W^{186}, present as an impurity in the molybdenum foil.

In the final experiment, a study of the behavior of MoF_6 on a sodium fluoride column, two different methods were used for preparing the compound,

$$Mo + 3F_2 \longrightarrow MoF_6$$

and

$$2MoF_5 + F_2 \longrightarrow 2MoF_6$$

For preparation by the first method, 10 mg of irradiated molybdenum powder was placed in a platinum-lined reaction vessel, at the downstream end of which was a trap cooled with dry ice. Fluorine, flowing at 5.4 g/hr, was passed over the molybdenum at room temperature for 80 min, but no volatilization of the molybdenum activity occurred during this time. The temperature of the molybdenum was then increased slowly, and at approximately 300 to 400°C the molybdenum activity was almost completely transferred from the reaction vessel to the cold trap. The trap was warmed to room temperature and fluorine was passed through for 5 hr, but no transport of activity was detected by the spectrometer and the run was discontinued. It was concluded that some compound less volatile than MoF_6 had been produced in this run.

To ensure high-yield production of MoF_6, 250 mg of pure MoF_5 was irradiated in the water-cooled facility of the Graphite Reactor and was then

transferred, in a helium atmosphere, to the reaction vessel. Downstream from this vessel were placed a sodium fluoride column, a dry ice cold trap, and a waste trap. The gamma spectrometer was positioned to monitor the line leading from the sodium fluoride column to the dry ice trap. A fluorine flow of 6.7 g/hr was maintained for 6 hr, during which time approximately 90% of the Mo^{99} activity was transferred from the reaction vessel to the sodium fluoride column, which was operating at 100°C.

Desorption of the $Mo^{99}F_6$ was started by increasing the column temperature to 400°C while the fluorine flow was maintained for an additional 5 hr. Activity in the line leading from the sodium fluoride column to the cold trap is plotted vs time in Fig. 161.

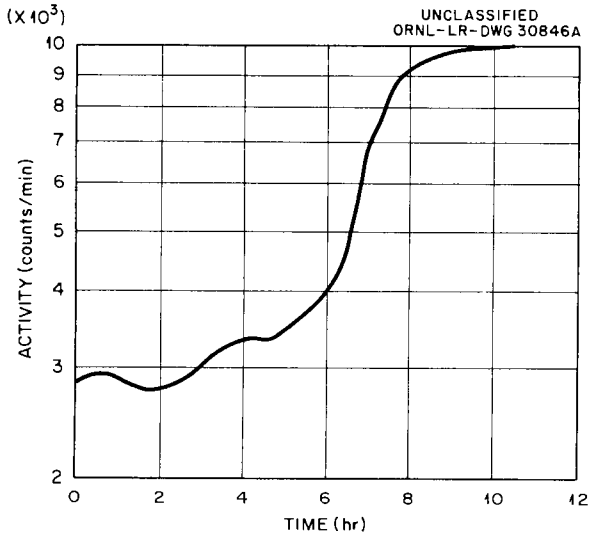

Fig. 161. Absorption and Desorption of $Mo^{99}F_6$ on Sodium Fluoride Column.

Radiochemical Mo^{99} analyses were obtained on the reaction vessel, the NaF trap after desorption, the cold trap after adsorption at 100°C, the cold trap after desorption at 400°C, the Teflon gasket at the top of the waste trap, and the upper half of the soda lime from the waste trap; the results are given in Table 14.

The following conclusions are based on the radiochemical analyses:

1. Most of the MoF_5 was converted to MoF_6, which volatilized into the NaF column (90%).
2. Molybdenum hexafluoride and technetium fluoride are strongly adsorbed on NaF at 100°C. There is less than 0.3% which is not adsorbed.
3. The technetium is more strongly held than the molybdenum on the NaF.
4. Molybdenum hexafluoride may not be completely trapped by a dry ice trap because of its vapor pressure of approximately 0.3 mm at −80°C.

The behavior of the volatile fission product fluorides investigated may be summarized as follows:

1. Ruthenium and niobium fluorides are volatile from fused salts during fluorination.
2. Molybdenum and technetium are not volatile during the hydrofluorination step in fused salt at 630°C.
3. Molybdenum hexafluoride is easily adsorbed from NaF, while technetium is not. The MoF_6 is not completely trapped with dry ice and trichloroethylene.
4. Molybdenum and technetium fluorides are volatile in excess fluorine at less than 100°C but are adsorbed strongly on NaF.

Future investigations should include studies of the volatile oxyfluorides of molybdenum.

Table 14. Distribution of Tracer Molybdenum

Location	Gross Gamma Activity		Molybdenum Activity	
	Counts per Minute	Per Cent of Total	Counts per Minute	Per Cent of Total Molybdenum
Reaction vessel	9.9×10^5	8.8	6.2×10^5	8.9
NaF column	2.7×10^6	23.9	5×10^5	7.2
Cold trap after adsorption	2.2×10^4	0.2	2.2×10^4	0.3
Cold trap after desorption	4.5×10^6	39.8	3.0×10^6	43.2
Waste trap gasket	2.0×10^6	17.7	1.8×10^6	26.0
Waste trap	1.1×10^6	9.7	1.0×10^6	14.4

EFFECT OF RADIATION ON CORROSION OF STRUCTURAL MATERIALS BY MOLTEN FLUORIDES[1]

G. W. Keilholtz J. G. Morgan W. E. Browning, Jr.

The use of molten fluorides as reactor fuels requires that they be stable, both thermally and in intense radiation fields. The fission process in the salt causes regions of high ionization density to exist, as well as very high heat fluxes. However, since molten salts are generally ionic liquids, there is no crystalline lattice to disrupt, nor are there covalent bonds to sever. Thus fast neutrons, fission fragments, and gamma radiation cannot cause severe damage of the type found in crystalline materials. However, the interface between the molten salt and its container offers a site where radiation effects might make themselves evident in an acceleration of the corrosion process. With this possibility, it has been necessary to test the compatibility of various salts with structural metals in the highest neutron fluxes available.

The effects of irradiation on the corrosion of metal containers exposed to various fluoride fuel mixtures have been investigated by irradiation of capsules filled with static fuel and by operating in-pile forced-circulation loops in the LITR and in the MTR. Capsule tests have been made with nickel, types 316 and 347 stainless steel, and Inconel. The in-pile loop tests are with Inconel components. The salts have included various compositions of NaF-KF-UF_4, NaF-BeF_2-UF_4, NaF-ZrF_4-UF_4, NaF-ZrF_4-UF_3, and KOH.

The principal variables studied in the static corrosion program have been flux, fission power, time, and temperature. In a fixed neutron flux, the fission power is varied by adjusting the U^{235} content of the fuel mixture. Thermal neutron fluxes have ranged from 10^{11} to 10^{14} neutrons·cm^{-2}·sec^{-1}, and fission power densities from 80 to 8000 w/cm^3. Capsules have generally been irradiated for 300 hr at 1500°F (815°C), although in recent tests the experiments have been extended to 600 to 800 hr. The techniques used for examining capsules after irradiation include pressure tests (in-pile), melting point determinations, petrographic analyses, chemical analyses, mass spectroscopic studies, gamma-ray spectroscopic studies, and metallographic examination of containers.

In the many capsule tests and in the three in-pile loop tests made to date, no major changes have occurred in the fuel mixtures that can be attributed to irradiation, other than normal burnup of uranium. Metallurgical examinations of the Inconel capsules and tubing have likewise shown no changes in corrosion that can be the result of radiation damage. The low corrosion results obtained for the in-pile loops have been confirmed by chemical analyses for corrosion products in the fuel mixtures.

[1] G. W. Keilholtz, *Effect of Radiation on Corrosion of Structural Materials by Molten Fluorides*, ORNL CF-58-2-4 (Feb. 2, 1958); presented at the 1958 Annual Meeting of the American Nuclear Society, Los Angeles, June 2–5; approved for publication in *Nuclear Sci. and Eng.*

EFFECT OF RADIATION ON STATIC CORROSION OF STRUCTURAL MATERIALS BY FUSED SALT FUELS

W. E. Browning, Jr. H. L. Hemphill

The study of the effect of radiation on the corrosion of structural materials by fused salt fuels has been continued. Irradiation in the MTR of two Hastelloy B capsules was completed with NaF-KF-LiF-UF_4 fuel at 1500°F. Metallographic examination showed them to have thin films on the surfaces that were exposed to the fuel. Composition of the film could not be determined. Corrosion of these capsules was negligible.

One more Hastelloy B capsule containing NaF-KF-LiF-UF_4 fuel was irradiated at 1250°F for 2496 hr and at an initial power density of 6000 w/cm^3. There was no indication of failure when the capsule was withdrawn. This capsule will be examined metallographically to identify the film and to determine the extent of corrosion.

Two capsules were irradiated in the MTR to determine the stability of graphite in contact with

fuel No. 130 (LiF, 62 mole %; BeF_2, 37 mole %; UF_4, 1 mole %) during exposure to radiation. If this combination of materials proves satisfactory, the graphite moderator of a reactor could be cooled by the fluoride fuel, thus simplifying the heat recovery system of the reactor and resulting in greater power economy. These capsules are shown in Fig. 162. Existing Inconel capsules were used for the outer container. Graphite liners having a wall thickness of 0.025 in. were prepared with a 0.100-in.-dia bore and 1-in. length. These graphite liners had loose plugs at the top end and

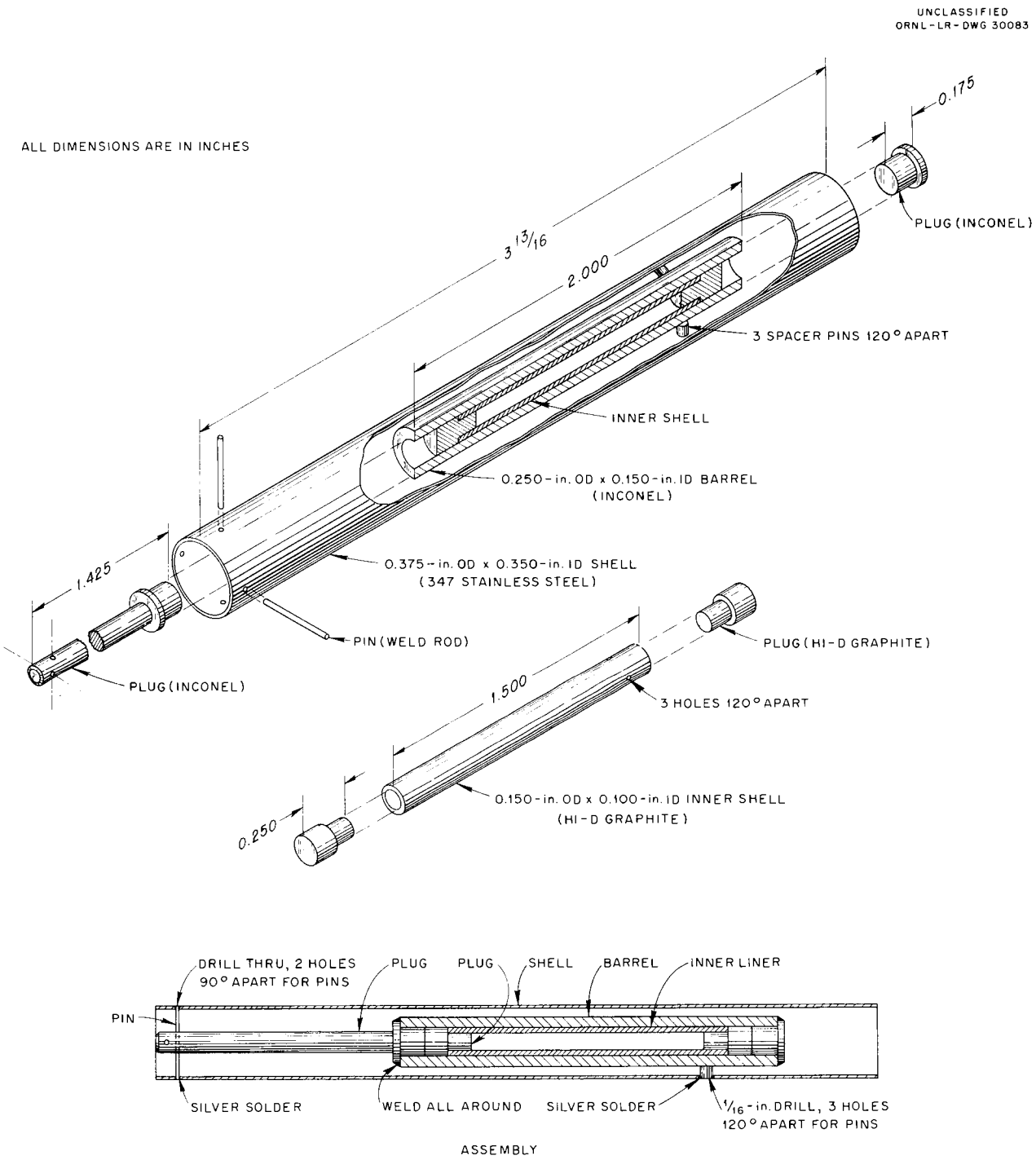

Fig. 162. Capsule for Irradiation of Fused Fluorides in Contact with Graphite and Inconel.

three small holes near the bottom which allow the fuel to fill the space in the graphite liner and the Inconel outer can. The purpose of this was two-fold. First, the fuel provides heat transfer between the graphite and the Inconel wall and permits more accurate estimation of the graphite temperatures based on measurement of the temperature of the wall. Second, it is of interest to observe the stability of a system comprised of fuel, graphite, and Inconel. These capsules were irradiated for 2000 hr at a graphite wall temperature of 1250°F.

The graphite temperatures are somewhat uncertain but were estimated by calculation using the thermal conductivity of graphite and the heat generation by fission in the fuel. The capsules will be examined in the Solid State Division hot cells to determine whether the graphite has disintegrated. If the graphite is still intact, measurements will be attempted to determine the distribution of fuel components and fission products in the graphite. The graphite and the Inconel will be examined metallographically for evidence of corrosion, and the fuel will be chemically analyzed.

Preparations for irradiation of fuel No. 130 in INOR-8 capsules in the MTR were continued. The fuel used in this test will be the same as that used in the in-pile convection loop. The INOR-8 tubing intended for these capsules had to be rejected because of high aluminum content. Another batch of INOR-8 tubing of satisfactory composition contained a large number of flaws. Short sections of this batch of tubing were selected for use in MTR capsules. INOR-8 tubing for MTR capsules is more difficult to fabricate than that used in the convection loop because of the small diameter and large wall thickness (0.200 in. OD and 0.100 in. ID). These capsules were prepared for irradiation and are awaiting insertion at the MTR. They are shown in Fig. 163.

Fig. 163. INOR-8 Capsule for Corrosion Studies in the MTR.

MOLTEN SALT REACTOR PROGRAM IN-PILE CONVECTION LOOP

W. E. Browning, Jr. W. H. Montgomery H. E. Robertson

An in-pile thermal-convection loop fabricated of INOR-8 alloy is being prepared for operation in the LITR with a lithium-beryllium-uranium fluoride fuel mixture. The purpose of the experiment is to demonstrate the reliability of this combination of materials and to determine the effects of radiation on corrosion of the container material by fluoride fuel in the Molten Salt Reactor design temperature range. The fuel container will be examined metallographically for evidence of corrosion after irradiation, and an analysis will be made of the corrosion products in the fuel. The design of the loop is based on calculations by F. E. Romie.[1] Design features and operating conditions for the loop are described below:

Fuel composition	BeF_2-LiF-UF_4 (37-62-1 mole %) with Li^7 and U^{235}
Container material (wt %)	INOR-8 (Ni, 71; Mo, 17; Cr, 7; Fe, 4.5; Co, 0.6)
Power density (w/cm^3)	50 or higher as necessary to achieve desired temperature differential
Maximum temperature (°F)	1250
Axial temperature differential (°F)	150
Desired duration of in-pile operation (hr)	Up to 10,000

The loop will be air-cooled and will have external electrical resistance heaters. The mechanical details are similar to those of the miniature vertical dynamic corrosion loop recently operated in the LITR. This loop design can be converted to a forced-circulation loop with a minimum of modification after suitable pump bearings have been developed.

The parts which will be assembled to form the loop are shown in Fig. 164. It may be noted that the loop consists essentially of two parallel tubes with connecting bends at the top and bottom. The loop will be cooled by air passing through an air annulus which will, in general, follow the loop all the way around.

The fuel tube is 35 in. long and $\frac{3}{8}$ in. in outside diameter and will contain 45 cm^3 of fuel. The total power will be approximately 2 kw.

A full-scale mockup of the in-pile loop has been prepared, with electrical resistance heating of the fuel tube used to simulate fission heating. The purpose of this out-of-pile test is to demonstrate the workability of the design and to provide operational information that will aid in an evaluation of hazards in the reactor. The parts shown in Fig. 164 were fabricated for the bench test and have been assembled. Figures 165 and 166 show the loop mockup at two stages of assembly. This mockup is now in operation at design temperature and at approximately half the design power. Tests are being conducted to optimize the air flow arrangement to obtain the desired axial temperature differential.

Mechanical mockup tests were performed on a series of designs for the thermocouple leads in the cooling-air annulus of the loop. It was desired to select a design which would prevent plastic deformation of the thermocouple lead wire. The mechanical mockup test was performed in an apparatus similar to a portion of the fuel tube and cooling-air-annulus tube, with the outer parts made of transparent plastic to permit observation of the thermocouple during movement of the fuel tube. The various designs of thermocouple lead wires were tested in this apparatus with longitudinal movement of the fuel tube as large as $\frac{1}{2}$ in. Radial movement of the fuel tube is prevented in the design of the convection loop by radial spacing pins. The thermocouple design selected uses a thin-walled stainless steel tube which fits closely around the ceramic insulator tube. The stainless steel tube is split open at the end and resistance spot-welded to the fuel tube near the point where the thermocouple bead is joined to the fuel tube. The stainless steel thermocouple jacket is nearly parallel to the fuel tube and is brought out along a straight line at a small angle from the fuel tube. As the fuel tube moves longitudinally during thermal

[1] F. E. Romie, *MSR Prog. Rep. Sept. 1, 1957*, ORNL-2378, p 7 (classified).

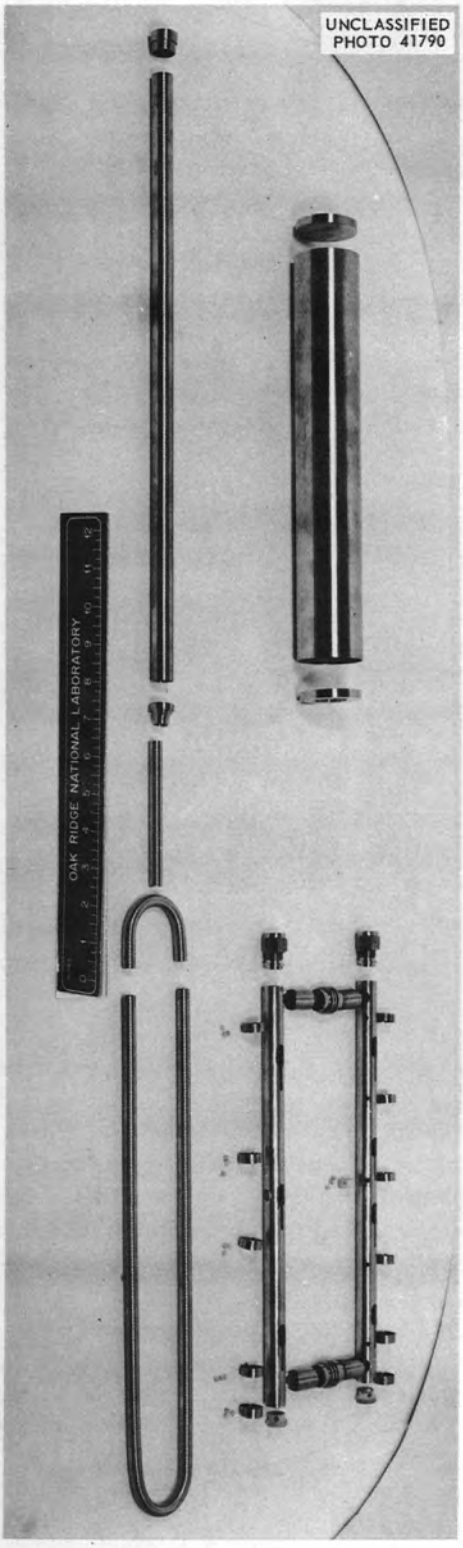

Fig. 164. Parts for INOR-8 Thermal-Convection Loop To Be Operated in the LITR.

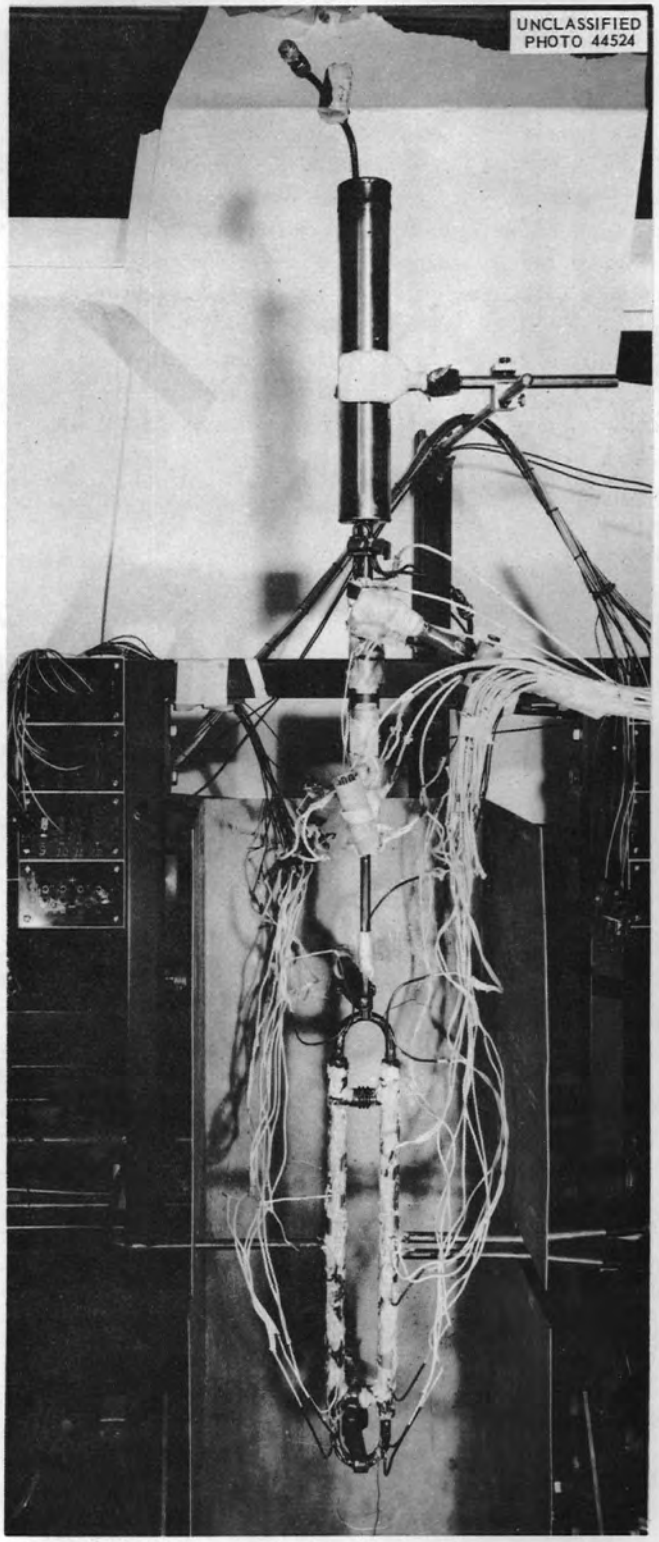

Fig. 165. MSR Convection Loop Mockup with Thermocouples Installed Through Walls of Air Channel.

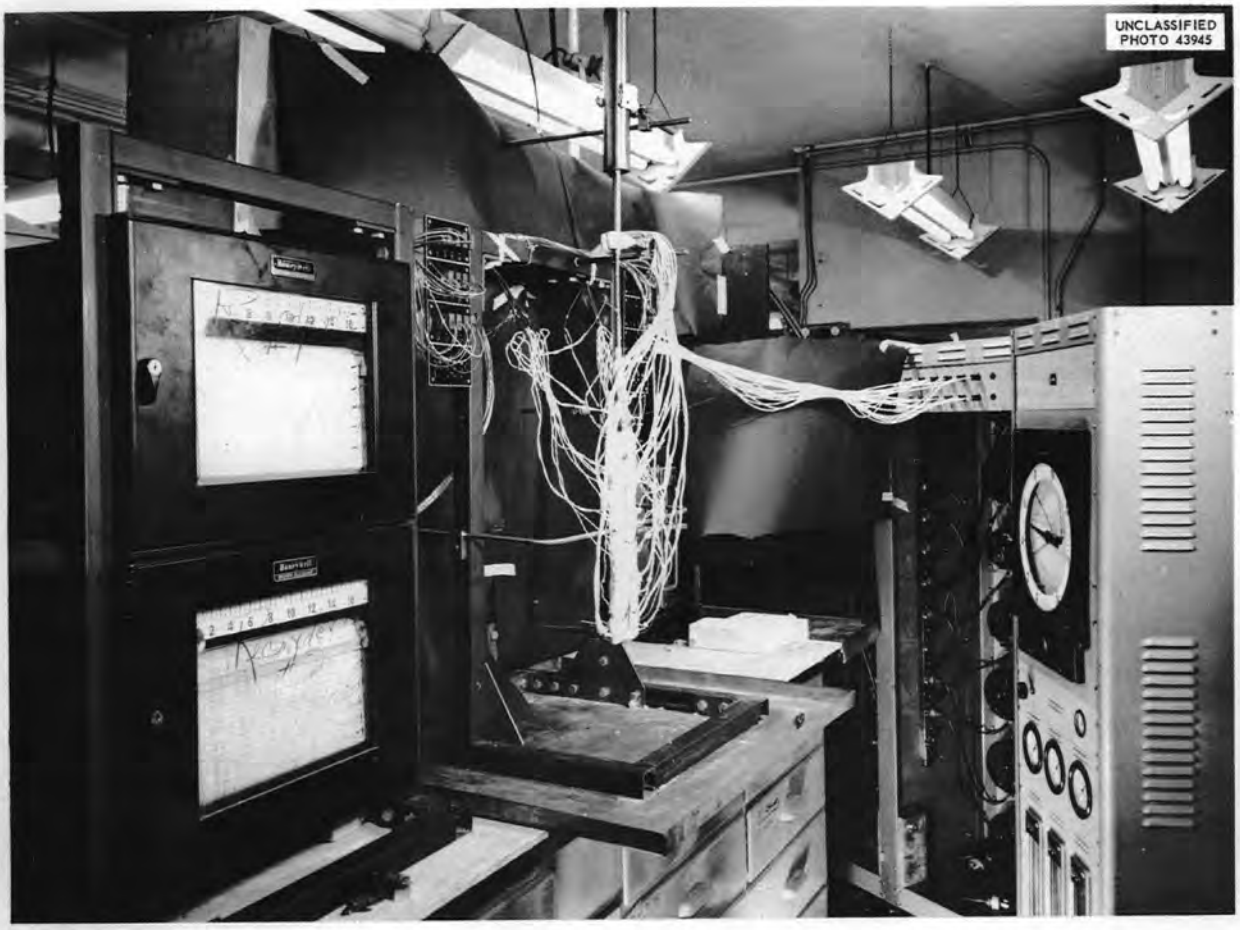

Fig. 166. MSR Convection Loop Mockup with External Resistance Heaters Installed.

expansion, the thermocouple jacket can move longitudinally along its own axis through the port in the air annulus and through the heater assembly. During thermal expansion the thermocouple jacket can move slightly with respect to the bundle of lead wires. This arrangement provides a relatively rigid structural member which does not move with respect to the thermocouple wire or thermocouple bead, thus preventing the application of stresses to the thermocouple. Thermocouples of this design survive dozens of cycles corresponding to thermal expansion many times greater than that expected in the loop.

A charcoal trap is provided in the design of the loop to remove xenon which diffuses from the surface of the fuel. Any organic material and water occurring in the charcoal as an impurity would be decomposed by radiation from adsorbed fission products, and the decomposition products could contaminate the fuel and interfere with interpretation of the results of the experiment. The charcoal used in the loop will be vacuum-baked for 48 hr at 500°C to decompose organic impurities. The charcoal which was installed in the mockup loop was subjected to this same treatment. The holdup time of the charcoal for radiokrypton in a flowing helium stream was measured to determine whether the heat treatment had reduced the capacity of the charcoal for noble gases. The charcoal was 10% more effective as an absorber for krypton after the heat treatment than it had been before. This effect was no doubt due to dehydration of the charcoal.

Calculations have been made for the equilibrium distribution of fission gases in the system. It is estimated that 9×10^{-4} mole of stable xenon and 1.5×10^{-4} mole of stable krypton will accumulate during 10,000 hr of operation at 2 kw. This amount

of xenon and krypton will be absorbed in the 500-g charcoal trap to such a degree that the remaining partial pressure of xenon will be 600 μ Hg and that of krypton will be 150 μ Hg. These equilibrium partial pressures are sufficiently low for the adsorption efficiency of the charcoal to be unimpaired. The combined decay-heat generation of all the daughters of fission gases having half lives greater than 10 sec is only 6 w, according to the calculations. Cooling of the charcoal trap will not be a difficult problem.

Calculations were made to determine the magnitude of undesirable effects of the isotope Li^6 in fuel for the in-pile loop. The following undesirable effects were considered:

1. flux depression by absorption of thermal neutrons by Li^6,
2. biological hazard in the event of an accidental release of tritium produced by the (n,α) reaction in Li^6,
3. generation of internal gas pressure by nuclear reaction products from Li^6,
4. possible chemical effects of the tritium equivalent of HF with consequent interference with the interpretation of the results of the experiment.

All the effects were of marginal importance except the last one. The possible effect of traces of tritium in the loop cannot be evaluated with sufficient confidence to risk operating the in-pile loop under such conditions. It was decided, therefore, to procure the highest available grade of Li^7 for use in the in-pile test. Fifty grams of lithium containing 99.8% Li^7 was obtained and has been incorporated into a batch of fuel composition No. 130 which has been ground to a powder in the dry box for filling the in-pile loop. Sufficient fuel was prepared for three loops.

Parts for the in-pile convection loop have been fabricated and will be assembled after the mockup test has been run.

Preparations have been continued in the ORR building for the future molten-salt pumped loop. The loop housing assembly and lead tube have been subjected to tests in the reactor to determine whether they are damaged by flow of reactor coolant water. Flux profile measurements were made at reduced reactor power levels with a poison load simulating that of the in-pile loop, including the molten salt.

Several different plans are being considered for the development of bearings which will withstand the radiation conditions surrounding the pump of an in-pile loop. An ordinary carbon steel ball-bearing assembly is being modified to use a silver separator. A similar arrangement has been found satisfactory by some manufacturers in the absence of lubrication. Another ball-bearing assembly being prepared will use specially prepared titanium carbide balls. Both these bearing systems will be tested in the absence of radiation without lubrication.

Another plan is being considered which shows promise of solving the bearing problem. This plan at the same time would solve the problem of removing xenon from the atmosphere above the fluoride fuel without contaminating the fuel with impurities in the sweep gas and without contaminating the environment with fission products from the loop. This plan involves recirculating helium from above the liquid fuel through a charcoal holdup trap which adsorbs most of the xenon and delays the return of short-lived fission gases until they have decayed to such a low level that they will not damage the lubricant in the bearings. The helium, after passing through the charcoal trap, passes down over the pump and through an impeller. Then the purified gas passes over the bearing and through an orifice to prevent diffusion of fission gases, after which it returns to the chamber containing the liquid fuel. Experimental tests and calculations are being planned to evaluate the probability of success of this arrangement.

The motor of the pump used in in-pile loops is being slightly redesigned to increase the available torque and to eliminate a universal joint which is judged to be a possible source of trouble in future loops.

FUSED SALT FORCED-CIRCULATION LITR LOOP

W. E. Browning, Jr. R. P. Shields J. E. Lee, Jr.

The Inconel forced-circulation loop[1] which circulated a molten salt in a vertical hole in the LITR for 235 hr at a maximum temperature of 1600°F and a temperature differential of 235 to 250°F was examined for corrosion, and the fuel mixture was analyzed for fission products. The corrosion was the same as that which would have been expected under the same conditions in the absence of radiation.

A section of Inconel tubing including fuel (NaF-ZrF_4-UF_4, 60.8-27.4-11.8 mole %) was cut from each region of the loop that contained a thermocouple. Several sections were examined metallographically, and a maximum depth of penetration of 4 mils was found. The 4 mils of penetration was in a section of the hot leg of the loop approximately 12 in. from the hairpin nose portion of the loop. Etched and unetched pieces of metal from the hot leg of the loop are shown in Fig. 167, and a section of tubing from the cold leg of the loop is shown in Fig. 168. The penetration found in a section of the hairpin of the loop is shown in Fig. 169.

A new fuel salt sampling method in which the salt is melted out of the tubing was developed. An induction furnace (Fig. 170) was set up for melting out salt samples from the Inconel fuel-tube specimens. The melt-out chamber is glass, and it can be evacuated and filled with helium to prevent contamination of the new salt by the atmosphere. When the Inconel tube walls are heated quickly, the salt slides out as a solid pellet. Tests were conducted to determine whether the salt and the metallography specimens were affected by this method of sample preparation. In order to compare the old and the new techniques of sampling, one sample of salt was drilled from the tube and a second sample was obtained by suspending the tube in an atmosphere of helium and heating it by induction until the salt dropped out as a pellet.

The results of radiochemical analysis of the salts obtained by the two methods are given below:

Constituents Analyzed For	Amount Found (mc/mg)	
	In Drilled Sample	In Melted Sample
Zr^{95}	6.7×10^{-2}	6.7×10^{-2}
Cs^{137}	1.40×10^{-4}	1.41×10^{-4}
Ce^{144}	6.85×10^{-3}	7.65×10^{-3}
Sr^{89}	1.84×10^{-2}	1.92×10^{-2}
Sr^{90}	5.45×10^{-4}	5.68×10^{-4}

The data show that the two sampling techniques are equivalent as far as radiochemical results are concerned. Analyses of the fuel samples for Fe, Cr, and Ni are under way.

In order to test the effect of the melt-out technique on metallographic samples, specimens from which the fuel was drilled and from which the salt was melted were submitted for examination. A metallographic sample cut from a piece of tubing from which the fuel was melted is shown in Fig. 171. The temperature was deliberately allowed to go to 200°F higher than necessary during melting of the fuel, and the specimen was held at this temperature for 1 min. Normally the salt drops out within 15 sec after the induction heater is turned on. The longer heating period was used to exaggerate any effect of the melting-out procedure. It is apparent in Fig. 171 that no significant amount of corrosion occurred during the melting-out operation.

[1] W. E. Browning *et al.*, *Solid State Ann. Prog. Rep. Aug. 31, 1957*, ORNL-2414, p 13 (classified).

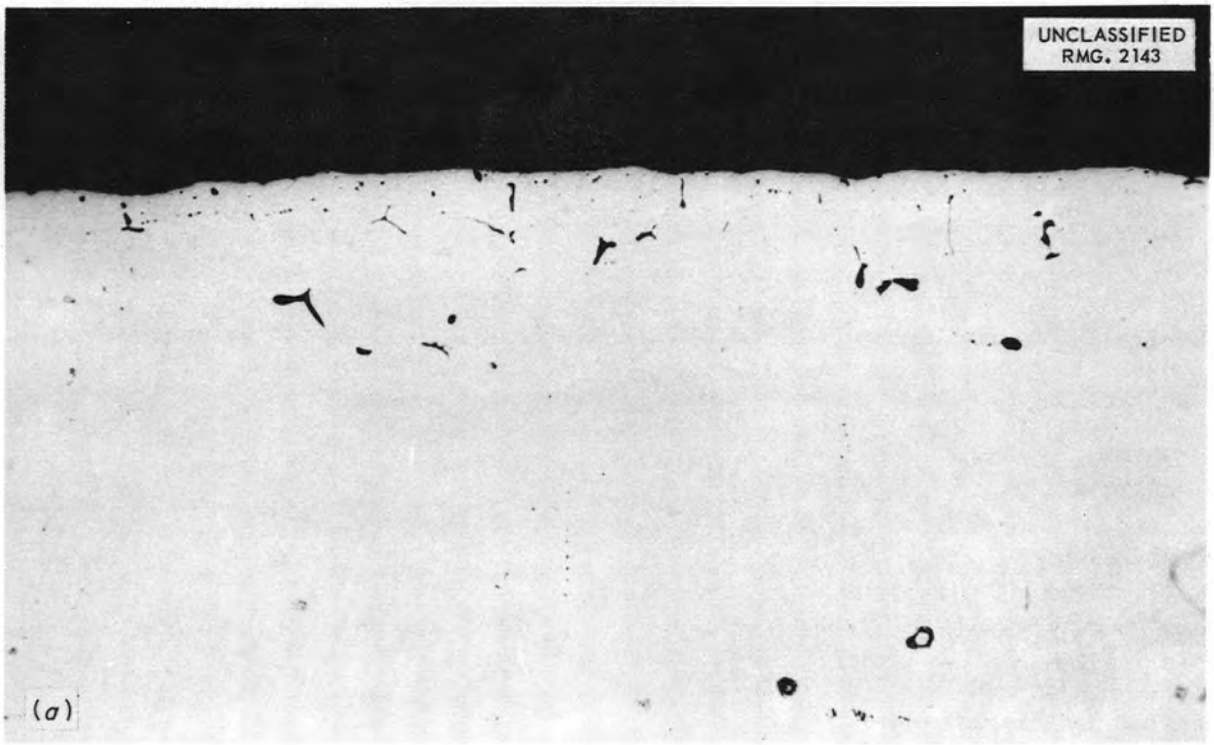

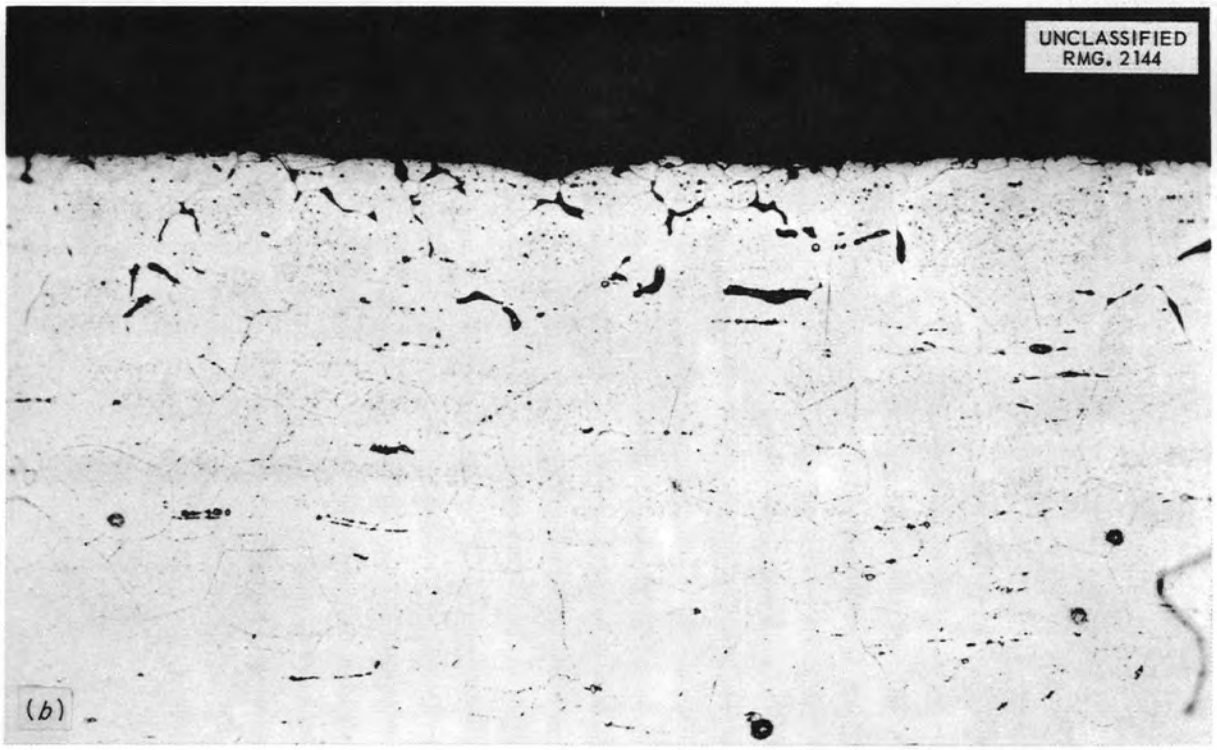

Fig. 167. Sections of Inconel Tubing from Hot Leg (1490°F During Operation) of LITR Vertical In-Pile Loop. (*a*) Unetched; (*b*) etched. 250X.

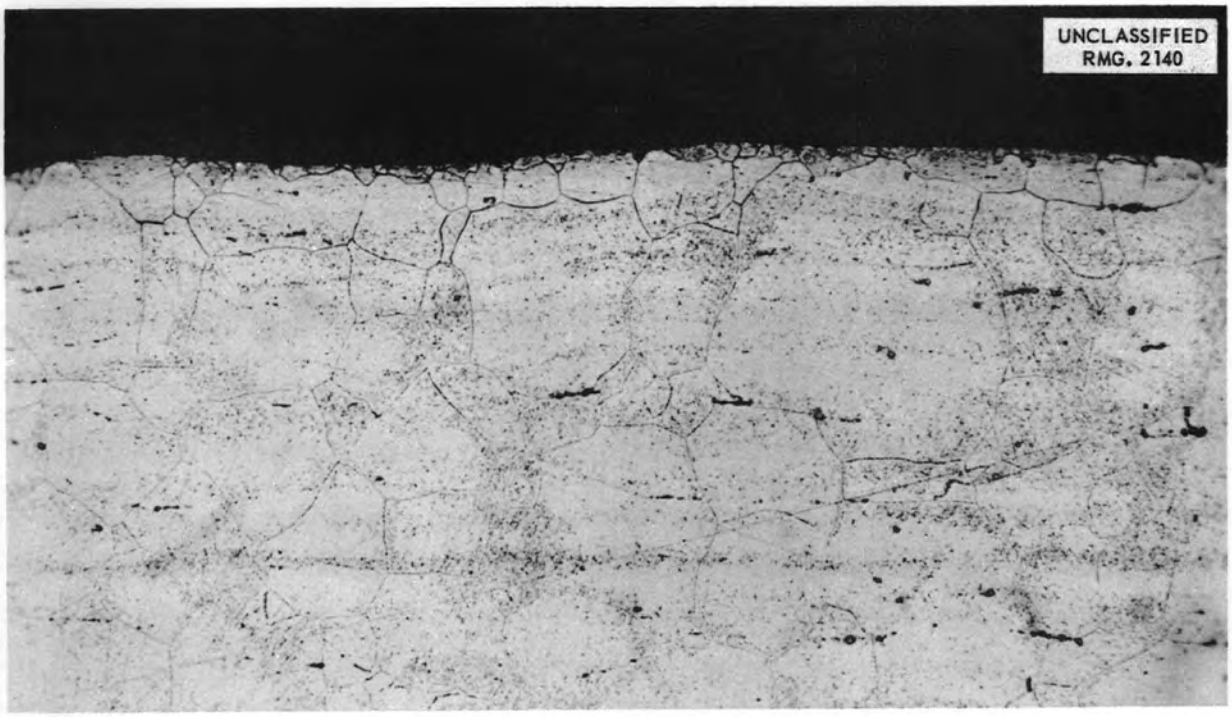

Fig. 168. Section of Inconel Tubing from Cold Leg (1290°F During Operation) of LITR Vertical In-Pile Loop. Etched. 250X.

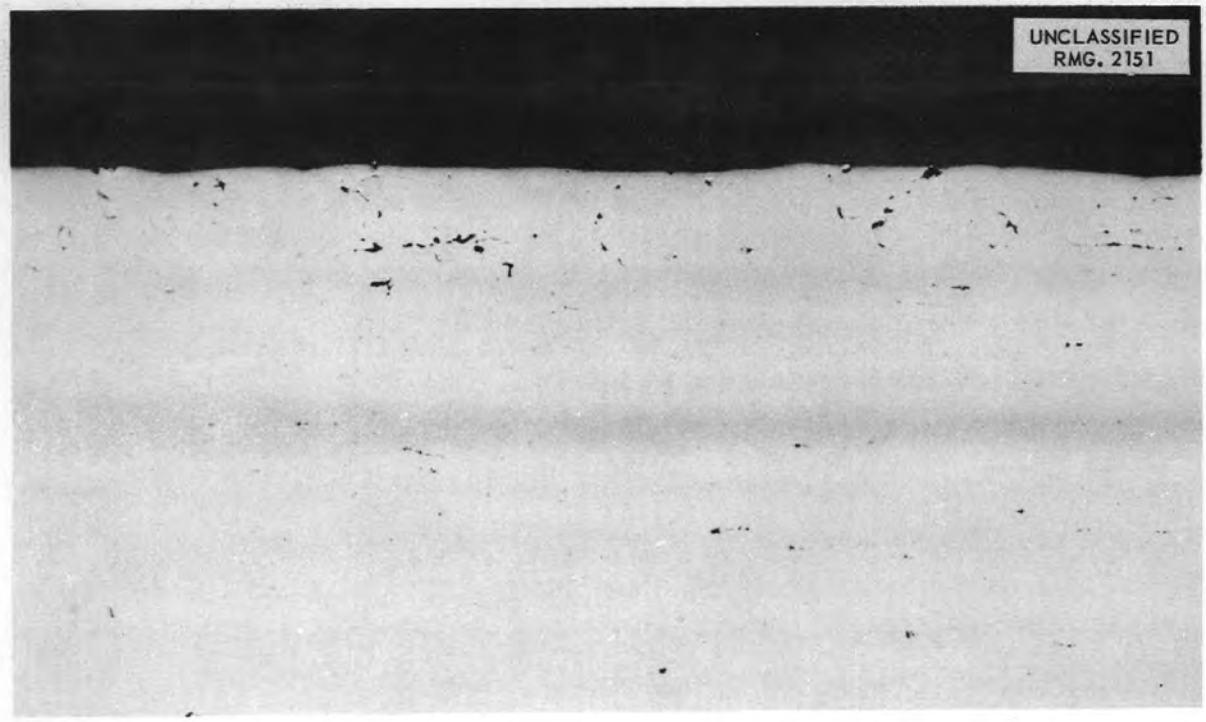

Fig. 169. Section of Inconel Tubing from Hairpin Nose Loop (1510°F During Operation) of LITR Vertical In-Pile Loop. Unetched. 250X.

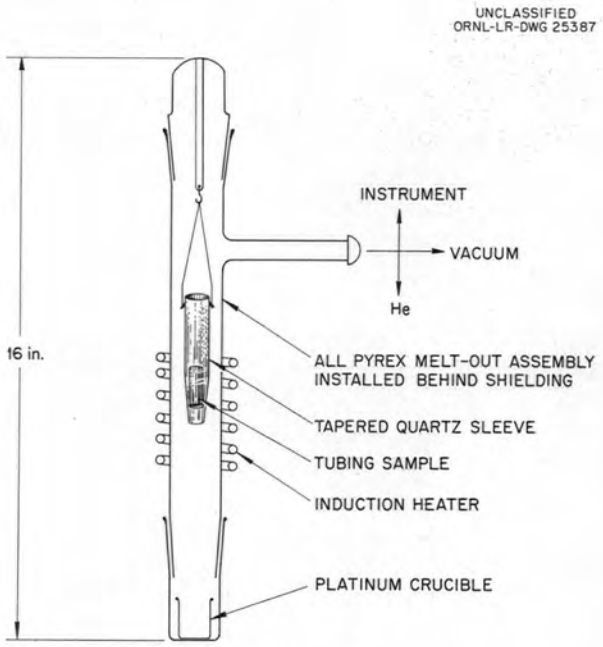

Fig. 170. Induction Furnace for Removing Fluoride Fuel from Inconel Tubing.

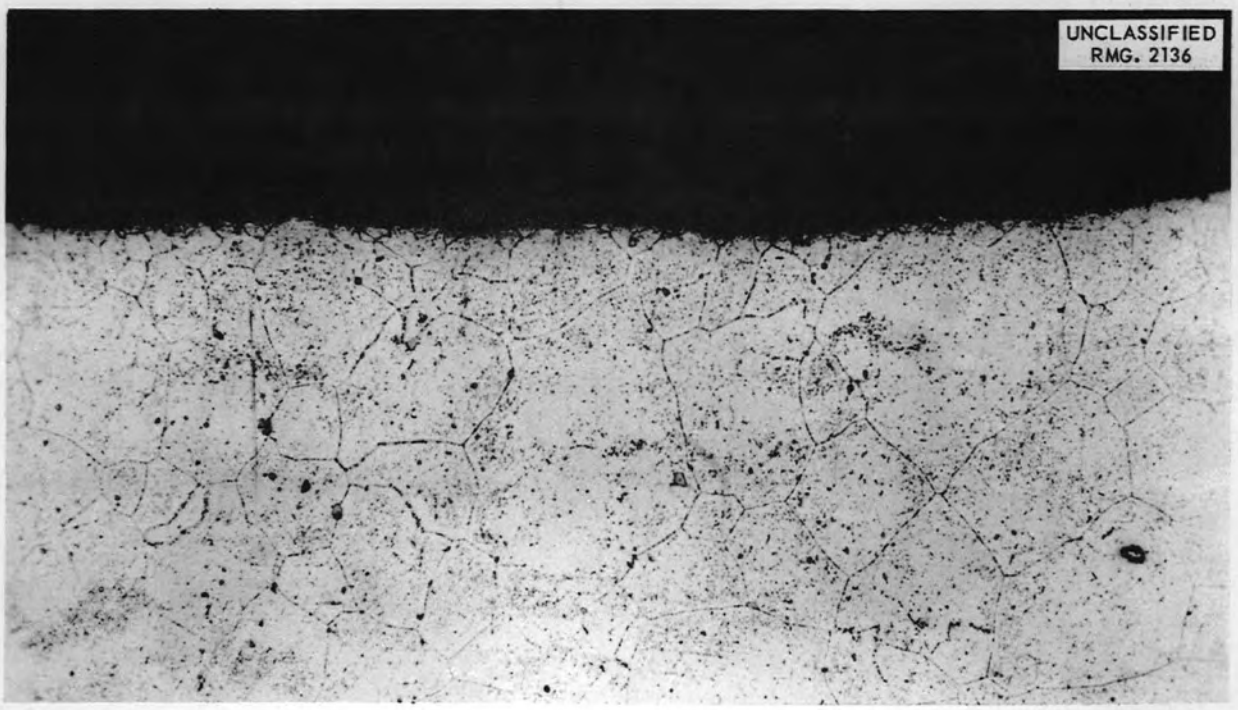

Fig. 171. Section of Inconel Tubing Held at 1390°F for 1 min During Melting-Out of Fuel Sample. 250X.

GASEOUS FISSION PRODUCT DISPOSAL

W. E. Browning, Jr. R. E. Adams R. D. Ackley

A problem which is often encountered in reactor operation and in experiments involving fission is the disposal of gaseous fission products. The latter, which include various isotopes of krypton, xenon, and iodine, may be present in such concentrations that venting them directly to the atmosphere would produce a biological hazard. While this problem is of a general nature, the most immediate interest in fission gas disposal at ORNL is in connection with the Homogeneous Reactor Test. In the HRT, iodine is removed chemically and the fission gases krypton and xenon in an oxygen purge stream from the reactor are passed through charcoal adsorbers. As a result of adsorption-desorption processes, the krypton and xenon molecules are delayed in their passage through the charcoal so that short-lived isotopes will decay and their concentration in the oxygen stream will thereby be greatly reduced. Gases leaving the adsorbers are then released into the atmosphere through a stack. Accordingly, the purpose of this program is to investigate methods of disposal of fission gases, with particular attention being given to the HRT adsorber system. As of the present time, virtually all the effort expended has been concerned with the holdup of fission gases by adsorbents, but other methods of disposal have been and will continue to be considered.

Previous to this period, experimental studies[1-3] indicated that (1) the efficiency of charcoal for holding up fission gases decreases with increasing temperature, (2) moisture on the charcoal surface has a deleterious effect on its adsorptive capacity, (3) the presence of gross voids and channels in a charcoal bed significantly reduces its holdup performance, and (4) holdup times with helium purge gas are higher than when nitrogen is used. All these observations are in accordance with expectations. In addition to the experimental measurements, a mathematical treatment of the gas holdup process, where an adsorber is regarded as being composed of a number of theoretical chambers, was postulated.[1]

In much of this work a gas-solid chromatographic technique, with Kr^{85} as a tracer, is used.[1] A block diagram of a typical setup is shown in Fig. 172, and a photograph of equipment employed in a current experiment is shown in Fig. 173. This

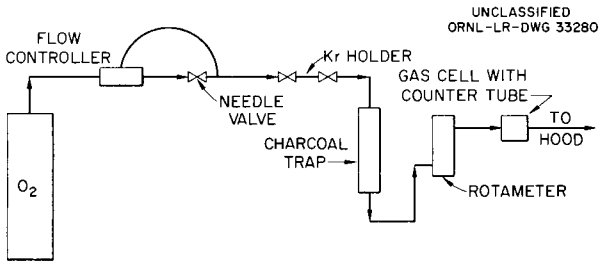

Fig. 172. Diagram of Apparatus for Investigating Fission Gas Holdup.

experiment is designed to study the effect of linear velocity over a wide range of linear velocities necessitating, on occasion, several charcoal columns connected in series and the measurement of pressures at various points throughout the system. Referring to Fig. 172, the instrument panel on the left shows the operating controls and the recorder for the proportional counter; the panel on the right shows the analogous equipment for the Geiger-Mueller counter (each panel also includes a recorder for temperatures). The counter tubes are located in the two lead containers in the left portion of the hood. A picture of one of the gas-tight counter tube cells with a Geiger-Mueller counter tube is shown in Fig. 174. In practice, Kr^{85} elution curves (counts per minute vs time) are obtained.

Experimental and Theoretical Studies

Brief summaries covering most of the work performed in the period ending August 31, 1958, are given in this section; however, investigations which are substantially unfinished and those of

[1] W. E. Browning and C. C. Bolta, *Measurement and Analysis of the Holdup of Gas Mixtures by Charcoal Adsorption Traps*, ORNL-2116 (July 27, 1958).

[2] R. A. McNees *et al.*, *HRP Quar. Prog. Rep. July 31, 1957*, ORNL-2379, p 137.

[3] W. E. Browning, R. E. Adams, and D. E. Guss, *ANP Quar. Prog. Rep. June 30, 1957*, ORNL-2340, p 279 (classified).

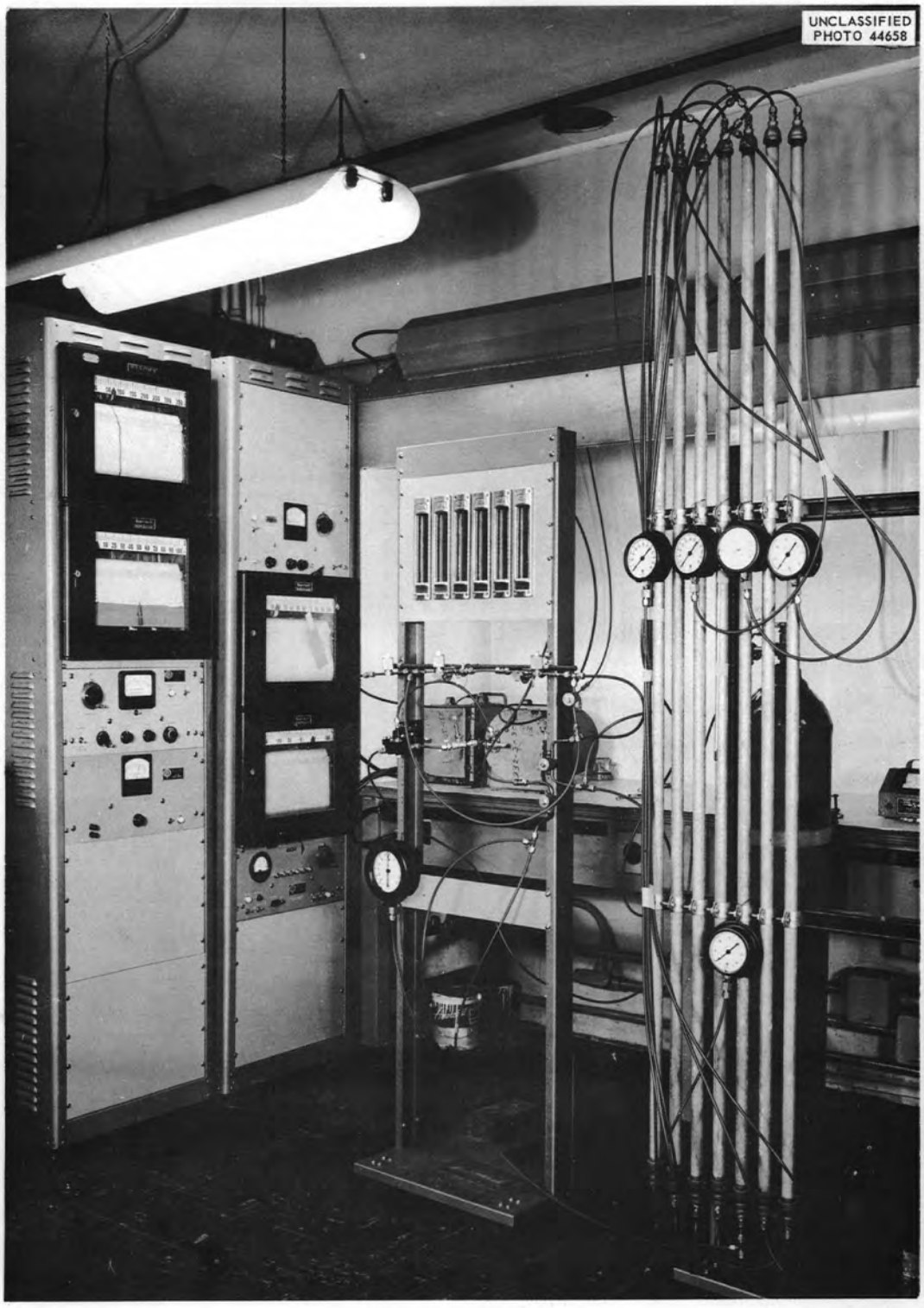

Fig. 173. Equipment for Study of the Holdup of Fission Gases in Adsorption Columns.

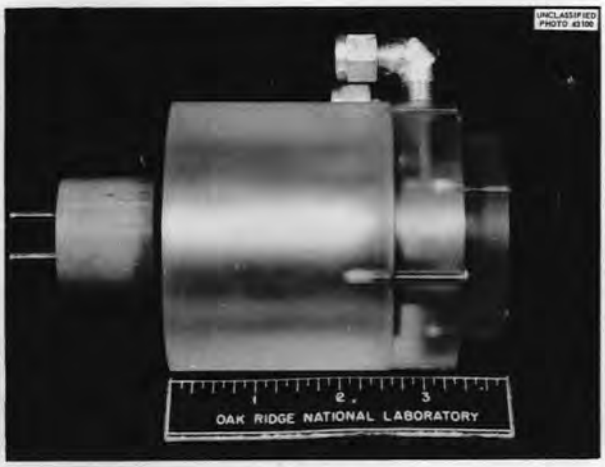

Fig. 174. Gas Cell with Geiger-Mueller Counter Tube.

a very brief or preliminary nature have been omitted.

In a number of these studies, the dynamic adsorption coefficient k (cc/g) is used as a criterion of holdup performance. It is defined as follows:

$$k = \frac{N}{N-1} \cdot \frac{Ft_{max}}{m} ,$$

where

N = number of theoretical chambers,

F = sweep (or carrier) gas flow rate, cc/min,

t_{max} = retention time corresponding to maximum in elution curve, min,

m = weight of adsorbent, g.

In calculating the values of k appearing herein, the factor $N/(N-1)$ was deleted from the above equation. This simplifying approximation is valid for long adsorber beds.

Also, k, or the product Ft_{max}, will deviate from constancy at very low and at very high flow rates; however, in most of the work described here, rather moderate flow rates were employed (of the order of 2 fpm in terms of linear velocity).

Comparison of Various Adsorbents. – Holdup characteristics of a wide variety of materials were determined by using Kr^{85} with oxygen as the sweep gas.[4] Activated carbon samples were dried at 150°C, and the other materials were activated at appropriate temperatures. The results obtained are shown in Figs. 175–177. As may

[4] R. A. McNees *et al.*, *HRP Prog. Rep. for Quarters Ending April 30 and July 31, 1958*, ORNL-2561 (in press).

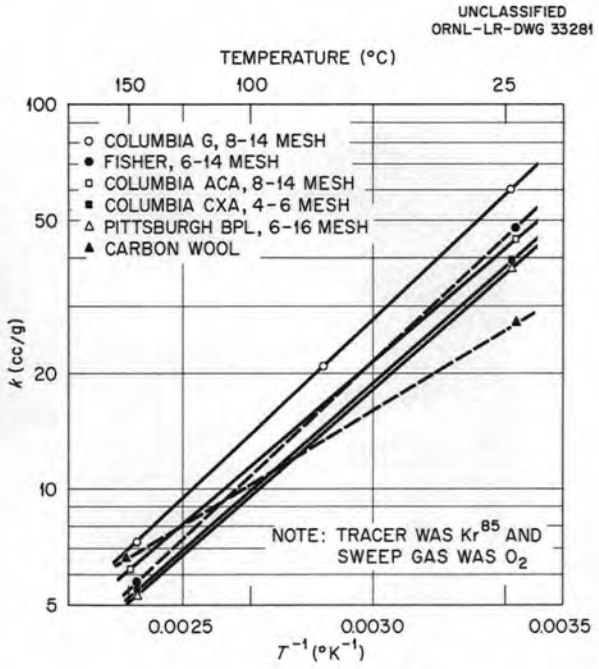

Fig. 175. Dynamic Adsorption Coefficients (k) for Activated Carbon.

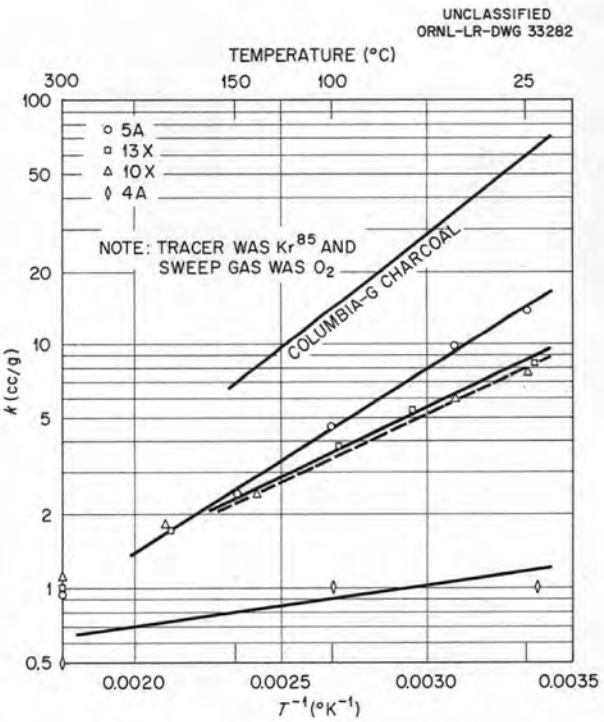

Fig. 176. Dynamic Adsorption Coefficients (k) for Linde Molecular Sieves.

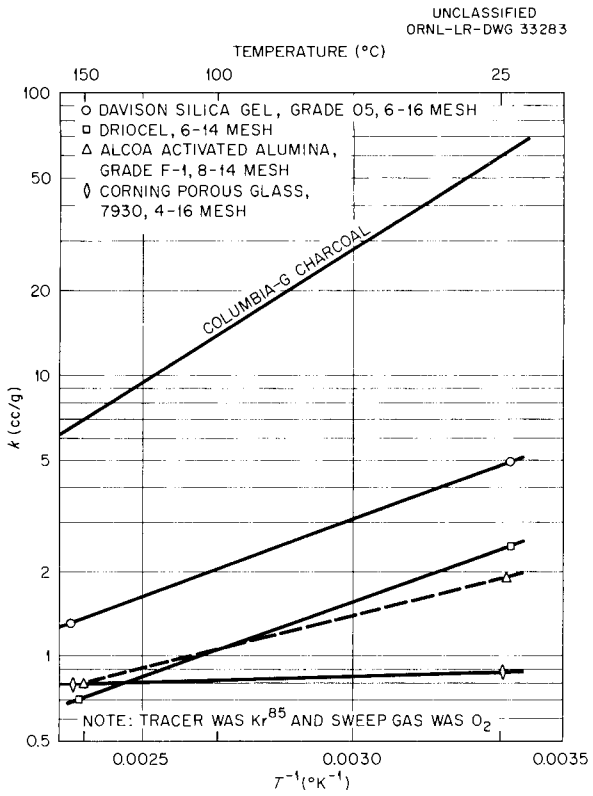

Fig. 177. Dynamic Adsorption Coefficients (k) for Miscellaneous Adsorbents.

be seen, activated carbons are clearly superior in this regard, with Columbia G appearing, under the conditions of this experiment, to be the most efficient of those tested. Linde molecular sieve, type 5A, was observed to be the most promising of the materials other than activated carbon. The principal interest in these other materials arises from the possible need for filling adsorbers with a noncombustible adsorbent, since a potentially hazardous situation is present when the sweep gas is oxygen and the adsorbent is activated carbon as in the HRT. Furthermore, the possibility of combustion is increased as a result of radiation effects, which include heating of the charcoal by radioactive decay of the fission gases and the production of ozone by beta radiation of the oxygen.

Drying of Charcoal. – It was observed, using Kr^{85}, that the dynamic adsorption efficiency of Columbia G charcoal as received could be increased by as much as 45% by drying.[5] Analysis indicated that the original moisture content of the charcoal was 3.4%. Various methods of removing moisture from charcoal were investigated. Sweeping gas through the bed at elevated temperatures was the preferred method.

Effect of Sweep Gas on Holdup. – Since adsorption of the sweep gas interferes with adsorption of the fission gases and since different sweep gases will be adsorbed to varying extents, fission gas holdup will depend on the particular sweep gas employed. This effect is illustrated in Fig. 178, Kr^{85} again having been used to typify the

[5] J. M. Funderburg and L. I. Moss, *Drying of Charcoal Used for Adsorption of Gaseous Fission Products from Homogeneous Reactors*, KT-307 (Dec. 20, 1957).

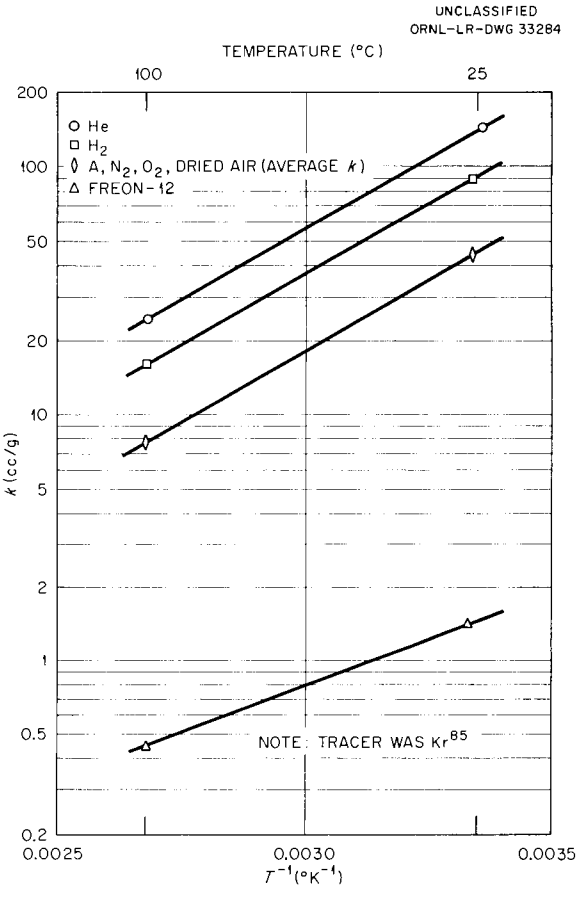

Fig. 178. Dynamic Adsorption Coefficients (k) for Columbia G Charcoal with Various Sweep Gases.

fission gases.[4] Results for argon, nitrogen, oxygen, and dried air did not differ appreciably. Results for all the sweep gases are consistent with respect to their adsorption characteristics. It is not anticipated that Freon-12 will be employed as a sweep gas, and it was selected only to demonstrate a large interference effect.

Effect of Fission Gas Partial Pressure on Holdup. – In reactor operations the fission gas partial pressures may be higher than the trace quantities employed in these experiments by orders of magnitude. Consequently, an experiment[4] was performed wherein normal krypton was continuously added to the oxygen sweep gas to provide a constant partial pressure of krypton throughout the dynamic system. Krypton-85 elution curves were then obtained and k values calculated in the usual manner. Results are shown in Fig. 179, where the point corresponding to a pressure of 740 mm Hg reflects the use of pure krypton as the sweep gas. As may be seen, relatively high krypton partial pressures are required to cause important reductions in the dynamic adsorption coefficient k.

Comparison of Krypton and Xenon Holdup. – In this experiment[6] the tracer was Xe^{133} which contained a small amount of Kr^{85}. Thus, two peaks were present in the elution curves. The adsorbent was Columbia G charcoal and the sweep gas was oxygen. The average ratio of the k value obtained with xenon to that obtained with krypton was 17 at 28°C and was 8 at 100°C.

Fission Gas Holdup Tests on HRT Charcoal Beds. – Prior to operation of the HRT reactor, measurement of the actual holdup characteristics of each of the four charcoal beds constituting the HRT adsorber system appeared necessary. This was done with Kr^{85} in a manner analogous to that employed in the laboratory. It was observed that the holdup performance of the beds exceeded design specifications and was better than that anticipated on the basis of laboratory data; on the other hand, the values which were obtained for N, the number of theoretical chambers, were smaller than those expected. These discrepancies are probably due, at least in part, to the linear velocity of the sweep gas in the larger sections of the HRT beds having been much lower than the linear velocities commonly employed in the laboratory. The results obtained and their significance with respect to HRT operations under various conditions have been reported.[7]

Prediction of Charcoal Trap Performance. – A method for predicting the fission gas holdup performance of charcoal traps has been presented and applied in the evaluation of the traps designed for use in the ORNL-MTR-44 loop experiment.[8] This is an in-pile molten fluoride fuel experiment in which one charcoal trap continuously handles fission gases from the loop pump purge system and in which a second trap serves in the event of a fuel leak.

Ignition of Charcoal in Oxygen. – As indicated earlier, the possibility of combustion exists in the HRT adsorber beds. In this connection the ignition temperature of Columbia G charcoal in flowing oxygen was measured and was found to be 290°C. The experimental conditions were intended to simulate those prevailing in the inlet sections of the HRT charcoal beds; however,

[6] R. A. McNees *et al.*, *HRP Quar. Prog. Rep. Oct. 31, 1957*, ORNL-2432, p 147.

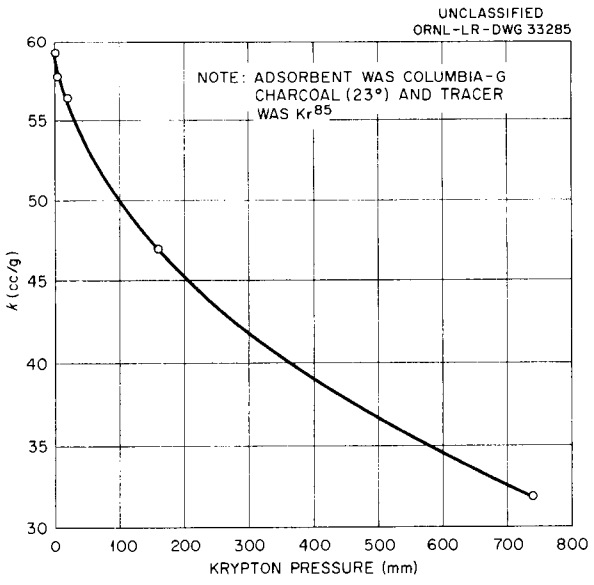

Fig. 179. Dynamic Adsorption Coefficient (k) vs Krypton Partial Pressure.

[7] R. E. Adams and W. E. Browning, *Fission Gas Holdup Tests on HRT Charcoal Beds*, ORNL CF-58-4-14 (April 2, 1958).

[8] R. E. Adams and W. E. Browning, *Evaluation of Fission Gas Adsorption Traps for ORNL-MTR-44 Loop Experiment*, ORNL CF-58-7-71 (July 18, 1958).

radiation conditions were absent. After the charcoal was ignited, combustion could be readily halted by stopping the flow of oxygen. The propagation rate of the combustion front as a function of oxygen flow rate was measured. These results, together with theoretical calculations of charcoal temperatures in the HRT adsorbers, were employed in a study concerned with the possibility of ignition in the HRT charcoal beds.[9]

Removal of Iodine from Gas Streams by Adsorbents. – The experimental phase of this study was concerned with the removal of I^{131} from an air stream with a linear velocity of 180 fpm by charcoal and Linde molecular sieve material, type 13X. After injection of the iodine, the air sweep was continued for 20 hr. At least 99.9% of the iodine was retained by each of the adsorbents. The distribution of iodine along the length of the traps is shown in Fig. 180. Indications were that there was no movement of the iodine along the charcoal after the initial deposition but that there was slight movement of iodine in the case of the sieve material.

The problem of removing radioiodine which might accidentally be released from reactor experiments into the experiment off-gas system of the ORR was investigated, and a conceptual design for an iodine trap containing activated charcoal was presented.[10] However, it was recommended that additional laboratory experiments be conducted before a final design is established. Such information would also be valuable in other reactor applications.

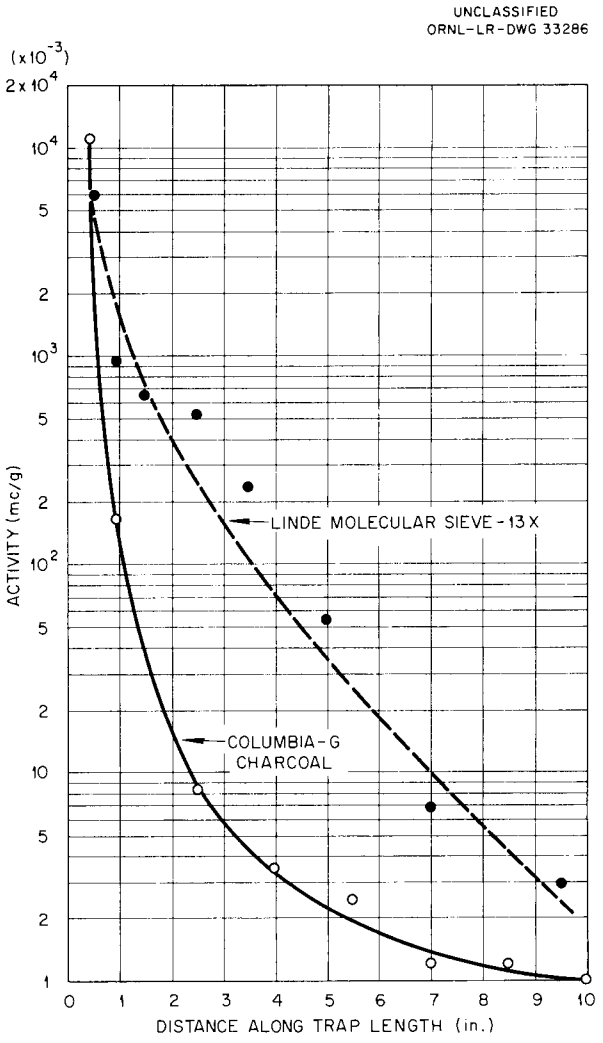

Fig. 180. Iodine-131 Activity Distribution on Adsorber Traps.

Current Projects

Work is under way on fission gas disposal problems including (1) the afore-mentioned linear velocity experiment involving charcoal traps and an approximate linear velocity range of 0.3–200 fpm for the oxygen sweep gas; (2) determination of the relationship between *N*, the number of theoretical chambers or plates, and trap geometry; (3) analysis of gas samples from the exit lines of the HRT adsorbers by gamma spectrometry, and interpretation of the results obtained; (4) measurement of the thermal conductivity of Columbia G charcoal; and (5) additional experimental studies of removal of iodine from gas streams.

Future Work

It is anticipated that a number of the investigations discussed here will be extended so as to provide information which is more detailed and broader in scope. In addition, work will probably be initiated on other studies which appear to be of value from the standpoint of the fission gas disposal program. These include such projects as (1) differences in holdup characteristics of isotopes, (2) determination of mixed adsorption isotherms for fission gases and various sweep gases, and (3) the effect of radiation on the adsorptive properties of adsorbents and on ignition.

[9] R. E. Adams and W. E. Browning, *Estimate of the Probability and Consequences of Ignition of the HRT Charcoal Beds*, ORNL CF-58-6-6 (June 3, 1958).

[10] R. E. Adams and W. E. Browning, *Proposed Method for Removal of Radio-Iodine Vapor from Experiment Off-Gas System of the ORR*, ORNL CF-58-5-59 (May 21, 1958).

HOT CELL OPERATIONS

S. E. Dismuke A. E. Richt E. S. Schwartz

The Hot Lab Section has operated strictly as a service group, with no budget of its own, since July 1, 1957. In the year's operating experience as a service facility it was determined that hot cell charges averaged approximately the same as those in other major hot laboratory facilities throughout the country.

Data concerning hot cell utilization are shown below:

	1957 (%)	January–June 1958 (%)
Installation and testing of equipment and techniques	6	4
Experimental (actual disassembly, data taking, examination, etc.)	27	19
Decontamination and removal of material	5	3
Maintenance		
Scheduled	3	7
Emergency	5	1
Miscellaneous	2	4
Operational down time (cell occupied but not actually in use)	45	52
Vacant	7	10
Total	100	100

During the last year metallographic preparation and examination of over 450 radioactive specimens were completed, along with an appropriate number of control specimens, and the results have been reported (see the "Publications and Papers" section of this report). The number of radioactive specimens handled increased approximately 15% over the previous year. This was accomplished in spite of 33% reduction in technical man power and a significant increase in down time for emergency maintenance.

In addition, 54 experiments were completed in the cells during the year. These experiments included the dismantling and examination of in-pile experimental assemblies, physical measurements, mechanical and metallurgical testing, and preparation of special specimens. Work was performed for members of the Chemical Technology, Metallurgy, Physics, Reactor Experimental Engineering, and Reactor Projects Divisions, and the GE-ANP group at ORNL. This work was in addition to that resulting from requests originating within the Solid State Division, and constituted supporting work for most of the major reactor projects at the Laboratory.

New equipment placed in operation during the past year included a metallographic laboratory for low-level radioactive specimens, an improved remote abrasive cutoff machine, a Kollmorgan wall periscope, one pair of model 8 master-slave manipulators, an in-cell storage coffin, and a modified lathe. In addition, an integral in-cell vacuum cleaning system and a permanent facility for the dry storage of radioactive materials are under construction. Preparations are being made to transfer the remote metallographic specimen preparation cell from cell 2 to cell 1, and modifications to equipment for use in the new cell are under way.

Design is in progress for the modification of cells 5b and 6 into a single cell for the handling of alpha-, beta-, and gamma-active specimens. The cell will have inside dimensions of $11 \times 5 \times 12$ ft. It will be air-tight, and a recirculating air cleaning system will result in a low-volume, filtered exhaust to the stack. The cell will open into an air lock in which glove box and frogman techniques can be used for equipment repair and cleaning.

At the present time radiation exposures to members of the Hot Lab Section are averaging considerably less than the accepted Laboratory tolerance of 100 mrem/week. Efforts are being continued to reduce these exposures even further by means of new and improved operating techniques and equipment.

PUBLICATIONS AND PAPERS

R. E. Adams and W. E. Browning

Fission Gas Holdup Tests on HRT Charcoal Beds, ORNL CF-58-4-14 (April 2, 1958).

Proposed Method for Removal of Radio-Iodine Vapor from Experiment Off-Gas System of the ORR, ORNL CF-58-5-59 (May 21, 1958).

Estimate of the Probability and Consequences of Ignition of the HRT Charcoal Beds, ORNL CF-58-6-6 (June 8, 1958).

Evaluation of Fission Gas Adsorption Traps for ORNL MTR-44 Loop Experiment, ORNL CF-58-7-71 (July 18, 1958).

D. S. Billington

"Radiation Effects on Physical and Metallurgical Properties of Metals and Alloys," chap. 3 in *Effects of Radiation on Materials* (ed. by J. J. Harwood), p 99, Reinhold Publishing Corp., New York, 1958.

D. Binder

"Variation of Irradiation Effects in Graphite and Germanium with Neutron Flux Spectrum," *Bull. Am. Phys. Soc.* **3**, Series II, 31 (1958).

T. H. Blewitt, R. R. Coltman, C. E. Klabunde, and T. S. Noggle

"Stored Energy Measurements in Irradiated Metals," paper presented at Commission I of the International Institute of Refrigeration, Delft, Netherlands, June 17–21, 1958.

W. A. Brooksbank, Jr., and G. W. Leddicotte

"Activation Analysis of Aluminum Base Alloys – A Study of Precision and Accuracy," paper presented at the Pittsburgh Conference on Analytical Chemistry, Pittsburgh, Pennsylvania, March 3–7, 1958.

W. A. Brooksbank, Jr., R. J. Carter, and M. F. Osborne

Volatility Studies of Some Fission Product Fluorides, ORNL CF-58-6-86 (June 25, 1958).

J. W. Cleland

"Radiation Effects in Semiconductors," talk presented at the U.S. Naval Ordnance Laboratory Colloquium, Washington, D.C., December 5, 1957.

J. W. Cleland and J. H. Crawford, Jr.

"Low Temperature Fast Neutron Irradiation of Germanium," *Bull. Am. Phys. Soc.* **3**, Series II, 31 (1958).

J. W. Cleland and J. H. Crawford, Jr.

"Radiation Effects in Indium Arsenide," *Bull. Am. Phys. Soc.* **3**, Series II, 142 (1958).

"Low Temperature Irradiation of *n*-Type Germanium," *J. Appl. Phys.* **29**, 149 (1958).

A. F. Cohen

"Low Temperature Thermal Conductivity in Neutron Irradiated Vitreous Silica," *J. Appl. Phys.* **29**, 591 (1958).

"Low Temperature Thermal Conductivity of Lithium Fluoride Crystal upon Irradiation by Thermal Neutrons and Co^{60} γ-Rays," paper presented at Commission I of the International Institute of Refrigeration, Delft, Netherlands, June 17–21, 1958.

"The Thermal Conductivity of Monoisotopic Ionic (Sodium Fluoride and Cesium Iodide) at Low Temperatures," paper presented at the International Low Temperature Conference, Leiden, Netherlands, June 23, 1958.

"The Thermal Conductivity of Sodium Fluoride Crystal at Low Temperatures," *J. Appl. Phys.* **29**, 870 (1958).

A. F. Cohen and L. C. Templeton
"Low Temperature Thermal Conductivity of Lithium Fluoride Crystal upon Irradiation by Co^{60} γ-Rays, Fast Neutrons and Thermal Neutrons," *Bull. Am. Phys. Soc.* **3**, Series II, 226 (1958).

R. R. Coltman, T. H. Blewitt, and J. T. Howe
"Cryogenic Techniques Developed in the Oak Ridge Graphite Reactor," paper read by T. H. Blewitt at Commission I of the International Institute of Refrigeration, Delft, Netherlands, June 17–21, 1958.

J. H. Crawford, Jr.
"Radiation Effects in Nonmetals," talk given at Arizona State College, Tempe, Arizona, January 7, 1958.

"The Influence of Radiation-Induced Defects on the Behavior of Diamond-Structure Semiconductors and Devices," paper presented at the International Conference on Solid State Physics in Electronics and Telecommunications, Brussels, Belgium, June 2–7, 1958.

J. H. Crawford, Jr., and A. F. Cohen
"The Effect of Fast Neutron Bombardment on the Thermal Conductivity of Silica Glass at Low Temperatures," paper presented at Commission I of the International Institute of Refrigeration, Delft, Netherlands, June 17–21, 1958.

O. L. Curtis and J. W. Cleland
"Investigation of Minority Carrier Recombination in Irradiated Germanium," *Bull. Am. Phys. Soc.* **3**, Series II, 14 (1958).

O. L. Curtis, J. W. Cleland, and J. H. Crawford, Jr.
"Radiation-Induced Recombination Centers in Germanium," to be published in *J. Appl. Phys.*

O. L. Curtis, J. W. Cleland, J. H. Crawford, Jr., and J. C. Pigg
"The Effect of Irradiation on the Hole Lifetime of *n*-Type Germanium," *J. Appl. Phys.* **28**, 1161 (1957).

D. K. Holmes
"Low Temperature Studies of Mechanical Properties of Metals," *Bull. Am. Phys. Soc.* **2**, Series II, 355 (1957).

"Effects of Imperfections and Their Interactions on the Properties of Crystalline Solids," paper presented to the Congressional Hearings on Physics Research Program Before Subcommittee on Research and Development, Washington, D.C., February 3, 1958.

R. E. Jamison
"A Theory of Irradiation Effects in Alloys," *Bull. Am. Phys. Soc.* **3**, Series II, 118 (1958).

G. W. Keilholtz, J. G. Morgan, and W. E. Browning
"Effect of Radiation on Corrosion of Structural Materials by Molten Fluorides," to be published in *Nuclear Sci. and Eng.*

R. H. Kernohan
"The Effect of Fissionable Particle Size on Fission Damage in Graphite," paper presented at the Joint French–U.S. Meeting on Graphite Reactors, New York, November 1957.

R. H. Kernohan and M. S. Wechsler
"The Effect of Neutron Irradiation on Cu-Al Alloys," *Bull. Am. Phys. Soc.* **3**, Series II, 118 (1958).

D. S. Lieberman, T. A. Read, and M. S. Wechsler
"Graphical Analysis of Diffusionless Phase Changes – The Cubic to Twinned Orthorhombic Transformation," *J. Appl. Phys.* **28**, 532 (1957).

E. J. Manthos
ORNL CF-58-1-16 (Secret).
ORNL CF-58-2-43 (Secret).
ORNL CF-58-3-35 (Secret).
ORNL CF-58-3-92 (Secret).

J. G. Morgan, P. E. Reagan, and M. T. Morgan
ORNL-2522 (Secret).

C. M. Nelson and J. H. Crawford, Jr.
"Optical and Spin Resonance Absorption in Irradiated Quartz and Fused Silica: I. Optical Absorption," *Bull. Am. Phys. Soc.* **3**, Series II, 136 (1958).

W. W. Parkinson
"The Effects of Nuclear Radiation on Organic Polymers," paper presented at the American Institute of Chemical Engineers – American Chemical Society Joint Section Meeting, Beaumont, Texas, March 15, 1958.

J. C. Pigg
"Radiation Effects in Electronic Components," paper presented at the American Institute of Electrical Engineers Winter Meeting, New York, February, 1958.
"Radiation Effects in Semiconductor Devices," *Proceedings of Transistor Reliability Symposium, September 17–18, 1956*, p 77, New York University Press, New York, 1958.

A. E. Richt
"Metallographic Examination of L6Z-114 In-Pile Autoclave Pins," ORNL CF-58-2-15 (Feb. 5, 1958).
"Metallographic Examination of Components and Coupons from HRP In-Pile Loop L-2-17 – Part I," ORNL CF-58-2-57 (Feb. 18, 1958).
"Metallographic Examination of Components and Coupons from HRP In-Pile Loop L-4-18," ORNL CF-58-4-30 (April 3, 1958).
"Metallographic Examination of Components and Coupons from HRP In-Pile Loop L-2-19," ORNL CF-58-6-20 (June 3, 1958).
"Metallographic Examination of Irradiated Cermet Fuel Elements – Report No. 6," ORNL CF-58-8-35 (Aug. 4, 1958).
"Irradiation Stability of APPR-1 Type Fe-B Cored, Stainless Steel Clad Control Rod Specimens," ORNL CF-58-5-60 (May 15, 1958).
ORNL CF-57-11-62 (Secret).
ORNL CF-58-1-96 (Confidential).

A. E. Richt, C. F. Lietten, and R. J. Beaver
"Stainless Steel Clad Dispersion of Boron in Iron for Pressurized Water Reactors," paper presented by R. J. Beaver at American Nuclear Society Convention in Los Angeles, California, June 2–5, 1958.

M. T. Robinson
"The Reaction of Uranium Tetrafluoride with Calcium Sulfate," *J. Am. Chem. Soc.* **79**, 5418 (1957).

M. T. Robinson, J. F. Krause, F. P. Green, and D. F. Weekes
"Electronic Analog Simulation of an In-Pile Circulating Fuel Loop," *Nuclear Sci. and Eng.* **3**, 648 (1958).

E. S. Schwartz
"Hot Cell Operation at the ORNL Solid State Division," *Hot Laboratory Operation and Equipment*, p 63–66, Pergamon Press, New York, 1957.

Participation in Panel Discussion: "Operational Aspects of Hot Laboratories," Sixth Hot Laboratories and Equipment Conference, Chicago, Illinois, March 19–21, 1958.

R. H. Silsbee
"Focusing in Collision Problems in Solids," *J. Appl. Phys.* **28**, 1246 (1957).

O. Sisman
"The Effects of High Energy Radiation on Organic Polymers," paper presented at a seminar at Minnesota Mining and Manufacturing Corp., St. Paul, Minnesota, January 20, 1958.

"Irradiation of Organic Polymers in Nuclear Reactors," a talk to be given at the AAAS Meeting in Washington, D.C., December 27–28, 1958.

O. Sisman and J. G. Morgan
"In-Pile Loop Technology," paper presented at Flight Propulsion Meeting of the Institute of the Aeronautical Sciences, Cleveland, Ohio, March 1958.

E. Sonder and D. K. Stevens
"Magnetic Susceptibility of Electrons and Donors in *n*-Type Silicon," paper read by J. H. Crawford at the Kamerlingh Onnes Conference on Low Temperature Physics, Leiden, Netherlands, June 23–28, 1958.

"Magnetic Properties of *n*-Type Silicon," *Phys. Rev.* **110**, 1027 (1958).

D. K. Stevens, W. J. Sturm, and R. H. Silsbee
"Magnetic Susceptibility of Neutron-Irradiated Quartz," *J. Appl. Phys.* **29**, 66 (1958).

J. O. Stiegler
"Metallographic Examination of Components and Coupons from HRP In-Pile Loop L-4-16," ORNL CF-57-9-99 (Sept. 30, 1957).

"Metallographic Examination of HRP In-Pile Loop System Valve 28," ORNL CF-57-11-130 (Nov. 11, 1957).

"Metallographic Examination of Components and Coupons from HRP In-Pile Loop L-2-14," ORNL CF-57-12-40 (Dec. 9, 1957).

W. J. Sturm and M. S. Wechsler
"Density and Resistivity Changes in Au-Cd upon Quenching," *J. Appl. Phys.* **28**, 1509 (1957).

D. O. Thompson and D. K. Holmes
"Temperature Dependence of the Dislocation Modulus and Internal Friction in Copper Single Crystals," *Bull. Am. Phys. Soc.* **3**, Series II, 107 (1958).

M. S. Wechsler
"Phase Transformations in Solids," talk presented at Research Institute for Advanced Study, Baltimore, Maryland, June 3, 1958.

M. S. Wechsler and R. H. Kernohan
"Effect of Quenching on Cu-Al Alloys," *Bull. Am. Phys. Soc.* **3**, Series II, 118 (1958).

R. A. Weeks
"Optical and Spin Resonance Absorption in Irradiated Quartz and Fused Silica: II. Electron Spin Resonance," *Bull. Am. Phys. Soc.* **3**, Series II, 136 (1958).

R. A. Weeks, R. H. Silsbee, J. E. Wertz, and P. Auzins

"Electron Spin Resonance of *F*-Centers in Magnesium Oxide; Confirmation of the Spin of Magnesium-25," *Phys. Rev.* **107**, 1535 (1957).

J. C. Wilson

"Metallurgy with New Rules," talk presented at Albuquerque Chapter of American Society for Metals, Albuquerque, New Mexico, October 17, 1957.

"Radiation Effects in Metals," talk presented at Research Colloquium, Sandia Corporation, Albuquerque, New Mexico, October 16, 1957. Also presented at Canton-Massillon Chapter of American Society for Metals, Canton, Ohio, March 4, 1958, and at Pennsylvania State University Summer Engineering Seminar on Mechanical Properties of Metals, University Park, Pennsylvania, July 10, 1958.

"Experimental Approaches to Radiation Studies – Radiation Sources and Dosimetry," chap. 2 in *Effects of Radiation on Materials* (ed. by J. J. Harwood), p 48, Reinhold Publishing Corp., New York, 1958.

J. C. Wilson and D. S. Billington

"Effect of Nuclear Radiation on Structural Materials," in *Selected Papers from First Nuclear Engineering and Science Congress* (ed. by D. J. Hughes), vol I, *Problems in Nuclear Engineering*, p 97, Pergamon Press, New York, 1957.

M. C. Wittels

"Structural Behavior of Neutron Irradiated Quartz," *Phil. Mag.* **2**, 1445 (1957).

F. W. Young, Jr.

"Polygonization of Copper," *Bull. Am. Phys. Soc.* 3, Series II, 107 (1958).

"Polygonization of Copper," *J. Appl. Phys.* **29**, 760 (1958).

INTERNAL DISTRIBUTION

1. R. E. Adams
2. C. D. Baumann
3. R. G. Berggren
4. J. O. Betterton, Jr.
5. D. S. Billington
6. D. Binder
7. T. H. Blewitt
8. A. L. Boch
9. E. G. Bohlmann
10. C. D. Bopp
11. G. E. Boyd
12. H. Brooks (consultant)
13. W. E. Browning
14. W. E. Brundage
15. N. Cabrera (consultant)
16. D. W. Cardwell
17. R. M. Carroll
18. C. E. Center
19. R. A. Charpie
20. J. W. Cleland
21. R. G. Cleland (consultant)
22. R. R. Coltman
23. A. F. Cohen (consultant)
24. J. H. Crawford, Jr.
25. F. L. Culler
26. J. E. Cunningham
27. O. L. Curtis
28. W. W. Davis
29. R. R. Dickison
30. S. E. Dismuke
31. G. Dresselhaus (consultant)
32. L. B. Emlet (K-25)
33. J. H. Frye, Jr.
34. J. L. Gabbard
35. B. R. Gossick (consultant)
36. R. J. Gray
37. C. S. Harrill
38. H. L. Hemphill
39. N. E. Hinkle
40. A. Hollaender
41. D. K. Holmes
42. A. S. Householder
43. H. B. Huntington (consultant)
44. J. T. Howe
45. R. E. Jamison
46. L. H. Jenkins
47. L. K. Jetter
48. R. W. Johnson
49. R. J. Jones
50. W. H. Jordan
51. C. E. Klabunde
52. G. W. Keilholtz
53. C. P. Keim
54. M. T. Kelley
55. R. H. Kernohan
56. J. A. Krumhansl (consultant)
57. J. E. Lee
58. G. Leibfried
59. A. B. Lewis (consultant)
60. T. A. Lincoln
61. S. C. Lind
62. R. S. Livingston
63. H. G. MacPherson
64. C. J. McHargue
65. W. D. Manly
66. E. J. Manthos
67. A. J. Miller
68. E. C. Miller
69. J. G. Morgan
70. K. Z. Morgan
71. M. T. Morgan
72. E. J. Murphy
73. J. P. Murray (Y-12)
74. C. M. Nelson
75. M. L. Nelson
76. T. S. Noggle
77. R. B. Oliver
78. M. F. Osborne
79. V. Paré
80. W. W. Parkinson
81. D. Phillips
82. J. C. Pigg
83. T. A. Read (consultant)
84. P. E. Reagan
85. J. K. Redman
86. P. M. Reyling
87. A. E. Richt
88. H. E. Robertson
89. C. C. Robinson
90. M. T. Robinson

91. O. E. Schow
92. E. S. Schwartz
93. H. C. Schweinler
94. W. C. Sears (consultant)
95. F. Seitz (consultant)
96. S. T. Sekula
97. F. A. Sherrill
98. R. P. Shields
99. E. D. Shipley
100. R. H. Silsbee (consultant)
101. O. Sisman
102. M. J. Skinner
103. G. P. Smith
104. A. H. Snell
105. E. Sonder
106. R. L. Sproull (consultant)
107. E. E. Stansbury
108. J. O. Stiegler
109. C. D. Susano
110. J. A. Swartout
111. E. H. Taylor
112. L. C. Templeton
113. D. O. Thompson
114. M. S. Wechsler
115. R. A. Weeks
116. A. M. Weinberg
117. E. P. Wigner (consultant)
118. G. C. Williams
119. J. C. Wilson
120. C. E. Winters
121. M. C. Wittels
122. F. W. Young
123. J. C. Zukas
124. Biology Library
125–127. Central Research Library
128. Health Physics Library
129–148. Laboratory Records Department
149. Laboratory Records, ORNL R.C.
150. ORNL – Y-12 Technical Library, Document Reference Section
151. Reactor Experimental Engineering Library

EXTERNAL DISTRIBUTION

152. W. W. Shaver, Corning Glass Works, Corning, New York
153. S. H. Liebson, Naval Research Laboratory, Washington, D.C.
154. Boeing Airplane Company
155. Division of Research and Development, AEC, ORO
156. J. R. Johnson, Minnesota Mining and Manufacturing Co., St. Paul
157. R. N. Little, ANP Project Office, Fort Worth
158. G. L. Stiehl, Convair Division of General Dynamics Corp., San Diego
159. C. C. Webster, Engineering Center, Westinghouse Electric Corp., E. Pittsburgh
160. R. O. Bolt, California Research Corp., Richmond
161. Benjamin Lax, Lincoln Laboratory, Lexington, Massachusetts
162. George H. Wagner, Linde Air Products Company, Tonawanda Laboratory, East Park Drive and Woodward Avenue, Tonawanda, New York
163. D. K. Stevens, Materials and Metallurgy Branch, Division of Research, U.S. Atomic Energy Commission, Washington, D.C.
164. J. B. Trice, General Electric Company – ANPD, Applied Materials Research, Building D, Cincinnati 15, Ohio
165. R. I. Leininger, Battelle Memorial Institute, 505 King Avenue, Columbus, Ohio
166. L. F. Connell, Jr., Dept. of Physics, N. Texas State Col., Denton, Texas
167. Westinghouse Electric Corp., Research Laboratories, Pittsburgh, Pennsylvania
168. J. G. Castle, Jr., Physics Dept., Westinghouse Electric Corp., Research Laboratories, Pittsburgh, Pennsylvania
169–776. Given distribution as shown in TID-4500 (14th ed.) under Physics and Mathematics category (75 copies – OTS)